The design and operation optimization of liquid air energy storage within multi-vector energy systems

Ting Liang

Degree of Doctor of Philosophy

University of Birmingham

School of Chemical Engineering

College of Engineering and physical Sciences

University of Birmingham

July 2022

Declaration

This dissertation is the result of my own work, and includes nothing which is the outcome of work done in collaboration except as declared in the Preface and specified in the text. I further state that no substantial part of my dissertation has already been submitted, or, is being concurrently submitted for any such degree, diploma or other qualification at the University of Birmingham or any other University of similar institution except as declared in the Preface and specified in the text.

This thesis contains 49366 words (excluding acknowledgement, abstract, list of tables, list of figures, appendix, bibliography etc.), as well as 93 figures and 34 tables. It does not exceed 50,000 words or 150 figures as set out by the Department of Engineering degree committee.

Acknowledgement

To my supervisors

First, I would like to acknowledge my first supervisor at University of Birmingham, Prof Yulong Ding. It was his continuous supervision, great vision, profound knowledge, instant feedback and careful revision that led me to develop the extensive academic research in energy storage field smoothly. It was his continuous trust, generous support and care that led me to finish this work in good quality. His dedication into research and work, his sense of responsibility, his rigorous work style and his care for students and the team inspired me to dedicate more and achieve more. I also would like to thank my second supervisor at University of Birmingham, Prof Yongliang Li, who is an excellent researcher with great vision and passion for research in my eyes. His sharing the insights and new ideas generously, and his discussing the research problems and confusions patiently has led me to develop the research work smoothly and fruitfully. I also would like to acknowledge my first supervisor in Melbourne, Prof Paul A. Webley, in the first year, he co-supervised me through remote connection in Melbourne, listening to my progress report carefully every month and providing his ideas and insights to me, my first paper was finished under his co-supervision and careful revision. I also would like to acknowledge my second supervisor in Melbourne, Prof Michael Brear, in the second year, he helped co-supervise me remotely for a period of time, and helped with my research confirmation report in Melbourne.

To research colleagues

I also would like to acknowledge my research colleagues, thanks to Dr. Xiaohui She for helping me with starting the thermodynamic analysis and simulation, I was impressive on his solid knowledge on thermodynamics. Thanks to Dr. Yichung Chen, who has provided me with much help on coding and gave me encouragement when I was discouraged by research

problems. Thanks to Dr. Wei He, he gave me much support in getting into the dynamic simulation, I was impressed by his solid knowledge of dynamic simulation and his quick mind. Thanks to Dr. Abdalqader Ahmad, who has given me much help at the last stage, both on developing my research work and test rig, as well as adjusting to a good mind-set. Thanks to Dr. Binjian Nie, I have learned a lot from him on research methodology and skills, as well as on managing multiple tasks both in work and life. Many thanks to Dr. Zhu Jiang, Dr. Tongtong Zhang, Dr. Boyang Zou, Dr. Yan Hong and Dr. Andrea Vecchi, they have helped me a lot to deal with different challenges of my life in the UK. Thanks to other research colleagues in our BCES centre as well. I cannot achieve my Ph.D. degree without their generous help and support.

To my families and friends

I would like to express great gratitude to my families, my parents, my brother and my sister-in-law, they gave me lots of courage and confidence to pursue my dream, and provided me with unconditional support and love to help me get through all the difficulties during this process. Thanks to my aunt Junxia Liang, she gave me mental support when I was down, telling me to keep my dream in mind and to be an independent lady whatever happened. I would also like to thank Dr. Jiani Mao, who has given me continuous support and gentle care to get through challenges, to build a good mindset for research and for life. Finally, I would like to commend myself as well, I insisted on finishing this journey in good quality even if I have experienced long-term insomnia, great pressure and mental difficulties in life.

To funding

I would like to acknowledge the support from Priestley Joint Ph.D. Scholarship from the University of Birmingham (UK) and University of Melbourne (Australia). Thanks to the partial support from UK EPSRC under grants EP/N032888/1, EP/P003605/1 and EP/S032622/1.

Abstract

Climate changes call for the construction of a net-zero-carbon energy system across the globe. Such a massive need become more urgent due to the recent war on Ukraine, which has led to energy poverty, sharp rise in living costs and economic challenges particularly in Europe. Renewable energy represents a critical pathway towards the decarbonisation. A high share of renewable could trigger multiple problems due to the intrinsic intermittency and variability. Energy storage technologies offer the major solution to resolve such problems.

There are many energy storage technologies at different development stages; among which, Liquid Air Energy Storage (LAES) is considered as a promising large-scale energy storage technology. The key advantages of the LAES include high scalability, no geographical constraints, cost-effectiveness, and capability of providing multi-vector energy services, which is expected to play an increasingly crucial role in future energy systems with a high renewable penetration. However, there are few studies working on the optimization and discussing the functions and benefits of LAES when it is applied into net-zero carbon energy systems. This forms the main motivation of this Ph.D. work, to address the research gaps. In the first and second parts of the thesis, the thermo-economic and dynamic simulation and optimization of the LAES system were conducted, which can provide the basis for discussing its key roles in distributed and grid-scale multi-vector energy systems. The given results can provide evidence for the optimal design, operation and improvement of LAES integrated systems. Meantime, the outcome can provide the enlightening views on the business investment decisions, and on developing renewable energy policies and storage expansion plans, to help achieve carbon mitigation ambitions in the UK by 2050. The following is a brief summary of the work and major conclusions:

In the first part of this work, the multi-objective thermo-economic optimization of a stand-alone LAES system by using a Genetic algorithm was conducted, taking the round-trip efficiency (RTE) and economic indicators as the optimization objectives. The optimization has lead to a 9%~14% of increase in energy efficiency and a 14% of decrease in exergy destruction. The optimal design and operational parameters of LAES under different configurations and scenarios can be determined, including the optimal charging and discharging pressure, heat transfer areas, and mass flow rates of hot and cold storage media etc. Meantime, the design and operational guidelines of LAES can be derived. A LAES system with lower machine efficiencies requires lower charging and discharging pressure, while a system with worse heat transfer performance needs higher charging pressure but lower discharging pressure. Finally, the Pareto Front of capital costs, efficiencies and the occupied space energy density (OSDE) was obtained to provide system operators good investment advice of LAES. It indicated that a higher capital cost lead to a higher RTE, NPV and OSDE. Specifically, when the RTE increases by 1%, the optimized capital investment increases by 0.5-1%. If the investment budget is over 48 M£, a LAES system with three-stage compressors and four-stage turbines can produce better RTE than three-stage and four-stage LAES systems .

In the second part of this work, the dynamic simulation and analysis of the LAES discharging unit were conducted to investigate its dynamic characteristic and response time when integrated with wind power. The results revealed that the LAES discharging unit is more suitable for responding to the wind power component at a time scale more than its start-up time, which can help compensate the wind power deficiency and reduce the motor fatigue. Meanwhile, the combined storage scheme with LAES and battery was proposed to smooth the varying wind power. The economic comparison among different storage schemes indicated the suitable storage system for wind power integration. The annual cost of solely battery storage is more than two times higher than that of the combined LAES and battery storage system,

meantime, the larger the wind farm, the more obvious the economic advantages of the combined storage system.

In the third part of this work, the multiple functions of LAES in decarbonizing a hybrid renewable micro-grid with high share of wind power were investigated. A mixed-integer linear programming (MILP)-based system design framework with the decoupled model of LAES was developed, which can determine the optimal sizes and operation of the micro-grid components and the LAES units. Specifically, the optimal charge/discharge energy to power ratio (27/14 h) and the storage tank size (608 t) of LAES in a micro-grid with 75% of wind power were obtained, leading to ~60% of carbon emission reduction on the 2016 level. The results also revealed the key roles of LAES in supporting a micro-grid with high share of wind power by providing multiple functions. The total benefits were split into six explicit revenue streams for the first time, including the time shifting (13.2%), renewable firming (11.4%), peak shaving (28%), flexibility (21%) and reserve value (20.4%), as well as the waste heat recovery (6%). It also indicated that a higher renewable percentage (over 50%) would be the major driving force to increase the attractiveness of LAES in micro-grids than the mildly reduced LAES capital cost and the enlarged electricity price differences.

In the fourth part of this work, the cost-effective pathways and the storage needs for the transition to a net-zero carbon energy system in the UK by 2050 were assessed. A MILP-based energy expansion model was developed to achieve the optimal design and operation of the system. Firstly, the results revealed that a future 100% renewable or net-zero carbon power system is feasible with levelised cost of energy (LCOE) at 65~80 £/MWh, and a net-zero carbon heat system is affordable with the levelised cost of heat (LCOH) at 45~63 £/MWh. The major expansions are onshore wind power (94.5 GW) in power sector and air-source heat pump (~80 - 90 GW) in heat sector. Secondly, storage technologies would play crucial roles in a net-zero carbon system, only ~10-12% of investments in electric storages would reduce the total

annual costs by ~15.1% - 28%. The major storage expansions lie in LAES (384 GWh) in power sector and the short-term heat storage (330 GWh) in heat sector. Thirdly, the newly deployed capacities of renewables and storages in different zones are correlated with each other, the LAES and renewable capacity ratio is around 20%. It also indicated that the LAES with the charge durations at 8~10 h and discharge durations at 14~15 h is more suitable for the wind-dominated case in the UK than short-duration batteries (~4/5h).

List of Figures

Figure 1.1. The global renewable deployment map....2
Figure 1.2. The layout representation of cycles: (a) Brayton-based PTES; (b) Rankine-based PTES [19]....5
Figure 1.3. The working principle of hydrogen storage....6
Figure 1.4. The working principle of VRFB....9
Figure 2.1. (a) Process flow diagram of a LAES (solid line – air cycle, dashed line – hot/cold recovery cycle) and (b) the associated *T-s* diagram (solid line – charging cycle, dashed line – discharging cycle)....13
Figure 2.2. The common liquefaction cycles (a) Linder-Hampson cycle (b) Claude cycle (c) Kapitza cycle (d) Heylandt cycle (e) Collins cycle....15
Figure 2.3. The common power recovery cycle of cryogen energy: (a) Direct expansion cycle; (b) Direct expansion with Rankine cycle; (c) Direct expansion with Brayton cycle; (d) Combined cycle....17
Figure 2.4. The LAES plants: (a) 350 kW/2.5 MWh at University of Birmingham (b) 50 MW/250 MWh in North of England....18
Figure 2.5. LAES integrated with different heat recovery technologies for excess compression heat utilisation....20
Figure 2.6. The approaches to integrate LNG regasification process with LAES....26
Figure 2.7. The illustration of the MES concept....33
Figure 2.8. A smart energy city configuration in Aalborg....35
Figure 2.9. The flowsheet of an integrated energy system with renewables and hydrogen....38
Figure 2.10. The superstructure of a multi-vector energy system....40
Figure 2.11. An energy hub model of a distributed energy system....41
Figure 2.12. The schematic of a HRES in HOMER....43
Figure 2.13. The flow chart of a hierarchical MILP method....46
Figure 2.14. The schematic of the multi-energy system with hydrogen storage....50
Figure 3.1. LAES thermodynamic layout....58
Figure 3.2. The system optimization framework....67
Figure 3.3. The composite temperature profiles of key heat exchangers: (a) compressor cooler; (b) turbine heater; (c) air-propane evaporator; (d) air-propane cold box....69
Figure 3.4. The effects of charging pressure on (a) RTE and Y; (b) excess oil percentage (the ratio of thermal oil left in hot storage tank to the total cooling thermal oil)....71
Figure 3.5. The effects of discharging pressure on (a) RTE and Y; excess oil percentage (the ratio of thermal oil left in hot storage tank to the total cooling thermal oil)....72

Figure 3.6. The effects of expansion stage on excess oil percentage and RTE 72
Figure 3.7. The effects of machine efficiencies on RTE 73
Figure 3.8. The effects of HEX pinch points on RTE of LAES 74
Figure 3.9. Single-objective optimization of LAES from different initial points.....77
Figure 3.10. The exergy destruction comparison of the LAES system before and after optimization 79
Figure 3.11. LAES system components cost comparison before and after optimization 80
Figure 3.12. Single-objective optimization of LAES with different stages of machines 81
Figure 3.13. Detailed parameters comparison of LAES with different stages of machines 82
Figure 3.14. The Single-objective optimization of LAES under worst scenarios 83
Figure 3.15. The sensitivity analysis of NPV under different economic assumptions 85
Figure 3.16. The optimal Pareto front of RTE and CAPEX 86
Figure 3.17. Two-objective optimization of LAES with different stages of machines 88
Figure 3.18. The optimal Pareto front of three-objective optimization 89
Figure 4.1. Representation of LAES system.....95
Figure 4.2. The pump pressure and mass flow rate validation curve 98
Figure 4.3. The performance characteristic map of turbine under different speed ratio 100
Figure 4.4. Packed-bed model simulation results and validation 102
Figure 4.5. The validation results of air outlet temperature of heat exchangers.....103
Figure 4.6. The liquid air level in tank.....104
Figure 4.7. The first pilot LAES plant configuration.....106
Figure 4.8. Power time response characteristics of LAES discharging model 108
Figure 4.9. The original wind power curve.....109
Figure 4.10. The control strategy of LAES discharging unit.....110
Figure 4.11. The 1st decomposition scheme of the wind power curve: (a) The power signal respond by LAES, (b) The power signal respond by a fast-speed storage 112
Figure 4.12. The LAES response characteristic to the 1st decomposition scheme: (a) The power tracking error, (b) The rotor speed.....112
Figure 4.13. The 2nd decomposition scheme of the wind power curve: (a) The power signal respond by LAES, (b) The power signal respond by a fast-speed storage 114
Figure 4.14. LAES time response to the 2nd decomposition scheme: (a) LAES power tracking error, (b) LAES rotor speed 114
Figure 4.15. The 3rd decomposition scheme of the rest power curve: (a) signal feeds to L ..115
Figure 4.16. LAES time response to the 3rd decomposition scheme: (a) LAES power tracking error, (b) LAES motor speed 116
Figure 4.17. The 4th decomposition scheme of the rest power curve: (a) signal feeds to LAES, (b) signal feeds to fast-speed storage 116

Figure 4.18. LAES time response to the 4th decomposition scheme: (a) LAES power tracking error, (b) LAES rotor speed 117
Figure 4.19. The economic comparison of different storage combinations 120
Figure 4.20. Temperature profiles: (a) low-temperature evaporator; (b) re-heaters 122
Figure 4.21. The turbine torque and mass flow rate profile: (a) Turbine torque; (b) Air mass flow rate 123
Figure 4.22. The turbine pressure and temperature profiles: (a) the valve and turbine outlet pressure; (b) the turbine inlet and outlet temperature 124
Figure 5.1. Future HRMG scheme for the campus 129
Figure 5.2. The decoupled LAES system 130
Figure 5.3. The electricity/heat/cooling demands in campus for four representative weeks 132
Figure 5.4. The methodology and framework of this work 137
Figure 5.5. The logic and structure of discussion part 138
Figure 5.6. Effects of different Cha/Dis E/P ratio on system ROI when achieving energy arbitrage 139
Figure 5.7. The effects of tank sizes on system economics 141
Figure 5.8. Effects of Cha/Dis E/P ratio on LAES revenue and ROI when wind curtailment occurs 142
Figure 5.9. Total revenue of LAES with different Cha/Dis E/P ratio 143
Figure 5.10. Effects of LAES nominal efficiency on economics 144
Figure 5.11. Cost comparison of different system scenarios 147
Figure 5.12. Value decomposition of three storage technologies 148
Figure 5.13. LAES effects on gas engine output and wind curtailment 150
Figure 5.14. Value of LAES serving as an operating reserve in micro-grid 151
Figure 5.15. MILP optimization iteration curve 152
Figure 5.16. Optimal power dispatch of the micro-grid with De-LAES and more wind power 154
Figure 5.17. Optimal heat dispatch of the micro-grid with De-LAES and larger price differences 156
Figure 6.1. District zones in Great Britain (a) 16 separate zones; (b) three aggregated zones (yellow – zone 1, green – zone 2, orange – zone 3) 170
Figure 6.2. The heat demand profile: (a) Monthly heat demand in a year; (b) Hourly heat demand in a day 172
Figure 6.3. The representative renewable capacity factor profiles: (a) Solar energy; (b) Onshore wind energy; (c) Offshore wind energy 173
Figure 6.4. The COP of ASHP varying with outdoor temperature 176
Figure 6.5. Country-level MILP-based energy system expansion model framework 182

Figure 6.6. The validation results of the case study in Italy 190
Figure 6.7. The installed capacity of electricity generators of different scenarios 192
Figure 6.8. The annual generation capacity of electricity generators of different scenarios . 193
Figure 6.9. The installed capacity of heat generators of different scenarios 194
Figure 6.10. The annual generation capacity of heat generators of different scenarios 195
Figure 6.11. The fuel consumption of heat generators of different scenarios 196
Figure 6.12. The annual investment cost, LCOE and LCOH of different scenarios 198
Figure 6.13. The renewable development in different zones 199
Figure 6.14. The capacity expansions of LAES and other storages (Hsto short stands for heat store for short time period) 201
Figure 6.15. The power and energy investment costs of LAES and other storages 202
Figure 6.16. The installed discharge power capacities of LAES and other storages in different zones 204
Figure 6.17. The annual storage generation in different zones 206
Figure 6.18. The effects of different hydrogenation rates on system costs 207
Figure 6.19. The effect of different storage durations on storage capacities and renewable generation 209

List of Tables

Table 1.1. The techno-economic performance of different storage technologies.....8
Table 2.1. Summary of the recovery of LAES excess compression heat.....24
Table 2.2. Literature summary of LAES integrated with renewables.....29
Table 3.1. Literature review and summary of thermodynamic analysis of LAES.....55
Table 3.2. Cost estimation models of major components of LAES.....63
Table 3.3. Thermodynamic input parameters for LAES.....67
Table 3.4. Single-objective optimization of LAES from different initial points.....77
Table 3.5. The detailed parameters comparison of LAES under worst scenarios.....84
Table 3.6. The selected points and parameters from the optimal Pareto front.....87
Table 3.7. The optimal design and operational parameters of three-objective optimization...89
Table 4.1. The comparison of thermodynamic states of LAES plants.....106
Table 4.2. The four decomposition schemes of wind power curve.....111
Table 4.3. Different storage system combination and their power and energy capacity.....118
Table 4.4. The components cost model of LAES.....119
Table 4.5. The technical details of commonly used batteries.....121
Table 4.6. The economic details of commonly used batteries.....121
Table 5.1. LAES nominal operating conditions.....130
Table 5.2. Technical and economic parameters of other system components.....131
Table 5.3. Model other input 'environment' parameters.....133
Table 5.4. Optimization results comparison.....145
Table 5.5. System components candidates.....146
Table 5.6. Optimal design & operation of micro-grid with LAES cost reduction.....153
Table 5.7. Optimal design & operation of micro-grid with increasing wind penetration.....154
Table 5.8. Optimal design & operation of micro-grid with future grid scenarios.....155
Table 5.9. Optimal design & operation considering different sizes of micro-grids.....156
Table 6.1. The literature summary of 100% renewable energy systems planning.....165
Table 6.2. Electricity demand of different zones in UK in 2020 (unit: GW).....171
Table 6.3. The capacities, CAPEX, FOM, VOM and performance metrics of electricity generators.....175

Table 6.4. Techno-economic performance parameters for heat generators.....177
Table 6.5. Fuel price prediction and CO_2 emissions in 2050.....178
Table 6.6. The techno-economic performance parameters of different storage technologies 180
Table 6.7. The techno-economic performance parameters of different heat storage.....180
Table 6.8. Different future energy system scenarios 181
Table 6.9. The average capacity factor of renewables in different zones.....199
Table 6.10. The discharge power capacity expansion in different zones and cases (unit: GW) 204

Abbreviations

ABC	Absorption chiller	LCC	Life cycle cost
ABSO	Advanced bee swarm optimization	LCES	Liquid CO_2 energy storage
ACO	Ant colony optimization	LCOE	levelized cost of electricity
A-CAES	Advanced compressed air energy storage	LCOS	Levelized cost of storage
AIGV	Adjustable inlet guide vane	LFU	Liquefaction unit
AU/AUS	Australia	LNG	Liquid natural gas
AVD	Adjustable vanned diffuser	LOA	Level of liquid air
ASU	Air separation unit	LOP	Loss of power
ASHP	Air-source heat pumps	LOLE	Loss of load expectation
BEV	Battery electric vehicles	LOPP	Loss of power probability
BES	Bulky energy storage	LPSP	Loss of power supply probability
BFPSO	Butterfly particle swarm optimization	MES	Multi-vector energy system
CAC	Carbon dioxide avoided cost	MILP	Mixed-integer linear programming
CAES	Compressed air energy storage	MOGWO	Multi-Objective Grey Wolf Optimizer
CAPEX	Capital expenditure	Mt	Million tonnes
CCHP	Combined cooling, heat and power	NE_RTE	Equivalent round trip efficiency
CCGT	Combined cycle gas turbines	NG	Natural gas
CCS	Carbon capture storage	NGCC	Natural gas combined cycle
CDR	Carbon Dioxide Removal	NPV	Net present value
CES	Cryogenic energy storage	NPSHR	Net positive suction head required
CWHE	Coil-wound heat exchanger	OCGT	Open cycle gas turbines
CHP	Combined heat and power	OMC	Operation and maintenance cost
C-ORC	Cryogenic organic Rankine cycle	ORC	Organic Rankine cycle
COP 26	Conference of the Parties 26	O&M	Operation & Maintenance
COE	Cost of energy	PBP	payback period
CSP	Concentrated solar power	PCM	Phase change material
DPBP	Dynamic Payback period	PFHE	Plate fin heat exchanger
DSM	Demand-side management	PHES	Pumped hydro energy storage
EU	European Union	PID	Proportion, Integration, Differentiation
ESS	Energy storage systems	PGES	Poly-generation energy systems
FCI	Fixed capital investment	PRU	Power recovery unit

FES	Flywheel energy storage	PSO	Particle swarm optimization
FIT	Feed-in tariff	PTES	Pumped thermal energy storage
FOM	Fixed operation and maintenance costs	P2G	Power-to-gas
GE	Gas engine	P2M	Power-to-methane
GHG	Green-house gas	PV	Photovoltaic
GSHP	Ground-source heat pumps	RM	Ratio of mass flow rate
Gt	Giga tonnes	RFB	Redox flow batteries
HES	Hydrogen energy storage	ROI	Return on investment
HESs	hybrid energy systems	RP	Ratio of power
HEX	Heat exchanger	RTE	Round trip efficiency
HDI	Human development index	SC-CAES	Supercritical CAES
HG	Heat generators	SEC	Specific energy cost
HP	Heat pumps	SPC	Specific power cost
HRES	Hybrid renewable energy system	SPBP	Static Payback period
HRMG	Hybrid renewable micro-grid	SQP	Sequential quadratic programming
HS	Heat storage	STOR	Short term operating reserve
HTF	Heat transfer fluid	TEG	Thermo-electric generator
ICE	Internal Combustion Engines	TES	Thermal energy storage
IEA	International Energy Agency	TG	Thermal generators
IGV	Inlet guide vane	TLBO	Teaching-learning based optimization
IPCC	Intergovernmental Panel on Climate Change	TNPV	Total net present value
IR	Interest rate	US (USA)	The United States(America)
IRR	Internal rate of return	UK	The United Kingdom
JC	Job creation	VRFB	Vanadium Redox Flow Battery
KC	Kalina cycle	VWM	Value web model
LAES	Liquid air energy storage	VPP	Virtual power plant
LCA	Life cycle assessment	VOM	Variable operation and Maintenance costs

Symbols

A	Area [m^2]	*online*	Online number or capacity
A	Constraints matrix for continuous variables	*offline*	Offline number or capacity
Amf	Amortized factor	*Obj*	Optimization objective
amb	Ambience	*OR*	Operating reserve
ann	Annual	***of***	On_off status matrix
ava	Available number or capacity	***of_num***	On_off number matrix
b	Known-term vector	*opm*	optimum value
B	Constraints matrix for binary variables	*P*	Power capacity or output
BAT/bat	Battery	*pv*	Photovoltaic
C1	Constant 1	*PinG*	Power injected in to the Grid
C2	Constant 2	*PfmG*	Power withdrawn from the Grid
c	Cost matrix for continuous variables	*PinH*	Heat power injected into the heat network
C	Compressor	*PfmH*	Heat power withdrawn from the heat network
capaf	Renewable capacity factor	*Pcha*	The charging power
Cos	The incurred cost	*Pdis*	The discharging power
Cha/cha	Charge	*Pr*	Price [£/kWh]
com	The committed number or capacity	*R*	Real number set
col	Cooling	*r*	The rated power
curt	The curtailed power or energy	*ratio*	The capacity percentage
d	Cost matrix for binary variables	*rev1*	The primary reserve
Des	Design variable set	*rev2*	The secondary reserve
Dis/dis	Discharge	*Rew/rew*	Renewable power
dn	The downward reserve	*RM*	Ratio of mass flow rate
DT	Duration time	*rtr*	Retired number or capacity
ele	Electricity	*RP*	Ratio of power
ext	Existing number or capacity	***S***	Selection value, 0/1
Eloss	The energy loss	*shut*	The shut-down number or capacity
ems	Emission of CO_2 [kg/kWh]	*SOC*	Storage level
emf	Emission factor [kg CO_2/kg]	*sta*	The start-up number or capacity
eff	Efficiency	*sto*	Storage technology
Elevel	Energy level	*up*	The upward reserve

ep	Equipment	*a*/*b*/*p*/*q*	Regression coefficients
EPR	Energy to power ratio	*t*	Time
fuel	Fuel consumption	$\boldsymbol{T}$	Time domain
grid	Electricity grid	*Tax*	CO_2 tax [£/kg]
HG	Heat generators	*TG*	Thermal electricity generators
h	Enthalpy [kJ/kg]	*Tr*	Expansion turbines
hex	Heat exchanger	*tot*	Total
$\boldsymbol{I}$	Design variable space	*U*	heat transfer coefficients (W/m2·K)
inc	Incentive	*V*	Volume [m^3]
Invc	Investment cost	*wt*	Wind turbines
in	Inlet parameters	$\boldsymbol{Z}$	Integer set
out	Outlet parameters	Q_h	Heat power [kW]
$\boldsymbol{J}$	Auxiliary variable space	Q_f	Fuel power [kW]
J	The moment of inertia	*i*	The i^{th} equipment
los	Loss	*j*	The j^{th} equipment candidate
L	Load	*t*	The t^{th} time period
la	Liquid air	*k*	The k^{th} renewable energy
Lf	Lifetime [years]	*z*	The z^{th} zone
$\boldsymbol{M}$	Mode vector of heat pump	$\boldsymbol{x}$	Continuous variable vector
min	Minimum number or capacity	$\boldsymbol{y}$	Binary variable vector
max	Maximum number or capacity	$\boldsymbol{\varepsilon}$	The escalation rate
$\boldsymbol{N}$	Selected number vector	$\boldsymbol{\sigma}$	The discount rate
num	The number of generators	β	Expansion ratio
new	Newly installed	η	Mechanical efficiency
need	Needed power or energy	ρ	Density [kg/m^3]
n	Selected number	φ	Valve opening rate
Num	Turbine speed	ω	Turbine in speed rad/s
Nx	Dimension of continuous variables	‘	Normalized parameters
Ny	Dimension of binary variable	*0*	The initial value
		¯	Reduced parameters

Publications

Liang, T., Webley, P.A., Chen, Y.C., She, X., Li, Y. and Ding, Y., 2022. The optimal design and operation of a hybrid renewable micro-grid with the decoupled liquid air energy storage. *Journal of Cleaner Production*, *334*, p.130189.

Liang, T., Vecchi, A., Knobloch, K., Sciacovelli, A., Engelbrecht, K., Li, Y. and Ding, Y., 2022. Key components for Carnot Battery: Technology review, technical barriers and selection criteria. *Renewable and Sustainable Energy Reviews*, *163*, p.112478.

Liang T, Zhang T, Li Y, Tong L, Wang L, Ding Y. Thermodynamic Analysis of Liquid Air Energy Storage (LAES) System. Ref. Modul. Earth Syst. Environ. Sci., 2021. https://doi.org/10.1016/B978-0-12-819723-3.00128-1.

Vecchi, A., Knobloch, K., Liang, T., Kildahl, H., Sciacovelli, A., Engelbrecht, K., Li, Y. and Ding, Y., 2022. Carnot Battery development: A review on system performance, applications and commercial state-of-the-art. *Journal of Energy Storage*, *55*, p.105782.

Kheshti, M., Zhao, X., Liang, T., Nie, B., Ding, Y. and Greaves, D., 2022. Liquid air energy storage for ancillary services in an integrated hybrid renewable system. *Renewable Energy*, *199*, pp.298-307.

Table of Contents

Declaration ..... **I**
Acknowledgement ..... **II**
Abstract ..... **IV**
List of Figures ..... **VIII**
List of Tables ..... **XII**
Abbreviations ..... **XIV**
Symbols ..... **XVI**
Publications ..... **XVIII**
Table of Contents ..... **XIX**
1 Introduction **1**
1.1 Background 1
1.1.1 Net zero carbon emissions with renewables 1
1.1.2 Different storage technologies 3
1.1.3 Multi-energy system 9
1.2 Objectives and layout of the thesis 10
2 Literature review **12**
2.1 Liquid air energy storage 12
2.1.1 Basic principle 12
2.1.1.1 Working principle description 12
2.1.1.2 Air liquefaction process 13
2.1.1.3 Air expansion process 15
2.1.2 Development history 17
2.1.3 Literature review on LAES 18
2.1.3.1 Stand-alone LAES systems 18
2.1.3.2 LAES integrated systems through compression heat 19
2.1.3.3 LAES integrated with external heat sources 22
2.1.3.4 LAES integrated with external cold sources 26
2.1.3.5 LAES integrated with renewables 28
2.1.3.6 LAES integrated with other storage technologies 31
2.2 Multi-energy system and design 33

2.2.1 Basic concepts 33
2.2.2 Literature review on multi-energy systems 34
2.2.2.1 MES studies at different spatial levels 34
2.2.2.2 MES studies from multi-fuel perspective 36
2.2.2.3 MES studies from multi-service/generation perspective 38
2.2.3 Modelling of multi-energy systems 40
2.2.3.1 Modelling methods for MESs 40
2.2.3.2 Commercial modelling tools of MES 42
2.2.3.3 Modelling of MES by using evolutional algorithms 44
2.2.3.4 Modelling of MES by using MILP algorithm 45
2.2.4 Assessment criteria of multi-energy systems 46
2.3 Review of energy storage value in MES 48
2.3.1 Energy storage value in micro-scale MES 48
2.3.2 Energy storage value in grid-scale MES 49
2.4 Summary of the review 50
3 Thermo-economic multi-objective optimization of the liquid air energy storage system 53
3.1 Introduction 53
3.1.1 Literature review 53
3.1.1.1 Thermodynamic analysis of LAES 53
3.1.1.2 Multi-objective optimization of LAES and other thermal systems 54
3.1.2 Research aim 56
3.2 Liquid air storage system 58
3.2.1 System description 58
3.2.2 Thermodynamic model and indexes 59
3.2.2.1 Energy analysis model 59
3.2.2.2 Performance indicators 61
3.2.2.3 Exergy analysis model 61
3.2.2.4 System economic model 62
3.3 Optimization model and parameters 66
3.3.1 Optimization formulation 66
3.3.2 Surrogate optimization 66
3.3.3 Assumptions and input parameters 67

3.3.4 Model validation 68
3.4 Results and discussion 70
3.4.1 Parametric sensitivity analysis 70
3.4.1.1 The effects of charging pressure 70
3.4.1.2 The effects of discharging pressure 71
3.4.1.3 The effects of expansion stages 72
3.4.1.4 The effects of machine efficiencies 73
3.4.1.5 The effects of HEX pinch points 74
3.4.2 Single-objective optimization and analysis 75
3.4.2.1 Single-objective optimization - energy analysis 75
3.4.2.2 Single-objective optimization - exergy analysis 78
3.4.2.3 Weighted Single-objective optimization - economic analysis 79
3.4.2.4 Single-objective optimization of LAES with different machine stages 80
3.4.2.5 Single-objective optimization under different device parameters 82
3.4.3 Two-objective optimization for three-stage system 84
3.4.4 Two-objective optimization for multi-stage system 87
3.4.5 Three-objective optimization of LAES system 88
3.5 Summary 90
4 The dynamic analysis of Liquid air energy storage integrated with wind power 92
4.1 Introduction 92
4.1.1 Literature review 92
4.1.1.1 Dynamic analysis of LAES without control strategy 92
4.1.1.2 Dynamic analysis of LAES with control strategy 93
4.1.2 Research aim 94
4.2 LAES system description 94
4.3 Component dynamic model and validation 95
4.3.1 Pump model 95
4.3.2 Turbine model 98
4.3.3 Packed-bed model 100
4.3.4 Heat exchanger model 102
4.3.5 Liquid air tank model 103
4.3.6 Valve model 105
4.3.7 Turbine rotor model 105

4.3.8 System-level validation 105
4.3.8.1 Thermodynamic states validation 106
4.3.8.2 The system response time validation 107
4.4 Case study and methodology 108
4.4.1 Case study 108
4.4.2 Methodology 109
4.5 Results & discussion 111
4.5.1 Wind power decomposition and storage response 111
4.5.1.1 The first decomposition scheme and discussion 112
4.5.1.2 The second decomposition scheme and discussion 113
4.5.1.3 The third decomposition scheme and discussion 114
4.5.1.4 The fourth decomposition scheme and discussion 116
4.5.2 Storage combination scheme and economic comparison 118
4.5.3 The dynamic behaviour of LAES with wind farm 122
4.6 Summary 124
5 The optimal design and operation of a hybrid renewable micro-grid with the decoupled liquid air energy storage 126
5.1 Introduction 126
5.1.1 Literature review 126
5.1.1.1 Hybrid renewable energy system design methods 126
5.1.1.2 Hybrid renewable energy system with energy storage 127
5.1.2 Research aim 128
5.2 Case study and input definition 129
5.2.1 Hybrid renewable micro-grid 129
5.2.2 Micro-grid components models 130
5.2.3 Demand profiles 132
5.2.4 Other input parameters 132
5.3 MILP formulation for micro-grid 133
5.3.1 MILP algorithm description 133
5.3.2 Decision variables 134
5.3.3 Bounded constraints 134
5.3.4 Optimization objectives 136
5.3.5 The methodology 137
5.4 Results and discussions 138

5.4.1 Optimal E/P ratio of LAES 139
5.4.1.1 Optimal E/P ratios for energy arbitrage 139
5.4.1.2 Optimal tank sizes for energy arbitrage 140
5.4.1.3 Optimal E/P ratios for wind firming 141
5.4.1.4 Optimal E/P ratios for operating reserve 142
5.4.1.5 Effects of LAES efficiency on the E/P ratio 144
5.4.2 Optimal design of a micro-grid and energy storage value 145
5.4.2.1 Optimal design of a micro-grid with storage 146
5.4.2.2 Value of storage in a micro-grid without operating reserve 147
5.4.2.3 Value of LAES in a micro-grid with operating reserve 150
5.4.3 Optimal design and operation of a micro-grid with LAES 151
5.4.3.1 Effects of the cost reduction of LAES on system design 152
5.4.3.2 Effects of a higher wind penetration on system design 153
5.4.3.3 Effects of higher electricity prices on system design 154
5.4.4 Effects of different micro-grid sizes on system design 156
5.5 Summary 157
6 Achieving a net-zero carbon energy system with liquid air energy storage and the optimal storage combination 159
6.1 Introduction 159
6.1.1 Literature review 159
6.1.1.1 100% renewable energy system planning 159
6.1.1.2 Energy storage values in a 100% renewable energy system 162
6.1.2 Research aim 168
6.2 Case study introduction 169
6.2.1 Space and time resolution of the case study 169
6.2.2 Electricity demand 170
6.2.3 Heat demand 171
6.2.4 Renewable profiles 172
6.3 Techno-economic input data 174
6.3.1 Electricity generators 174
6.3.2 Heat generators 176
6.3.3 Storage technologies 178
6.3.4 Scenario development 179

6.4 Energy system modelling 181
6.4.1 Modelling framework 181
6.4.2 Modelling constraints 182
6.4.2.1 Electricity generators 182
6.4.2.2 Heat generators 185
6.4.2.3 Renewable generators 185
6.4.2.4 Storage technologies 186
6.4.2.5 Balance constraints 188
6.4.2.6 Optimization objective 188
6.4.3 Model validation 189
6.5 Results and discussions 190
6.5.1 Different pathways for a net-zero carbon energy system 190
6.5.1.1 The effects of different pathways on power sector 190
6.5.1.2 The effects of different pathways on heat sector 194
6.5.1.3 The economic performance of different pathways 197
6.5.1.4 Renewable deployment in different zones 198
6.5.2 The analysis of different storage technologies 200
6.5.2.1 The total capacity expansion of LAES and other storages 200
6.5.2.2 The zonal capacity expansion of LAES and other storages 203
6.5.3 Sensitivity analysis 206
6.5.3.1 Different heat hydrogenation rate 206
6.5.3.2 Different storage duration 207
6.6 Summary 209
7 Conclusion and recommendations 212
7.1 Major conclusions 212
7.2 Future research recommendations 214
Supplementary materials A 215
Bibliography 235

1 Introduction

1.1 Background

1.1.1 Net zero carbon emissions with renewables

In past decades, environmental deterioration and climate changes have drawn considerable attention across the world, which are strongly attributed to the green-house gas (GHG) emissions and primary fuel exhaustion, accompanied with the explosion of human populations and increasing demands in power, heating, cooling and transport sectors [1]. Especially the recent war on Ukraine has led to energy poverty, sharp rise in living costs and economic challenges particularly in Europe.

Therefore, the urgency for new energy provision and carbon emission reduction have been triggered globally. Many countries have proposed carbon reduction plans and made pledges in Paris Agreement 2015 [2]. The agreement set a long-term climate goal as: substantially reducing global GHG emissions to limit the global temperature increase to 2 ℃ in this century while pursuing efforts to limit the increase even further to 1.5 ℃, which needs international cooperation and global coordinated efforts [3]. Upon this fundamental protocol, COP 26 (Conference of the Parties 26) held in 2021 launched 'the Glasgow Climate Pact' [4], which has involved over 200 countries globally to further accelerate the action. It stated that the CO_2 emission must be reduced by 45% by 2030, and achieve net zero by 2050. Several major economies have set out legally binding targets. For example, the UK has pledged to achieve net-zero carbon emissions by 2050 [5], which had 454.8 million tons (Mt) of carbon emissions in 2019. China promised to achieve carbon neutrality by 2060, and India aimed at the net-zero carbon target by 2070 [4]. The United States America (USA) pledged to reduce

net greenhouse gas emissions by 50-52% in 2030, and reach net-zero emissions no later than 2050 [6].

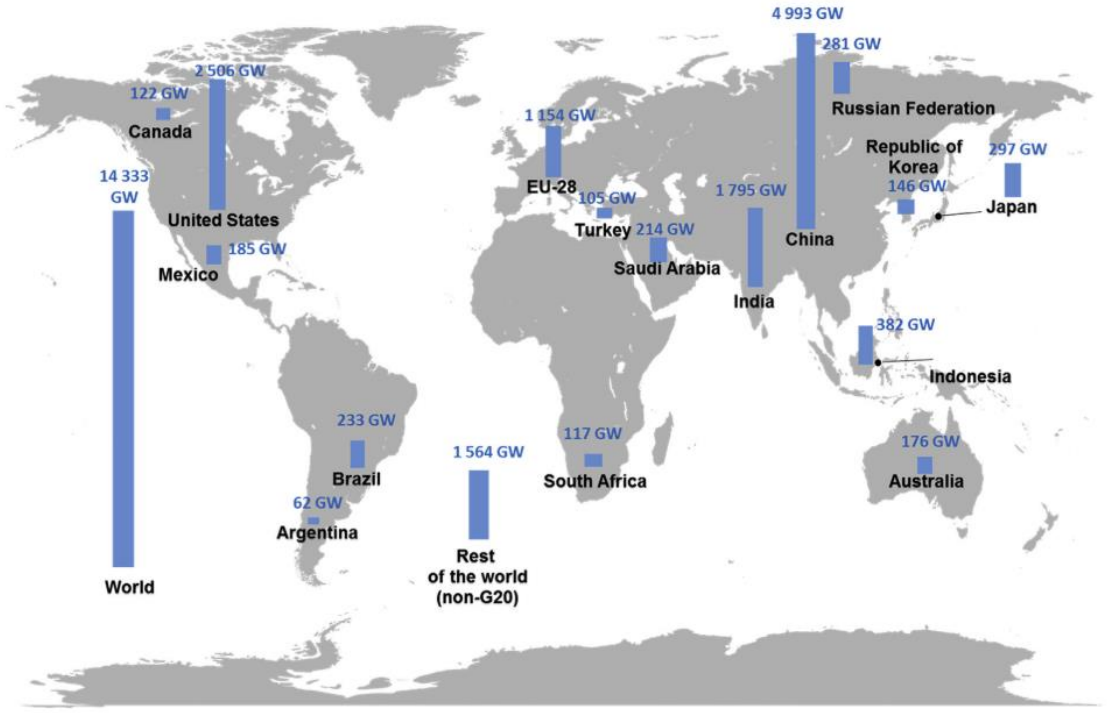

Figure 1.1. The global renewable deployment map [7]

Net-zero carbon means a huge reduction in the use of fossil fuels, falling from nearly four-fifths of total energy supply in 2020 to slightly over one-fifth by 2050. More specifically, this means cutting 98% of unabated coal demand to just less than 1% of total energy use in 2050, reducing oil demand by 75% from around 90 million barrels per day (mb/d) in 2020 to 24 mb/d in 2050, decreasing gas demand by 55% to 1750 billion cubic metres [2]. To make up the energy demand, the share of renewable energy in the total primary energy supply need to grow by 1.4% per year to 63% in 2050. Despite a significant progress has been made in increasing renewable penetration, this is far from the needs. Figure 1.1 shows the current global deployment status [7]. One can see that the major players include China (26%), the USA (15%), India (12%), and the EU (9%) [7].

Looking at the power sector specifically, renewable generation was predicted to provide ~90% of electricity by 2050, with wind and solar Photovoltaics (PV) together account

for nearly 70%. These imply the needs for rapid deployment of the solar and wind power with their capacities expected to increase to 7122 GW and 5445 GW respectively by 2050 [2]. Such a scale of deployment presents huge challenges in the stability and reliability of the power grids due to the intermittency, variability and unpredictability of the renewable generation. Various approaches have been proposed to address the challenges, including flexible dis-patchable power, transmission interconnection, multiple storage technologies, smart grids and demand-side management (DSM) [7][8]. Clearly, each of these approaches has their own disadvantages. The dis-patchable power is generally hydrocarbon-based, which emits carbon. Improving grid transmission capacity would trigger significant cost increase and implement delay. DSM relies upon customers' behavior, leading to uncertainties [9]. Energy storage technologies have a unique role, which will be discussed in the following (Section 1.1.2).

1.1.2 Different storage technologies

Energy storage provides one of the solutions to cope with challenges triggered by high renewable penetration as mentioned above and offers several advantages [9][10]. Firstly, energy storage decouples the renewable energy supply and demand due to its time-shifting function. Secondly, its can accommodate large untapped renewables, to avoid curtailments and green energy waste. Thirdly, energy storage can support isolated distributed energy systems with renewables by ensuring the supply and improving the system efficiency. Finally, energy storage can also provide other benefits for electricity market with higher renewable share, like achieving energy arbitrage, relieving transmission congestion, increasing the grid flexibility and reliability, and regulating the frequency and voltage etc. [11]. Various storage technologies are available for the provision of these services, which are briefly summarised in the following.

Pump hydro energy storage (PHES): This is a mechanical-based energy storage, it works by charging the upper water reservoir with water pumped from lower reservoir, and discharging when water drives turbines to produce power and return to the lower reservoir. It

is the mostly widely developed storage technology, with over 178 GW of capacities installed globally [12]. The advantages of this storage include: high efficiency (~80%), long lifetime (40~60 years), quick response time and fast ramp-up rate etc. The disadvantages are its low energy density (0.5 - 1.5 kWh/m^3), geographical constraints and significant initial cost [13].

Compressed air energy storage (CAES): This is a thermal-mechanical-based energy storage, consisting of the charging system (with air being compressed), compressed air storage reservoir, and the discharging system (with air driving turbines). It is another commercially mature storage technology. The widely studied CAES systems include the conventional diabatic CAES, the advanced adiabatic CAES (AA-CAES) and the isothermal CAES. The heat source for expansion and the operating temperature profile distinguish these three CAES plants [14][15]. The RTEs of CAES are between 50% ~ 70%, the energy density is about 0.4 - 20 kWh/m^3. The functions CAES can provide include load shifting, peak shaving, frequency and voltage control and renewable integration etc. [16]. At present, there are two well-known CAES plants which have been operating successfully for decades, namely the Huntorf (321 MW) in Germany and McIntosh (108 MW) in America. Other CAES plants in US, Chile and China are being planned and built during next decades [14].

Liquid air energy storage (LAES): This is a thermal-mechanical-based energy storage, consisting of three major sub-systems, air liquefaction unit (LFU), cryogenic storage tank and power recovery unit (PRU) [17]. LFU transforms electricity from the grid and renewables into liquid air through liquefaction process. The liquid air is then stored in cryogenic tanks at ambient pressure. PRU transforms cryogenic exergy of liquid air back into electric power through turbine train when needed. The RTE can reach 50%~60% when both the compression heat and the high-grade cold energy can be recovered. The energy density is ~ 120-200 kWh/m^3, and there is no geographical constraint [18].

Pumped thermal energy storage (PTES): This is a thermal-mechanical-based energy storage. During charging, input electricity is converted to thermal energy to establish a temperature difference between a hot and a cold reservoir. During discharging, the stored thermal energy is converted back to electricity through a power cycle, such as a Brayton or a Rankine cycle, corresponding to Brayton-based PTES and Rankine-based PTES [19] (shown as in Figure 1.2). Brayton-based PTES systems work with media like argon, air, super-critical CO_2 (sCO_2), helium hydrogen and nitrogen [20], with the RTE in the range of 45% [22] - 75% [25], and the energy density at ~30-70 kWh/m^3 [21]. Rankine-based PTES can be distinguished into different cycles based on their working media, including steam Rankine cycles [31], organic Rankine cycles (ORC) [29] and trans-critical CO_2 cycles [28] , as well as cascade ammonia and water steam cycles [22] and cascade trans-critical CO_2 [28] and subcritical NH_3 cycles [32]. The system RTEs are in the range of 40% [29] to 70% [31], which can be increased to over 100% based on electricity input when external low-grade heat [34] or waste heat sources [36] are utilized, and its energy density is at ~15 kWh/m^3 [20].

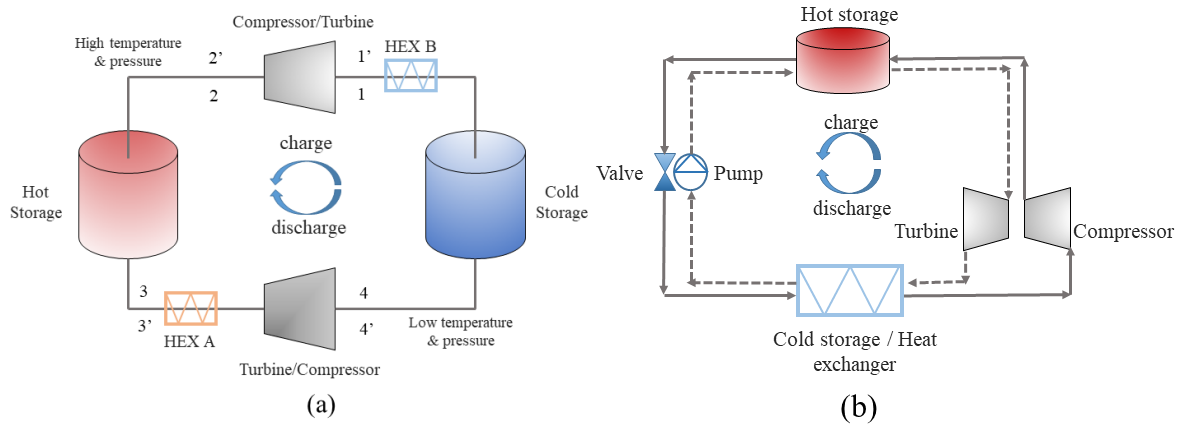

Figure 1.2. The layout representation of cycles: (a) Brayton-based PTES; (b) Rankine-based PTES [19]

Hydrogen energy storage (HES): This is a thermo-chemical energy storage as shown in Figure 1.3. A water electrolysis is adopted to produce hydrogen by using grid or renewable electricity. The hydrogen can be stored in high-pressure container or in liquid state, or injected into gas pipelines for transmission. Fuel cells or combustion turbines are two key technologies

to convert chemical energy of hydrogen into power with waste heat [16]. Three electrolyser technologies are currently available, including Alkaline electrolyser (efficiency 43–66%, mature), polymer electrolyte membrane electrolyser (efficiency 68–72%, early commercial), and high temperature Solid Oxide electrolysers (efficiency up to 98%, developing stage) [11]. Fuel cell technology is more efficient and quieter, and produces less pollution than the combustion technology [23]. The RTE of power-to-power system is at ~ 30% - 50%, the energy density is high at 530 – 750 kWh/m^3 (200 – 300 bar compressed gas state) or 2360 kWh/m^3 in liquid state [11]. It is a very promising technology when performing as a long-term energy storage [24], but it currently needs significant cost reduction and durability improvement to deploy this technology in large-scale.

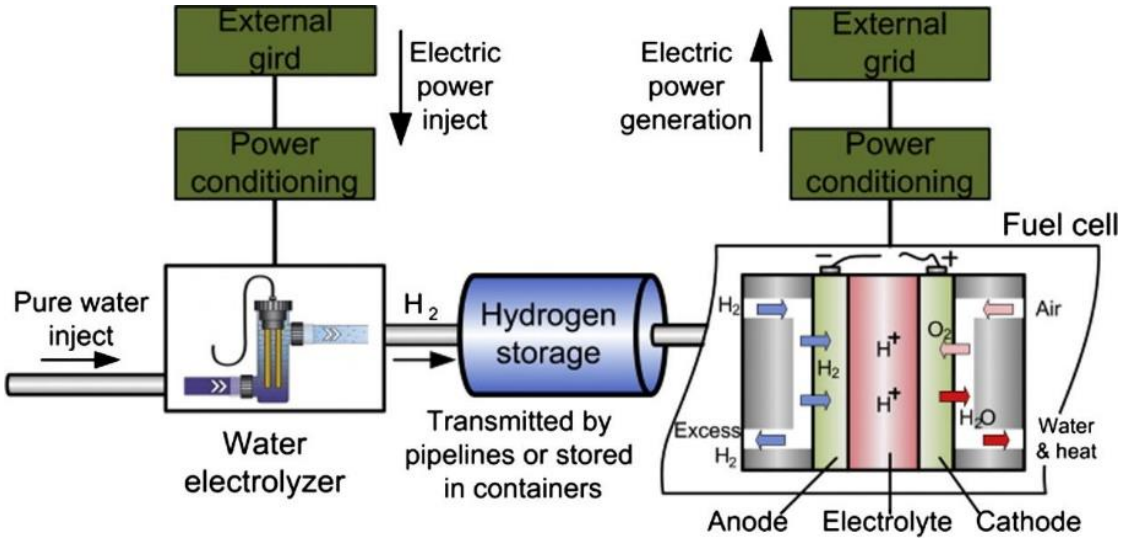

Figure 1.3. The working principle of hydrogen storage [16]

Flywheel energy storage (FES): This is a mechanical energy storage technology with high power density and low energy density. Energy is charged by accelerating rotating mass(flywheel) and discharged by deaccelerating the rotating mass. Its performance is mainly affected by the moment of inertia of the rotor and rotating speed [25], the efficiency is as high as 90% - 95%. There are two categories, namely the low-speed flywheel (<10,000 rpm) and high-speed flywheel (10,000–100,000 rpm). It suits for short-term electricity services, like frequency response and power quality [14].

Lithium-ion batteries (LIBs): This is an electrochemical energy storage technology, featuring high energy density (75 – 200 Wh/kg), quick response (~ms) and high efficiency (>80%) [25]. It consists of two electrodes, the cathode (lithiated metal oxide, like $LiCoO_2$ and $LiMO_2$) and anode (layered graphitic carbon), with the electrolyte of lithium salts (such as LiPF6) dissolved in organic carbonates [25]. Nowadays, it has been widely used in renewable integration and electric vehicles (EVs). A 32 MW/8 MWh Li-ion storage system for a 98 MW wind farm in 2011 has been established [26]. Another case is that 15-20 kWh and 50 kWh of Li-ion batteries have been applied into hybrid EVs and EVs [27]. However, the major drawbacks of LIBs are short lifetime and rapid degradation [16], which need significant improvement.

Redox flow batteries (RFB): This is an electrochemical energy storage technology, but is different from the conventional electrochemical batteries. A RFB system consists of the cell stack with two electrolyte flow compartments separated by the ion selective membrane, and two external liquid electrolyte tanks. Taking Vanadium Redox Flow Battery (VRFB) as an example, the working principle is illustrated as in Figure 1.4. The charging/discharging chemical reaction is $V^{4+} \leftrightarrow V^{5+} + e^{-}$, $V^{3+} + e^{-} \leftrightarrow V^{2+}$, the H^{+} irons are exchanged through the iron selective membrane [16]. This RFB can achieve the independence of power and energy capacity of batteries and has low capacity expansion cost [13], similar to CAES and LAES, which facilitates its large-scale (kW - multi MW) and long-duration (>10h) applications. Its advantages include the moderate energy density at 10-70 kWh/m^3, the high efficiency around 70%-85%, and the low self-discharge rate (0.1–0.4%/day), as well as long lifetime (10-15 years) [14]. However, research work is needed to improve the energy density, develop new cheaper materials and reduce the environment issues caused by acid solution.

Table 1.1. The techno-economic performance of different storage technologies [11][13][16][25][28][22][25][25][26][27][29]

EES	Energy density kWh/m^3	Power rating (MW)	Discharge energy/power ratio (hours)	Self-discharge rate (%)	Life time (years)	Stand-alone cycle efficiency (%)	Response time[2]	Specific power cost $/kW (avg[3])	Specific energy cost $/kWh (avg[3])
PHES	0.5-1.5	100-1000	~8-16	Neg[1]	40-60	~70-85	~min	2638	165
CAES	3-15	10-1000	~8-40	Neg	20-40	~50-70	~min	1669	105
LAES	60-120	10-300	~4-360	Neg	25+	~50+	~min	~2100	~280
PTES_Brayton	30-55	<150	~6-72	Neg	20	~40-80	~min	~3600	460-560
PTES_Rankine	15-20	<100	~6-72	Neg	20	~35-70	~min	~2700	275-376
HES	530-750	<100	~hours-days	Neg	20+	~20-50	~s	~2793	~279
FES	20-80	0.01-1	~0.25	>20%/hour	15+	~90-95	~s	2880	11520
Li-ion	200-400	0.1-100	~4-6	0.1-0.3%	10-15	~75-90	~ms-s	1446	362
VRFB	20-70	<100	~10-20	Neg	10-20	~75-85	~s	2598	650

Notes:

1. Neg – negligible.

2. Response time: min – minute level, s – second level, ms – millisecond level.

3. avg – average level.

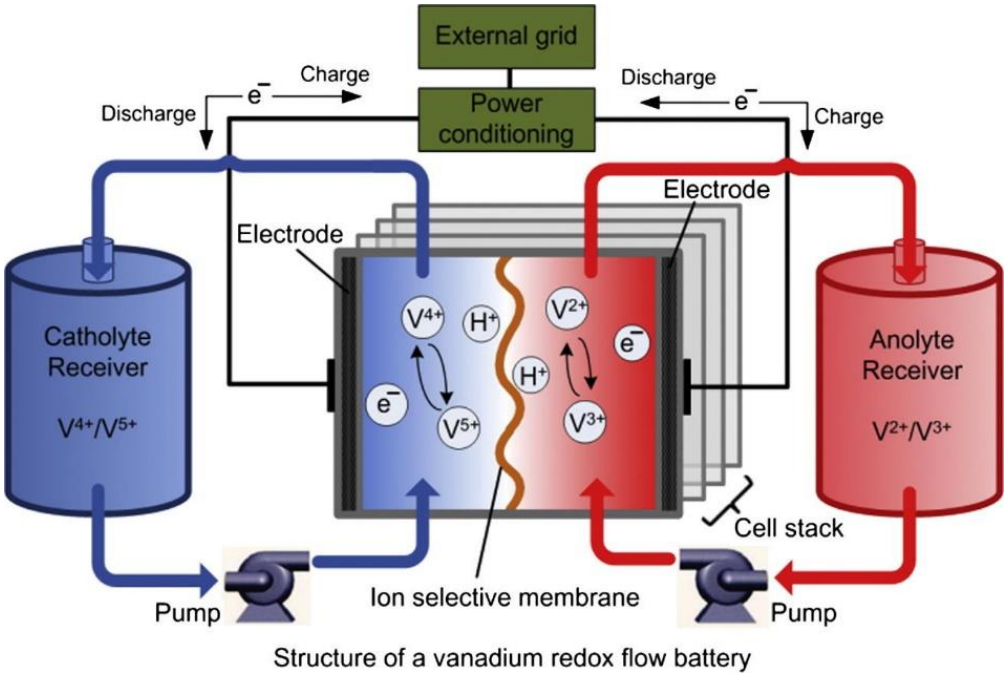

Figure 1.4. The working principle of VRFB [16]

1.1.3 Multi-energy system

By 2021, global CO_2 emissions from energy combustion and industrial processes have reached 36.3 Giga-tonnes (Gt) [30]. Thus, the de-carbonization of the whole energy system today, not only focusing on the electricity sector, but also attending to the heating, cooling and transport sectors, as well as incorporating different storage technologies, poses the greatest challenge that humankind has ever faced. This needs taking a holistic multi-energy system perspective for policy makers and researchers alike. The original concept of *multi-energy systems* (MES) is dated back to the 1990s [31], which has been extended to the newly ones in literatures [32,33]. Nowadays, the concepts, such as *multi-energy systems* (MES), *hybrid energy systems* (HES), *poly-generation energy systems* (PGES) have been put forward, which integrate multiple energy carriers (gas, electricity, hydrogen etc.), conversion technologies (gas turbines, heat pumps and fuel cells etc.) and energy sectors (power, heating, cooling and transport etc.) together at the system level [34]. These system concepts aim at investigating how energy systems can be designed, operated and regulated in an interconnected and collective way, to improve their technical, economic and environmental performance.

With regards to the planning and operating of MES, energy system models were developed to determine the selection, sizes and dispatch of multiple technologies, in order to optimize the overall techno-economic and environment metrics. The first multi-energy system model was proposed in the 1970s by the International Energy Agency (IEA) and the International Institute for Applied System Analysis (IIASA) [35,36]. Nowadays, these models have been developed significantly with more renewables penetrating into conventional energy systems, and with more complex and tight interactions within MES. New modelling challenges were introduced as well[34][37], they are: a) the modelling formulation to deal with the novel energy carriers, conversion and storage technologies; b) the modelling approaches to cope with the increasing complexity and interactions within multiple energy sectors; c) the modelling capacity to manage the uncertainties of future energy systems; d) the modelling skills to reveal more system details but reduce the high calculation volume; e) the complex optimization involving multiple objectives including technical, economic, environment and human development aspects. Among various optimization algorithms, the mixed-integer linear programming (MILP) or linear programming has been one of the most popular approaches to formulate the whole energy system model, which has been widely investigated among researchers and planners since 2000s [36,38–40]. It is capable of determining how energy is transported, converted, stored and dispatched due to its flexible formulations, reasonable computation cost and mature commercial solvers.

1.2 Objectives and layout of the thesis

Overall, this work aims to conduct the optimization of LAES system and investigate its applications in different-scale multi-energy systems (MES). Specifically, the optimal thermodynamic and dynamic optimization of LAES were conducted first. Secondly, the MILP-based design and operation framework for integrating LAES with a micro-grid-level MES and a country-level MES were developed, to explore its multiple functions and benefits in helping

managing higher renewable penetration and reducing CO_2 emissions. The layout of this thesis is presented as follows:

Chapter 2: Literature review, the work related to LAES system and MES all has been reviewed in details, including the system description and working principle, the development history, the related extensive research studies and analysis.

Chapter 3: The thermo-economic multi-objective optimization of a stand-alone LAES system. It aims at assessing the thermodynamic and economic performance of LAES by optimizing the design and operational parameters, and further to guide the design and investment of the system.

Chapter 4: The dynamic simulation and analysis of LAES integrated with wind power. It is to investigate the dynamic behavior and response characteristics of LAES when integrating with wind energy, and to find the methods to improve both the system steady and dynamic performance.

Chapter 5: The optimal design and operation of a hybrid-renewable micro-grid (HRMG) with the decoupled LAES. It aims at investigating the multiple functions and value streams of LAES in HRMG, in order to achieve the optimal deployment of LAES in HRMG and to increase its attractiveness.

Chapter 6: Achieving a net-zero carbon energy system with LAES and an optimal storage combination. It is to develop a net-zero carbon energy system at country-level with multiple conversion and storage technologies, discussing the key roles and compensation value of LAES and other storage technologies for supporting a net-zero carbon energy system in the UK.

Chapter 7: Conclusion. It summarizes the major results of the thesis, extracting the most relevant conclusions and draw the line for future developments and studies.

2 Literature review

2.1 Liquid air energy storage

2.1.1 Basic principle

2.1.1.1 Working principle description

A stand-alone LAES is illustrated in Figure 2.1, the system has three key subsystems, namely the air liquefaction unit (LFU, charging process), storage unit and power recovery unit (PRU, discharging process). The detailed working principle is introduced as: in the charging process, LFU absorbs off-peak electricity (low-cost) or excessive renewable power to compress the purified air to a high pressure (charging pressure) through multistage compression (state 1-6), which is then cooled in heat exchangers ('cold box', state 6-8) by recycling air and cold storage media. The compression heat is recovered and stored in thermal storage medium. Liquid air is produced after expansion machines, like cryo-turbine or throttling valve (state 8-9), and then is stored in cryogenic tanks at ~78 K and near-ambient pressure (state 9-11). In the discharging process, the stored liquid air is pumped to a higher pressure (discharging pressure, state 11-12), releasing cold energy to the cold storage media in the evaporators (state 12-13), the recovered cold energy can be reused in the air liquefaction process. The high-pressure air is then heated by the recovered compression heat before entering air turbine train, to generate electricity through expansion process (state 13-18). An efficient liquefaction process and power recovery process could significantly enhance the working performance of the whole system, thus the key technologies about these two processes are introduced next.

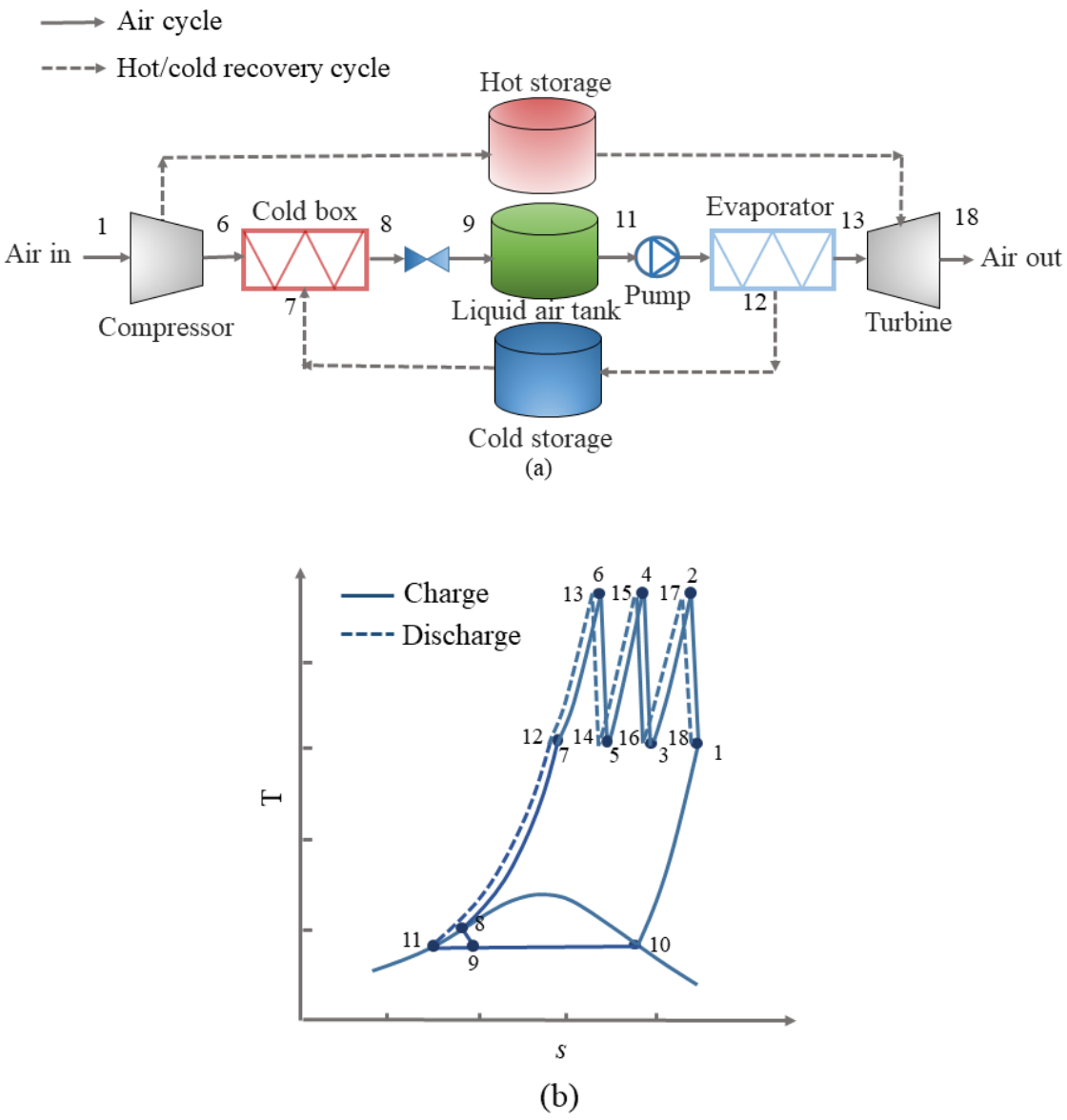

Figure 2.1. (a) Process flow diagram of a LAES (solid line – air cycle, dashed line – hot/cold recovery cycle) and (b) the associated *T-s* diagram (solid line – charging cycle, dashed line – discharging cycle)

2.1.1.2 Air liquefaction process

The air liquefaction process turns the high-pressure air into liquid at a suitable pressure (boiling point at -194.35 ˚C / 78.8 K at 1bar). This significantly reduces the volume by ~700 times [41]. Key parameters affecting the performance of the liquefaction process and liquid air yield include the type of liquefaction cycle used, the charging pressure, the performance of multi-stream heat exchangers (cold box), compressors and the cryo-turbine etc. The optimal charging pressure has been investigated in several studies, which was shown to be at around

12–18 MPa [42–45]. It has also been found that, the higher the efficiencies of the compressors and cryo-turbine, the better the liquefaction performance, with the impact of the compressor efficiency stronger than that of the cryo-turbine [46]. The role of the heat exchanger efficiency is also crucial, as illustrated by Guizzi et al. [42], who showed that an increase of 5 K in the pinch point of the 'cold box' could lead to a 2.2% of decrease in round trip efficiency (RTE).

Commonly used air liquefaction cycles include Linde-Hampson cycle, Claude cycle, Kapitza cycle, Heylandt cycle, and Collins cycle [41], as illustrated in Figure 2.2. The Linde-Hampson cycle has the simplest configuration (Figure 2.2(a)), featured by a long lifespan and a low cost. However, the exergy loss of the irreversible throttling process and the mismatch of the temperature profile in the cold box mean a low exergy efficiency of the cycle below ~10% [47]. The Claude cycle (Figure 2.2(b)), Kapitza cycle (Figure 2.2(c)), Heylandt cycle (Figure 2.2(d)) and Collins cycle (Figure 2.2(e)) are variants of the Linde-Hampson cycle, aimed for improving the liquid yield. The Claude cycle uses two expanding machines, a Joule Thomson valve and an expander, which has been shown to have a comparable efficiency but a better economics than Collins cycle [48]. However, the Collins cycle allows the system to work under a lower pressure. The disadvantages of Collins cycle are its complexity in system configuration, and high investment and maintenance costs due to multiple cryogenic expansion devices. Borri et al. [49] and Zhang et al. [50] investigated a LAES system with a Kapitza cycle, showed that the cycle was more suitable for low-pressure working conditions. The Heylandt cycle is a high-pressure cycle (up to 20 MPa) [41]. Hamdy et al. [51] compared the performance of six liquefaction processes. They found that the Claude cycle had the highest exergy efficiency of ~76 - 82%; whereas the Heylandt cycle gave the highest RTE with the lowest liquefaction power requirement, and the Kapitza cycle could achieve the lowest investment costs.

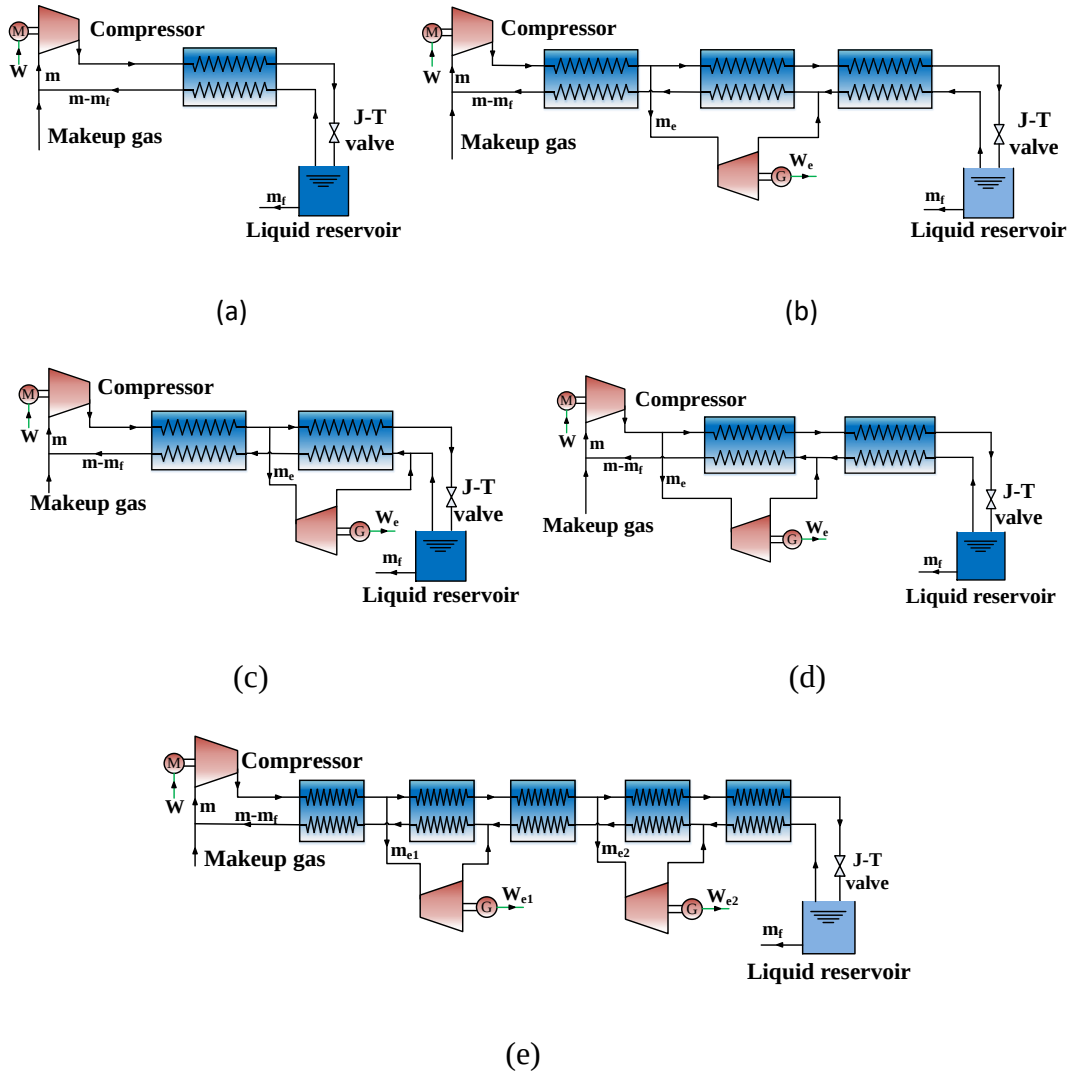

Figure 2.2. The common liquefaction cycles (a) Linder-Hampson cycle (b) Claude cycle (c) Kapitza cycle (d) Heylandt cycle (e) Collins cycle [52]

2.1.1.3 Air expansion process

The power recovery process extracts the cryogenic exergy in the stored liquid air and converts it back into electrical power when in demand, with the stored compression heat reused in the process. Key factors affecting the performance of the power recovery process include the discharging pressure, the cold recovery process in the evaporator, the reheating temperature before expansion, and the efficiencies of the cryo-pump and turbines. Studies of the effect of the discharging pressure have indicated an optimal operating pressure of ~9–12 MPa [53,54]. However, this optimal value varies depending on the system configuration and other operating conditions [55] [56]. Tafone et al. demonstrated that a 1% of increase in the reheating

temperature could produce a 1% of increase in the specific work output when the discharging pressure remains constant [56]; whereas Liang et al. [55] found that the turbine efficiency has the most important impact on the overall system efficiency with the effect of cryo-pump efficiency being lowest. Sciacovelli et al. [44] demonstrated that a 16% of enhancement in recoverable cold energy could lead to a 20%- 30% of increase in the RTE and the liquid yield, respectively.

There are four basic cycles for power recovery (electrical generation): direct expansion cycle, Rankine cycle, Brayton cycle, and combined cycle [17]; see Figure 2.3 for schematic illustrations. For a standalone LAES system, the commonly adopted cycle is the direct expansion. In such a cycle, liquid air is pumped to a high pressure, and then heated before expanding through turbines to generate power. It has the lowest cryogenic exergy utilization rate, because only the mechanical (pressure) part of the cryogenic exergy is used. The recovery and reuse of the thermal part of the cryogenic exergy are crucial, which can be stored in the high-grade cold store, and reused in the liquefaction process to enhance the liquid yield [57]. In fact, the use of a direct expansion cycle with high-grade cold recovery in the discharging process could lead to a much higher RTE than only a combined cycle is used [58]. In addition, as reported by Peng et al. [43], some 20–45% of the compression heat could be in excess and utilised through integrating with other processes to improve the overall system efficiency. Examples of such integration include LAES-ORC [45], LAES-ORC-VCRC [49] and LAES-ORC-ARC [59].

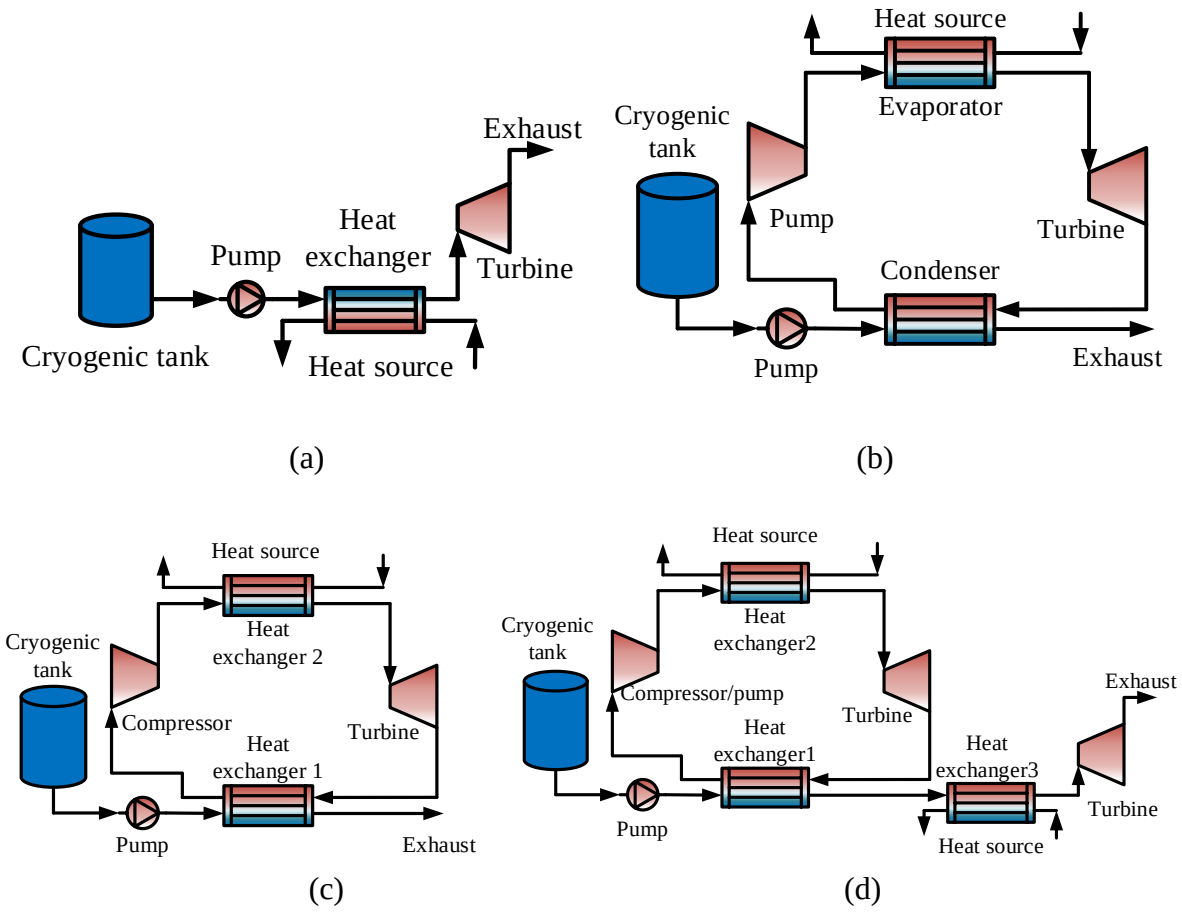

Figure 2.3. The common power recovery cycle of cryogen energy: (a) Direct expansion cycle; (b) Direct expansion with Rankine cycle; (c) Direct expansion with Brayton cycle; (d) Combined cycle [52]

2.1.2 Development history

The pioneering work on LAES can be dated back to 1977 when liquid air was proposed for peak-shaving of power grids by University of Newcastle upon Tyne [60]. This led to subsequent research by Hitachi in 1980-1990s and Mitsubishi Heavy Industries, aiming at replacing CAES in the late 1990s [61]. It was a collaborative research between the University of Leeds and Highview Enterprises Ltd. (now branded as Highview Power) started from around 2005, which has led to substantial development of the technology - the world's first LAES pilot plant (350 kW/2.5 MWh) between 2009 and 2012 (Figure 2.4 (a)) [62]. A pre-commercial LAES plant (5 MW/15 MWh) between 2018 and 2020 (Figure 2.4 (b)); and the announcement of the construction of the world's first commercial LAES plant (50 MW/250 MWh) in 2020

[63]. The first commercial plant is still under construction and is projected to be operational in late 2023 or early 2024, and the actual scale of the plant has been increased from 250MWh to 300 MWh.

(a) (b)

Figure 2.4. The LAES plants: (a) 350 kW/2.5 MWh at University of Birmingham (b) 50 MW/250 MWh in North of England [64]

2.1.3 Literature review on LAES

2.1.3.1 Stand-alone LAES systems

LAES was first proposed and studied without utilizing the excess compression heat. Most studies on such systems were on the analyses of system energy and exergy efficiencies and some on economic analyses.

Energy analyses Guizzi et al. [42] and Xue et al. [65] found that a 50% of RTE could be reached for a stand-alone LAES. Sciacovelli et.al [44] investigated a 100 MW/300 MWh stand-alone LAES system with packed-bed cold store. A RTE of around 50% can be reached, but the power consumption during the charging process increased by 25% due to the formation of thermocline in the packed bed. Liang et al. [55] and Liu et al. [66] developed an optimization scheme to optimize the operational parameters, including the charging/discharging pressures, temperatures, and system configurations. They found an optimal efficiency as high as 60% - 63%.

Exergy analysis Ameel et al. [67] studied the exergy destruction and recovery within a LAES cycle, and concluded that the cold and heat recovery was of high importance. Guizzi et al. [42] found that the major exergy loss came from the compression and expansion processes. Andrea et al. [68] analysed the exergy distribution of LAES at both component and system levels with the system operated under the design and off-design conditions. Hamdy et al. [69] conducted an overall exergy analysis of LAES by using a 'fuel/product' method and found the irreversibility of the liquefaction process accounted for as high as 75%. Jimena et al. [70] split the irreversibility of a LAES cycle into avoidable and unavoidable parts, and concluded that the major potential improvement would lie in the main heat exchanger of the power recovery unit, which could avoid 60% of exergy destruction.

Economic analyses Xie et.al [71] assessed the economics of a decoupled LAES system when participating in the UK electricity service markets. The results indicated that a large-scale LAES with high-grade waste heat (150 °C) would be profitable. Lin et al. [72] found similar results for a LAES system (~200 MW), which was shown to achieve a payback period of 25.7-39.4 years without introducing external waste heat. Wang et al. [73] found that the payback period of standalone LAES systems ranged between 9.6 and 31.7 years when the capacity increased from 10 MWh/day to 200 MWh/day at a peak-valley electricity price ratio of 3.3:1. Clearly, maximising the utilization rate of the compression heat and/or the introduction of external waste heat to the stand-alone LAES system would shorten the payback period and hence improve the economic benefits.

2.1.3.2 LAES integrated systems through compression heat

Around 20% - 40% of compression heat (recovered from the LAES charging process) was not effectively used in many analyses, which provides an opportunity to improve the system RTE [45,74,75]. As a result, different solutions have been proposed to use the excess compression heat and associated techno-economic analyses have been carried out. These

studies include power and cooling generation technologies at medium-to-low temperature, such as organic Rankine cycle (ORC), absorption chiller (ABC), Kalina cycle (KC), and thermo-electric generator (TEG), and district heating network, as illustrated in Figure 2.5.

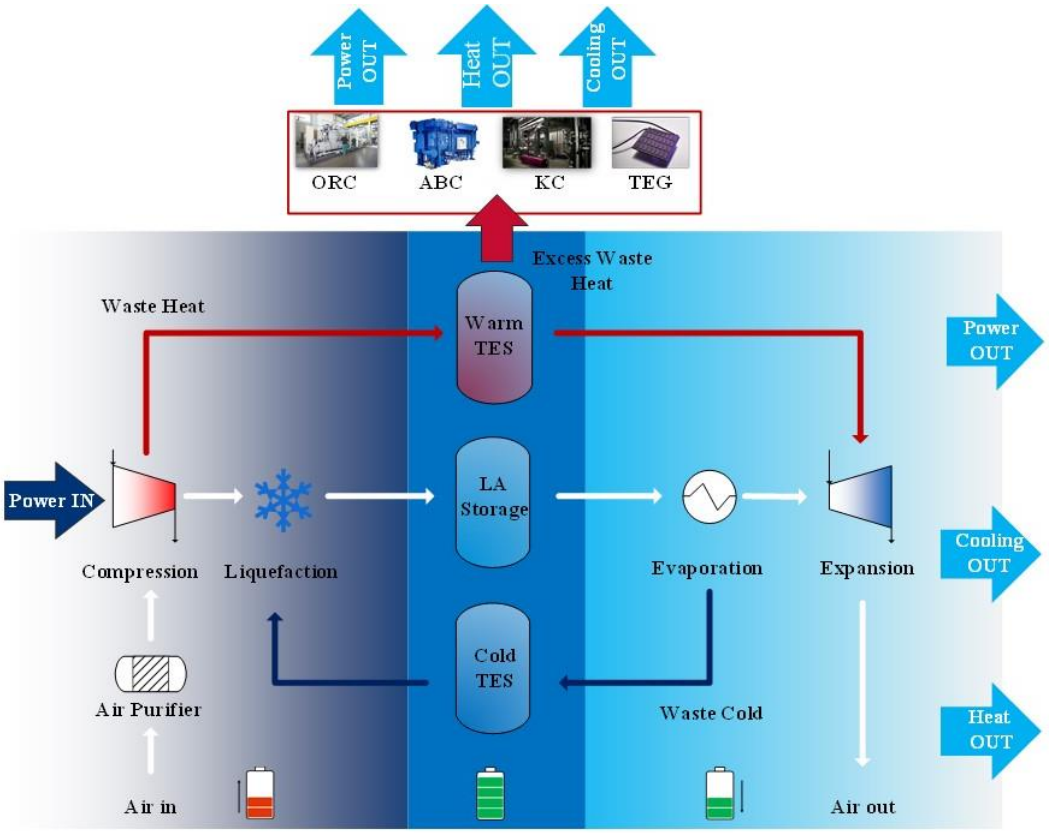

Figure 2.5. LAES integrated with different heat recovery technologies for excess compression heat utilisation [18]

The ORC is the most widely studied method for excess compression heat recovery and utilisation in LAES plants. She et al. [45] performed an thermo-economic analysis on an integrated LAES-ORC system. They found that, compared to the stand-alone configuration, the integrated system could increase the exergy efficiency and RTE by 9-12%, with a payback period of as low as 3 years when introducing a vapour refrigeration cycle as a heat sink for the ORC. Peng et al. [53] proposed a similar configuration to replace vapour compression chiller with a waste-heat powered water-ammonia ABC. Their technical analysis showed that the LAES-ORC system without the ABC (using ambient water as heat sink directly) had a simpler configuration but a higher RTE than the system with ABC, and both of them could have a RTE

over 60%. Tafone et al. [76] compared the economics of standalone LAES, LAES-ORC and Li-ion batteries. Their results showed that the levelised cost of storage (LCOS) of the stand-alone LAES was decreased by 10% when LAES-ORC system operated in a poly-generation mode.

The KC cycle can be used for recovering the excess compression heat efficiently. Ebrahimi et al. [77] proposed a LAES-KC cogeneration system, where phase change materials (PCMs) were used to recover and store the LAES excess compression heat. By reducing the charging pressure and increasing the discharging pressure of the LAES, the RTE and the electrical storage efficiency of this hybrid system were shown to be enhanced to 47.6% and 61.6% respectively. Zhang et al. [50] proposed an ammonia-water based KC cycle coupled with LAES for excess compression heat recovery. A 10% of increase in the RTE was obtained compared with the stand-alone LAES without KC. The same researchers [78] compared the performance of KC and ORC based cycles for LAES excess compression heat recovery and utilization. Their results showed that ORCs generally could outperform KCs with optimal working fluids and conditions. The subcritical ORCs with dry fluids were found to be more suitable for excess compression heat recovery. KCs, on the other hand, would require a higher operating pressure, which would require a more complex system design and a higher investment.

Apart from the use of ORC or KC individually for power generation, Nabat et al. [79,80] studied a combined ORC and KC system with TEG for power generation. For the ORC-TEG hybridization [80], both electrical power and hot water could be produced through a cascaded arrangement of ORC and TEG to fully utilize the excess heat, leading to an improved system RTE and exergy efficiency to 61.1% and 52.8%, respectively, 6.59% and 3.28% higher than systems without the excess heat utilization. A payback period of 3.91 years was shown, together with a final profit of $18.6 million. With a KC-TEG hybridization [79], the RTE was

shown to be increased to 61.6%, with a payback period of 3.5 years and a total profit of $26.3 million for a 30-year operation if an optimal charging pressure of 150.9 bar and a discharging pressure of 84.4 bar were adopted. The combined LAES-TEG system was investigated by Liu et al. [81] as well, their techno-economic analysis suggested an optimal hot water outlet temperature of 60-80 ℃, an overall efficiency increase of 1.7%, and a payback period as low as 3 years.

Tafone et al. [76,82] studied a LAES-based poly-generation system, with LAES integrated with an ORC and a waste heat-driven ABC to provide electricity, heat and cold energy for district heating and cooling networks. Their results showed that the overall RTE of the LAES for the tri-generation could reach 45 - 56%. She et al. [83] proposed a hybrid LAES system to provide cooling, heating, hot water and power simultaneously. The equivalent RTE was shown to be between 52% - 76%, with the highest achieved at a charging pressure of 5 MPa. Cui et al. [84] studied a novel multifunctional LAES system for the provision of heating, cooling, electricity and fresh air. Such a LAES system was shown to reach an energy efficiency of 75.4% with an LCOE at 0.79 CNY/kWh in Beijing. Al-Zareer et al. [85] proposed a LAES system for district heating and cooling applications, with a gas turbine and an ORC for power generation during discharging, and a solid-gas reactor for heating and cooling. They showed that the overall energy and exergy efficiencies of 72.1% and 53.7%, respectively, could be achieved. Vecchi et al. [86] performed a techno-economic analysis on a LAES-based system for heating, cooling and power applications, and showed that the RTE of the overall system increased by 54.8%, and the operational cost reduced by 8-12%.

2.1.3.3 LAES integrated with external heat sources

Although compression heat may not be effectively used in some cases, the use of external heat sources can be of an advantage from either or both economical and system efficiency aspects. Briola et al. [87] proposed a LAES system with a gas turbine cycle. Their

energy analysis revealed a specific work of the charging circuit at 486 kJ/kg, and a storage efficiency (a new indicator) of 2.173. Their economic analysis indicated a differential Net Present Value Ratio of 2.764 under an optimistic scenario. Hanak et al. [88] proposed the combination of cryogenic oxygen storage with an oxy-coal fired power plant to enhance overall efficiency and economics. Their results showed the enhanced flexibility by the combined system, as well as daily financial return by 3.8%-4.1%. Chino et al. [89] proposed and analysed the use of stored liquid air to a gas turbine combustor, and found that the generated power could be doubled compared with the system with air compressors, and the RTE could reach 70%. Piotr et al. [90] studied a LAES system (270 MW, 1080 MWh) with a combustion chamber. Under a charging pressure of 12 MPa, a discharging pressure of 2.1 MPa, and an expansion turbine inlet temperature of 1300 °C, the system RTE was found to be 55.2%.

Barsali et al. [91] modelled a hybrid system with liquid air as an energy storage medium and LNG as a fuel, an equivalent RTE ranging from 82% with carbon capture at 100 bar to 104% without carbon capture at 150 bar can be obtained. Kim et al. [92] investigated a combined renewable-LAES-LNG system, in which renewables were to provide electricity for charging LAES, and LNG regasification and combustion to help increase power generation during LAES discharging. The energy and exergy efficiencies of the combined system were shown to be 64.2% and 62.1%, respectively, and the system LCOE ranged from 142 to 190 $/MWh depending on the system sizes and storage time. Due to carbon emissions of natural gas (NG) and coal combustion, the use of external heat from non-carbon sources to the LAES

Table 2.1. Summary of the recovery of LAES excess compression heat

Authors/Ref.	The systems for compression heat utilization	Working fluids	Round trip efficiency (η_{RTE})	Exergy efficiency (η_{ex})	Economic indicators and values
She et al. [45]	LAES-ORC Heat source: compression heat Heat sink: vapor compression refrigeration cycle (VCRC)	Liquid air for LAES R32/ R502/ R134a for ORC R134a for VCRC	Up to 62%	Charging: 83-87% Discharging: 80-82%	PBP for the proposed ORC: ~3 years (based on 5 MW/40 MWh LAES)
Peng et al. [53]	LAES-ORC Heat source: compression heat Heat sink: ABC or ambient water	Liquid air for LAES R134a for ORC Ammonia-water for ABC	Up to 64%	Charging: 85%	/
Tafone et al. [76,82]	LAES-ORC – (ABC) Heat source: compression heat Heat sink: ambient	Liquid nitrogen for LAES R134a/R245fa for ORC water-LiBr for ABC	48-53% for electricity 45-56% for trigeneration[1]	/	LCOS: 0.16 €/kWh (100MW/400 MWh, 365 cycles per year)
She et al. [83]	LAES-ABC-direct heating Heat source: compression heat	Liquid air for LAES LiBr-water for ABC	52-76% for trigeneration[1]	Charging: 87% Discharging: 84%	Primary energy savings: 12.1 MWh Avoided carbon dioxide emissions: 2.3 ton (1MW/8MWh)
Cui et al. [84]	LAES-ABC-direct heating Heat source: compression heat	Liquid air for LAES	75.4% for trigeneration[2]	/	SPBP: ~5 years LCOE: 0.79 CNY/kWh (1.5 MW/12MWh)
Al-Zareer et al. [85]	LAES-ORC-solid gas reactor Heat source: compression heat/combustion heat Heat sink: ambient	Liquid air for LAES Ammonia for solid gas reactor	72.1% for cooling supply (0℃)[2]	53.7%	/

Vecchi et al. [86]	LAES-direct cooling-direct heating	Liquid air for LAES	72.8% for rigeneration[2]	/	Cost saving metric: 8-13%
Ebrahimi et al. [77]	LAES-KC (KC-based cogeneration unit) Heat source: compression heat	Liquid air for LAES Ammonia-water for KC	47.6% for cogeneration[2]	~40%	/
Zhang et al. [78]	LAES-ORC Heat source: compression heat	Liquid air for LAES n-Pentane for subcritical ORC R152a for supercritical ORC	~57%	~58-61%	/
Nabat et al. [80]	LAES-ORC-TEG Heat source: compression heat and high-temperature electric heater Heat sink: ambient water	Liquid air for LAES R717 for ORC	~61% for cogeneration[2]	~53%	SPBP: ~4 years (9.6MW/38.4MWh)
Nabat et al. [79]	LAES-KC-TEG Heat source: compression heat and high-temperature electric heater Heat sink: ambient water	Liquid air for LAES Ammonia-water for KC	~62%	Charging: 76.4% Discharging: 90.32%	SPBP: ~4 years (~7MW/14MWh)

Notes: [1] $\eta_{RTE} = \frac{W_{dis} + \frac{Q_{cooling}}{COPc} + \frac{Q_{heating}}{COPh}}{W_{ch}}$, [2] $\eta_{RTE} = \frac{W_{dis} + Q_{cooling} + Q_{heating}}{W_{ch}}$

system has been studied. For example, Li et al. [93] proposed the use of heat from a nuclear power plant for load-shifting and peak-shaving of nuclear power plants and increasing the power output of LAES. They showed that the RTE of LAES could reach ~70% and the peak power of the integrated system can be 2.7 times that of the rated nuclear power plant. Cetin et al. [94] developed a system combining LAES with a geothermal power plant, with the geothermal water serving as an external heat source of ~180 ℃ for the expansion process of LAES. Their analyses indicated 46.7% of RTE of a LAES, and an overall system efficiency at ~24.4%.

2.1.3.4 LAES integrated with external cold sources

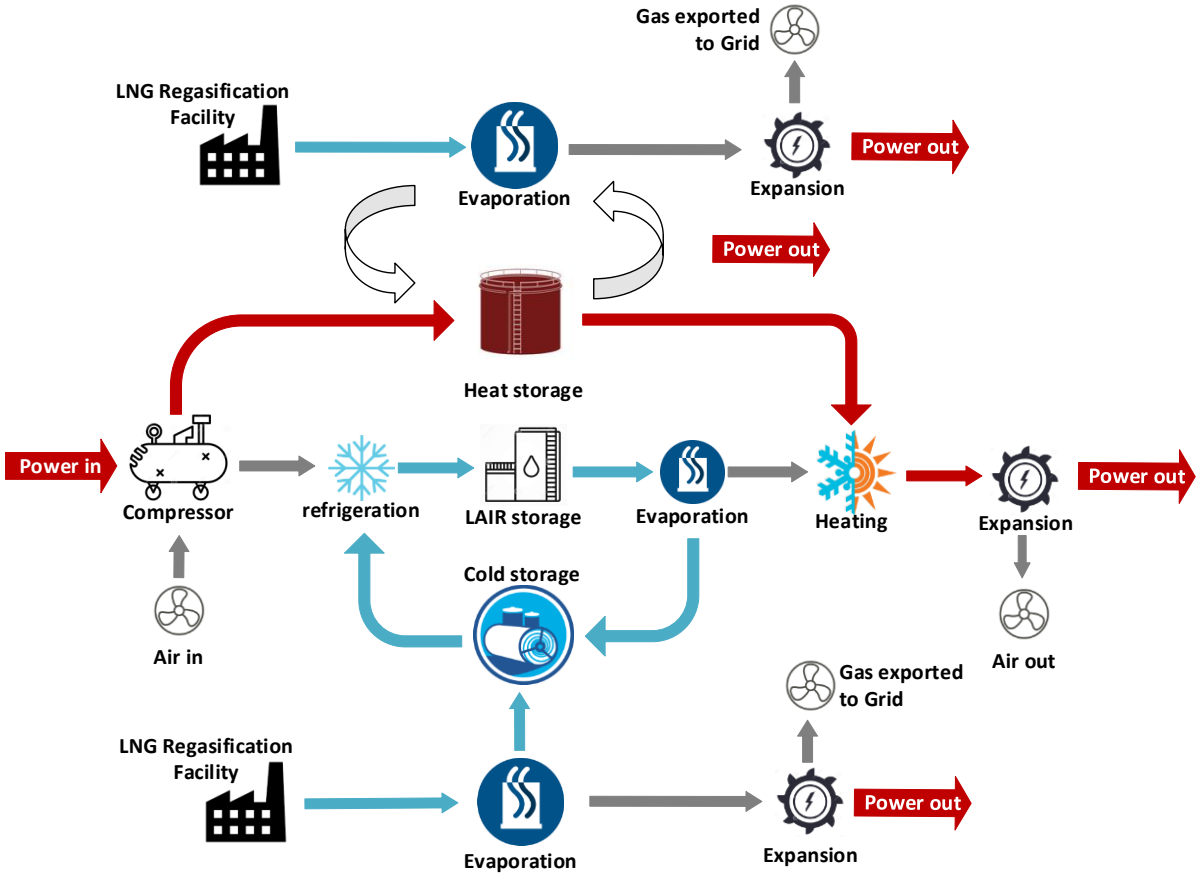

Figure 2.6. The approaches to integrate LNG regasification process with LAES [18]

A LAES system requires cold energy to liquefy air during charging, but the recovered cold energy during discharging is insufficient with ~18% of shortage [43]. The use of an external high-grade cold source can therefore improve the system RTE. An example of such

external cold energy source is from the regasification of Liquefied Natural Gas (LNG). This is discussed in the following.

The integration of LNG regasification with a LAES system is illustrated in Figure 2.6. The LAES-LNG integration can be divided into three sub-categories of direct utilization, indirect utilization through cold storage, and hybrid utilization:

- *Direct utilization* LNG regasification process happens with the LAES charging process. The high-grade cold energy from LNG regasification process is used to cool down and liquefy the charging air of LAES directly in cold box. The power recovered from LNG regasification can be output directly [95,96], or can be used in LAES compression process [97–99]. The energy efficiencies of this approach varied between 70.5% [100] - 141.88% [101]. The exergy efficiencies varied in the range of 35% [102] - 50.73% [100]. This sub-category has a lack of flexibility, as it requires LNG regasification and air liquefaction to operate simultaneously. Besides, the waste cold energy released from the LNG depends on the natural gas (NG) demands, which is often fluctuating, thus adding operational difficulties of such a LAES-LNG integrated system [97].
- *Indirect utilization* LNG regasification process happens with the LAES discharging process. The high-grade cold energy released from the LNG regasification is captured and stored by a cryogenic energy storage system (CES). During LAES air liquefaction process, the stored cold energy from the LNG regasification is reused for air liquefaction. The power recovered from LNG regasification can be output together with LAES discharging power [103], or the re-gasified LNG can be used as combustion fuel in LAES discharging process [92]. This approach increases the flexibility of the integrated system, and improved system exergy efficiency to be 64% (energy efficiency 88%) [103] and 62.1% (energy efficiency 64%) [92].

- *Hybrid utilization* LNG regasification process happens with both the LAES charging and discharging process. This is a combination of the direct and indirect utilization approaches. The high-grade cold energy from the LNG regasification is recovered either in the cold box/heat exchangers of the LAES directly [104] or through a CES unit [105,106], depending on the time of day (peak time and off-peak time [104]). A highest efficiency of 187.4% has been seen in the work [107], in which air liquefaction process used cold energy from LNG regasification and CES as cold source. The output power came from LAES discharging process at ambient temperature and LNG direct expansion power (cold recovery in CES).

2.1.3.5 LAES integrated with renewables

Recent years have seen a number of studies on the direct integration of LAES with renewable generation to deal with intermittency and time-shifting of renewables, including solar thermal heat, solar PV, wind, and geothermal energy. These studies are summarised in the followings:

- ***Integration with solar thermal energy*** Solar thermal system can provide medium and high-temperature heat. Such heat can be used to increase air inlet temperature of turbine during LAES discharging process. Li et al. [108] proposed the integration of LAES with a parabolic trough based concentrated solar power (CSP) system with solar heat stored in thermal oil at ~300-400 ºC. The integrated system was found to be able to provide 30% more output power than the summation of power provided by the CSP and LAES alone. Other studies include the use of other media to store heat from CSP, high temperatures ranging from 574 °C [109] to 1100 °C [110] for LAES discharging.
- ***Integration with solar PV*** Studies on LAES integration with solar PV have been focused on techno-economic analyses. Legrand et al. [111] investigated the LCOE of

Table 2.2. Literature summary of LAES integrated with renewables

LAES integrated with Renewables	Integration method	System scale/ MW/h	Turbine inlet temperature/K	RTE /%	Economic indicator
Concentrated solar heat [108]	Solar heat for expansion	1	~300-400 ºC	~27.55	\
Concentrated solar heat [110]	CSP power for liquefying air Solar heat for expansion	54	~400 ºC	~54.05	PBP: 2.42 years Overall profit: 137.4 $M
Solar PV & wind power [111]	Solar and wind power for charging LAES	100/3h	~377 ºC	~51.7	LCOE: 150 €/MWh LCOS: 50 €/MWh
Solar PV & wind power [112]	Solar and wind power for charging LAES	100/4h	~1300 ºC	~52.7	LCOE: 80-130 €/MWh SB: 5.43 €/MWh
Concentrated solar heat & wind power [113]	Solar heat for expansion Wind power for charging LAES	3.9	~60ºC	~45.7%	\
Wind power [55]	Wind power for charging LAES	3	~200 ºC	~47.9%	Total profits: k£ 729.2 -958.6
Geothermal power [94]	Geothermal power & heat for liquefaction and expansion	12/1h	~127 ºC	LAES: ~ 47% Overall: ~24.4%	\
Geothermal power [114]	Same as [94]	12/1h	~127ºC	LAES: ~ 47% Overall: ~28.4%	\

integrating LAES with solar power for the Spanish power grid. The effects of LAES capacity and renewable ratio (wind power to solar power) were investigated. The results indicated that the LCOE and LCOS (LCOE without accounting for electricity purchase costs) could be reduced to 150 and 50 €/MWh, respectively, with a sufficiently higher solar energy penetration in the Spanish power grid. They also evaluated the price arbitrage function of LAES in a future 2030 scenario in Spain with almost 100% renewables (wind + PV) in another study [112]. They found an optimal size of the LAES charging power which is about 80% of PV nominal power. Such an optimum scenario suggested a power ratio between charge and discharge is ~0.25 (short day-time charge and long night discharge). Damak et al. [115] performed an economic analysis on LAES integration with a PV power plant and a cold storage warehouse. Self-sufficiency and sound economics could be achieved at sufficiently high PV generation.

- ***Hybrid integration*** There have been studies on hybrid renewable integration with LAES; see the studies summarised above [25] [112]. Other studies include the integration of wind and solar with LAES [113], in which LAES was mainly charged by wind power, solar heat was used for LAES discharging process, while excess compression heat of LAES is used for domestic hot water. Such a hybrid plant could give a RTE of ~50% and an exergy efficiency of ~46%. Liang et al. [55] performed a detailed study on the integration of a decoupled LAES plant to a hybrid renewable micro-grid with ~50% of wind power. Their results revealed an optimal energy to power ratio of LAES with ~ 12 h charging and 6 h discharging for stabilising wind power generation. The major revenue streams included peak shaving (28%), flexibility (21%), operating reserve (20.4%), arbitrage (13.2%), wind firming (~11.4%) and waste heat benefits (6%) [55]. Zhou et al. [113] proposed the use of LAES to store solar and wind

energy, and showed, by modelling, the RTE and exergy efficiency of about 45.7% and 44.2%, respectively can be achieved.

- ***Integration with geothermal*** Two studies have been found on LAES integration with geothermal power generation. In one of the studies, energy generated from a single flash geothermal plant during off-peak hours is used to produce and store liquid air. LAES power recovery occurs at peak hours using geothermal heat at ~180ºC [94]. The RTE of the LAES was estimated at ~ 47%, while the overall efficiency of the integrated system was found to be only 24.4%. The other study considered a binary geothermal power plant (6 MW) integrated with an air liquefaction unit and a cryogenic organic Rankine cycle (C-ORC) (1.4 MW) [114]. The C-ORC is driven by the geothermal heat source (~180ºC). The overall efficiency of the combined system was estimated at ~28.4%. This study also indicated a viable solution for flexible operation of geothermal power plants for peak shaving.

2.1.3.6 LAES integrated with other storage technologies

Recent years have also seen reports on the integration of LAES with other storage technologies, including CAES, PTES, and TES. They are summarised in the following.

- Nabat et al. [80] investigated an integrated LAES system with a thermoelectric generator, a high-temperature thermal energy store, and an organic Rankine cycle. Their techno-economic analyses indicated the system energy and exergy efficiencies of 61.13% and 52.84%, respectively, with a payback period (PBP) of 3.91 years.
- Wu et al. [116] proposed an integrated system consisting of LAES and a thermochemical energy store. Their techno-economic analyses showed the system-level RTE and energy density at 47.4% and 36.8 kWh/m^3, respectively, with the PBP and LCOE respectively at 10 years and 179–186 $/MWh.

- Antunez et al. [117] examined an integrated LAES and PTES system, with the cold reservoir of LAES replaced by a cryogenic heat exchanger with helium from PTES as the heat transfer fluid. Their thermodynamic analysis indicated a similar RTE of ~60% as the systems operated separately, but with a significantly higher energy density. The study, however, did not include any economic analysis.
- Xu et al. [109] compared a liquid CO_2-based energy storage (LCES) system and a LAES system in terms of RTE, exergy efficiency, and volumetric energy density. Their results showed higher RTE (45.35%) and exergy efficiency (67.2%) of LCES compared with the data for LAES (37.83% and 45.48% respectively). The energy density of LAES (101.6 kWh/m^3) is about 6 times higher than that of LCES (18.06 kWh/m^3).
- Krawczyk et al. [90] compared a LAES (270 MW, 1080 MWh) and a CAES (290 MW, 1700 MWh) system. Their thermodynamic analyses indicated a major advantage of LAES over CAES in terms of energy density and efficiency. Peng et al. [54] obtained similar results with an energy density of LAES (40.49×10^4 kJ/m^3) ~7 times than that of CAES.
- Georgiou et al. [118] compared LAES and PTES by techno-economic analyses. The results indicated a lower power and energy capital cost of LAES, but PTES was found to be more competitive than LAES in terms of LCOS at an electricity purchasing price higher than 0.15 $/kWh.
- Kantharaj et al. [119] proposed a CAES system with liquid air storage, with an aim to overcome the needs for a pressurized large storage tank and the geological constraint of CAES. They found an efficiency of the hybrid system at about 42%, and concluded that the system was more economical than purely a LAES or a CAES system. Based on the similar concept, Pimm et al. [120] developed an optimization algorithm and control strategy to determine the optimal operation of a hybrid LAES and CAES system. Their

results indicated that the return on investment (ROI) could be maximized if the charging time of the hybrid system was higher than 36 h, with 80% of total storage capacity being liquid air at a charge time /discharge time of 2.5:1.

2.2 Multi-energy system and design

2.2.1 Basic concepts

For conventional energy systems, the energy vectors, including the electricity, heating, cooling, fuel and transport etc., are planned and treated 'separately' or 'independently'. However, the tight interconnections and interactions among these energy vectors have been seen to grow and be strengthened [121]. For example, the electricity network gets connected with the heating/cooling network through heat pumps, while electric vehicles facilitate the connection between the electricity grid and the transport sector.

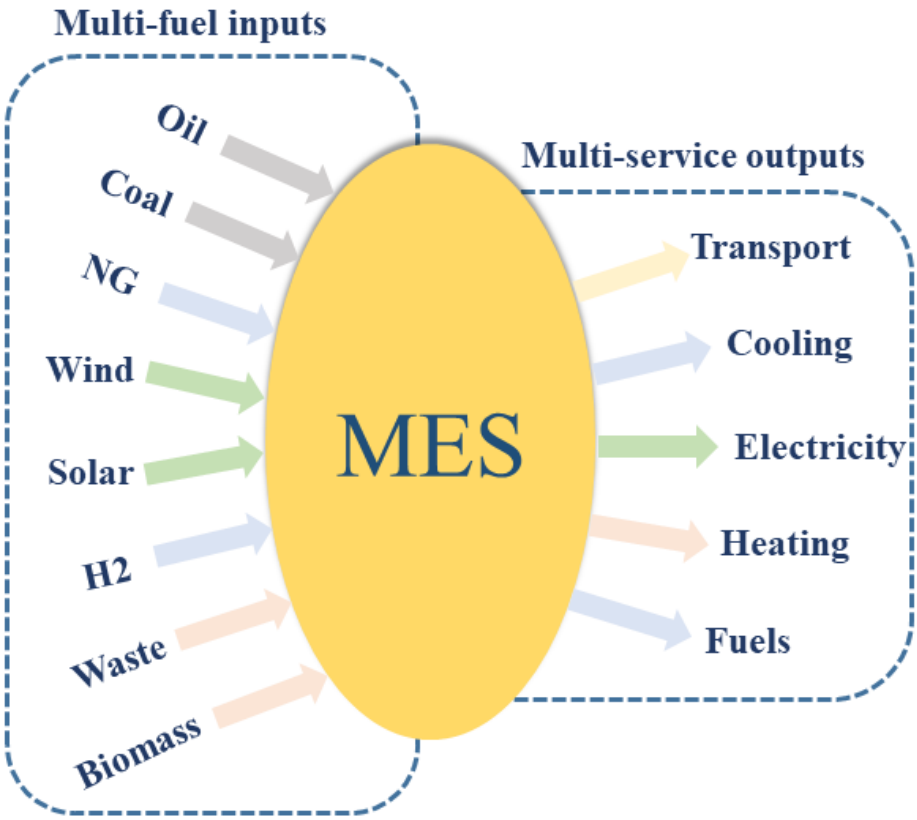

Figure 2.7. The illustration of the MES concept [34]

Multi-energy system (MES) was proposed to represent a system involving multiple fuels (from conventional NG to biomass to renewable energy), multiple services (electricity, heating, cooling and transport), and multiple networks, shown as in Figure 2.7. The electricity, heating, cooling, fuel and transport sectors and networks are optimally planned and operated at various levels (town, city, district, region or country), to achieve a cleaner, affordable and flexible energy system with better technical, economic and environmental performance [122].

2.2.2 Literature review on multi-energy systems

2.2.2.1 MES studies at different spatial levels

Starting from small-scale MESs, Cai et al. [123] designed a community-scale MES with solar PV, wind, and hydro-power, as well as diesel generator by using interval linear programming based on the superiority and inferiority of interval parameters. The optimal resources and services allocation plan were obtained to minimize the total cost, maximize the reliability and security. Schütz et al. [124] achieved the optimal design of different-scale micro-grids by using different optimization algorithms. The results showed that the cost and CO_2 emissions can be reduced by 4% and 23.7% respectively for the optimal scenario. Meanwhile, it indicated that the compact optimization is suitable for designing small-scale micro-grids, but the decomposed method is suitable for large-scale micro-grids. Expanding to the district level, Rieder et al. [125] have designed a distributed energy system with CHP, gas boiler, heat storage and the district heating network, to maximize the profit and minimize the CO_2 emissions. The optimal sizes of the system components can be determined under different weightings and different technology scenarios. Wouters et al. [126] have worked on designing the efficient and cost-effective distributed residential energy systems in South Australia. It connected distributed generation units with multiple micro-grids to meet the local electricity, heating and cooling demands, the optimal components' capacities and energy generation were obtained under different scenarios. Thellufsen et al. [127] have presented a methodology to design Smart

Energy Cities with 100% renewable energy in 2050 (shown as in Figure 2.8). The related challenges and practical issues have been coped with in the design process, including the fuel and its consumption, as well as the supply and demand balance solutions.

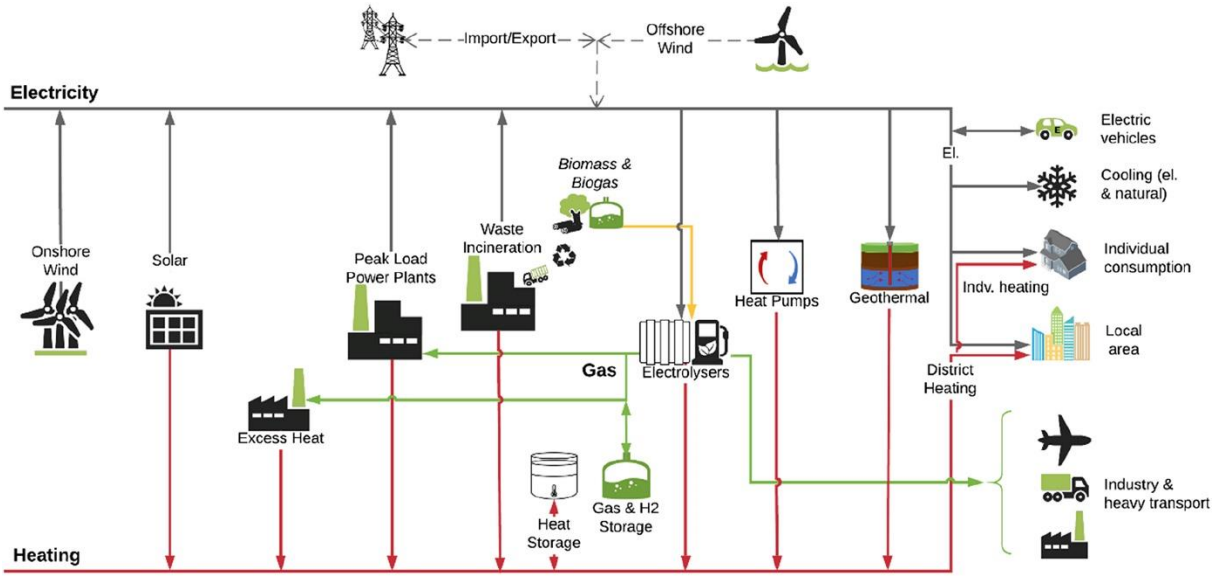

Figure 2.8. A smart energy city configuration in Aalborg [127]

For the country-level studies about MES, Elliston et al. [128] compared the investment costs of two different scenarios for Australia, namely 100% renewable power and low-emission fossil fuel power system. The results indicated the necessity of continuing researches on carbon capture and storage (CCS) to decarbonize the conventional fossil-fuel based energy systems, but 100% renewable electricity is also an economically feasible pathway at low risk for the future. Colbertaldo et al. [89] assessed the possibility and needs of hydrogen as the energy storage technology in California power system with 100% renewables. The results showed that massive electrolysers and fuel cells are needed to balance the supply and demand, like a combination of 94 GW of solar power and 40 GW of wind power required 77 GW of electrolysis systems. A techno-economic model was proposed by Rodriguez et al. [129] to minimize the back-up and transmission capacity, as well as the LCOE for a pan-European electricity system. It suggested that the optimal way to achieve high renewable penetration is to lower the costs of wind power, increase back-up power capacities and utilize excess

renewable energy wisely. For global-level studies, Pleßmann et al. [130] have estimated the energy storage demands for a 100% global renewable electricity system, the storage includes battery, high-temperature heat storage and power-to-methane (P2M). The results indicated that the average 142 € /MWh of LCOE can be achieved by integrating renewables and applying the optimal energy storage mix globally. McPherson et al. [131] assessed the impacts of future costs of electricity storage and hydrogen technologies on the transition to low-carbon energy system globally. It indicated that only the optimistic techno-economic performance of storage technologies can promote the large-scale deployment of energy storage and hydrogen technologies, thus, more related R&D projects on storage technologies are needed.

2.2.2.2 MES studies from multi-fuel perspective

Nowadays, inputs into MESs have expanded from conventional fuels, like coal, oil/diesel, NG, and Uranium (nuclear power plant), to biomass, biogas and waste, as well as to hydrogen and renewables, including wind energy, solar energy, geothermal and tidal energy etc. Chen et al. [132] achieved the optimal design of a poly-generation system involving coal, biomass, diesel, liquid fuels (methanol and diesel etc.) and CCS under different economic scenarios. Gan et al. [133] determined the optimum sizes of wind turbines, solar PVs, diesel generators and battery storage in a hybrid system through a model with graphical user interface (GUI). Ogunjuyigbe et al. [134] optimized the hybrid system with wind turbines, solar PVs, diesel generators and battery storage as well. The best scenario is a hybrid system with solar PV and wind power, diesel generator and battery storage, producing the cost of energy (COE) at 0.13 $/kWh and Life cycle cost (LCC) at $11,273. The net dumped energy and CO_2 emissions have been reduced by 82% and 94%. Wang et al. [135] conducted the thermodynamic analysis and optimization of a hybrid poly-generation system with closed combined heat and power (CCHP), solar energy (solar PVs and collectors), heat recovery system and absorption chillers. The results showed that the exergy efficiency can be improved

by incorporating solar PVs, and the energy efficiencies can be improved by integrating CCHP with solar collectors.

Mohammad et al. [136] conducted a comparative study among different MES systems in four cities in India by using HOMER from a techno-economic view, finding the PV-wind-diesel-battery system to be the best combined system with a LCOE at ~0.162 $/kWh. Maya et al. [137] proposed a poly-generation system fuelled by NG, solar energy and biomass, to produce electricity, heat and cold energy, and fresh water simultaneously. The results indicated the reliability and profitability of such a system. Giannakoudis et al. [138] studied a MES system with solar PVs, wind turbines, hydrogen (fuel cell), and diesel generator and battery storage (shown as in Figure 2.9), to minimize the total cost by using stochastic annealing optimization algorithm with different kinds of uncertainties being taken into account. Abedi et al. [139] investigated a MES system with solar PVs, wind, hydrogen, diesel generator and battery storage, to minimize the total cost, unmet load and fuel emission simultaneously by using differential evolution algorithm combined with fuzzy techniques. The optimum number of system components, installation data of solar panels and wind turbines, as well as the operational strategy were obtained. Samsatli et al. [140] have achieved the optimal design and operation of wind-hydrogen electricity network in the UK. The design framework can determine the optimal number, location and transmission network of the related components, like wind turbines and fuelling stations. It indicated that the domestic transport demand in the UK can be met by onshore wind turbines and hydrogen-electricity network.

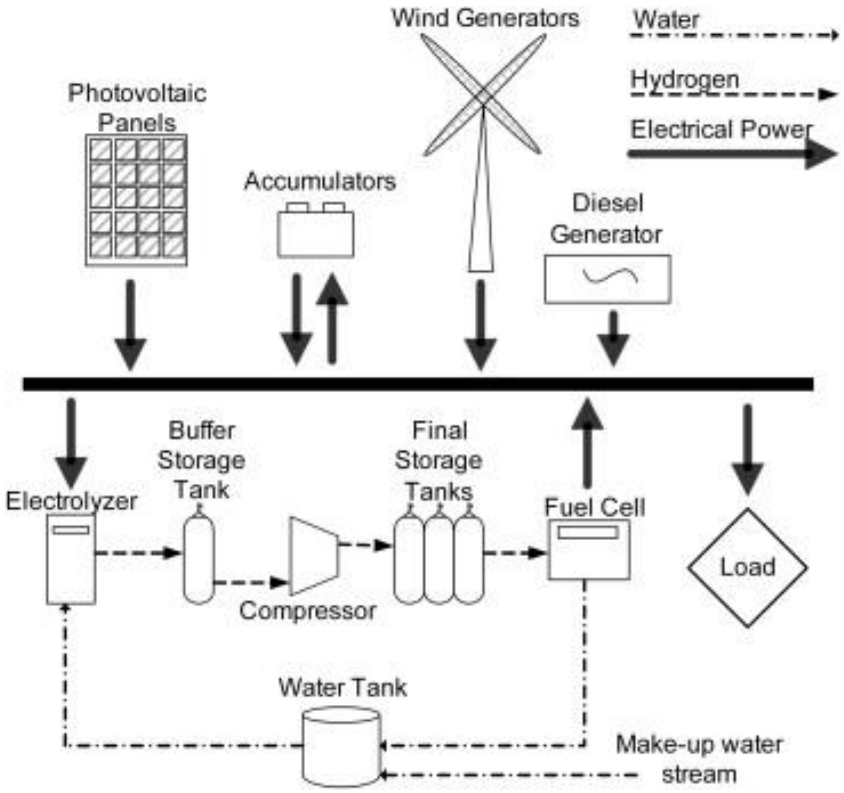

Figure 2.9. The flowsheet of an integrated energy system with renewables and hydrogen [138]

2.2.2.3 MES studies from multi-service/generation perspective

A MES can provide multiple outputs or services to consumers, including the electricity, heating, cooling, transportation and fuels, in the form of co-generation, tri-generation and multi-generation or poly-generation, which brings about significant energy, economic and environment benefits.

Starting from the basic co-generation cases, Casisi et al. [141] have determined the number of gas turbines and Internal Combustion Engines (ICE), as well as their optimal layout for a distributed urban co-generation system, to evaluate the total annual cost, energy performance and CO_2 emissions. Rasmus et al. [142] investigated the systems with large CHPs, renewable energy and biomass by using EnergyPLAN. The socioeconomic analysis indicated that CCHP plant was techno-economically more advantageous, and a regulatory framework should be introduced for planning the CHP in the long term. For tri-generation systems, Kavvadias et al. [143] studied the performance and economics of a tri-generation system to

supply the heating, cooling and electricity demands, the best operating strategy was determined as an electrical-equivalent load following approach. Li et al. [144] studied a tri-generation system in Beijing, the techno-economic optimization has determined the optimal plant configurations to maximize the thermodynamic efficiency, and to minimize the total cost and emissions (both CO_2 and NO_x emissions).

Further for multi-generation or poly-generation systems, Calise et al. have [145] provided a comprehensive review about poly-generation with various input fuels and output services. Liu [146] has provided a generic modelling and optimization framework for a poly-generation system. Ahmadi et al. [147] have established the thermodynamic and multi-objective optimization model for a poly-generation system which provides electricity, heating, cooling, and hot water. The Pareto front of the total system cost and exergy efficiency was obtained, and the optimal operating parameters of system components were determined. Sigarchian et al. [148] compared different operating strategies of a poly-generation system, including following thermal load, following electric load, and the modified base load. It showed that the reduction in total cost, CO_2 emissions and fuel consumption were in the range of 17–19%, 30–38%, and 35–43% respectively with various operating strategies. Liu and Mancarella [149] illustrated the interconnection among heat, electricity and gas network under different scenarios by using efficiency matrix and Sankey diagrams. The results showed that the case with district-level CHP and local gas boilers generated the least carbon emissions, and the case with district-level CHP and local CHP produced the lowest-price electricity by 2030. Samsatli et al. [150] have taken transportation as another energy vector in addition to the electricity and heating sectors, using energy chain model and MILP to achieve the optimization of the MES, as shown in Figure 2.10. The work has answered the questions of what resources should be used, when to invest certain technologies and where to locate them. Overall, different researchers have looked at the capability of MES to supply various services, it has been

demonstrated that multiple services provided by MES can greatly improve the system flexibility, reliability and economics.

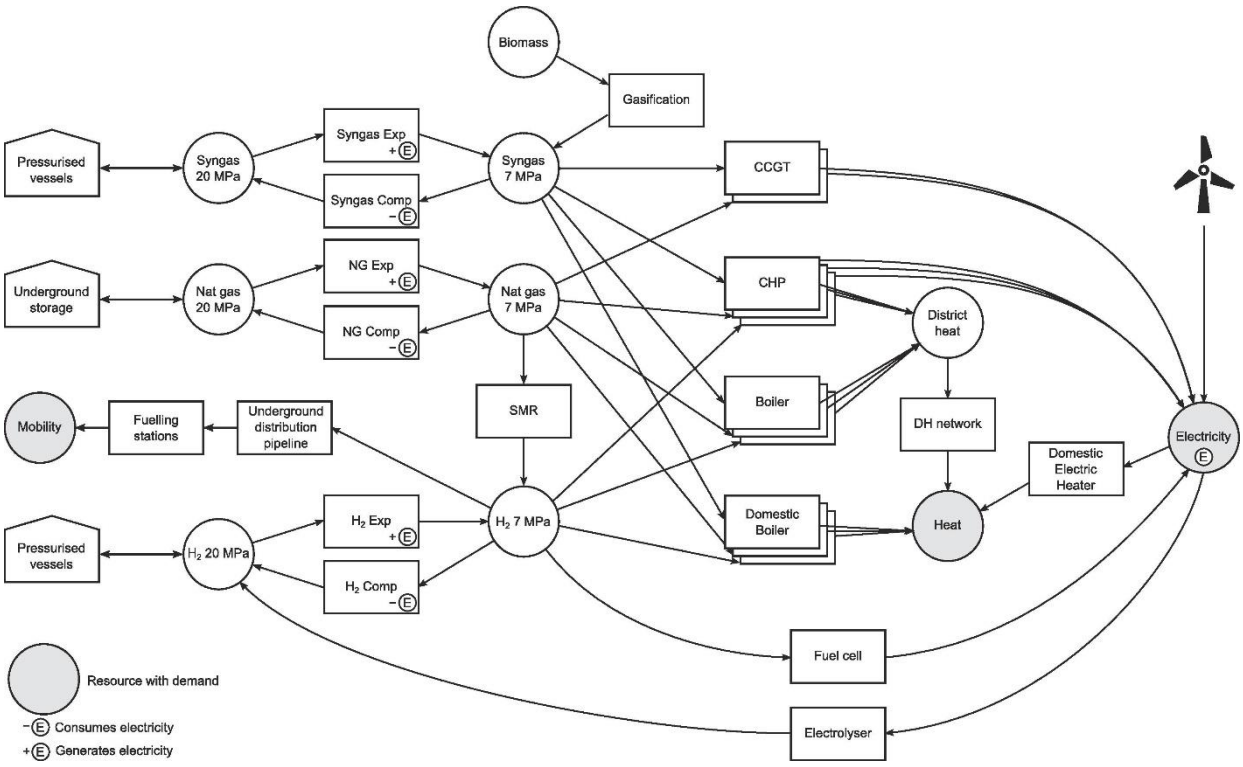

Figure 2.10. The superstructure of a multi-vector energy system [150]

2.2.3 Modelling of multi-energy systems

Considering the complexity and multi-energy interactions within and outside the MES, it calls for advanced modeling techniques and tools to perform the planning and operational optimization, as suitable modelling methods are key to help understand the system and study the performance.

2.2.3.1 Modelling methods for MESs

The energy hub concept is a generic approach for steady-state modelling and optimisation of future interconnected multi-energy networks. An energy hub normally consists of various inputs and outputs, conversion and storage technologies, the connections are described by simplified models with constant conversion and storage efficiencies [121]. It is flexible and needs less computing resource, but this method is based on a set of assumptions

and simplifications, such as the constant conversion efficiency, which might overestimate or underestimate the components and system performances [37]. The traditional energy hub model has been widely adopted by a few researchers in their work. Orehounig et al. [151] have adopted energy hub concept (shown as in Figure 2.11) to evaluate the energy autonomy and ecological performance of distributed energy systems, the CO_2 emissions can be reduced by 46% under the optimal scenario. Maroufmashat et al. [152] have applied the energy hub network to optimize distributed energy systems. It indicated that the connection of multiple energy hubs (more than three) can reduce system costs and CO_2 emissions significantly.

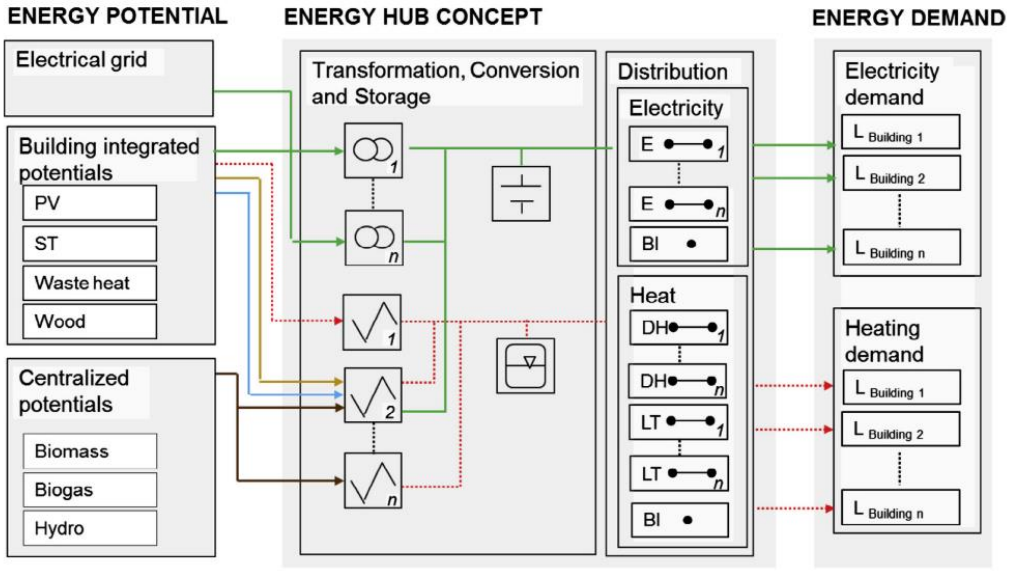

Figure 2.11. An energy hub model of a distributed energy system [151]

Besides the energy hub modelling, Mancarella [122] also proposed to include another two modelling concepts, namely 'Micro-grids' and 'Virtual power plant (VPP)'. The aggregation concept 'Micro-grid' refers to a distributed energy system with various energy resources and conversion technologies, of which the modelling details are determined by researchers, it can work in grid-connected mode or islanded mode [122]. Stadler et al. [153] have investigated the integration of EVs to smart grids and the impacts on system emission reduction. Schwaegerl et al. [154] have explored the potential economic, technical and environmental benefits of Micro-grids by using multi-objective optimization, demonstrating

the benefits in increasing renewable penetration and supply reliability. The VPP concept refers to a distributed energy system with flexible boundary (resources and technologies are geographically close or not), and can provide multiple services for customers as well. Mancarella [155] introduced the 'equivalent cogeneration plant' and 'equivalent efficiencies' to investigate a small VPP, showing its high generality and effectiveness for the modelling. Mancarella and Chicco [156] have studied the costs and benefits of distributed multi-generation systems, showing their contribution in real-time demand response by energy shifting. Recently, a new concept 'value web model' (VWM) has been proposed by Samsatli [150] to study MES. In this modelling concept, each resource and technology, their costs, efficiencies and losses, as well as their relationships and interactions are represented by value web diagram and in a generalized approach, a superstructure can be constructed to represent a whole MES. This modelling method has been applied by Samsatli et al. to study the decarbonisation of the transportation sector [140], heat sector [157] and the multi-vector energy systems [150] in the UK.

In respect of modelling and simulation tools, there are mainly three categories, namely the commercial tools (such as EnergyPLAN, AEOLIUS, SimREN, HOMER, MARKAL/TIMES, Sifre, MATLAB/SIMULINK), the mathematical MILP programming and the evolutional algorithms, which will be introduced in details in the next sections.

2.2.3.2 Commercial modelling tools of MES

Zakeri et al. [158] adopted EnergyPLAN tool to comprehensively model an energy system involving electricity, heat and transportation, to investigate the maximum penetration ratio of different renewables and the optimal combination of different technologies. It indicated that a maximum 69%-72% of renewables in Finland was achievable. Ghenai et al. [159] adopted HOMER to design a clean energy system (shown as in Figure 2.12) for a desalination plant with high renewable fraction (47.3%), low gas emissions (264.25 kg CO_2/MWh) and

low COE ((90 $/MWh). Sawle and Gupta [160] designed a renewable hybrid system to fulfil the load demand of a telecom base station by using HOMER software. It foundthe optimal combined system with solar PVs, wind power and battery storage, andthe optimal LCOE at 50.2 $/MWh. Lagorse et al. [161] designed a hybrid energy system by using MATLAB/SIMULINK, it found that the most cost-effective system is the one with solar PVs, Fuel cells (FC), electrolysers and battery. Rosen et al. [162] applied AEOLIUS tool, which can manage the time scale as low as 10 min, to achieve the scheduling of a hybrid renewable power plant. Sveinbjörnsson et al. [163] have investigated the net-zero carbon pathways for a city in Denmark by using the software Sifre. The optimization goal is to maximize the energy efficiency, and to minimize the total cost, CO_2 emission and biomass consumption. The results indicated that the scenarios with higher electrification rate performs better than the systems with higher biomass consumption. Overall, these commercial software tools make the planning and optimization of MESs more accessible and faster, but they lack flexibility and adjustability.

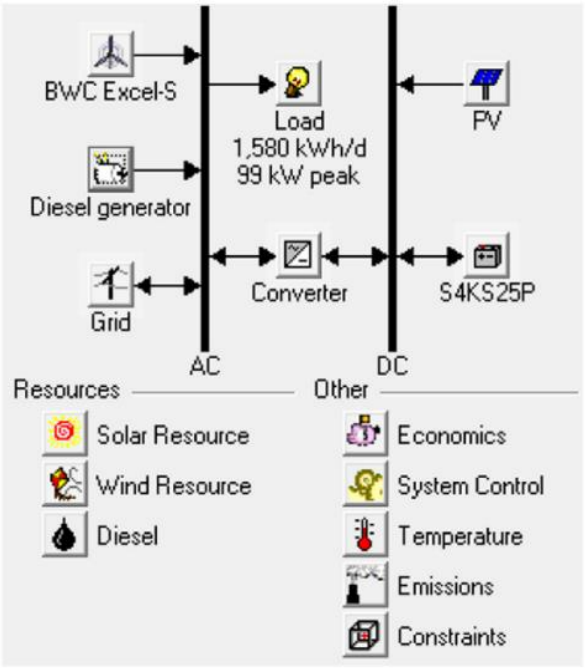

Figure 2.12. The schematic of a HRES in HOMER [159]

2.2.3.3 Modelling of MES by using evolutional algorithms

Various evolution algorithms were developed by researchers to achieve the optimal design and operation of MESs. Zahra et al. [121] developed a new multi-objective particle swarm optimization algorithm (PSO) to design a PV/diesel hybrid system with the operating reserve. The Pareto set was obtained which coordinated the total net present value (TNPV), CO_2 emissions, and loss of power supply probability (LPSP), demonstrating that the new PSO can achieve a well-distributed Pareto front of the objectives. Maleki and Pourfayaz [164] have compared the optimization performances of different evolutionary algorithms, including the improved particle swarm optimization (IPSO), improved harmony search (IHS), improved harmony search-based simulated annealing (IHSBSA), and advanced bee swarm optimization (ABSO) algorithms, to optimally size a hybrid wind/PV/battery energy system. The results showed that the ABSO was more promising and robust than other algorithms. Dong et al. [165] optimized the sizes of solar PVs, wind turbines, battery and hydrogen storage in a hybrid renewable energy system. The improved ant colony optimization (ACO) was adopted to minimize the cost and LPSP. The results showed that the improved ACO with sorting was more efficient than the original one. Maleki et al. [166] evaluated the effects of different PSO variants on sizing PV/wind/battery hybrid energy systems to minimize the annual cost. It concluded that the PSO with constriction factor was more favourable than with other variants in respect of accuracy and computational cost. M. Sharafi et al. [167] adopted the Dynamic Multi-objective Particle Swarm optimization (DMOPSO) to determine the sizes and types of components in a hybrid renewable system. The results implied that wind generators were preferred to solar PVs, and hydrogen storage was not selected due to its high investment and maintenance costs.

Overall, various evolution algorithms were developed to achieve the design and operation of MESs, showing good accuracy and efficiency, but the shortcomings are that these

algorithms can easily get stuck in local optimal point, and they are very sensitive to the initial start points, which can be avoided by using MILP algorithm.

2.2.3.4 Modelling of MES by using MILP algorithm

In addition to the commercial planning tools and the developed evolutional algorithms, the MILP has been one of the powerful tools to achieve the optimal design and operation of MESs. This is due to its moderate calculation complexity, and the capability to find the global optimal point, as well as the available commercial solvers, like Gurobi (commercial), CPLEX (commercial), and YALMIP (open source).

Urbanucci [168] has discussed the limits and advantages of MILP for the design and operation of multi-energy systems. Yokoyama et al. [169] proposed a hierarchical MILP method to achieve the optimal design and scheduling of a poly-generation system (shown as in Figure 2.13), demonstrating its higher efficiency and equal accuracy than the conventional MILP method. Yang et al. [170] constructed a MILP model for a distributed energy systems in Guangzhou (China), which can optimize the resource locations, technologies combinations and operation strategies. Weber and Shah [171] proposed a DESDOP tool (District Energy System Design and Optimisation, MILP based) to explore the optimal combination of vast of generation technologies, in order to reduce annual cost and CO_2 emissions, but the energy storage devices were not considered. Arcuri et al. [172] developed a MILP optimal design and scheduling model for a tri-generation plant for a hospital. The short-term (gross operational marginal) and long-term optimization (net present value) have led to decent energy savings and economic returns, but renewable energy was not considered in the model. Bischi et al. [173] presented a detailed MILP model for the planning and optimization of a CCHP system. The model was capable of determining the operational scheduling of system components and minimizing the cost of the CCHP system, taking time-varying conditions, off-design behaviours and on-off limitations and penalizations into account. Deetjen et al. [174] adopted

a MILP model to improve rooftop solar integration and maximize the profits under different electricity rate structure. The results showed the reverse power flow, peak demand and annual cost can be reduced by 43%, 51% and 9.1% respectively. Tu et al. [175] constructed a two-level MILP model to design a stand-alone hybrid renewable micro-grid, aiming at minimizing the overall annual cost. The positive effects of load deferring on battery sizes, renewable penetration and system costs have been investigated. Zhou et al. [176] studied the effects of components' off-design performance curve on the system design by implementing a MILP model. It indicated that the off-design characteristics have small effects on the system optimal design (the error was within 5%).

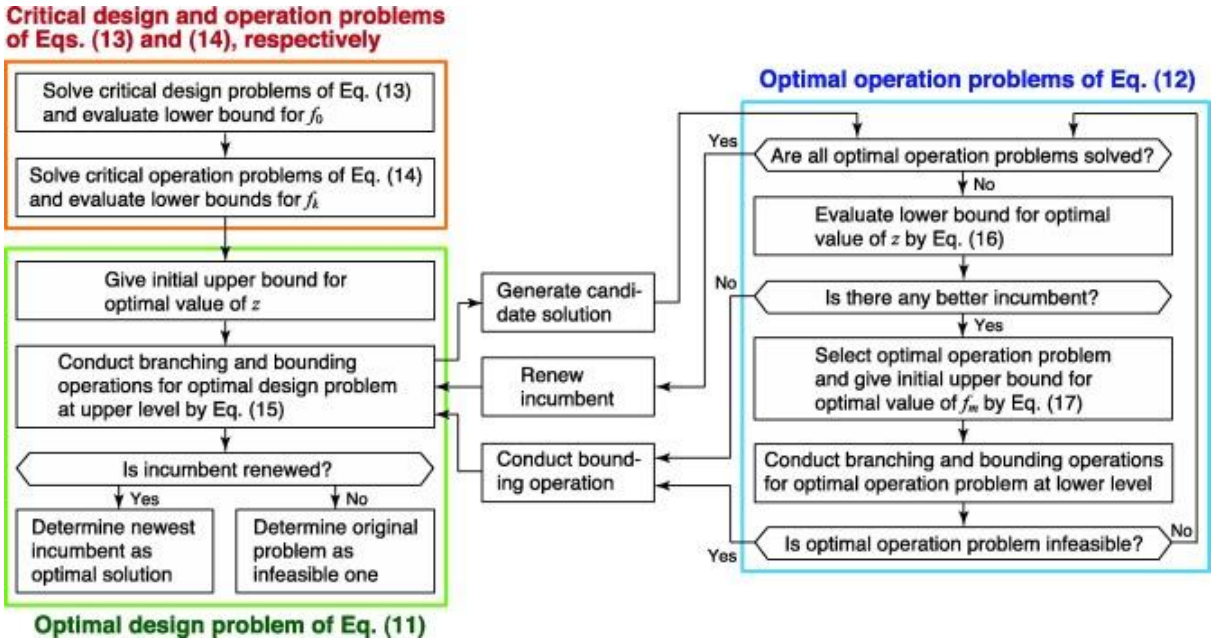

Figure 2.13. The flow chart of a hierarchical MILP method [169]

2.2.4 Assessment criteria of multi-energy systems

The optimal design and operation of MES aims to accomplish various assessment criteria or objectives, which can be categorised into the energy, economic and environment performances [122]. From the studies above about the MES at different perspectives, the general energy performance indicators include electrical and thermal efficiencies, the equivalent energy efficiencies [144], exergy efficiency [135], primary energy saving [82], fuel

consumption reduction [148], unmet load [139], and loss of power probability (LOPP) [165] etc. The economic indicators include the total capital cost or annual cost (including operational costs) [141], the gross operational margin [172], NPV [121], Internal Rate of Return (IRR) [177], LCOE [130], cost of energy (COE) [134], Life cycle cost (LCC) [134], payback period time (PBP) [178], and exergy cost of electricity and heat [147] etc. The environmental indicators include CO_2 emissions [141], other pollutants emissions (NO_x, CO, SO_2 etc.) [144], "Eco-indicator 99" (cradle-to-grave life cycle assessment (LCA)) [179], Ozone Depletion Potential [180] etc. Different work would choose different objectives or their combinations based on the study aims and application scenarios. Recently, some researchers have expanded the objectives to social aspects, like the human development index (HDI) and job creation (JC) indicators etc. [181] [182]. Carvalho et al. [179] have applied the LCA and "Eco-indicator 99" (overall environment load in points, evaluate the damages to human health, ecosystem quality, and resources) methods to design and optimize an energy system for a hospital. Sawle et al. [181] aimed at determining the optimal configurations of hybrid systems by constructing a multi-objective function with six objectives (including the technical, social and economic parameters). It found that the system with PV/wind/ biomass/diesel generator/battery bank is the optimal one, and the teaching-learning-based optimization algorithm (TLBO) performed better than PSO, butterfly particle swarm optimization (BFPSO) and genetic algorithm (GA) in term of convergence time. Rodolfo et al. [182] first time ever proposed to minimize net present cost and the LCOE, and to maximize HDI and JC simultaneously for a hybrid PV-wind-diesel-battery system, using two layers of multi-objective optimisation algorithms (the main algorithm and GA) to obtain the optimal Pareto set of three objectives. One of the optimal results gave the LCOE at 0.56 kWh, HDI at 0.615, and JC at 0.119.

2.3 Review of energy storage value in MES

2.3.1 Energy storage value in micro-scale MES

Some researchers have investigated the integration of ESS with micro-grids, exploring the functions and value of storage technologies. Macedo et al. [183] determined the optimal operation and location of energy storage devices in distributed renewable energy systems by using MILP. Djelailia et al. [184] proposed a hybrid renewable energy system with PHES, and have proved the effectiveness of hydroelectric storage in irrigation, power dispatch, fuel saving and CO2 emissions. Pablo [70] proposed a grid-connected combined system with battery and hydrogen storage, in which wind and solar PV served as primary sources. Three energy management systems have been developed to minimise the utilization cost and maximize the ESS efficiency and life cycle cost. The results were consistent with those of Rodolfo obtained [71], who minimized the total cost, CO_2 emissions and unmet load simultaneously for a PV-wind-diesel-hydrogen-battery hybrid system.

Li et al. [185,186] developed a sizing method for a hydrogen-based micro-grid, which was based on the combined evolution algorithm and MILP. It considered the degradation of hydrogen and battery storage, as well as the uncertainties of PV output and load demand, to obtain the optimal operation strategy and system components' sizes. Ceseña et al. [187] conducted the techno-economic analysis of a multi-vector energy system with battery storage and thermal storage to provide energy, reserve and reliability services simultaneously. It showed that the electricity cost saving (decreasing by 40%), reserve revenue (increasing by 47.3%) and reliability revenue (increasing by 12.7%) were achieved by adding electric storages, but the flexibility value of storage systems was not considered. Quashie et al. [188] developed a bi-level planning model for a micro-grid with operating reserve, achieving the co-optimization of investment, operation and outage cost. It indicated that CAES storage can help provide reserve capacity, improve reliability and defer additional investment.

2.3.2 Energy storage value in grid-scale MES

Besides, there were also some studies exploring the value of grid-scale energy storages. A. Khan et al. [189] have discussed the impacts of demand response and medium-term EES on energy and capacity markets. Hejazi and Rad [190] formulated a stochastic programming framework to investigate the energy and reserve value of energy storage in hour-ahead market, as well as the effects of capacity and sites of storage on the profits. Byrne and Monroy [191] have investigated the potential arbitrage and regulation value of grid-scale energy storage by developing a MILP model. The results revealed that the revenue coming from regulation markets is four times than that from arbitrage. Pudjianto et al. [192] studied the value of grid-scale energy storage on system cost and security, as well as the benefits on the transmission and distribution. It discussed the impacts of types (distributed and bulk energy storage (BES)), capacity scales, storage costs, locations and efficiencies on storage revenue in the whole system. The results indicated that the net benefits of the distributed and bulk energy storage are £50/kW.year and 100/kW.year respectively. The value of both storages decreased with capacity increasing.

A MILP model has been developed by Moreno et al. [193] to investigate the potential benefits of distributed energy storages in grid distribution management, energy arbitrage and reserve, and frequency regulation markets, aiming at coordinating the multiple services and maximizing the storage net profits. Sisternes et al. [194] have explored the potential value of energy storage in the de-carbonization of the electricity sector by using the expanded IMRES (MILP-based planning model). The effects of different CO_2 emission limits on energy storage value, technologies' generation and costs have been compared. But the author did not consider the complementary characteristics of electric storage technologies. Gabrielli et al. [195] proposed a MILP-based model to achieve the optimal design of a multi-vector energy system with hydrogen storage (as shown in Figure 2.14). It discussed the impacts of different

modelling methods on the sizing results, including the time horizons, CO_2 emission limits, PV panels' surface areas and battery cost reductions. The results indicated that seasonal storage is favoured when a system requires significant CO_2 emission reduction, as well as a larger ratio of thermal to electrical demand, and higher renewable penetration.

Overall, various storage technologies, from small-scale to grid-scale, and from battery, and PHES toCAES and heat storage etc., as well as their different benefits, including the arbitrage, reserve, frequency regulation and flexibility values have been studied. But there are gaps in investigating the integration of LAES with MES, and its energy storage models and functions and benefits in MESs, which motivates this work to fill the gaps.

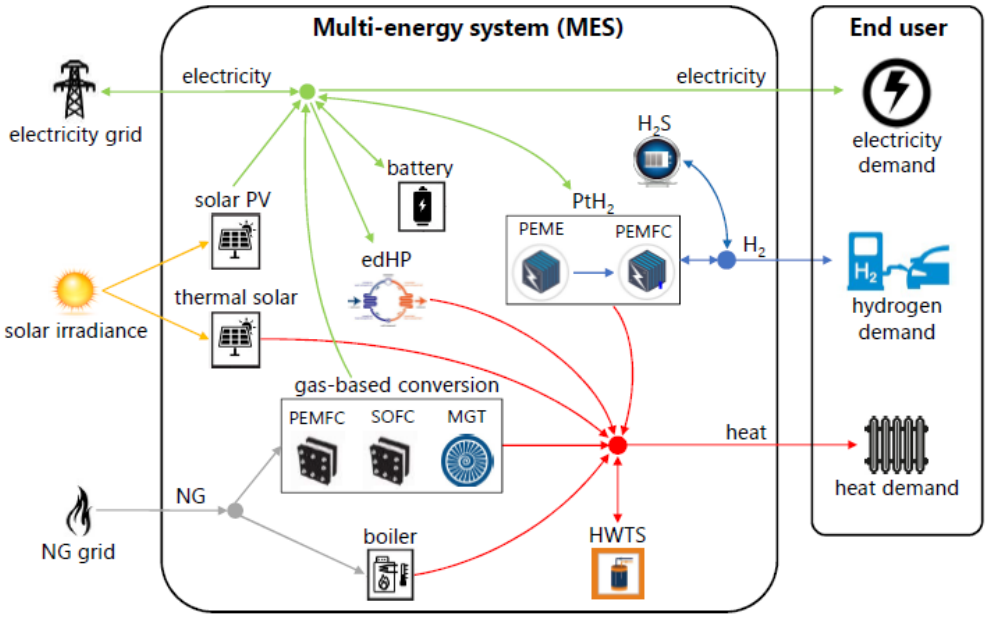

Figure 2.14. The schematic of the multi-energy system with hydrogen storage [195]

2.4 Summary of the review

In summary, firstly, the work about the LAES system, expanding from the basic working principle, system configuration and development history to the thermodynamic and techno-economic analysis of the stand-alone and integrated LAES systems, ha been reviewed comprehensively. Secondly, the work about MES, including the basic concept, the studies at

different spatial levels, the systems with multiple fuels and services it provides, the modelling methods and simulation tools, and the assessment criteria, were all reviewed extensively. Thirdly, the applications, multiple functions and benefits of energy storage technologies in micro-grids and grid-scale MESs all have been reviewed as well. After the systematic and comprehensive literature review, there are four major gaps that were identified to motivate the work involved in this Ph.D. thesis, they are:

a. The thermodynamic analysis and techno-economic analysis of LAES systems were mainly based upon the parametric studies by using the exhaustive method, which does not have a whole system view and also is human-resource consuming. There is few work focusing on the optimization of key design and operational parameters of the whole LAES system by using artificial intelligence (AI) algorithms, which can overcome the limitations of the exhaustive method.

b. Though thermodynamic analysis and techno-economic analysis of LAES are important to understand the theoretical energy and exergy efficiencies, as well as its economic performance, there is few work that has paid attention to the dynamic analysis and simulation of LAES systems. This is crucial to understand the system design and control logic, as well as to promote the practical application of LAES technology.

c. Though the stand-alone and integrated LAES systems have been investigated widely and comprehensively, the applications of LAES into micro-grids, and its integration and interaction with other generators have not been covered so far. The design and operation of LAES within a micro-grid, as well as the discussion of its multiple functions and benefits in a micro-grid were not reported so far.

d. Under the background of constructing the net-zero carbon energy system globally, the application of LAES into a country-level energy system, the integration of LAES with

renewables, the overall energy system design and operation, as well as the key roles of LAES and other storage technologies in zero-emission energy system were not reported so far.

Based on the above gaps identified from the literature review, the specific contents and objectives of this work include:

a. To establish a thermo-economic multi-objective optimization framework based on genetic algorithm for a stand-alone LAES system. It aims at optimizing the thermodynamic and economic performance of LAES by searching for the optimal design and operational parameters, to guide the design and investment of the system.

b. To develop the component- and system-level dynamic models of a LAES system. It is to investigate the dynamic behavior and response characteristics of LAES when integrating with renewables, and to find the proper methods to improve the system dynamic performance, including the heat transfer process, response time, the start-up and load-following behaviour etc.

c. To determine the optimal design and operation of a hybrid-renewable micro-grid with the decoupled model of LAES by using hierarchical MILP method. It aims at investigating the multiple functions and benefits of LAES in a micro-grid, in order to guide the micro-grid design with LAES and increase the attractiveness of LAES systems in micro-grids.

d. To develop a MILP-based design and operational framework for a country-level net-zero carbon energy system with LAES and other storage technologies. It is to assess the key roles of LAES and other storage technologies for supporting the future net-zero carbon energy systems. The results can provide decision makers a new perspective about the energy system transformation and planning with storage technologies.

3 Thermo-economic multi-objective optimization of the liquid air energy storage system

3.1 Introduction

3.1.1 Literature review

3.1.1.1 Thermodynamic analysis of LAES

In terms of the investigation of LAES systems, most researchers have revealed the crucial effects of charging and discharging pressures, and cold energy recovery. Lee et al. [196] designed an integrated LAES system with LNG, in which the expansion power and external cold energy recovered from LNG gasification process were used to compress air and liquefy air simultaneously. The results showed that the RTE of the new system was as high as 172.1%. Hamdy et al. [58] proposed two types of cold exergy recovery methods, namely the direct expansion of liquid air through main heat exchangers, and the combined expansion of liquid air with an extra Rankine cycle. The analysis results indicated that the second method performs better, the power output increased by 25%, the exergy efficiency and energy efficiency can be improved to be 45% and 40.4% respectively. Peng et al. [53] argued the external cold resource (10% - 20%) is still needed to enhance the RTE further. It is also reported that if the recoverable cold energy was enhanced by 16%, it would lead to 20% and 30% of increases in RTE and liquid yield respectively [44].

Peng et al. [54] studied a LAES system with packed-bed storage, as well as compared the system performance with those of CAES. It found that the RTE of LAES can be between 50% - 62% depending on the charging/discharging pressure and inlet temperature of cold box. Tafone et al. [197] developed the performance map for LAES systems, applying it to determine the operative parameters of LAES. The results indicated that the specific consumption and RTE

can be determined by a specific charging and discharging pressure, as well as the cold and hot energy utilization factor. But this method is too lengthy to determine the system operational parameters efficiently. Wang et al. [198] techno-economically analysed a LAES system which can produce power, oxygen and heat energy simultaneously. The results showed that the multi-functional LAES system has a 5.7 years of PBP but with lower overall efficiency (0.39). Cui et al. [198] proposed a multi-generation LAES system to provide heat and cold energy and fresh air simultaneously. The techno-economic analysis gave about 75.4% of overall efficiency and 0.79 ¥/kWh of LCOE. The above studies have been summarized as shown in Table 3.1.

3.1.1.2 Multi-objective optimization of LAES and other thermal systems

So far, few researchers have worked on the multi-objective optimization of the whole LAES system. Only Li et al. [199] investigated a combined system with solar thermal heat and LAES, the system has been optimized by using a sequential quadratic programming method. The results indicated that the optimal system produces 30% of higher power output and 15.3% of higher exergy efficiency. Liu et al. [66] applied GA to optimize LAES system. The results revealed the optimal RTE (as high as 63.1%) and the optimal system configuration with two compression stages and three expansion stages). But the author only take the RTE as the optimization objective. Khani et al. [200] investigated the optimal dispatch of LAES to serve as arbitrage function in a day-ahead and weekly-head electricity market. It showed that the weekly dispatch was more beneficial. J. Pimm et al. [201] developed an optimization algorithm and control strategy to determine the optimal operation of a hybrid storage system (CAES and LAES). The results suggested the ROI can be maximized if the charging time of the hybrid system is higher than 36 h, and 80% of total storage capacity is in liquid air form (charge time /discharge time is 2.5:1).

Table 3.1. Literature review and summary of thermodynamic analysis of LAES

Ref.	Charge pressure (MPa)	Discharge pressure (MPa)	Turbine inlet temperature (K)	RTE (%)	Exergy efficiency (%)	Energy density (kWh/kg)	Power cost (£/kW, 2020)	LCOE (£/MWh, 2020)
Morgan et al. [202,203]	15	12	323	60	\	\	750 ~ 1250	135
Guizzi et al. [42]	18	6.5	616	54.4	84.7 (charging) 78 (discharging)	\	\	\
Sciacovelli et al. [44]	18	12	613	49.4	\	\	\	\
She et al. [45]	12	12	458	53.5	87 (charging) 77 (discharging)	\	\	\
Peng et al. [204]	13.5	8	480	59.4	84 (charging) 81 (discharging)	\	\	\
Hamdy et al. [205]	15	15	474	41.6	55.5 (overall)	\	1040~1324	246
Kim et al.	16	7	1673	64.2 (with combustion)	62.1(overall)	\	\	110.8~148.2
Peng et al. [54]	12.1	5	585.8	56.3	\	7.74	\	\
Wu et al. [116]	14	5	1123	52.8	\	8.82	\	75~150 (integrated LAES system)
Wang et al. [206]	15	12	470	54.4	59.1 (overall) 85.8 (charging) 87 (discharging)	\	\	\
Cui et al. [198]	11.2	11.8	438.2	74.8 (multi-generation)	\	\	\	94.8

However, there were some studies working on optimizing other thermal systems. Ghasemkhani et al. [207] conducted both mono-objective (using algorithms like simplex, conjugate-direction, and genetic algorithm etc.) and multi-objective optimization (using algorithms like non-dominated sorting genetic algorithm (NSGA-II)) for a combined cycle based on finite-time thermodynamics. The results revealed that the optimal dimensionless power, maximum efficiency, and minimum exergy destruction were 0.186, 75.9% and 0.00078 respectively. Punnathanam et al. [208] optimized three Stirling engine systems by using multi-objective Front-based Yin-Yang-Pair algorithm, taking the output power, thermal efficiency and pressure drop as the objectives. The results proved that this new optimization algorithm is more effective than Multi-Objective Grey Wolf Optimizer (MOGWO) and GA.

An organic Rankine cycle was optimized by Pierobon et al. [209], which took the thermal efficiency, total volume and NPV as objectives. The results suggested two optimal working fluids for the system, namely acetone and cyclopentane, and the Pareto Fronts of three objectives have been identified. The thermo-economic optimization of different configurations of trans-critical CO_2 cycle were conducted by Morandin et al [210]. A two-level optimization scheme was developed, in which the heat exchangers' and storage tank's design parameters were optimized by GA first, and the mass flow rates were optimized by using the nested linear programming. The Pareto Front of RTE with system investment cost was presented to guide system design. Gebreslassie et al. [211] designed the absorption cooling systems by using mathematical programming method and LCA, to minimize the system cost and environmental impact. The Pareto Front of these two objectives was identified.

3.1.2 Research aim

Above all, the literature reviewed about LAES systems mainly focused on the parametric studies of key performance indicators like RTE and exergy efficiency by using exhaustive method, meanwhile, the economic analyses related to indicators like LCOE and

specific power and energy costs were separated with performance analyses. But fewer work has covered the thermo-economic optimization of whole LAES system by using artificial intelligence (AI) algorithm, like GA and PSO etc. Thus, this study aims to achieve the thermo-economic multi-objective optimization of LAES by using GA, the novelties of this part of work lie in:

a. It is capable of optimizing the design and operational parameters of LAES under different initial conditions to reach the optimum RTE, including the optimal charging and discharging pressure, the heat transfer areas of heat exchangers, as well as the optimum mass flow rates of hot and cold storage media.

b. The system design guideline can be derived to tailor different optimal parameters for LAES systems with different system configurations (like systems with different compressor and expander stages), and systems with different initial conditions.

c. The investment advice of LAES can be obtained by identifying the Pareto Front of system efficiency and capital cost, to provide system operators good guidance to make a proper investment in LAES systems.

The layout of this part of work is: section 3.2 describes the basic system configuration and modelling methods. Section 3.3 introduces the economic and optimization models of the system, as well as the model validation. Section 3.4 presents the main results and discussion. Finally, the conclusion is given in section 3.5.

3.2 Liquid air storage system

3.2.1 System description

The thermodynamic diagram of a stand-alone of LAES is shown in Figure 3.1, which consists of an LFU (the liquefaction unit), a storage unit and a PRU (the power recovery unit). During the charging process, there is a three-stage compression which can compress the inlet air 1 to a high pressure state 7. The air goes through the cold box and cryo-turbine, being liquefied (9) and stored (12) in storage tank. During the discharging process, the stored liquid air is pumped to a high pressure (14) and goes through two cold-recovery evaporators, achieving three-stage reheating and expansion (16 – 22) to produce power. The compression heat can be stored in thermal oil (H1 – H2) and applied in the reheating process (H3 - H4) to enhance power output. The cold energy can be recovered by propane (C1 – C2) and methanol (C3 – C4), and then utilized to liquefy air in cold box during charging.

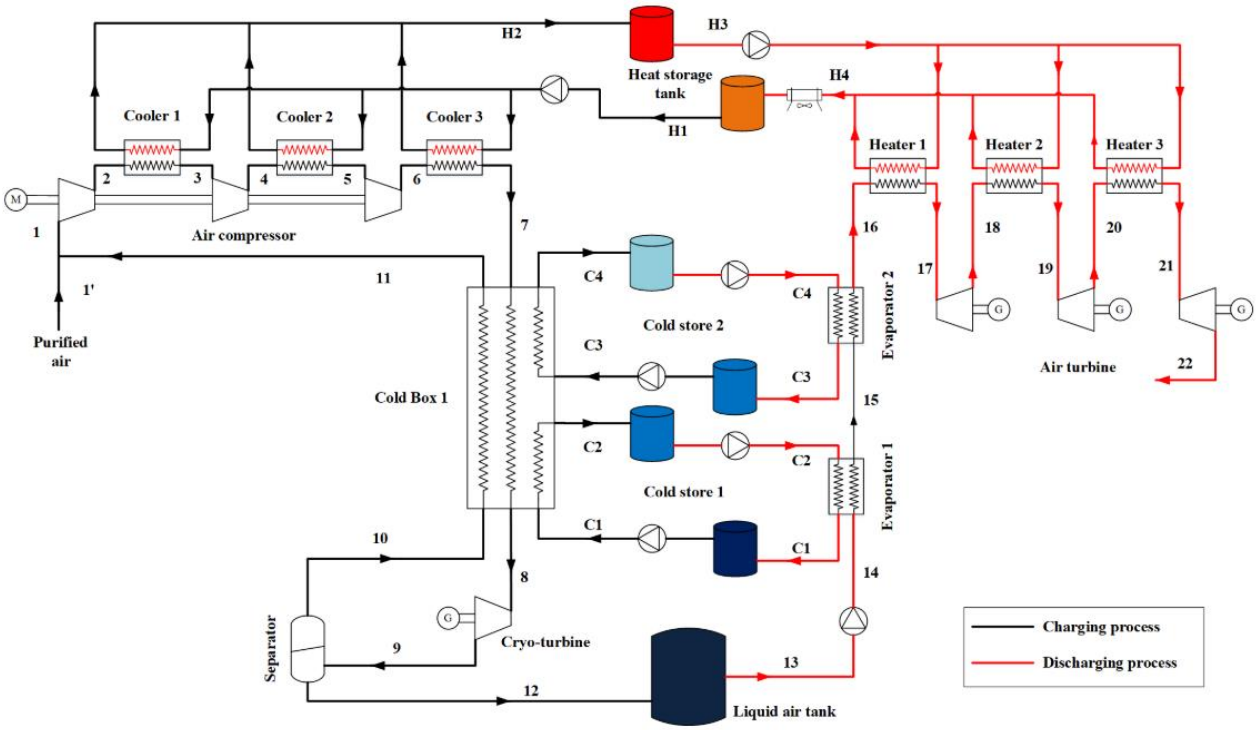

Figure 3.1. LAES thermodynamic layout [17]

3.2.2 Thermodynamic model and indexes

The thermodynamic model of LAES was built in Aspen HYSYS 11.0 by adding the corresponding modules and adjusting the parameters. The simulation iterations were constrained by the given pinch points of different heat exchangers to make sure it converges at last. The simulation principle is based on the first and second law of thermodynamics, which are explained in section 3.2.2.1 to section 3.2.2.3.

3.2.2.1 Energy analysis model [204,212]

During charging, the purified air is compressed to a high pressure by a three-stage air compressor (stage n = 1, 2, 3), the air outlet enthalpy and compressor power of each stage are given by eq. (3.1) ~ eq. (3.2):

$$h_{i+1} = h_i + \frac{h_{i+1,s} - h_i}{\eta_c} \qquad \text{eq.(3.1)}$$

$$W_{cmi} = q_{ma}(h_{i+1} - h_i) \qquad \text{eq.(3.2)}$$

where, h_i is the specific enthalpy at state i, with subscript i = 1, 3, 5 denoting the inlet state of the compressor; η_c is the isentropic efficiency, q_{ma} is the mass flow rate of air, W_{cmi} is the compressor power output; Subscript s - the isentropic process, cm - the compressor.

The compression heat is transferred to the cooling medium through intercoolers, and the heat exchanged with the cooling medium is given by eq. (3.3):

$$Q_i = q_{ma}(h_i - h_{i+1}) \qquad \text{eq.(3.3)}$$

where, Q_i is the heat exchange rate in intercoolers, subscript i = 2, 4, 6 represents the inlet state of intercoolers.

The compressed air (state 7) is cooled down by the recycling air and cold storage media in the cold box, and the outlet state 8 and liquid yield ratio (Y) are calculated by using the energy conservation within the controlled volume (cold box) as in eq. (3.4) and eq. (3.5), with the pinch point limitations considered in heat exchangers:

$$q_{m7} \cdot (h_7 - h_8) = (1 - Y) \cdot q_{m10} \cdot (h_{11} - h_{10}) + \cdots$$

$$q_{mC1} \cdot (h_{C2} - h_{C1}) + q_{mC3} \cdot (h_{C4} - h_{C3}) \qquad \text{eq.(3.4)}$$

$$Y = 1 - \frac{q_{m10}}{q_{m7}} \qquad \text{eq.(3.5)}$$

where, q_{m7}, q_{m10}, q_{mC1} and q_{mC3} are mass flow rates of the compressed air, recycling air, the first cooling medium (propane) and the second cooling medium (methanol). The cooled air (state 8) expands in the cryo-turbine to the ambient pressure with a fraction (*Y*) of air mass flow liquefied. The air enthalpy h_9 at the outlet of cryo-turbine and turbine power are given by eq. (3.6) and eq. (3.7):

$$h_9 = h_8 - \eta_{c,t} \cdot (h_8 - h_{9,s}) \qquad \text{eq.(3.6)}$$

$$W_t = q_{ma}(h_8 - h_9) \qquad \text{eq.(3.7)}$$

where, $\eta_{c,t}$ is the isentropic efficiency of the cryo-turbine; W_t – the power output of cryo-turbine.

During discharging, the liquid air with a mass flow rate q_{la} is pumped to a high pressure by a cryo-pump with an isentropic efficiency η_p, and its outlet enthalpy h_{14} and power consumption W_p are given by eq. (3.8) and eq. (3.9):

$$h_{14} = h_{13} + \frac{h_{14,s} - h_{13}}{\eta_p} \qquad \text{eq.(3.8)}$$

$$W_p = q_{la}(h_{14} - h_{13}) \qquad \text{eq.(3.9)}$$

The high-grade cold energy of liquid air is recovered by exchanging heat with one or more cold storage media (e.g. propane and methanol), and the energy balances for the processes are governed by eq. (3.10) and eq. (3.11):

$$q_{la} \cdot (h_{15} - h_{14}) = q_{mC2} \cdot (h_{C2} - h_{C1}) \qquad \text{eq.(3.10)}$$

$$q_{la} \cdot (h_{16} - h_{15}) = q_{mC4} \cdot (h_{C4} - h_{C3}) \qquad \text{eq.(3.11)}$$

where, q_{la}, q_{mC2}, q_{mC4} are the mass flow rates of liquid air, propane and methanol. Subscript 14, 15, 16 represents the inlet and outlet state of liquid air going through evaporators. C_2 and

C_1 represent the inlet and outlet of propane, and C_4 and C_3 represent the inlet and outlet of methanol across evaporators.

In the turbine train, the high-pressure air is heated before entering each stage and the outlet enthalpy and output power W_{Tr} of each turbine stage are given by eq. (3.12) and eq. (3.13):

$$h_{i+1} = h_i - \eta_{Tr}(h_i - h_{i+1,s}) \quad \text{eq.(3.12)}$$

$$W_{Tr} = q_{la}(h_i - h_{i+1}) \quad \text{eq.(3.13)}$$

where, η_{Tr} is the isentropic efficiency of the turbine, and the subscript i = 17, 19, 21 represents the inlet state of turbines.

3.2.2.2 Performance indicators

The following indicators are defined to study the LAES system performance.

- *Round trip efficiency (RTE)* is defined by eq. (3.14) as the ratio of the net total output work eq .(3.15) produced in the discharging process to the net total input work eq. (3.16) consumed in the charging process [212]:

$$RTE = \frac{q_{la} \cdot w_{dis}}{q_{ma} \cdot w_{cha}} \quad \text{eq.(3.14)}$$

$$w_{dis} = (h_{17} - h_{18}) + (h_{19} - h_{20}) + \cdots$$
$$(h_{21} - h_{22}) - (h_{14} - h_{13}) \quad \text{eq.(3.15)}$$

$$w_{cha} = (h_2 - h_1) + (h_4 - h_3) + (h_6 - h_5) - (h_8 - h_9) \quad \text{eq.(3.16)}$$

- *Liquid yield ratio* is the ratio of compressed air that can be directly liquefied to the total compressed air flow. This is an indicator of the efficiency of liquefaction process [212]:

$$Y = \frac{q_{m12}}{q_{m7}} = \frac{q_{la}}{q_{ma}} \quad \text{eq.(3.17)}$$

3.2.2.3 Exergy analysis model

Exergy is the maximum work output available in the working fluid and the exergy analysis is based on the second law of thermodynamics given by eq. (3.18) [41,42]:

$$0 = \sum(1 - \frac{T_0}{T_k})\dot{Q}_k - W_{cv} + \sum q_{mi}\, e_i - \sum q_{mj}\, e_j - E_d = 0 \quad \text{eq.(3.18)}$$

where, T_0 is the environment temperature; T_k is the temperature of the k^{th} control volume; $\dot{Q}_k$ is the heat production rate; W_{cv} is the work output of a control volume; $\sum q_{mi}\, e_i$ is the total exergy inflow; $\sum q_{mj}\, e_j$ is the total exergy outflow; and E_d is the exergy destruction. The exergy flow *e* is defined by eq. (3.19) [41,42]:

$$e_i = h_i - h_0 - T_0(s_i - s_0) + 0.5{v_i}^2 + gz_i \quad \text{eq.(3.19)}$$

where, $h_i - h_0$ is the enthalpy difference; $T_0(s_i - s_0)$ is the entropy difference, representing the irreversibility in adiabatic control volumes; The kinetic energy term $0.5{v_i}^2$ and the potential energy term gz_i are usually negligible.

Based on the above the exergy balance equation, the exergy efficiency and exergy destruction for each component and each specified control volumes can be derived.

3.2.2.4 System economic model

The economic evaluation of the whole system requires the estimation of the costs of major components, including compressors, expanders, pumps, heat exchangers, motor-generator, tanks and reservoirs, as well as thermal oil, methanol and propane. The cost functions of these components and fluids were collected and shown in Table 3.2. Based on the currency and the year built in these cost functions, the currency inflation and transfer to pound (2020) were considered. The total capital expenditure (CAPEX) of a LAES plant was determined by adding the purchasing cost of each component, as it is the simplest and least

Table 3.2. Cost estimation models of major components of LAES

Components	Cost model	Currency	Parameters introduction	References
Compressors	$C_{fc} \cdot \dot{m}_{fc} \cdot \frac{log\beta_c}{0.9 - \eta_{is,c}}$	$ 2017	$\dot{m}_f$ - mass flow rate (kg/s), η_{is} – the isentropic efficiency, β_c – the compression ratio, C_{fc} – compressor cost factor, 670 $/(kg/s), c - compressors	[214]
Turbines	$C_{fTr} \cdot \dot{m}_{fTr} \cdot \frac{log\beta_{Tr}}{0.92 - \eta_{is,Tr}}$	$ 2013	Tr - Turbines, β_{Tr} – the expansion ratio, C_{fTr} – turbine cost factor, 1100 $/(kg/s)	[214]
Heat exchangers	$log_{10}(C_{hex0}) = (4.325 - 0.303 \cdot log_{10}(A) + 0.1634 \cdot log_{10}(A)^2$ $P_f = 1.63 + 1.66 \cdot 10\text{^}(0.0388 - 0.1127 \cdot log_{10}(P) + 0.08173 \cdot log_{10}(P)^2)$ $C_{hex} = C_{hex0} \cdot P_f$	$ 2009	A - heat transfer area (m^2), C_{hex0} – the base cost of heat exchangers, P_f – pressure factor, P – HEX pressure (bar), C_{hex} – total HEX cost	[215]
Thermal oil tank	$41.055 \cdot X + 92872$	$ 2016	X – tank volume (m^3)	[205]
Cold storage tank	$17400 + 79 \cdot X^{0.85}$	$ 2002	X – tank weight (tons)	[216]
Liquid air tank	$0.256 \cdot (\frac{X}{100})^{0.9}$	Million £ 2012	X – tank weight (tons)	[203]
Pump	$644 \cdot (\frac{X}{10})^{0.6}$	k€ 2009	X – shaft power (kW)	[205]
Cryo-turbine	$6975 \cdot X^{0.7}$	$ 2012	X – shaft power (kW)	[205]
Motor-generator	$60 \cdot X^{0.95}$	$ 2009	X – power (kW)	[215]

Thermal oil	0.5~1 $/kg	$ 2018	For large mass scale purchase order	[217]
Methanol	519 $/ton	$ 2018	\	[116]
Propane	264 $/$m^3$	$ 2018	\	[116]

uncertain economic metric. Other costs, including the installation, piping, electric and land and so on were all not taken into account, as this study is only focused on the design stage.

Besides, the NPV was considered as another economic indicator. It takes into account the operation and maintenance costs and energy market factors, including electricity prices, inflation rate, taxes and insurance etc. The expression of NPV is given by eq. (3.20) [213]. It is the value of all future cash inflows and outflows discounted to the present over the whole life of an investment. The annual O&M cost is assumed to be 1.5% of total CAPEX [116].

$$NPV = \sum_{t=1}^{Lf} \frac{(p_{rd} W_{dis} T_{dis} - p_{rc} W_{cha} T_{cha} - C_{OM} - C_{other}) \cdot (1+\varepsilon)^t}{(1+\sigma)^t} - C_{invc} \cdot Amf \quad \text{eq.(3.20)}$$

$$Amf = \frac{IR(1+IR)^{Lf}}{(1+IR)^{Lf}-1} \quad \text{eq.(3.21)}$$

where, Lf – lifetime of LAES plants, t – a specific year, p_r- the electricity price (£/kWh), W – power (kW), C_{OM} – maintenance cost, C_{other} - other cost. T – charge/discharge duration (hours), Amf – annual amortized factor, IR – the interest rate, ε – the escalation rate, σ – the discount rate. Subscripts: *cha* – charging process, *dis*- discharging process, *invc* – capital investment.

Occupied Space Energy Density (OSDE) is the ratio of the net output power during discharging to the sum of the volume of stored tanks. The higher OSDE means more compact system.

$$OSDE = \frac{\dot{W}_{net,out}}{V_{tot}} \quad \text{eq.(3.22)}$$

$$V_{tot} = V_{LA} + V_{ms} + V_{ps} + V_{hs} \quad \text{eq.(3.23)}$$

where, $\dot{W}_{net,out}$ is the system net output power, V is the volume of tanks, subscripts *LA* – liquid air, *ms* – methanol storage, *ps* – propane storage, *hs* – hot storage.

3.3 Optimization model and parameters

3.3.1 Optimization formulation

For the optimization model, it consists of the optimization variables, constraints and objectives, as well as the optimization algorithms. In this study, the parametric analysis in Aspen HYSYS was first conducted to understand the effects of key design and operational parameters on the system performance. The selected design and operational variables are the charging pressure, the discharging pressure, the inlet and outlet temperature of air-propane cold box, as they are crucial to improve the system performance. The optimization objectives include RTE, NPV and CAPEX of a LAES plant. There are various algorithms that have been used to do system optimization, including the GA [210], Multi-Objective Grey Wolf Optimization (MOPSO) algorithm [208] and Yin-Yang-Pair optimization algorithm [208] etc. In this study, in order to reduce the computation time, the GA optimization based on the surrogate model was adopted.

3.3.2 Surrogate optimization

For the optimization, a ‘surrogate model’, which is simpler and cheaper, was first constructed to replace the complex thermodynamic model of LAES built in Aspen HYSYS. The optimization based on the surrogate model is termed as ‘surrogate optimization’, which can reduce the computing time significantly. An interface between MATLAB and HYSYS was built to achieve the optimization.

MATLAB has been configured to control the custom interface server of Aspen HYSYS by creating a COM object through the commands (actxserver) [24]. Data exchange between MATLAB and HYSYS has been implemented by the commands structured according to the procedures shown in Figure 3.2. The MATLAB Surrogate Model Toolbox (MATSuMoTo) was used for the single-objective optimization [218], and the optimization algorithm

'Thompson sampling efficient multi-objective optimization (TSEMO)' was used for multi-objective optimization due to its higher efficiency [219][220].

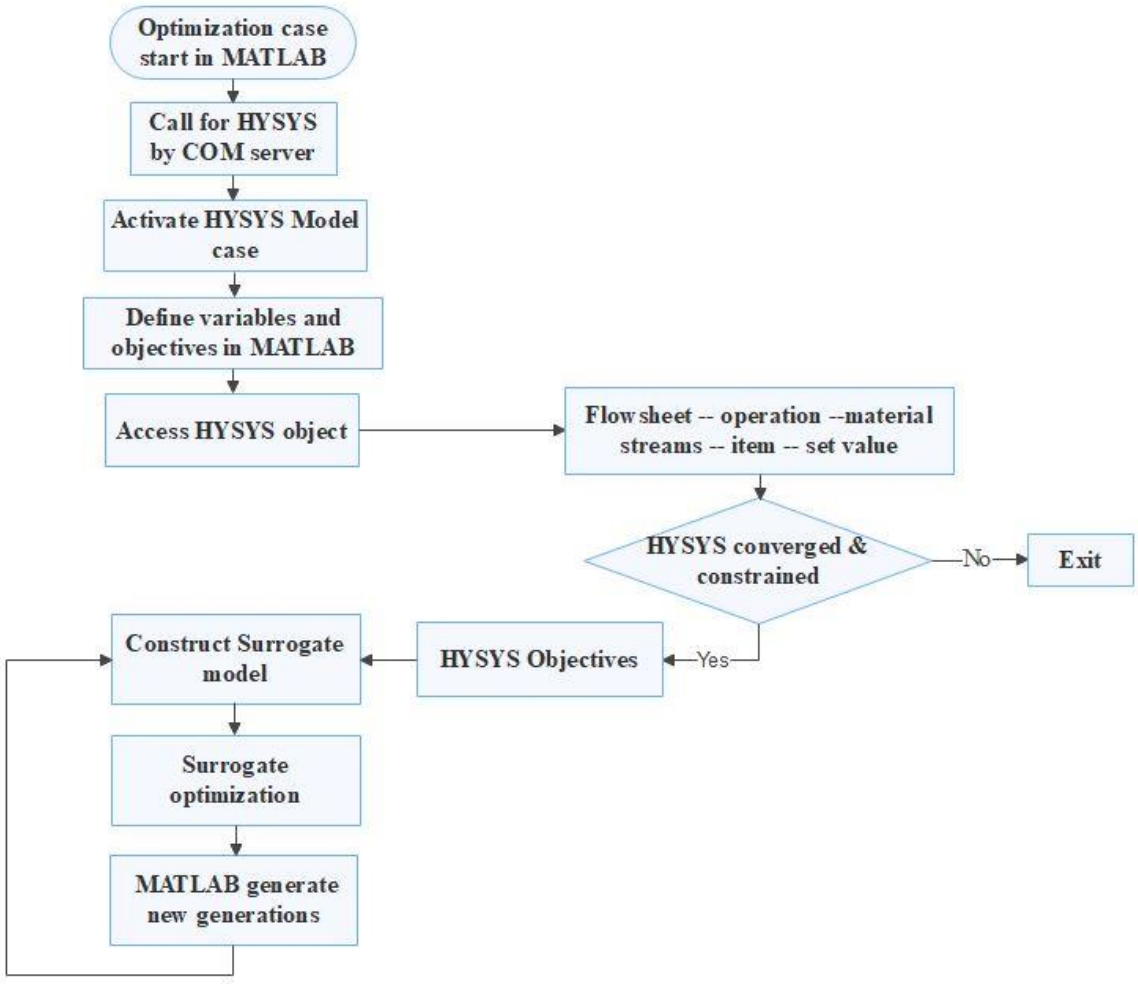

Figure 3.2. The system optimization framework

3.3.3 Assumptions and input parameters

The thermodynamic and economic parameters of LAES applied in this study are listed in Table 3.3.

Table 3.3. Thermodynamic input parameters for LAES [45][116]

Thermodynamic parameters		Economic parameters	
Ambient air temperature (K)	293	Charge pressure (MPa)	9~16
Ambient pressure (kPa)	101.3	Discharge pressure (MPa)	10~15
Liquid air storage pressure (kPa)	101.3	O&M cost	1.5% of CAPEX

Thermal oil inlet temperature (K)	293	Charging electricity price (£/MWh) [221]	20
Methanol temperature range (K)	210~310	Discharging electricity price (£/MWh) [221]	80
Propane temperature range (K)	85~220	Discount rate	6%
Pinch point in evaporators (K)	2	Escalation factor	2%
Pinch point in cold box, heaters and coolers (K)	5	Annual operating days of LAES	330 days
Isentropic efficiency of compressor	89%	Lifetime of LAES	25 years
Isentropic efficiency of turbine	90%	Maximum generations	100
Isentropic efficiency of cryo-turbine	75%	Minimum surrogate points	60
Isentropic efficiency of cryo-pump	70%	Convergence criteria	0.1%

3.3.4 Model validation

The nominal conditions and parameters of LAES system are shown in Table 3.3. The thermodynamic simulation in this study was conducted in Aspen HYSYS. The results have been compared with those of She's work [45]. At nominal conditions, the charging pressure is 9 MPa, the inlet ait is cooled down to 125.97 K before expansion, resulting in 64% of liquid yield ratio (Y), which is 3.5% higher than that of She's work (60.5%). It is mainly due to larger flow rate of cold propane, which can provide more recoverable cold energy to cool air down. The RTE is 52.6%, which is 4.5% higher than that of She's work (50.3%) due to higher liquid yield ratio. Thus, the error was considered reasonable within 5% of range [222], the model developed in Aspen HYSYS was considered accurate to do the thermodynamic simulation of the LAES system. Figure 3.3 shows the composite temperature profiles of major heat exchangers, illustrating that the temperature gradients of working fluids match well under the specified pinch point constraints, which can ensure the effective heat transfer.

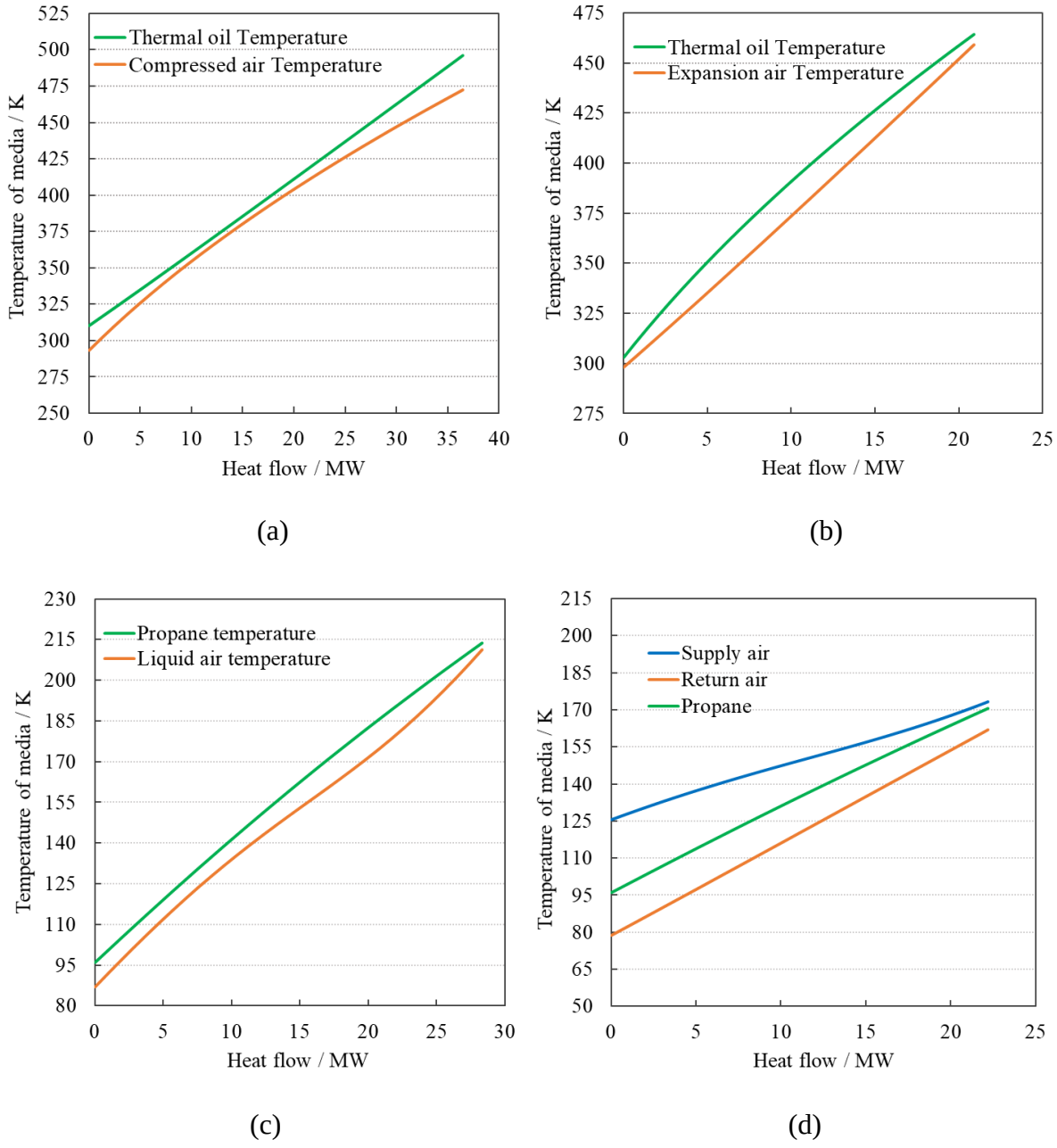

Figure 3.3. The composite temperature profiles of key heat exchangers: (a) compressor cooler; (b) turbine heater; (c) air-propane evaporator; (d) air-propane cold box

3.4 Results and discussion

3.4.1 Parametric sensitivity analysis

3.4.1.1 The effects of charging pressure

The effect of charging pressure on RTE of LAES in this work has been validated by the work of She et al. [45], shown in Figure 3.4 (a). When keeping the discharging pressure constant at 12 MPa, the charging pressure increases from 6 MPa to 15 MPa, the liquid yield ratio increases remarkably in the range of 6-12 MPa, and then changes slowly at higher pressures. It is mainly due to the average specific heat capacity of supercritical air can be reduced remarkably first and then subtly when the charging pressure goes up. Accordingly, the RTE increases notably first and then presents the maximum value at 12 MPa before decreasing, as the RTE strongly depends on Y which rises slowly after 12 MPa, where a significant increase in compression work is observed. When the discharging pressure is at 8MPa, the Y of '8 MPa case' is higher than '12 MPa case', it is due to that more cold energy is recovered at lower discharging pressure. However, the RTE of '8 MPa case' is lower due to less specific expansion power produced through turbines.

From Figure 3.4 (b), when the charging pressure rises, the mass flow rate ratio of thermal oil to charging air increases, as the outlet temperatures of compressors get higher, more thermal oil is needed to maintain the low inlet temperatures of the next stage compressor. But the excess oil percentage declines, it is due to that the liquid yield ratio becomes larger, there is more liquid air expanding through turbines, thus, more thermal oil is needed and less oil (30% ~ 45%) left in hot storage tank.

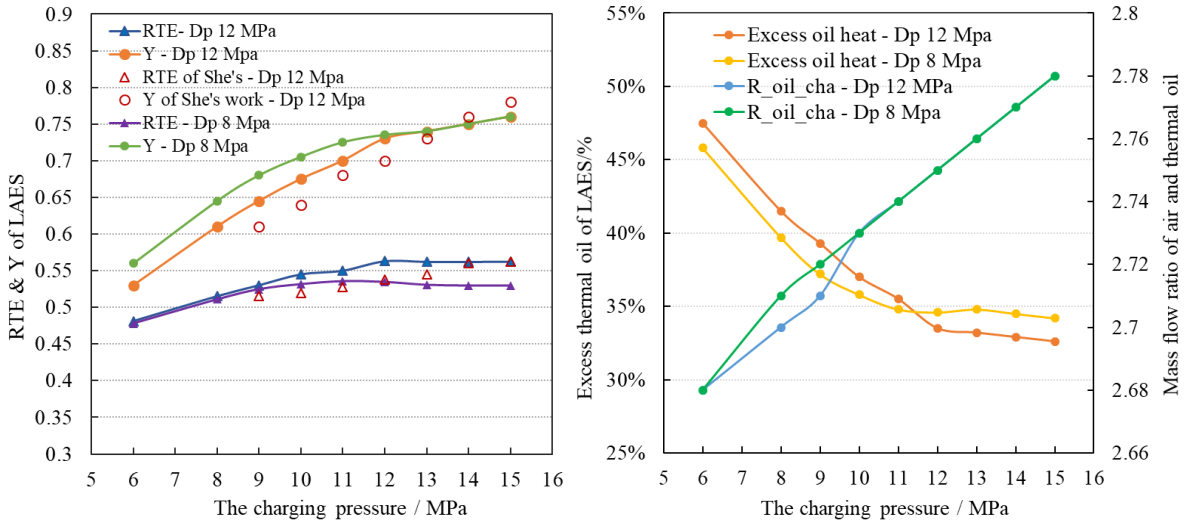

Figure 3.4. The effects of charging pressure on (a) RTE and Y; (b) excess oil percentage (the ratio of thermal oil left in hot storage tank to the total cooling thermal oil)

3.4.1.2 The effects of discharging pressure

From Figure 3.5 (a), it can be seen that there exists an optimal discharging pressure as well when there is no external cold source, which is ~12 MPa when the charging pressures are at 9 and 12 MPa respectively. The RTE increases first and then decreases with the discharging pressure rising from 6 MPa to 16 MPa. It is due to that higher turbine inlet pressure means larger expansion power. But if the discharging pressure is higher than 12 MPa, more pump work is needed to elevate the liquid air head, resulting in higher liquid air temperature at the pump outlet, and hence much more cold exergy loss across pump. This further leads to the drop in the liquid yield ratio, accordingly, the RTE declines as well.

From Figure 3.5 (b), the mass flow ratio of thermal oil to discharging air increases remarkably when the discharging pressure goes up. It is due to that higher discharging pressure means larger expansion ratio, accordingly, the air-side temperature difference across turbines and the need for hot thermal oil all increase. The excess oil declines first and then increases significantly after 12 MPa, because the mass flow rate of discharging air declines when the liquid yield ratio goes down at higher discharging pressure (> 12 MPa, Figure 3.5 (a)), thus there is much more excess thermal oil in hot storage tank left.

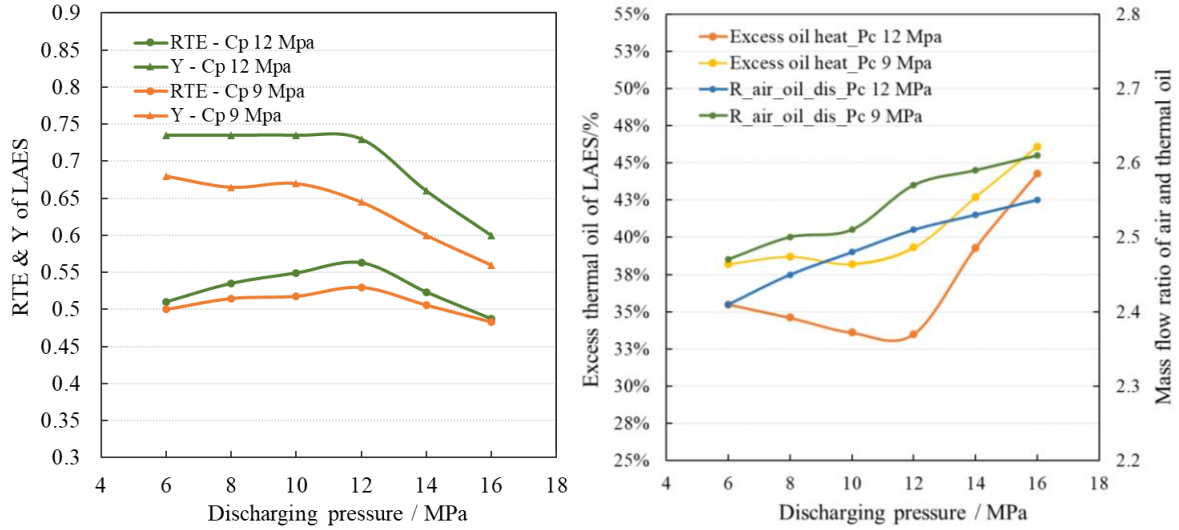

Figure 3.5. The effects of discharging pressure on (a) RTE and Y; excess oil percentage (the ratio of thermal oil left in hot storage tank to the total cooling thermal oil)

3.4.1.3 The effects of expansion stages

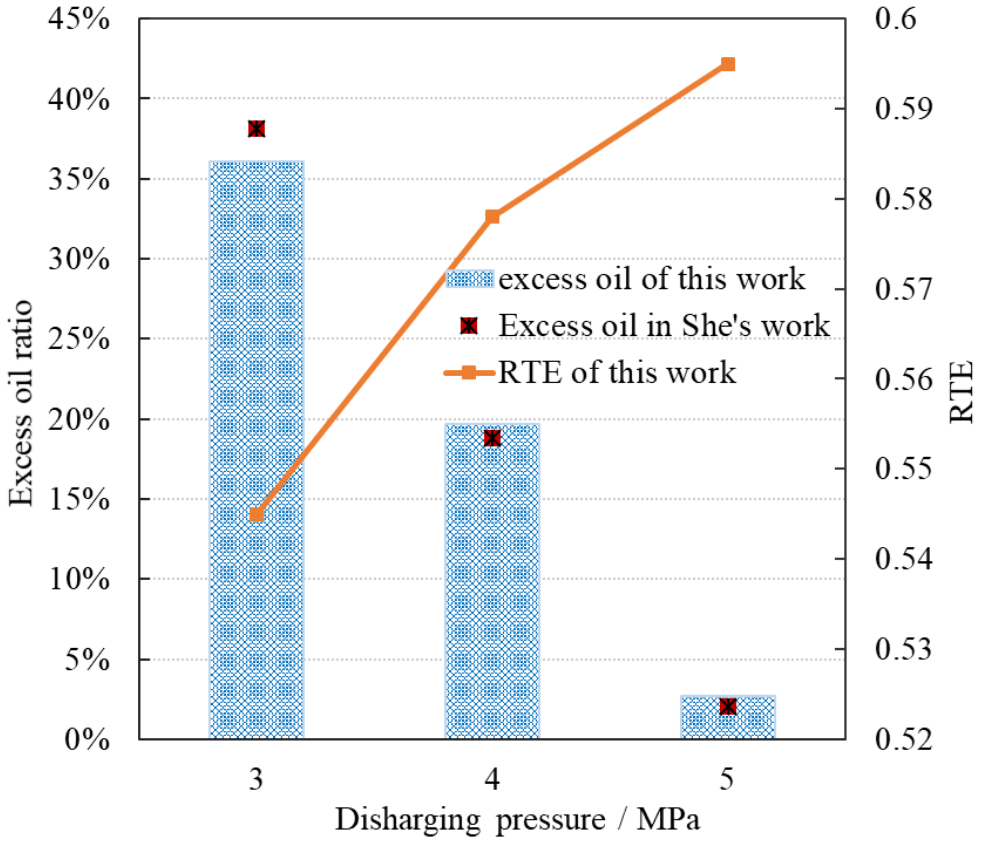

Figure 3.6. The effects of expansion stage on excess oil percentage and RTE

From *sections 3.3.1 and 3.3.2*, there is about 30% ~ 45% of excess thermal oil in hot storage tank left after three-stage expansion during LAES discharging. One way to utilize the excess oil is to add more expansion turbines. From Figure 3.6, when the expansion turbines increase from three to four, and then to five stages, the excess thermal oil percentage is reduced from 36.1% to 19.1% and then to 2.7%.. Correspondingly, the RTE of LAES is improved from 0.548 (there-stage expansion) to 0.575 (four-stage expansion) and then to 0.595 (five-stage expansion), which is consistent with the results of She's work [212] (red solid points in Figure 3.6), as more output power can be produced under more expansion stages. But more expansion turbines also mean more investment cost, there is a thermo-economic balance which can be struck by multi-objective optimization discussed in *section 3.4.2.4*.

3.4.1.4 The effects of machine efficiencies

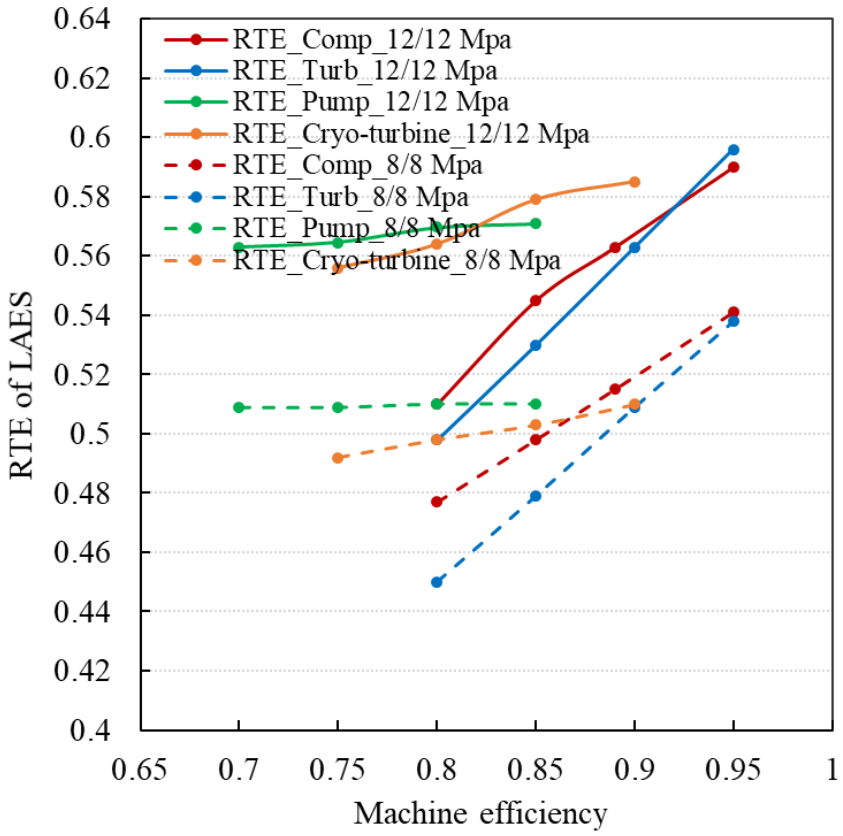

Figure 3.7. The effects of machine efficiencies on RTE

From Figure 3.7, the effects of machine efficiencies on system RTE at different charging/discharging pressures (8/8 MPa, 12/12 MPa) can be seen. To be noted, when one machine's efficiency changes, the efficiencies of other machines keep constant. The RTE is enhanced remarkably by 19.7% when the turbines' efficiencies increase from 80% to 95%. The second most significant impact on RTE comes from the improvement of compressors' efficiencies (increasing from 80% to 95%), the RTE is improved by 15.7%. The effects of efficiencies of cryo-turbine and cryo-pump are less impactful. There is only 4.3% of increase in RTE when cryo-turbine efficiency goes up from 70% to 90%. About 1.4% of increase in RTE can be seen when cryo-pump's efficiency is improved from 70% to 85%. Overall, in order to obtain higher RTE, it is essential to keep high efficiencies of turbines and compressors, but to focus more on reducing the investment costs of cryo-turbines and cryo-pump.

3.4.1.5 The effects of HEX pinch points

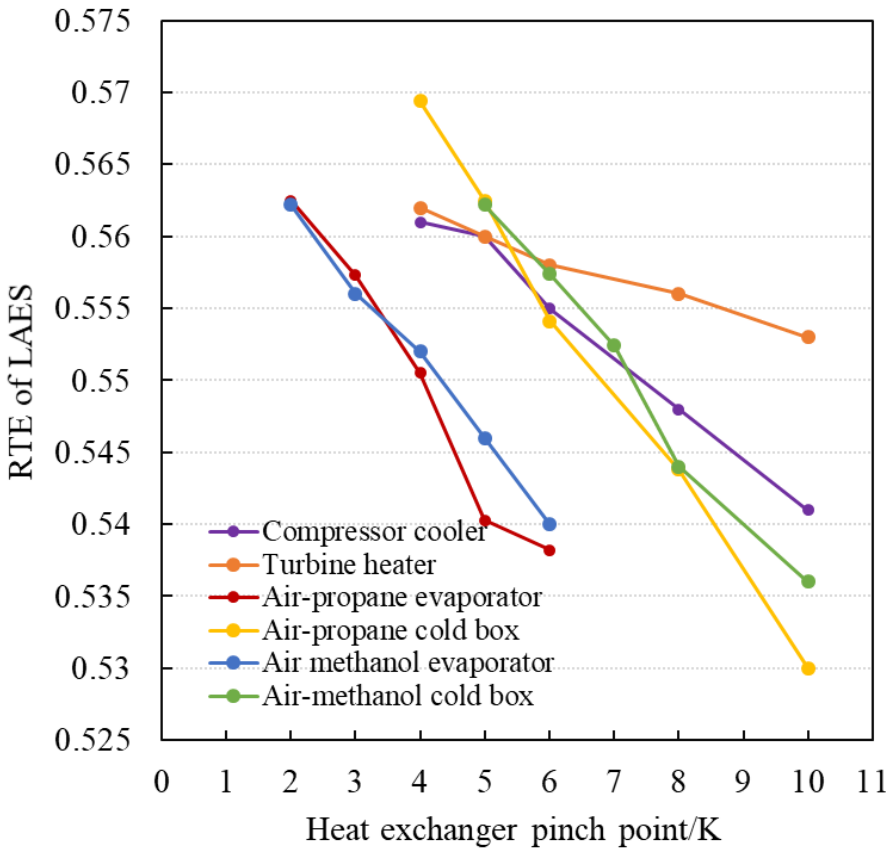

Figure 3.8. The effects of HEX pinch points on RTE of LAES

From Figure 3.8, the effects of pinch points of different heat exchangers (HEXs) on the RTE of LAES were studied. It can be seen that the most sensitive effects come from the air-propane and air-methanol evaporators. When their pinch points vary between 2 ~ 6 K, the RTE decreases by 4.7%, as larger pinch point means worse heat transfer performance, and thus, more cold exergy loss in these HEXs and lower liquid yield ratio. Besides, the higher pinch points (from 4 to 10 K) of air-propane and air-methanol cold box also get the system RTE deteriorated remarkably by 7.5% and 5% respectively. It is due to these four HEXs play key roles in recovering cold exergy from liquid air, and feeding cold exergy back to liquefy air. By comparison, compressor coolers have larger effects on RTE than turbine heaters, as larger pinch points (from 4 to 10 K) of coolers mean more heat transfer losses, leading to more compression work and lower RTE decreasing by 3.5%. For turbine heaters, there is only 1.8% of drop in RTE accordingly due to ~6 K of increase in the pinch point.

3.4.2 Single-objective optimization and analysis

Based on the analysis in *section 3.4.1*, the key factors that affect system efficiency and economics include the charging pressure, discharging pressure, number of machine stages, as well as the efficiencies of machines and pinch points of heat exchangers. Thus, in *section 3.4.2*, the charging and discharging pressure, as well as the inlet and outlet temperature of air-propane cold box are considered as the key design and operational variables for the optimization of LAES. The optimization objective is to maximize RTE (*section 3.4.2.1*) and maximize NPV (*section 3.4.2.3*)). The discussions about the optimizations under different machine stages (*section 3.4.2.4*), machine efficiencies (*section 3.4.2.5*) and HEX pinch points (*section 3.4.2.5*) were also presented.

3.4.2.1 Single-objective optimization - energy analysis

For the LAES system with the configuration shown in Figure 3.1, the single-objective optimization of the system was first conducted. It starts from three different initial points and

runs for 100 generations, the results are listed in Table 3.4, the optimization curves are shown in Figure 3.9. It can be seen that the optimal RTEs from three different initial points all have been optimized by 9.5% ~ 14.4%, reaching around 61% under the nominal conditions shown in Table 3.3. The corresponding optimal charging and discharging pressures are ~15 MPa and 11.2~11.8 MPa respectively. The optimal inlet and outlet air temperature of air-propane cold box are ~218 K and ~105 K (in the following sections, the optimum charging/discharging pressure, as well as the optimum inlet and outlet temperature of cold box are written as X = [15 MPa, 11.6 MPa, 218 K, 105 K]). These parameters further indicate the optimal sizes of air-propane and air-methanol cold boxes and evaporators, as well as the optimal mass flow rates of propane and methanol for recovering cold energy, which are given in Table 3.4. It can be seen that the heat transfer areas of cold boxes and evaporators, as well as the mass flow rates of cold media all increase remarkably. The most significant increases in heat transfer areas lie in air-propane cold box and air-propane evaporator, which is directly related to lowering the inlet temperature of cryo-turbine, leading to higher liquefaction rate and hence more turbine power output.

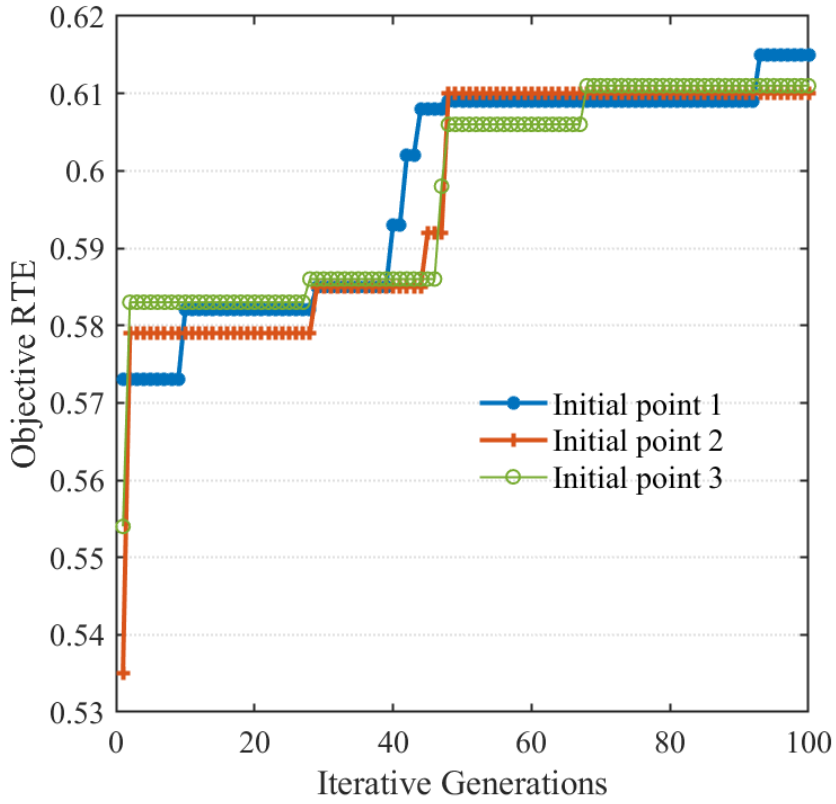

Figure 3.9. Single-objective optimization of LAES from different initial points

Table 3.4. Single-objective optimization of LAES from different initial points

Parameters	3-3 stage system before optimization	3-3 stage system after optimization[1]	Percentage increase
Initial points	X_{01} = [12, 10, 220, 119] X_{02} = [13, 13, 222, 120] X_{03} = [11, 12, 217, 115]	X_{opm1} = [15, 11.7, 217.8, 104.8] X_{opm2} = [15, 11.8, 218, 104.9] X_{opm3} = [15, 11.2, 218.2, 105.1]	/
RTE %	57.3 (X_{01}) 53.5 (X_{02}) 55.4 (X_{03})[2]	61.5 (X_{opm1}) 61.1 (X_{opm2}) 60.9 (X_{opm3})	7.3% 14.2% 9.9%
Compressor consumption/MW	107.12	113.57	6.02%
Compression temperature/K	474.40	482.30	1.67%
Liquefaction rate %	70.1	81.5	16.3%
Turbine output/MW	56.97	69.32	21.68%
Methanol flow rate (kg/s)	47.10	56.90	20.81%
Propane flow rate (kg/s)	155.20	176.50	13.72%
Air-methanol CB area (m^2)	2504.63	5249.06	109.57%[3]
Air-propane CB area (m^2)	5329.08	7325.88	37.47%
Air-methanol EVAP area (m^2)	4541.53	5208.15	14.68%
Air-propane EVAP area (m^2)	4114.70	5624.45	36.69%

Notes:

1. Other parameters except for initial points were from the optimization started from point X0 = [12, 10, 220, 119];
2. The RTEs are for three different initial points respectively, 01/02/03 – three initial points, opm1/opm2/opm3 – three optimum points.
3. The large increase in heat transfer area of air methanol CB is mainly due to its mean temperature difference decrease remarkably.

3.4.2.2 Single-objective optimization - exergy analysis

Taking the optimization case from the initial point X_0 ([12 MPa, 10 MPa, 220 K, 119K]) and RTE_0 (0.573) as an example, the optimized design and operation variables are X_{opm} = [15 MPa, 11.6 MPa, 217.8 K, 104.8 K] and RTE_{opm} is 61.5%. The exergy destruction comparison was conducted to reveal the optimization effects, shown as in Figure 3.10. The total exergy destruction decreases by 16.6% (from 256.1 to 213.2 kJ/kg.K), which is mainly due to the remarkably increased heat transfer areas and the reduced heat transfer losses. From Figure 3.10, specifically, these include the declines of exergy destruction in air-propane cold box (by 31.5%) and air-propane evaporator (by 11%), as well as in air-methanol cold box (by 58.3%). The other decreases of exergy destruction in turbines and cryo-turbine are 5.3% and 4.8% respectively, which are resulted from their optimum working conditions that produce less entropy increases and irreversible losses. However, the exergy destructions in compressors and cryo-pump (due to the higher charging and discharging pressure), as well as in coolers and heaters (due to higher compression heat temperature and heat transfer losses) were observed to grow by 1~4%.

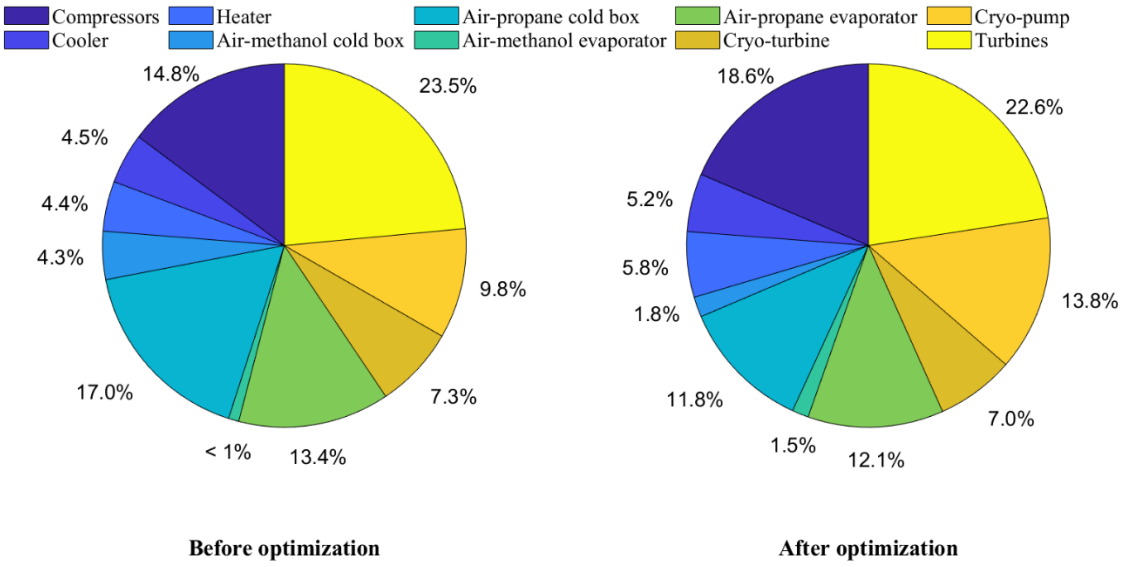

Figure 3.10. The exergy destruction comparison of the LAES system before and after optimization

3.4.2.3 Weighted Single-objective optimization - economic analysis

After the optimization, the economic analysis of the LAES system was discussed and the results are shown in Figure 3.11. The results showed the total CAPEX of LAES increases by 13.4% to obtain the optimum RTE, and the NPV increases by 66.95% from 25.7 million £ to 42.7 million £. Specifically, almost the capital costs of major system components all increase in different degrees (Figure 3.11).

The percentage increases in machines' costs include 4.7% of compressors, 19.7% of turbines, 19.1% of cryo-pump and 19.1% of the generator, which results from higher charging and discharging pressure, as well as higher air flow rate and power output during discharging. The significant cost increases of heat exchangers are observed as well, including 97.5% of air-methanol cold box and 41.2% of air-propane cold box, as well as 35.3% of air-propane evaporator and 15.5% of air-methanol evaporator. Higher liquefaction rate produces more liquid air and hence higher liquid air storage cost (increase by 14.5%). The costs of cold storage and heat storage enhance by 9.2% and 1.1% respectively. It indicates that the system prefers to enhance the costs of major components to obtain higher RTE and NPV. Overall, after optimization, four major cost contributors of the whole LAES system still are turbines (22.3%),

the liquid air tank (15.2%), heat storage (including thermal oil, 15.4%) and compressors (12.3%).

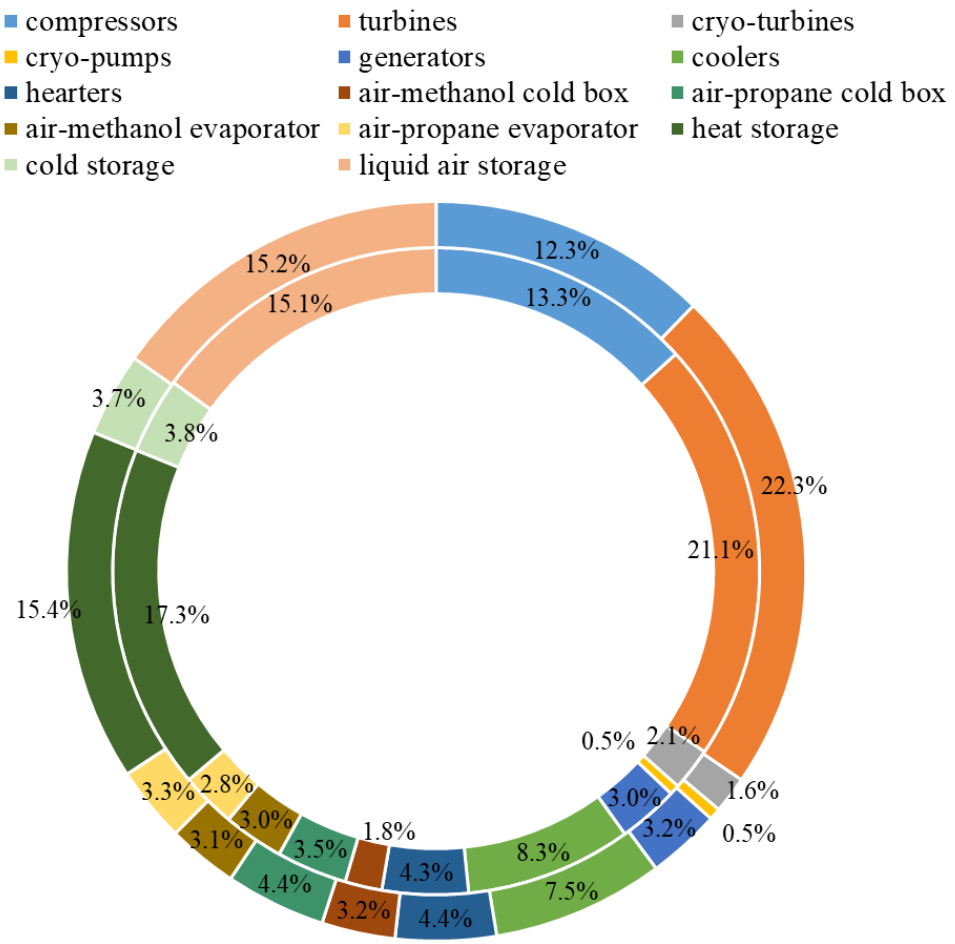

Figure 3.11. LAES system components cost comparison before and after optimization

3.4.2.4 Single-objective optimization of LAES with different machine stages

The single-objective optimization of LAES with different machines stages was conducted, the comparison results are shown as in Figure 3.12. For LAES with four stages of compressors and turbines (termed as four-stage system), the optimal variables and objective are X_{opm} = [16.5 MPa, 13.3 MPa, 210 K, 105 K] and RTE_{opm} is 0.61. Compared with the LAES with three stages of machines (termed as three-stage system), the charging pressure increases from 15 to 16.5 MPa, and the discharging pressure from 11.5 to 13.3 MPa.. It is due to that the compression ratio and expansion ratio per stage both decrease for four-stage system, leading to the decreases in the compressor power per stage and compressor outlet temperature, as well

as the turbine output power per stage. However, as the hot storage temperature and expansion power of turbines are all reduced. Thus, the charging pressure was optimized to be higher to produce a higher temperature of thermal oil, in order to increase turbine power output at higher discharging pressure and to obtain better RTE.

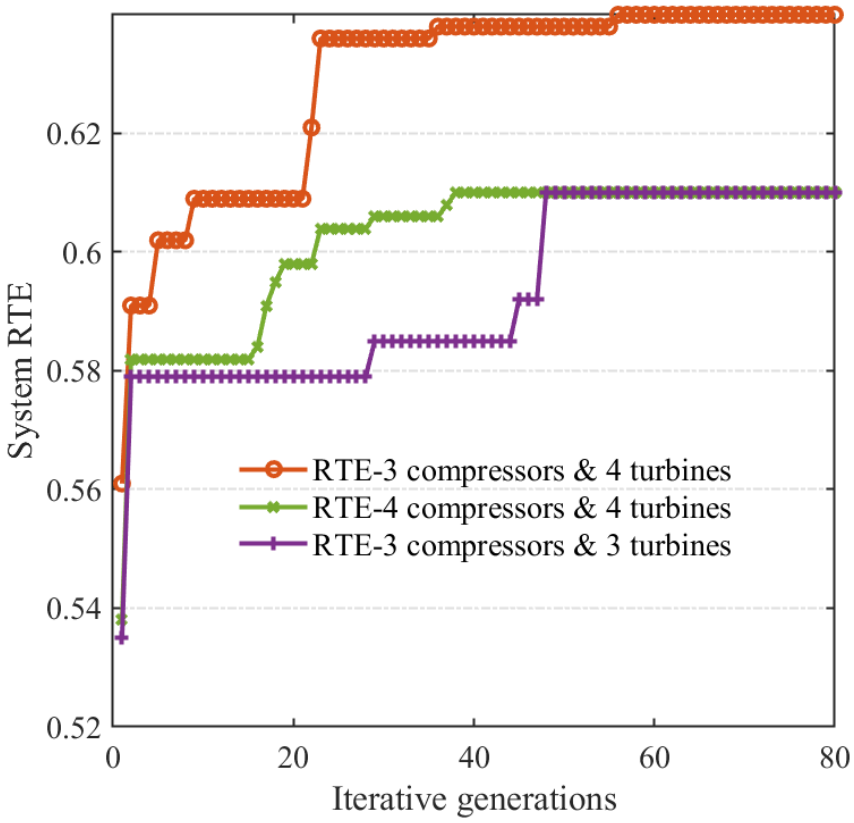

Figure 3.12. Single-objective optimization of LAES with different stages of machines

For the LAES system with three-stage compressor and four-stage turbine (three-four stage system), after optimization, the optimal variables are X_{opm} = [15.4 MPa, 11.7 MPa, 210 K, 105 K] and RTE_{opm} is 0.633. The optimum pressure and temperature are close to those of the LAES system with three-stage machines, but the efficiency has been optimized from 0.575 (section 4.1.3) to 0.633. It is mainly due to that one more stage of turbine can help fully utilize the excess compression heat, producing more output power and higher efficiency, accordingly, the NPV is the highest at 50 M£ and specific power cost is the lowest at 756.9 £/kW respectively for three-four stage system, the detailed comparison of these parameters are shown as in Figure 3.13.

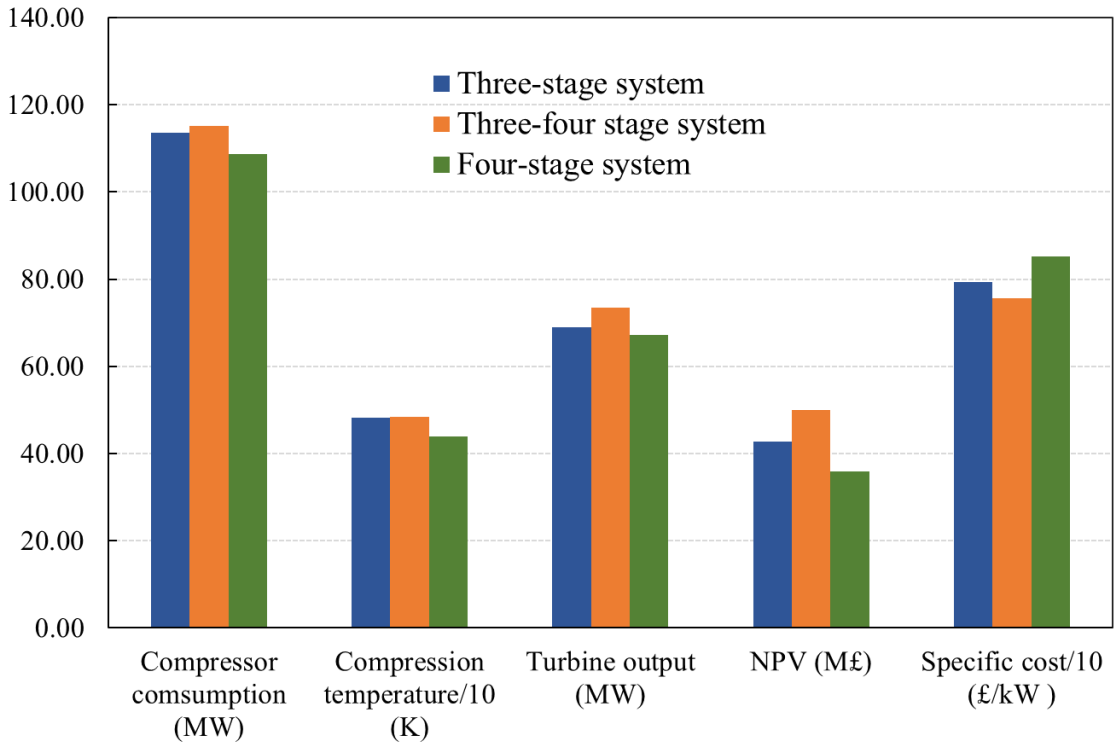

Figure 3.13. Detailed parameters comparison of LAES with different stages of machines

3.4.2.5 Single-objective optimization under different device parameters

The single-objective optimization of the LAES system with the worst machine efficiencies and worse heat transfer performance were studied, shown as in Figure 3.14, the detailed results comparison is shown in Table 3.5. After the optimization, the optimal design parameters and objective for the worst machine efficiency scenario are X_{opm} = [13.7 MPa, 9 MPa, 210 K, 105.7 K] and RTE_{opm} is 0.459. Compared with the optimum results of LAES working under the nominal conditions, a lower charging pressure is to reduce the compressor power consumption, and a lower discharging pressure is to reduce the cold exergy loss across the pump, as their efficiencies both get worse. The inlet and outlet temperature of air-propane cold box are kept at lower value to increase the liquefaction rate. Thus, for three-stage LAES with compressor efficiency in the range of 75% ~ 90%, the optimal charging pressure is between 13~15 MPa. If the turbine and pump efficiency vary between 80%~90% and 60%~70%, the optimal discharging pressure is between 9 ~11.5 MPa.

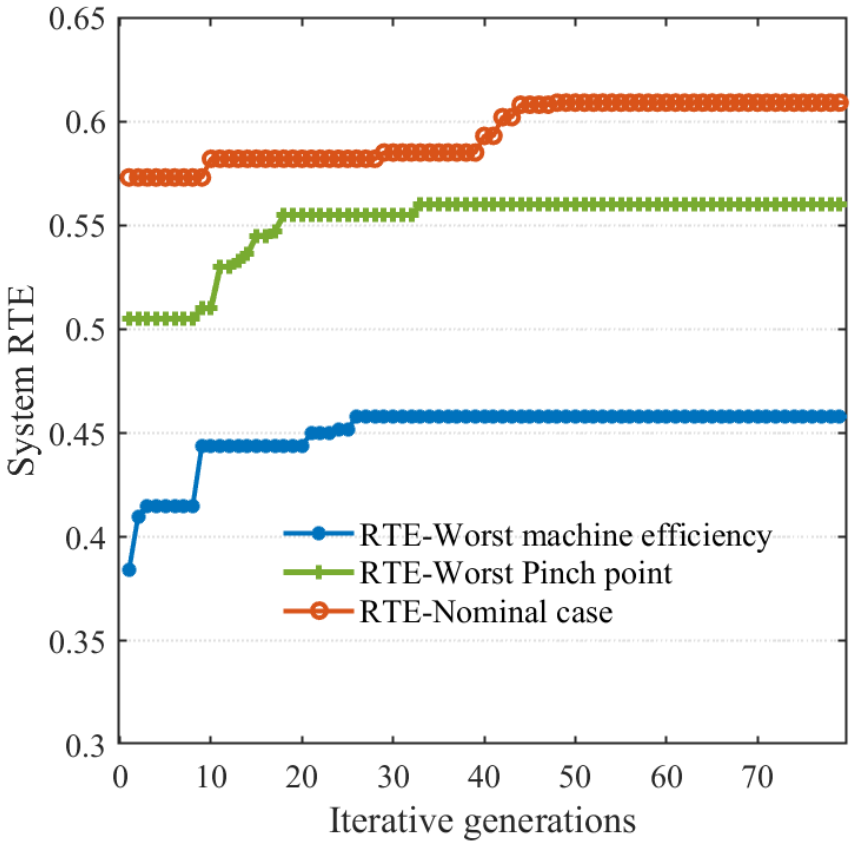

Figure 3.14. The Single-objective optimization of LAES under worst scenarios

When the pinch points of heat exchangers within LAES increase to larger values, it means the heat transfer performance gets worse. The optimization curve in Figure 3.14 gave the optimum design parameters X_{opm} = [16.8 MPa, 10 MPa, 217.6 K, 105.2 K] and the optimum objective RTE_{opm} (0.553). Compared with the optimization results of LAES working under nominal conditions, operating at a higher charging pressure is to obtain higher compression heat temperature, which can compensate the heat transfer losses in compressor coolers and enhance the discharging power output. A lower discharging pressure is selected to avoid much cold exergy loss across pump, as the cold exergy losses in evaporators increase when their pinch points are higher. Thus, for designing LAES systems, if the heat transfer performance of HEXs gets worse, the charging pressure should be elevated but the discharging pressure should be reduced. Meanwhile, larger heat transfer areas and mass flow rates of cold storage media are required to keep higher RTE. Overall, from the comparison shown in Table

3.5, lower machines' efficiencies lead to more compressor power and lower power output, leading to lower RTE and NPV. The effects of worse machine efficiency have worse impacts on LAES than those of the case with worse heat transfer performance. To be noted, the heat transfer areas of HEXs with larger pinch points are all smaller than those of LAES at the nominal and worst efficiency scenarios, as the logarithm mean temperature differences of HEXs all increase remarkably.

Table 3.5. The detailed parameters comparison of LAES under worst scenarios

Optimum parameters	Three-stage system under nominal conditions	Three-stage system with the worst machine efficiencies	Three-stage system with higher pinch points of HEX
Variable scenarios	Compressors 89% Cryo-turbine 80% Cryo-pump 70% Turbines 90%	Compressors 75% Cryo-turbine 70% Cryo-pump 60% Turbines 80%	Cooler-10 K (nom 5 K) Heater-10 K (nom 5 K) Cold box-10 K (nom 5 K) Evaporator-5 K (nom 2 K)
Optimization variables	[15, 11.6, 218, 105.1]	[13.7, 9, 210, 105]	[16.8, 10, 217.2, 105.2]
RTE	0.611	0.451	0.553
Compressor consumption/MW	113.57	131.63	116.74
Compression temperature/K	482.30	504.23	472.60
Turbine output/MW	68.97	60.77	65.30
Methanol flow rate (kg/s)	56.90	53.84	56.90
Propane flow rate (kg/s)	176.50	188.62	184.30
Air-methanol cold box area (m2)	5249.06	4262.22	3034.79
Air-propane cold box area (m2)	7325.88	7024.76	4180.72
Air-methanol evaporator area (m2)	5208.15	5187.63	3048.54
Air-propane evaporator area (m2)	5624.45	5664.39	5397.58
NPV M£	51.40	27.30	34.33

Notes:

1. 'nom' means at the nominal conditions.

3.4.3 Two-objective optimization for three-stage system

Based on the results from *section 3.4.2.3*, RTE is synergistic with NPV but in conflict with capital cost. As NPV is highly dependent on economic factors, like electricity price

difference, discount rate and operating days etc., the sensitivity analysis result of NPV under different economic assumptions (the possible minimum and maximum value) is shown in Figure 3.15. It can be seen that the most significantly impactful factors are electricity price, discount rate and charging hours, like when the electricity selling price varies between 0.06 and 0.1 £/kWh (keep the electricity purchasing price 0.02 £/kWh constant), the NPV increases from million £ 0.193 to million £ 85.49. The less impactful factors include annual working time, lifetime, maintenance cost and escalation factor.

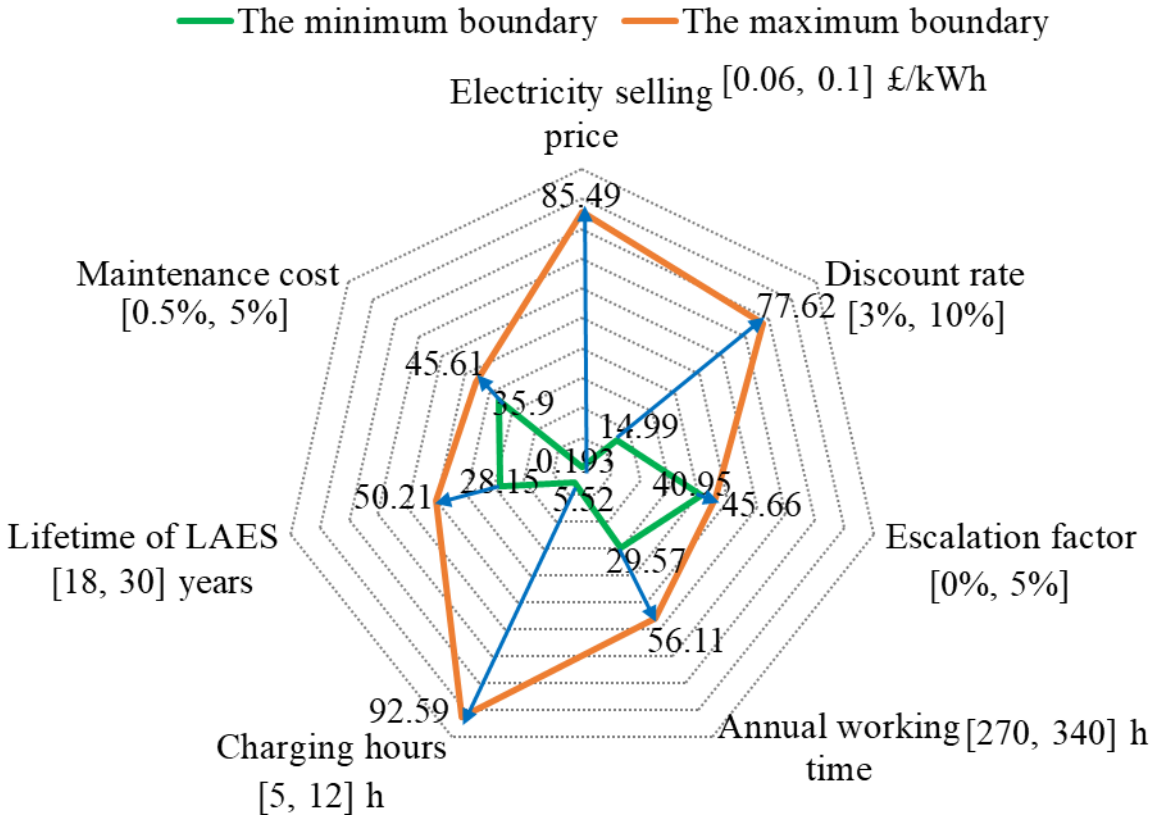

Figure 3.15. The sensitivity analysis of NPV under different economic assumptions

Thus, for the two-objective optimization, the CAPEX of LAES was chosen as another objective due to it is less uncertain, the optimal Pareto front is shown in Figure 3.16. Selecting four optimal points from the Pareto front, the results are listed in Table 3.6. It can be seen that higher RTEs are at the cost of higher capital investments, but also producing higher NPV. Specifically, when the RTE increases by 1%, the optimized CAPEX increases by 0.5-1% (the regression relationship between RTE and CAPEX on Pareto front is shown in Figure 3.16).

Comparing to single-objective optimization (RTE_{opm} is ~0.61), the two-objective optimization gave the optimum RTE at 56.5%, to avoid a significant increase in the CAPEX of LAES.

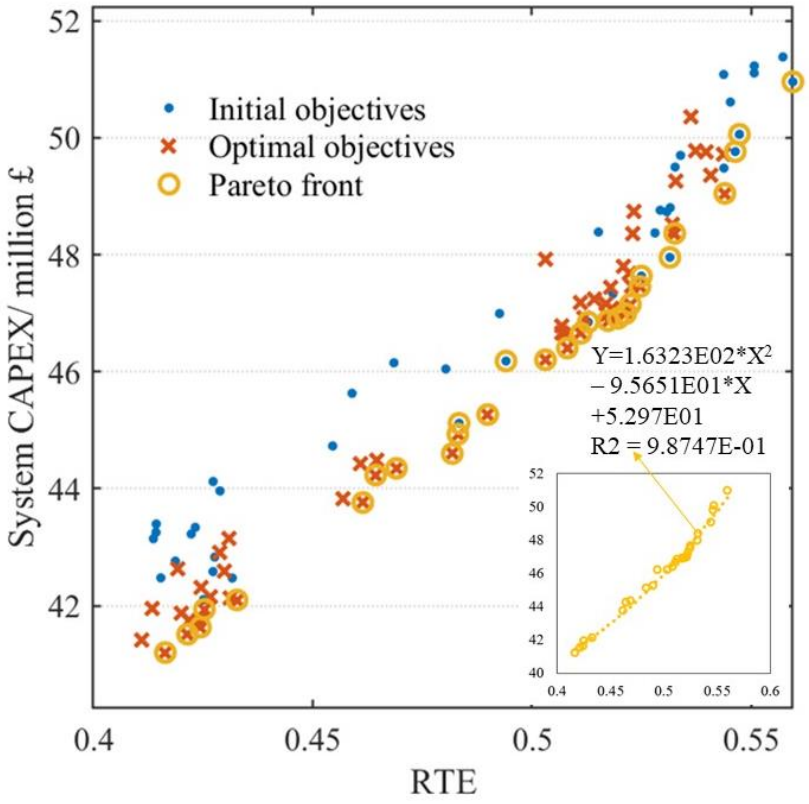

Figure 3.16. The optimal Pareto front of RTE and CAPEX

Further form Table 3.6, when the system investment budget is limited, the optimization prefers to have a lower charging pressure, to reduce the compressor power consumption and its investment cost. When the system investment budget is large, it chooses a higher charging pressure, the discharging pressure is near the optimal value (~11.5 MPa), to produce higher compression heat and more power output, and hence higher RTE at a reasonable system cost. After the two-objective optimization, it is also observed that the inlet and outlet temperatures of air-propane cold box decrease remarkably, accordingly, the heat transfer areas of HEXs are enhanced significantly, but the increases in their CAPEXs are limited, as the HEX costs only account for 3%-5% of total CAPEX of LAES (from Figure 3.11). Thus, the investors should balance the trade-off between RTE and investment cost at the beginning, choosing to

investment more on HEXs at first (larger heat transfer areas) and then more on compressors and turbines (higher charging/discharging pressure).

Table 3.6. The selected points and parameters from the optimal Pareto front

Optimal Point [MP, MPa, K, K]	Methanol mass flow rate kg/s	Propane mass flow rate kg/s	Methanol CB area / m2	Propane CB area / m2	Methanol EVAP area / m2	Propane EVAP area / m2	RTE/%	CAPEX/M£	NPV/M£
[11, 12.7, 227, 139]	37.4	110.0	1502.3	2386.5	3479.7	3321.0	42.5	41.7	4.2
[12.3, 11, 218, 124]	45.5	144.1	2322.9	4522.0	4300.5	4123.4	49.2	46.1	19.2
[11.7, 10, 224, 117]	47.5	155.2	2643.0	5966.5	4613.7	4020.4	52.2	47.5	25.0
[13.5, 10.8, 217, 108]	54.1	173.9	4493.4	7223.3	5083.9	5076.5	56.3	51.3	35.6

3.4.4 Two-objective optimization for multi-stage system

The Pareto front of two-objective optimization of LAES with different stages of machines is shown in Figure 3.17. The optimal Pareto front comparison indicates that if the CAPEX budget is below 42 M£, there is a better trade-off between RTE and CAPEX for three-stage system. If the CAPEX budget is between 42 M£ and 44 M£, the optimal RTE of three-stage system is around 44%, while that of four-stage system is around 46%-48%. When the CAPEX budget is between 44 to 48 M£, the Pareto front shows that three different LAES systems present similar trade-offs between the optimal RTE and CAPEX. But when CAPEX budget is above 48 M£, the three-four stage system presents the best RTE (55% - 61%), which is 7.3% and 3.6% higher than RTEs of three-stage system and four-stage system. The regression relationship between RTE and CAPEX of three-four stage system on the green Pareto front is shown in Figure 3.17. Overall, after crossing a specific investment threshold, the advantages of three-four stage system are obvious. Thus, it is not wise to add more machines stages at lower CAPEX budget, but to focus on optimizing heat transfer areas to enhance the

overall efficiency. If more budget is allowed, except for increasing heat transfer areas, more machine stages and their good combination can produce better RTE.

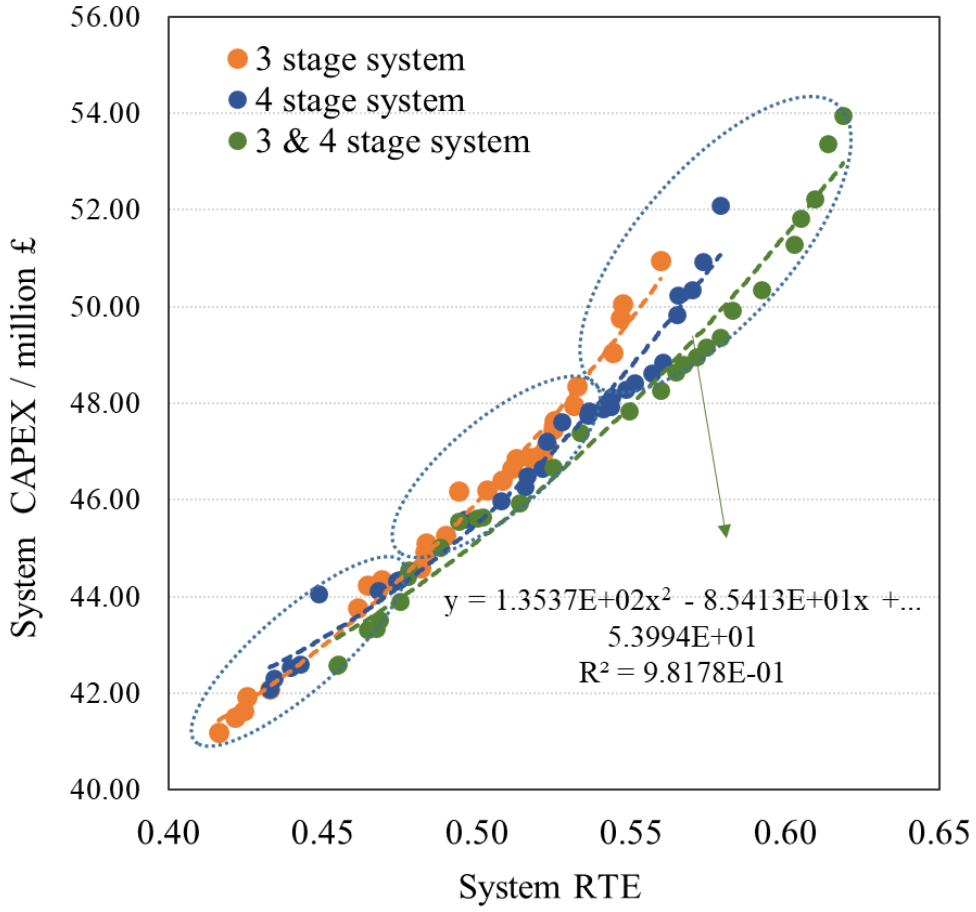

Figure 3.17. Two-objective optimization of LAES with different stages of machines

3.4.5 Three-objective optimization of LAES system

In this case study, take the LAES configuration with three-stage compressor and four-stage turbine as an example, three-objective optimization was conducted, to optimize the RTE, CAPEX and OSDE simultaneously, the optimal design and operational parameters were obtained (four points are shown in Table 3.7) and the optimal Pareto front is shown as in Figure 3.18. From Figure 3.18, the more investment made, the higher the RTE and OSDE. Though the higher RTE means more liquid air is produced, accordingly triggering larger volumes of liquid air tank and cold storage tank. But the enhancement in power output is more than the total increase in tank volume, producing higher OSDE. From the view of design and

operational parameters, in order to obtain higher RTE and OSDE, it prefers to increase the charging and discharging pressure, as well as the heat transfer areas of propane cold box and evaporators, but the increase in thermal oil storage volume is very limited in order not to lower the OSDE.

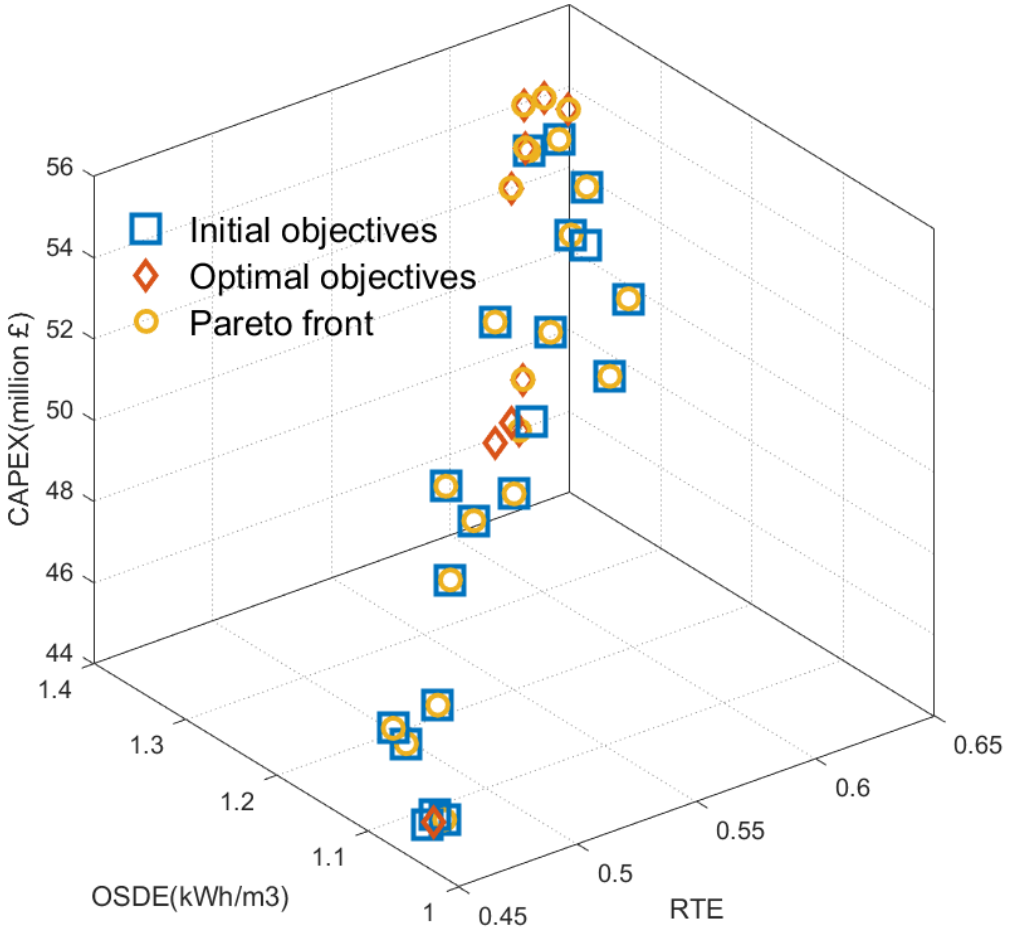

Figure 3.18. The optimal Pareto front of three-objective optimization

Table 3.7. The optimal design and operational parameters of three-objective optimization

RTE	CAPEX/ million	OSDE (kWh/m^3)	Charging pressure (MPa)	Discharging pressure (MPa)
0.48	46.30	1.11	13.60	12.52
0.54	49.31	1.18	13.14	11.67
0.58	51.55	1.24	12.01	13.58
0.61	55.24	1.34	15.94	14.32
Inlet T of cold box (K)	Outlet T of cold box (K)	V_hot/m^3	V_cold/m^3	V_LAES/m^3
221.57	132.96	14680.00	7705.00	3860.00
222.42	125.17	14668.08	8474.60	4204.42

210.66	122.68	14521.80	8624.67	4341.13
225.66	107.63	15088.67	9425.49	4824.93

3.5 Summary

This part of work conducted the parametric study and thermo-economic multi-objective optimization of a stand-alone LAES system, the major contributions and conclusions were drawn as the followings:

a. After the Single-objective optimization of a three-stage LAES system, the optimal design and operation variables were derived, including the optimal charging pressure (~15 MPa) and discharging pressure (~11.5 MPa), as well as the optimal inlet (~218 K) and outlet temperature (~105 K) of air-propane cold box. These parameters can further indicate the optimal heat transfer areas of coolers, heaters, cold boxes and evaporators, as well as the optimum mass flow rates of propane, methanol and thermal oil. The RTE can be optimized by 7%~14% to be ~61%.

b. After the sensitivity optimization, it indicated that a LAES system with three-stage compressor and four-stage expander performs better than three-stage and four-stage LAES systems. The RTE of three-four stage system can be optimized from ~57.5% to ~63%. LAES systems with different machine efficiencies and heat transfer performance need different optimal design and operating parameters. The overall guideline is: the system with lower machine efficiencies works well with lower charging and discharging pressure, but the system with worse heat transfer performance of heat exchangers need higher charging pressure and lower discharging pressure.

c. The two-objective and three-objective optimization of the LAES presented the Pareto Front of RTE, CAPEX and OSED. It indicated that more capital investment can lead to higher RTE, NPV and OSED. The investment budget should be on different LAES systems and configurations should be tailored depending on different investment budgets. For example, a

LAES system with three-stage compressor and four-stage expander can obtain better RTE and NPV if over 48 million £ of investment budget is allowed.

4 The dynamic analysis of Liquid air energy storage integrated with wind power

4.1 Introduction

4.1.1 Literature review

4.1.1.1 Dynamic analysis of LAES without control strategy

Several researchers have investigated the transient behaviours of packed-bed thermal storage in LAES plants, while other components' models were all in steady-state. The results from Sciacovelli et al. [44] indicated that the specific liquefaction work increased by ~25% due to the increasing cold end temperature of the packed-bed cold storage, but the specific expansion work was not affected obviously by the bed transient behavior. In consequence, the RTE changed from cycle to cycle, reaching ~48% after ~20 cycles and keeping constant after the steady-state inside the packed bed was established. Legrand et al. [111] investigated the effects of the transient behavior of packed-bed cold storage on the liquid yield ratio and pressure drop of a LAES system. The results indicated that the liquid yield ratio decreased dramatically but the pressure drop increased after 6~8 hours of charging.

Guo et al. [223] studied the dynamic characteristics of a two-stage packed-bed in a LAES system after multiple cycles. It considered the intermittent period between the charging and discharging processes, as well as the inevitable cold energy loss. The results indicated that the RTE of the LAES was lower than that of ideal cycle (without dynamics and cold exergy loss) by 16.8%. Wang et al. [224] evaluated the effects of dynamic performance of hot and cold packed-beds on a LAES system from start-up period to steady-state operation. The results concluded that the average liquid air yield increased from 0.23 (start-up) to 0.56 (steady-state), the RTE reached ~42.8% and a combined heat and power efficiency reached ~82.1%. However,

a complete dynamic system model should have time-dependent and dynamic sub-models of its all components, in order to study the transient performance of the system and to develop dynamic control strategy, which cannot be achieved by steady-state modelling.

4.1.1.2 Dynamic analysis of LAES with control strategy

Several researchers have worked on studying and developing the control strategy of LAES systems based on the full dynamic models. Guo et al. [225] developed a comprehensive dynamic model for a supercritical-CAES system (SC-CAES), in which the volume effect and thermal inertia were considered to study the transient performance and control methods. The results showed the different transient impacts of volume effect and thermal inertia of components. A 10% of load step-down method and a combined control model were proposed to achieve shorter load balance time and smaller dynamic overshoot.

Cui et al. [226] developed the modular dynamic model of the LAES discharging unit, which considered the performance characteristics of key components and dynamic changes of thermodynamic parameters. The control strategy design and the sensitivity analysis of rotor speed rising rate, as well as the frequency disturbance test can help expand the understanding of LAES systems and provide more practical application guidance. The same authors [227] have developed a dynamic model of a 12.5 MW LAES system as well. The dynamic simulation of different operating conditions of the LAES discharging unit can help develop the control schemes for the start-up process and the primary frequency regulation. Lu et al. [228] studied the impacts of rotor time constant and valve closing time on the rotor speed and shutdown time of the LAES discharging unit. It is recommended that the rotor time constant should be less that 7s, the closing time of the control valve should not exceed 1.5s, to meet the safety requirements of the system.

4.1.2 Research aim

From the literature review above, it found that few researchers have paid attention to the dynamic analysis of LAES, which is crucial to understand its practical operational behaviour and control strategy. Meanwhile, the dynamic characteristic of an LAES system when integrated with renewable energy is important to smooth the renewable power output and improve the stability of power grid, but such kind of analysis is currently unavailable. Thus, this part of work contributes to the dynamic studies of LAES, with a particular focus on investigating its dynamic characteristics when it is integrated with wind power. In order to achieve this, the major issues addressed by this work are presented as the following three parts: a) The component- and system-level dynamic models of a LAES discharging unit, as well as a proper control strategy were established, to capture and understand its transient behaviours when wind power fluctuates with time, to improve the dynamic performance of LAES. b) The wind power curve was decomposed into the components varying at different time scales and frequency bands which were fed to the storage systems with different response speeds, in order to identify the response time of LAES, to smooth and compensate the fluctuations of wind power properly. c) The economic comparison among the distributed LAES system with different battery technologies was conducted to identify the most practical and economical storage combination to respond to the fluctuating wind power.

The structure of this part of work is: section 4.2 presents the distributed LAES system and its layout. *Section 4.3* introduces the component dynamic mathematical models and validation results. *Section 4.4* introduces the case study and methodology. *Section 4.5* presents the major results and discussions. The conclusion is made in *section 4.6*.

4.2 LAES system description

A whole LAES system is represented in Figure 4.1. It is composed of three major sub-systems [17]: a liquefaction unit, a storage unit and a power recovery unit. However, for small-

scale application scenarios, like for a micro-grid or a distributed energy system, the capital investment on an air liquefaction unit would be very expensive and less efficient. A feasible approach to apply LAES systems into such cases is to introduce the LAES discharging unit, the related components include cryogenic tanks, pump, evaporators, heaters, heat storage units, turbines and generators. The needed liquid air or liquid nitrogen can be produced on-site by the LAES charging unit or can be purchased from market and stored in tanks for system operation. Such a distributed LAES system can help achieve multiple functions, including the energy arbitrage, renewable energy smooth, operating reserve, black-start, and the deferral of transmission capacity etc., providing its technical and economic benefits. In this part of work, it is mainly to discuss the response time, dynamic behaviour and control strategy when the distributed LAES system interacts with wind power from a distributed wind farm.

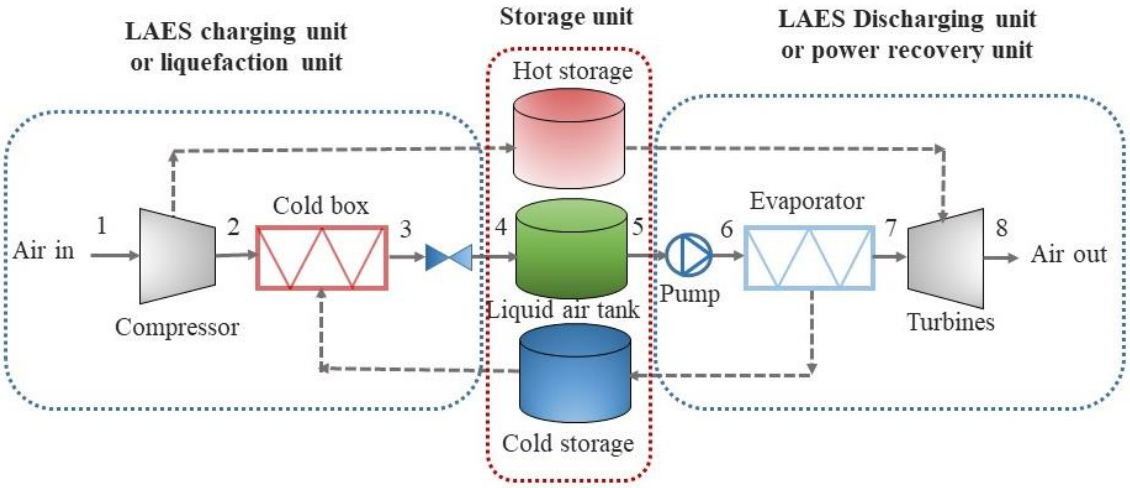

Figure 4.1. Representation of LAES system

4.3 Component dynamic model and validation

4.3.1 Pump model

A reciprocating cryogenic pump is used to pump liquid air from the tank to turbine train. The dynamic model of the pump and assumptions are described as followings [229][230]:

a. The liquid air is non-compressible, there was no heat transfer between pump and ambience. The nominal inlet and discharge pressure kept constant.

b. It was assumed the minimum level of liquid air in tank is enough to keep the reasonable Net positive suction head required (NPSHR).

c. The pump inlet and outlet valves open only depending on the valve pressure difference and spring force, the valve leakage was not considered, the cavitation effect was ignored as well.

The volume flow rate of the cylinder was derived based on Reynolds transport theorem [231], expressed as in eq.(4.1), the inflow and outflow air rate are expressed in eq. (4.2) and eq.(4.3) [232].

$$Q_c = Q_p - Q_{in} + Q_{out} \qquad \text{eq. (4.1)}$$

$$Q_{in} = A_{in} C_{f,in} \sqrt{\frac{2(P_{in} - P_c)}{\rho}} \qquad \text{eq. (4.2)}$$

$$Q_{out} = A_{out} C_{f,out} \sqrt{\frac{2(P_c - P_{out})}{\rho}} \qquad \text{eq. (4.3)}$$

where, Q_c – the cylinder flow rate (m^3/s), Q_p – the piston displacement flow rate (m^3/s), Q_{in} – the valve inflow rate (m^3/s), Q_{out} – the valve outflow rate (m^3/s), A_{in}- the flow area of inlet valve (m^2), A_{out}-the flow area of outlet valve (m^2), P_{in}- the inlet pressure before inlet valve (kPa), P_{out}-the outlet pressure after outlet valve (kPa), ρ – the density of fluid (kg/m^3), P_c- the pressure inside the cylinder (kPa). $C_{f,in}$- the flow coefficient of inlet valve, $C_{f,out}$- the flow coefficient of outlet valve.

The piston displacement x_p, linear speed v_p and cylinder displacement flow rate Q_p are the function of rotating angle θ (rad) or rotating speed ω (r/min, rpm) of crankshaft, they can be expressed as in eq. (4.4), eq.(4.5) and eq.(4.6) [233].

$$x_p = r[(1 - \cos\theta) + \frac{1}{\lambda}\left(1 - \sqrt{1 - \lambda^2 \sin^2\theta}\right)], \qquad \text{eq. (4.4)}$$

$$v_p(\theta) = r\omega(\sin\theta + \frac{\lambda \sin 2\theta}{2\sqrt{1-\lambda^2 \sin^2\theta}}), \quad \text{eq. (4.5)}$$

$$Q_p = \rho \cdot x_p \cdot A_p, \quad \text{eq. (4.6)}$$

where, r – radius of crankshaft (m), λ - radius and length ratio of crankshaft, A_p – piston area (m^2).

The pressure and enthalpy inside cylinder can be obtained from eq.(4.7) and eq.(4.8) [232,234].

$$\frac{dP_c}{dt} = -\frac{\beta}{V_p}\frac{dV}{dt} = -\frac{\beta}{V_p}Q_{in} = -\frac{\beta}{V_p}(Q_p - \sum(Q_{in} - Q_{out})), \quad \text{eq. (4.7)}$$

$$\frac{d(mu)}{dt} = \dot{Q} + \dot{W} + \dot{m_{in}}h_{in} - \dot{m_{out}}h_c, \quad \text{eq. (4.8)}$$

where, β – fluid bulk Modulus of Elasticity (Pa, N/m^2), the bulk modulus constant of liquid air is $2.5*10^9$ Pa, V_p – the volume of cylinder (m^3), u – the thermodynamic energy (J/kg), $\dot{Q}$- heat rate (W), $\dot{W}$ – power rate (W), $\dot{m}$– mass flow rate (kg/s), h - enthalpy (J/kg.K). Subscripts, *in* – inlet, *out* – outlet.

The pump model has been validated based on the pump input data and results given by Kim et al. [232]. The pressure variation curve (Figure 4.2 (a)), the mass flow rate varying with time (Figure 4.2 (b)), and the relationship of mass flow rate with pump pressure (Figure 4.2 (c)) and rotating speed (Figure 4.2 (d)) are shown as followings. It shows that mass flow rate is linearly correlated with pump speed (Figure 4.2 (d)), but is independent of the pump outlet pressure (Figure 4.2 (c)), it is due to the flow characteristics of reciprocating pump [235].

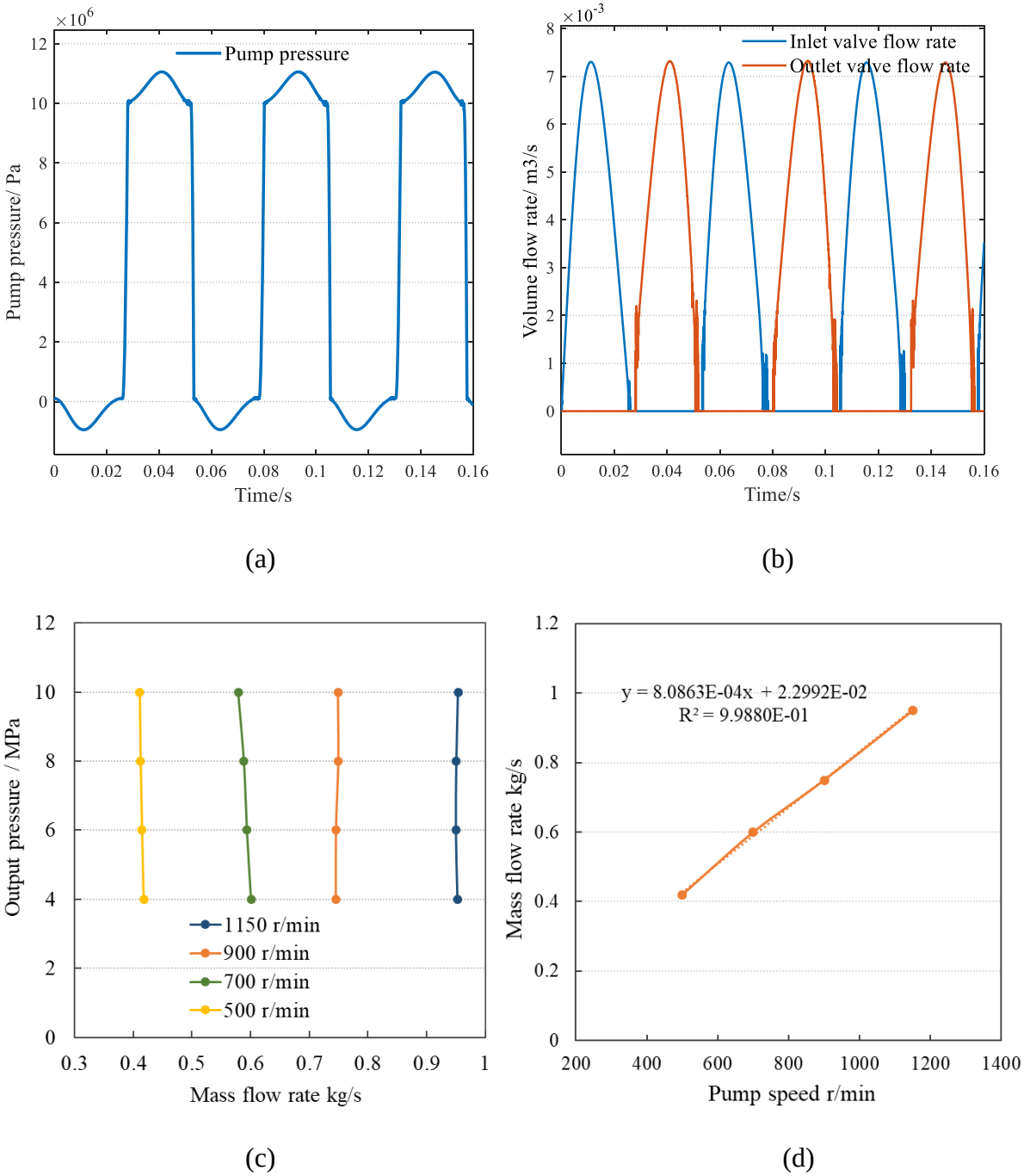

Figure 4.2. The pump pressure and mass flow rate validation curve

4.3.2 Turbine model

The stored liquid air is drawn from tanks to expand through multi-stage turbines to produce power. The off-design turbine model is built based on the thermodynamics, which is used in system Simulink model to determine outlet parameters at different time points. The

inlet temperature (T_{in}) and pressure (P_{in}), as well as the turbine speed (N_{Tr}) and mass flow rate (m_{Tr}) are all known. The output parameters are outlet temperature (T_{out}) and pressure (P_{out}), the efficiency (η_{Tr}) and expansion ratio β_{Tr}, the output power (W_{Tr}) and torque (T_{Tr}).

The operation of each turbine is described by the reduced characterized performance parameters [236] and Flugel formula [237], shown as in eq. (4.9) - eq. (4.15).

$$\dot{W_{Tr}} = \dot{m_{Tr}}(h_{Tr,out} - h_{Tr,in}) \quad \text{eq. (4.9)}$$

$$\frac{\eta_{Tr}}{\eta_{Tr,0}} = (1 - t(1 - n'_{Tr})^2)\frac{N'_{Tr}}{G'_{Tr}}\left(2 - \frac{N'_{Tr}}{G'_{Tr}}\right) \quad \text{eq. (4.10)}$$

$$N'_{Tr} = \frac{\bar{N}_{Tr}}{\overline{N_{Tr.0}}} \quad \text{eq. (4.11)}$$

$$\bar{N}_{Tr} = \frac{N_{Tr}}{\sqrt{T_{Tr,in}}} \quad \text{eq. (4.12)}$$

$$G'_{Tr} = \frac{\overline{\dot{m}_{Tr}}}{\overline{\dot{m}_{Tr,0}}} \quad \text{eq. (4.13)}$$

$$\overline{\dot{m}_{Tr}} = \frac{\dot{m_{Tr}}\sqrt{T_{Tr,in}}}{P_{Tr,in}} \quad \text{eq. (4.14)}$$

$$\frac{\dot{m}_{Tr}}{\dot{m}_{Tr,0}} = \alpha\sqrt{\frac{T_{in,0}}{T_{in}}}\sqrt{\frac{{\beta_{Tr}}^2 - 1}{{\beta_{Tr,0}}^2 - 1}} \quad \text{eq. (4.15)}$$

where, the subscripts *0* – the design/initial state, *Tr* – expansion turbine, the superscripts ‘’‘ means the normalized parameters, ‘-’ means the reduced parameters. Symbols W- the power output (W), $\dot{m}$ – the mass flow rate (kg/s), T- the temperature (K), η- the isentropic efficiency, *P* – pressure (kPa), *RP* – the pressure ratio, *RM* – the mass flow rate ratio, β- the expansion ratio, *N* – the turbine speed (rpm). The rated speed of turbine is 3000 r/min. Constant *t* is 0.3 [236].

The turbine performance characteristic map was plotted in Figure 4.3. It is used to obtain the thermodynamic parameters of turbine under off-design conditions.

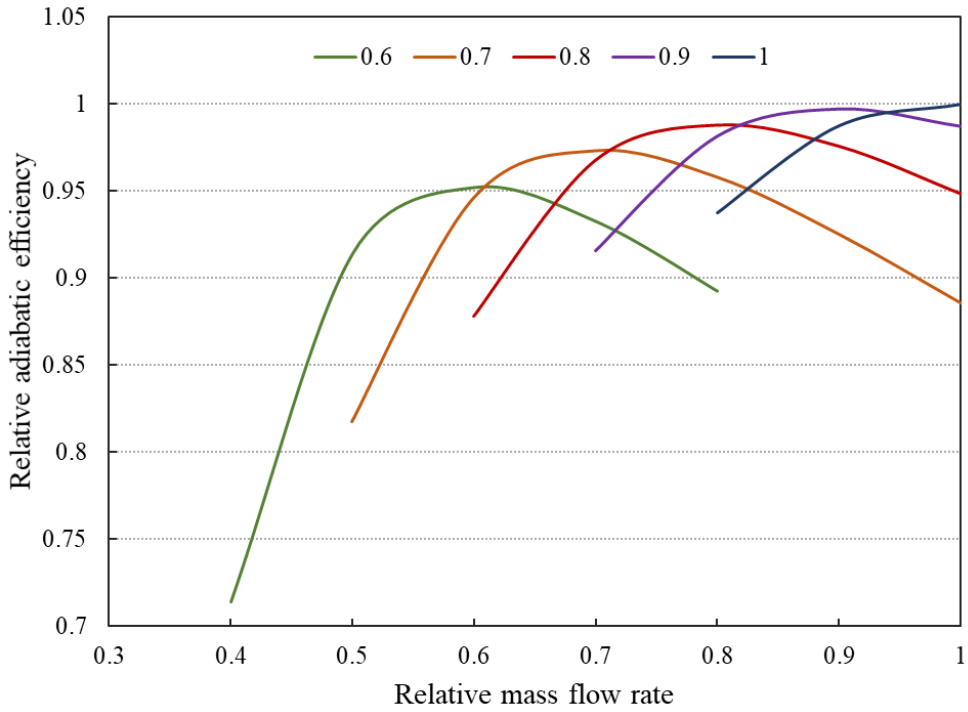

Figure 4.3. The performance characteristic map of turbine under different speed ratio

4.3.3 Packed-bed model

For high-grade cold storage, based on heat transfer governing equation derived from energy conservation and Fourier's law, one-dimensional differential energy balances were built for the packed-bed and liquid air, which cover the energy change rate, flow convection, conduction heat transfer, convective heat transfer between two media, shown as in eq. (4.16) - eq. (4.18), several assumptions were made as followings [44,111].

a. The dynamic performance was only dependent on time *t* and coordinate *x*, the wall effect was neglected. The heat transfer between packed-bed shell and ambience was neglected.

b. Packed bed was assumed with mono-dispersed particles and homogeneous distribution. The temperature was distributed uniformly in particles.

c. The heat conduction of liquid in flow direction was ignored. The liquid air is incompressible, the tracked mass in solid bed was not considered.

$$\rho_s C_{ps} \frac{\partial T_s}{\partial t} = \lambda_s \frac{\partial^2 T_s}{\partial x^2} + \frac{\alpha h_{eff}}{1-\varepsilon} (T_f - T_s), \qquad \text{eq. (4.16)}$$

$$\rho_f \frac{\partial(C_{pf}T_f)}{\partial t} + \rho_f u_x \frac{\partial(C_{pf}T_f)}{\partial x} = \frac{\alpha h_{eff}}{\varepsilon}(T_s - T_f), \quad \text{eq. (4.17)}$$

$$\frac{\partial(\rho_f)}{\partial t} + \frac{\partial(\rho_f u_x)}{\partial x} = 0, \quad \text{eq. (4.18)}$$

where, the cylinder height and diameter can be determined by users, the diameter of filling spheres d_{sp} is 0.015m, the void fraction ε is 0.38. The solid material heat capacity C_{ps} is 541 J/kg.K, density ρ_s is 2560 kg/m^3, the thermal conductivity λ_s is 8.99 W/m.K, the bed initial temperature T_s is 288 K. C_{pf}, ρ_f, T_f are specific heat capacity, density and temperature of heat transfer fluid, h_{eff} - the volumetric convective heat transfer coefficient [111], u_x – the air axial velocity, α – the heat exchange surface per unit volume.

The packed-bed model has been validated by the experiment data from pilot LAES plant [44], of which the packed-bed cold store is a 4U-shaped cylinder filled with quartzite rock. The validation result is shown as in Figure 4.4, the validation results deviation was caused by some uncertainties in the experiment, like the void factor estimation or the exact positions of thermocouples.

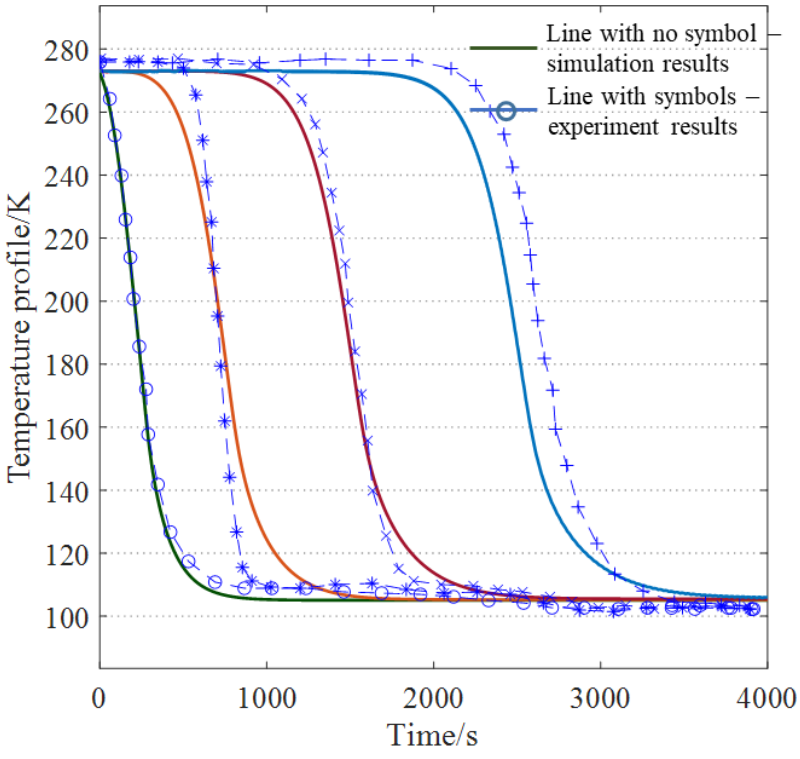

Figure 4.4. Packed-bed model simulation results and validation

4.3.4 Heat exchanger model

A LAES plant involves different heat exchangers for different applications, including the evaporators, coolers and heaters etc., which normally have two counter-flow streams, namely the hot and cold streams exchanging heat inside. The types can be brazed-plate, shell-and-tube or plate-and-plate frame etc. Some assumptions were made before building the model [238].

a. The heat conduction in flow direction and pressure drop were ignored. There was no heat source or sink inside the heat exchangers.

b. A lumped overall heat transfer coefficient was assumed for the convective heat transfer between two fluids.

Based on the assumptions, as well as the energy conservation and Fourier's law, one-dimensional governing heat transfer process is expressed as partial difference equations below eq.(4.19) – eq.(4.20) [239].

$$\rho_c C_{pc}\left(\frac{\partial T_c(x,t)}{\partial t} + v_c \frac{\partial T_c(x,t)}{\partial x}\right) = \frac{U_{hex}A(T_h(x,t) - T_c(x,t))}{V_c}, \qquad \text{eq. (4.19)}$$

$$\rho_h C_{ph}\left(\frac{\partial T_h(x,t)}{\partial t} + v_h \frac{\partial T_h(x,t)}{\partial x}\right) = \frac{U_{hex}A(T_c(x,t) - T_h(x,t))}{V_h}, \qquad \text{eq. (4.20)}$$

where ρ – density (kg/m^3), C_p – specific capacity (kJ/kg), v – specific volume (m^3/kg), A – heat transfer area (m^2), V – heat transfer volume (m^3), U – heat transfer coefficients (W/m^2·K). The subscripts *c* – cold working fluid, *ht* – hot working fluid, *hex* – heat exchanger.

The finite difference method and the first-order up-wind scheme were used to solve the partial differential equations. The overall heat transfer coefficient was estimated based on the empirical data from the work [240].The initial constant inlet temperature and zero-gradient boundary conditions are set as eq. (4.21) and eq. (4.22) for two working fluids [241][239].

$$T_h(x,0) = T_{h0,in},\ T_c(L,0) = T_{c0,in}, \qquad \text{eq. (4.21)}$$

$$\frac{\partial T_c(x,t)}{\partial x}|_{x=0} = 0,\ \frac{\partial T_h(x,t)}{\partial x}|_{x=L} = 0\ , \qquad \text{eq. (4.22)}$$

The heat exchanger model has been validated by the results from the work of Li et al. [241], which is shown in Figure 4.5.

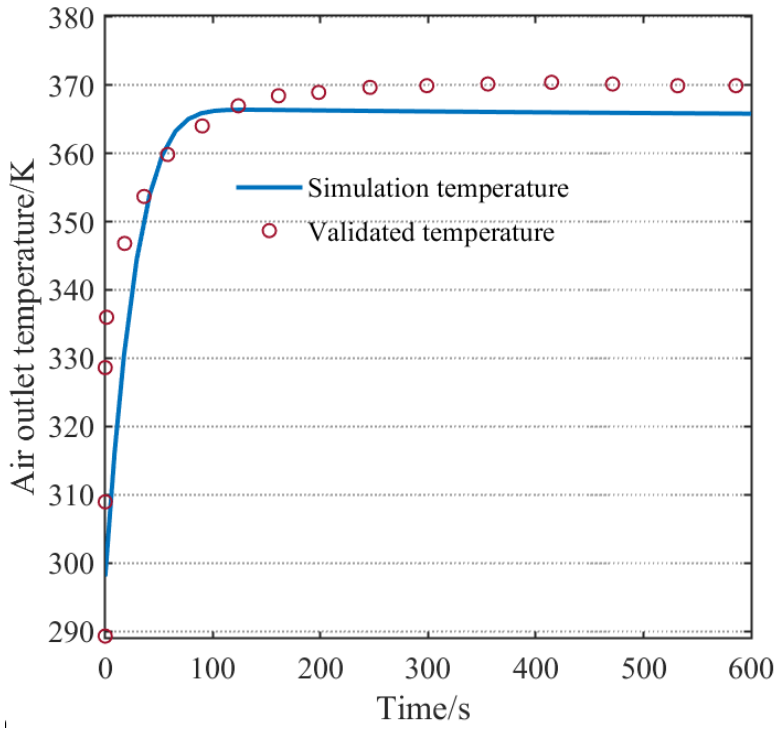

Figure 4.5. The validation results of air outlet temperature of heat exchangers

4.3.5 Liquid air tank model

For liquid air storage tank, it receives liquid air from liquefaction unit and supplies liquid air for expansion. The assumptions were made for LAES tank modelling as followings [241]:

a. No heat source / sink exists in the tank. The pressure change inside the tank was neglected.

b. The tank shape is cylindrical. The minimum liquid air level of tank met the requirement of NPSHA of the cryogenic pump.

The energy balance and the liquid air level change rate in the tank, as well as the related parameters are expressed in eq.(4.23) – eq.(4.26), which referred to the modelling of CAES

tank [241,242]. Figure 4.6 shows the variation of liquid air level for ~50s, it decreases linearly with time when a constant outlet mass flow rate was applied.

$$\rho_{la} V_{la} C_{pla} \frac{\partial T_{la}}{\partial t} = \dot{m}_{la,in} h_{la,in} - \dot{m}_{la,o} h_{la,o} - U_{tk} A_s \cdot (T_{la} - T_{amb}), \quad \text{eq. (4.23)}$$

$$\rho_{la} A_{bm} \frac{\partial H_{la}}{\partial t} = m_{la,in} - m_{la,o}\ , \quad \text{eq. (4.24)}$$

$$H_{la}(t) = H_{la}(t-1) + \frac{\partial H_{la}}{\partial t}, \quad \text{eq. (4.25)}$$

$$H_{min} \leq H_{la} \leq H_{max}, \quad \text{eq. (4.26)}$$

where, symbols: H – liquid air level (m), h – enthalpy (kJ/kg), ρ – density (kg/m^3), V – tank volume (m^3), $\dot{m}$ – mass flow rate (kg/s), U – heat transfer coefficient (W/m^2), T – temperature (K). Subscripts: *la* – liquid air, *tk* – tank, *s* – tank surface, *bm* – bottom, *min* – minimum, *max* – maximum.

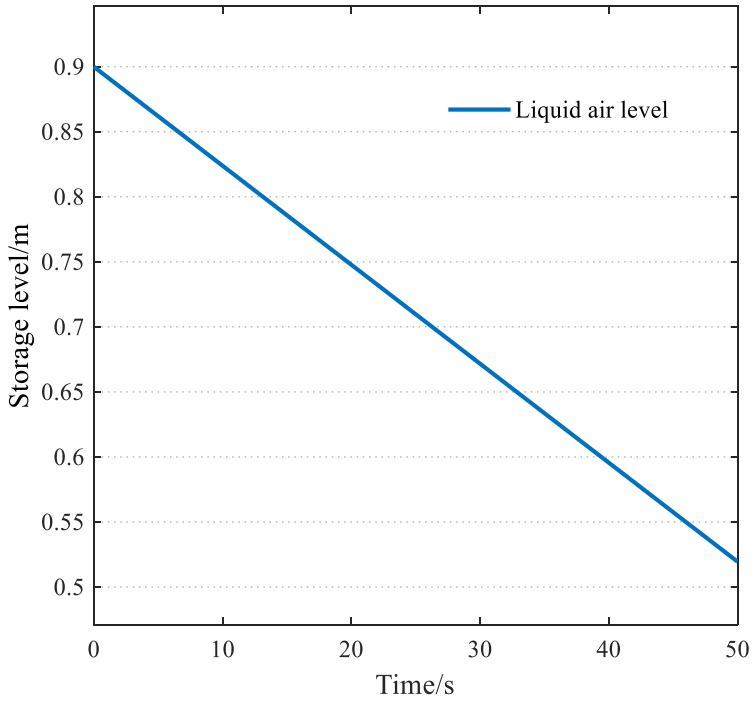

Figure 4.6. The liquid air level in tank

4.3.6 Valve model

The valve is used to regulate the air mass flow rate going through turbines. The pressure drop ΔP and mass flow rate q_m are presented as the non-dimensional relationship with the opening rate φ, the process is isenthalpic (constant h), shown as in eq.(4.27) – eq.(4.29) [243]:

$$q_m = -9 * 10^{-5}\varphi^2 + 0.0199\varphi - 0.0362, \quad \text{eq. (4.27)}$$

$$\Delta P = -3.3057 * 10^{-7}\varphi^3 + 1.5174 * 10^{-4}\varphi^2 - \cdots$$

$$-1.9563 * 10^{-2}\varphi + 1.7828 \quad \text{eq. (4.28)}$$

$$h_{in} = h_{out}, \quad \text{eq. (4.29)}$$

4.3.7 Turbine rotor model

The turbine rotor speed is determined by four factors, they are: the mechanical torque T_m, load torque T_L and friction torque T_f, as well as the moment of inertia *J*. ω (rad/s)/*N* (r/min) is turbine rotor speed. The rotor torque balance equation is shown as in eq. (4.30) – eq. (4.31) [226].

$$J\frac{d\omega}{dt} = T_m - T_L - T_f \quad \text{eq. (4.30)}$$

$$\omega = \frac{2\pi N}{60} \quad \text{eq. (4.31)}$$

4.3.8 System-level validation

The first pilot LAES plant was located in the University of Birmingham, which has a rated power of 350 kW and a rated capacity of 2.5 GWh. The system configuration is shown in Figure 4.7. It consists of a liquid air tank, reciprocating pumps, the packed-bed cold storage, two evaporators, the hot water storage system (temperature 45~65 ℃), heaters and four expansion turbines (inlet pressure ~56 bar) [41]. The plant tests have been conducted to study the system performance and dynamic behaviour, the results obtained from the tests have been validated by the dynamic model in this work.

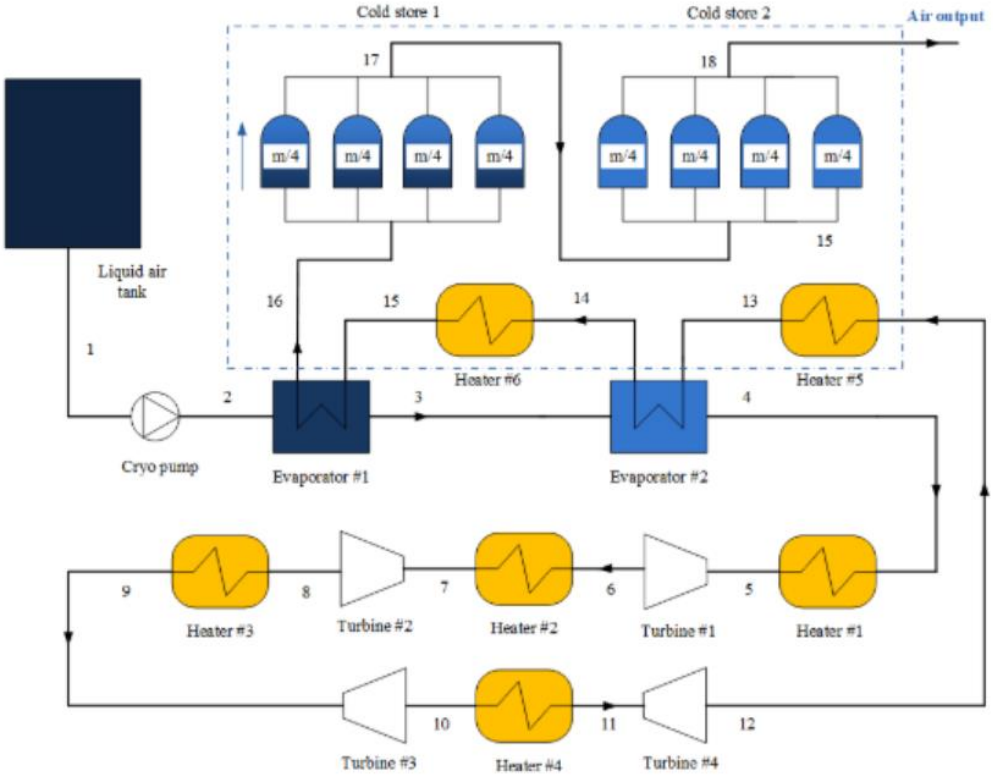

Figure 4.7. The first pilot LAES plant configuration [41]

4.3.8.1 Thermodynamic states validation

The key thermodynamic states of LAES system during the tests and simulation were compared, shown as in Table 4.1. The power output of the model at steady state is 299.08 kW (error 4.7%) when the mass flow rate is 1.6 kg/s. The temperature relative differences come from the coarse estimation of heat exchangers sizes. The pressure differences come from the simplicity of the model which does not consider the pressure drops before turbines. The results can confirm the validity of system model with around 0.2% - 5% of error differences [221].

Table 4.1. The comparison of thermodynamic states of LAES plants [244]

Thermodynamic states (Figure 4.7)	Tests/Simulation Temperature (K)	Temperature error (%)	Tests/Simulation Pressure (bar)
2	103/103	0	56/52
3	164.1/171.3	4.4%	56/52

4	216.2/215.7	0.2%	56/52
5	337.2/339	0.5%	51/51.6
6	298.2/293	1.7%	25/24.8
16	107.3/113	5.3%	1/1

4.3.8.2 The system response time validation

Based on the test result of the response time of the LAES pilot plant, this work divides the start-up process into two stages [41]. During 0-30s, turbine starts to increase its speed to the rated value (3000 r/min) without external load added. During 30-120s, turbines transfer mechanical torque to generator to output power. The simulation power curve (Figure 4.8) shows the turbine power varying with time, it increases to around 35 kW during 0-30s, and then decreases to ~0 to keep the turbine speed constant at 3000 r/min (constrained by the power swing equation [226]), as the generator load was added from zero at 30s. After about 130s (compared to ~120s for test results), the turbine power increases to the maximum value (the rated generator load power) and keeps constant after then. The whole simulation curve is nearly in consistent with the tested generator power curve after 30s, while the difference exists before 30s, it is due to two curves were observed from different views, the simulation curve was viewed from turbine rotor side, the tested curve was viewed from the generator side.

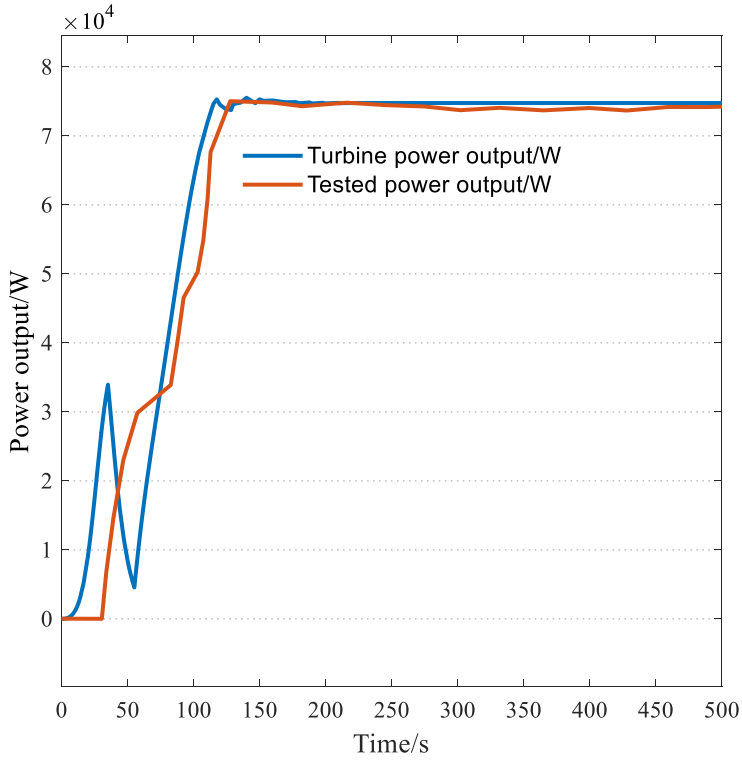

Figure 4.8. Power time response characteristics of LAES discharging model

4.4 Case study and methodology

4.4.1 Case study

LAES is an energy storage system which can be used to integrate with renewable energy, like wind power. However, wind power is fluctuating and intermittent, featuring multi-scale time and frequency components. Thus, it is necessary to discuss the time response characteristics of LAES when interacting with wind power, to find the feasible storage system to help absorb, compensate and smooth the fluctuating wind power, reducing its impacts on the stability and reliability of power grid.

A wind power curve was obtained from a small-scale distributed wind farm in China (CITIC Pacific Jiangyin Taineng Wind Power Co., Ltd.). The data was collected in seconds, shown as in Figure 4.9. The rated power capacity of the wind farm is 2MW, the average wind capacity factor is 0.35. It is assumed that the wind farm is equipped with a storage system to help deal with the power dispatch command. Another assumption is made to facilitate the

technical and economic analysis: two power commands are required by the system operator, a constant peak power at 1 MW and a constant off-peak power at 400 kW. When wind power is higher than the commanded power at off-peak period, the excess power is stored in LAES through the charging unit, but this study will not discuss the charging characteristics. When wind power is less than the commanded power at peak period, the rest needed power should be provided and compensated by the storage system, the dynamic behaviour of the LAES discharging unit will be discussed in *section 4.5.1*. The techno-economic analysis results can be applied to more general cases.

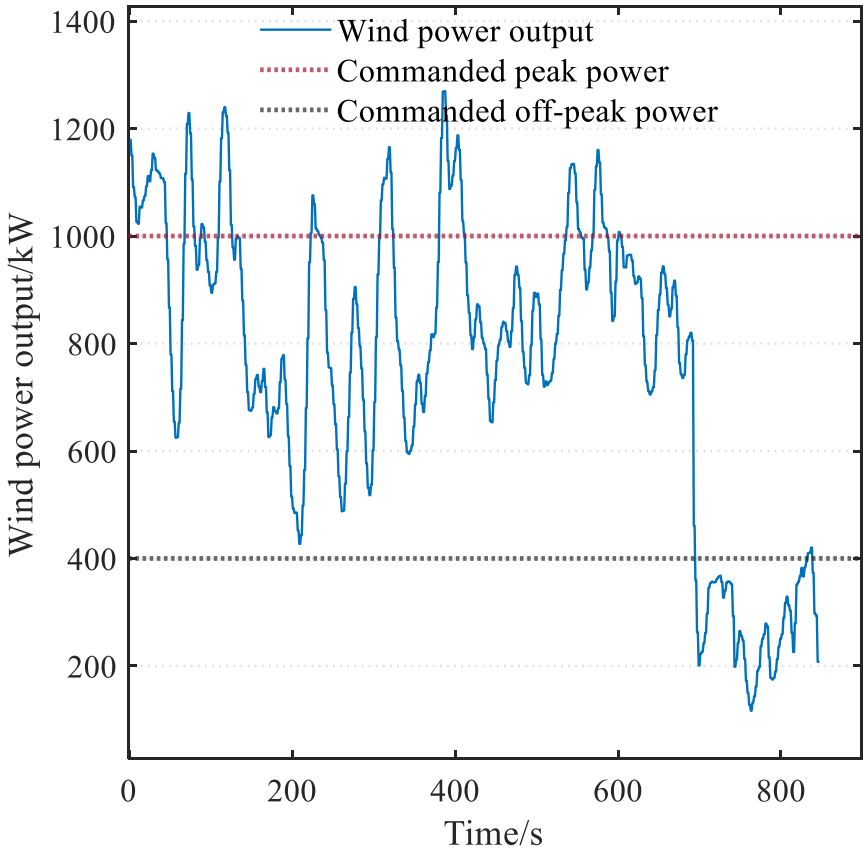

Figure 4.9. The original wind power curve

4.4.2 Methodology

For the LAES discharging unit, the pump provides liquid air for turbines to achieve expansion and power output, the pump can work under constant-speed or varying-speed modes, the discharging unit has four operation modes in practical way, they are the start-up process,

the steady-state operation, the idle operation and the shut-down period. During the start-up process, turbines slowly increase the speed to the rated value without connecting to a generator, in order to gradually increase the temperature of air flow and turbine casting [239]. Then turbines are connected with generators and the external torque is loaded if the inlet conditions of turbines are acceptable, the system is adjusted and goes into the steady-state mode. During the whole process, the PID controller is activated to adjust the opening rate of the regulating valve, changing the mass flow rate of air injected into turbines and power output to respond to the varying external load [227]. The control strategy is shown as in Figure 4.10.

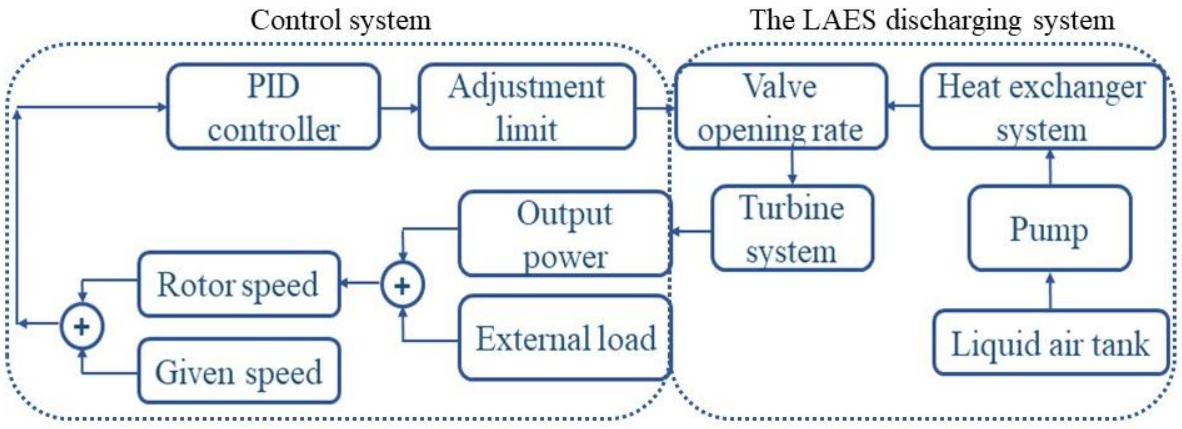

Figure 4.10. The control strategy of LAES discharging unit

Considering the multi-scale time components existing in wind power, a decomposition method is needed to split the original power signal into different time scales, or frequency bands. In this study, the empirical wavelet transform technique is adopted due to its fast computation and high accuracy [245], the spectrum segmentation and wavelet transform coefficients were applied to decompose the energy of the input signal into different time scales or frequency bands. Based on different time response characteristics of storage systems, the split signals can be reconstructed into different time-scale components for storage systems to respond, absorbing or compensating the power components.

4.5 Results & discussion

4.5.1 Wind power decomposition and storage response

Based on the methodology in *section 4.4.2*, the wind power curve was first decomposed into different components (components with 5~7 different frequency bands). They were then reconstructed into two power signals at different time scales which were fed to storage systems. The four decomposition schemes of wind power curve were listed in Table 4.2. The detailed discussion were introduced in *section 4.5.1.1 – 4.5.1.4*. This section only discuss the dynamic behaviour of LAES discharging units when a 1MW of power command is made at peak time. The first power signal was input into the controller of the LAES discharging unit as the external load. The power tracking error is defined as the difference between the external load signal and the actual power output of LAES. Both the power tracking error and the turbine motor speed of LAES were observed and compared, to obtain the time response characteristic of the LAES discharging unit. The second power signal was fed into another fast-speed storage system depending on its time scale.

Table 4.2. The four decomposition schemes of wind power curve

Wind power decomposition scheme	The first power component (energy content and frequency)	The second power component (energy content and frequency)
1	~99.7%, 0-0.03 Hz	~0.3%, 0.03-0.5 Hz
2	~97.9%, 0-0.016 Hz	~2.1%, 0.016-0.5 Hz
3	~96.4%, 0-0.008 Hz	~3.6%, 0.008-0.5 Hz
4	~95.06%, 0-0.00375 Hz	~4.94%, 0.00375-0.5 Hz

4.5.1.1 The first decomposition scheme and discussion

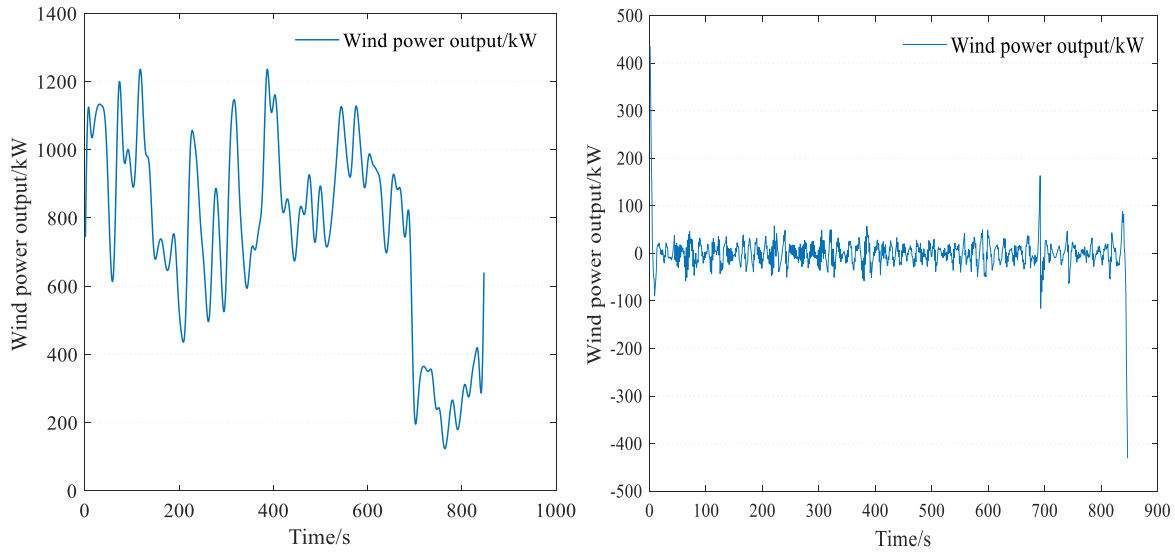

(a) **(b)**

Figure 4.11. The 1st decomposition scheme of the wind power curve: (a) The power signal respond by LAES, (b) The power signal respond by a fast-speed storage

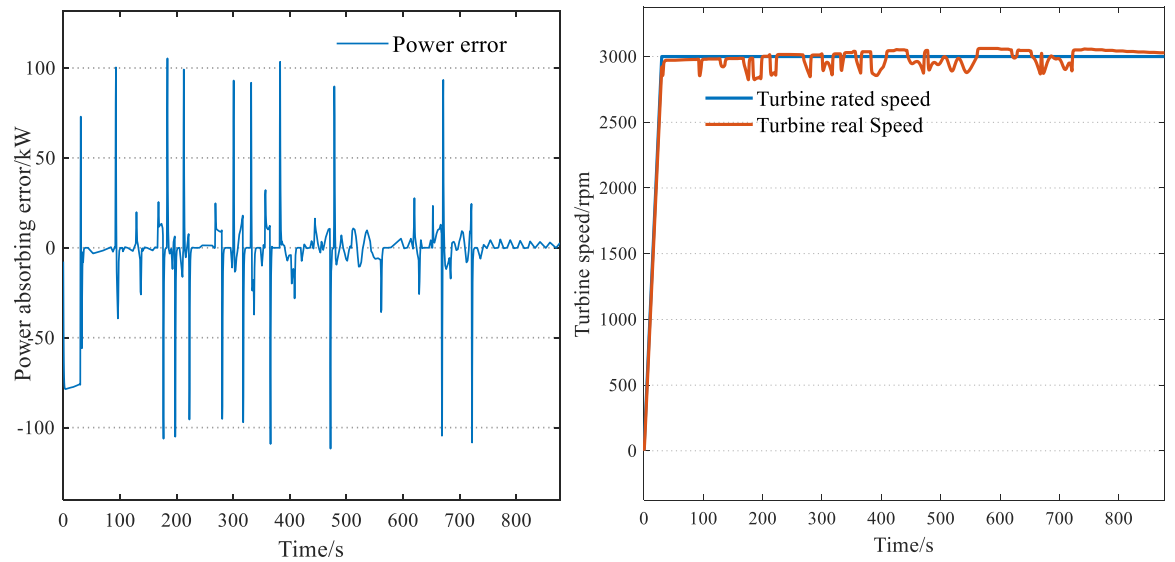

Figure 4.12. The LAES response characteristic to the 1st decomposition scheme: (a) The power tracking error, (b) The rotor speed

From Figure 4.11, the wind power curve was decomposed and then reconstructed into two components, the first one contains ~99.7% of low-frequency energy (0-0.03 Hz), and the second one has ~0.3% of fast-frequency energy (0.03-0.5 Hz) and presents low power magnitude (less than 50 kW). The low-frequency power component was responded by LAES

by inputting an external power signal into the storage system. Figure 4.12 shows the power tracking error and the varying turbine rotor speed of LAES. As shown by Figure 4.12 (a), due to the change of air mass flow through turbines and the large inertia of turbine system, the power output of turbine system cannot follow the corresponding input power signal well, leading to many tracking errors and instant peaks. Meantime, it can be seen from Figure 4.12 (b) that the rotor speed was adjusted very frequently in order to adapt to the varying load curve, which could cause significant mechanical fatigue. Thus, it is concluded that the LAES discharging unit cannot follow the power curve at ~30s time scale, it would lead to the instability of the system and reduce its longevity.

4.5.1.2 The second decomposition scheme and discussion

From Figure 4.13, the wind power curve was decomposed and then reconstructed into the first component containing 97.9% of low-frequency energy (0 Hz-0.016 Hz) and the second component having 2.1% of fast-frequency energy (0.016-0.5 Hz). When the low-frequency power curve was responded by the LAES discharging unit, Figure 4.14 shows the power tracking error and the varying turbine motor speed of the storage system. Compared to the first decomposition scheme and the storage time-response characteristic, the tracking errors and instant peaks (Figure 4.14 (a)) have been reduced but still obviously affect the system power-following accuracy, which is still considered as unacceptable [246], especially when there exist multiple start-up processes, as the start-up time of the unit is about 120 s. Similarly, the frequency of adjusting rotor speed slows down (Figure 4.14 (b)), varying at a ~60s time interval. Thus, it is concluded that the LAES discharging unit cannot follow well the power curve varying at ~60s time scale. But to be noted, the power magnitude of the second wind power component that responded by another fast-speed storage system increases greatly, the peak power is around 300 kW.

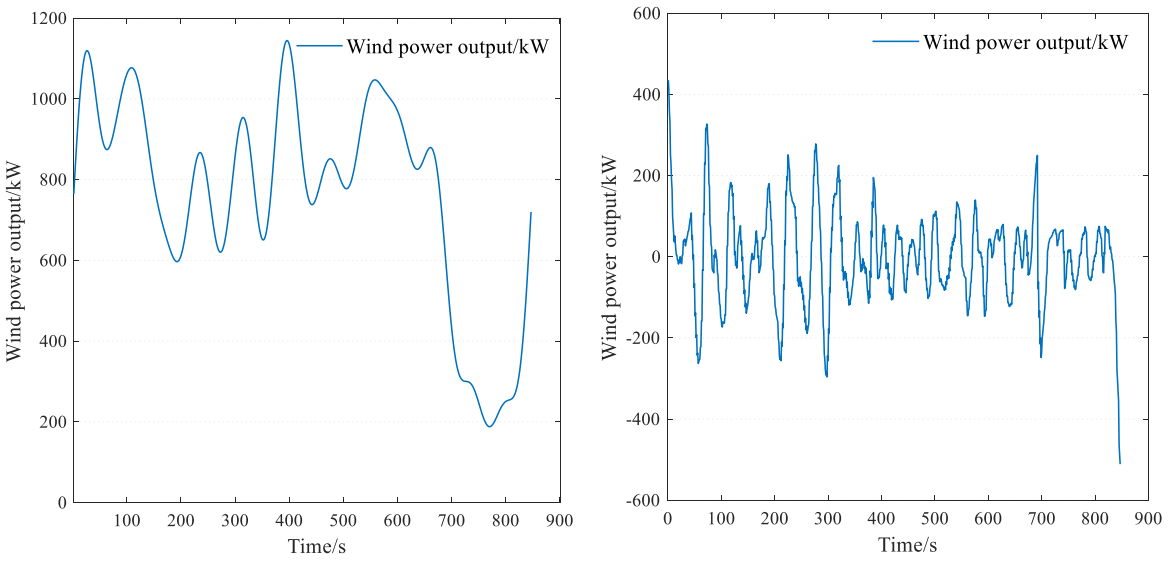

Figure 4.13. The 2nd decomposition scheme of the wind power curve: (a) The power signal respond by LAES, (b) The power signal respond by a fast-speed storage

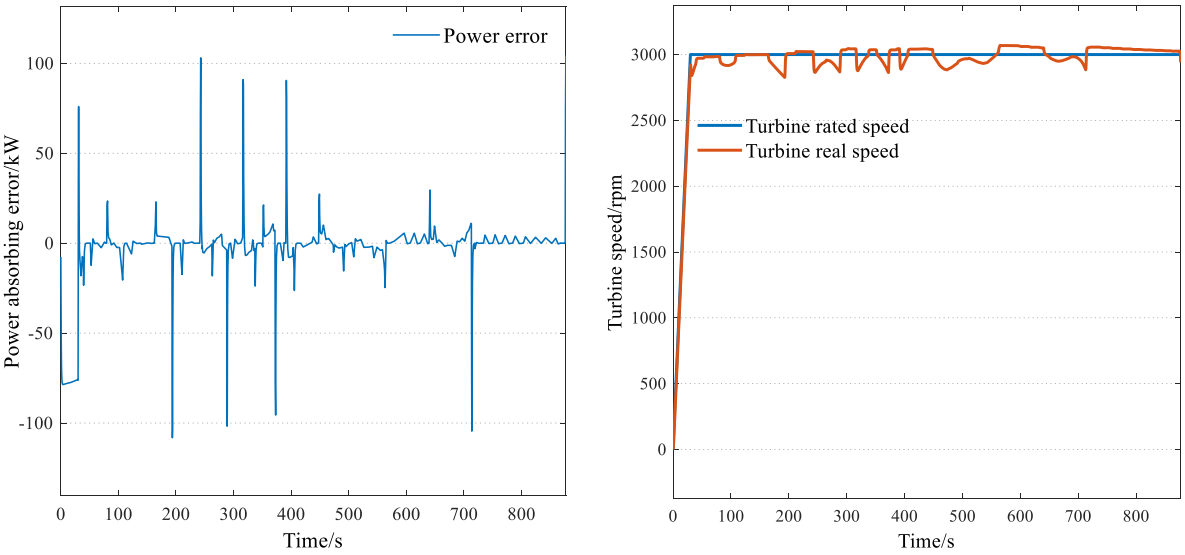

Figure 4.14. LAES time response to the 2nd decomposition scheme: (a) LAES power tracking error, (b) LAES rotor speed

4.5.1.3 The third decomposition scheme and discussion

From Figure 4.15, the wind power curve was decomposed and then reconstructed into the first component containing 96.4% of low-frequency energy (0 Hz – 0.008 Hz) (Figure 4.15(a)) and the second component having 3.6% of fast-frequency energy (0.008-0.5 Hz) (Figure 4.15(b)). Figure 4.16 shows the power tracking error and the varying rotor speed of the LAES discharging unit. The number and magnitude of tracking errors and instant peaks are

reduced remarkably seen from Figure 4.16 (a). The motor speed was controlled and adjusted to be slower and smoother seen from Figure 4.16 (b), which can help reduce the turbine motor fatigue. Thus, it is considered that the LAES discharging unit can follow the power curve at 100~120s time scale with limited minor tracking errors, it is due to that both the change of air mass flow and speed adjustment match well with the corresponding turbine inertia, and can adapt well to external load at such a time scale. Meanwhile, the 2nd wind power component responded by the fast storage system increases further, the peak power is around 400 kW, the maximum storage capacity increases as well.

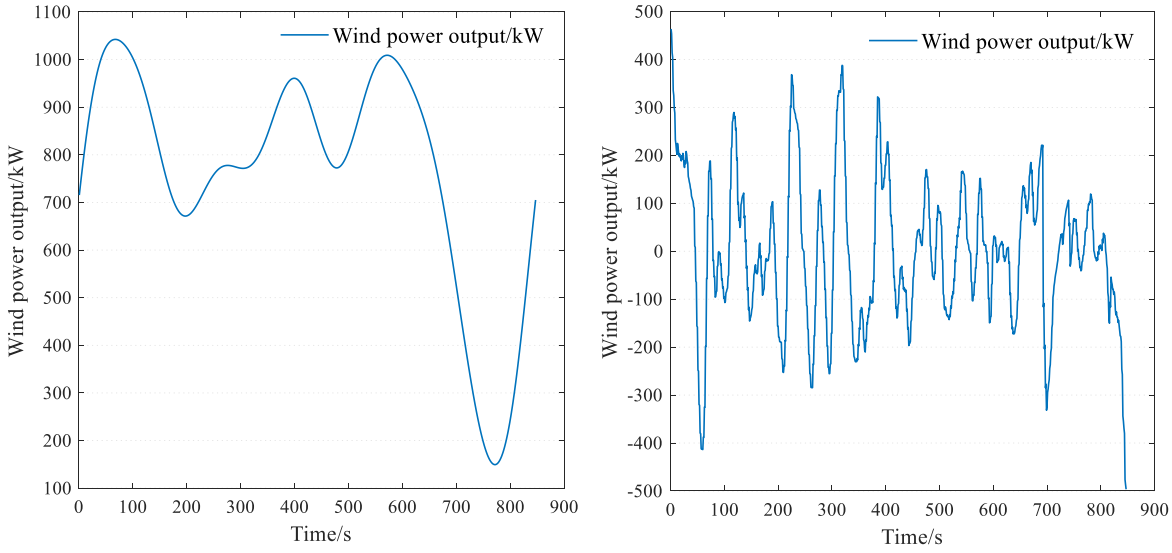

(a) **(b)**

Figure 4.15. The 3rd decomposition scheme of the rest power curve: (a) signal feeds to L AES, (b) signal feeds to fast-speed storage

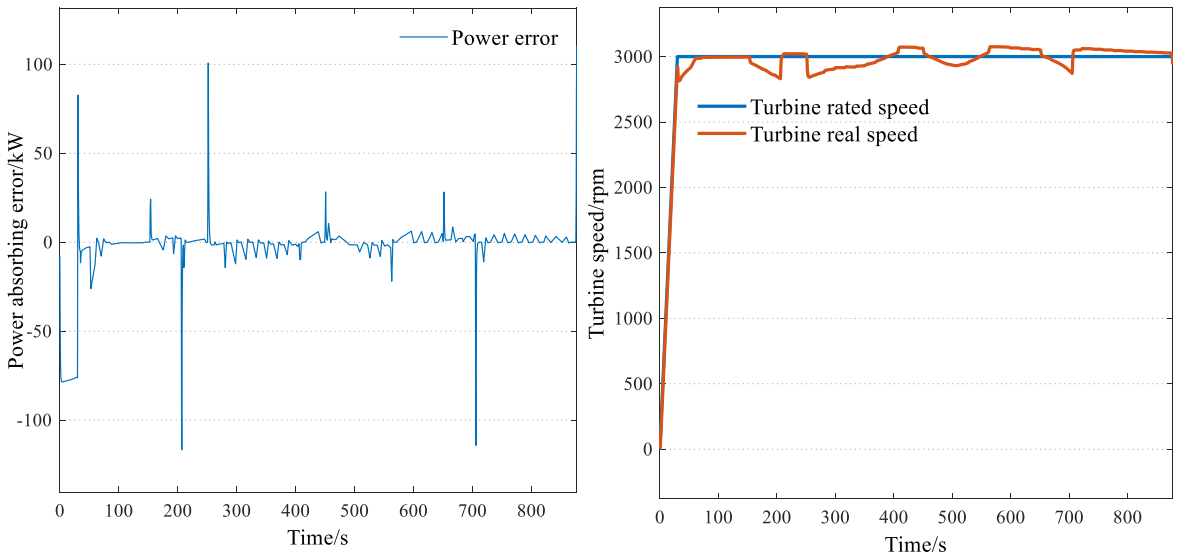

(a) **(b)**

Figure 4.16. LAES time response to the 3rd decomposition scheme: (a) LAES power tracking error, (b) LAES motor speed

4.5.1.4 The fourth decomposition scheme and discussion

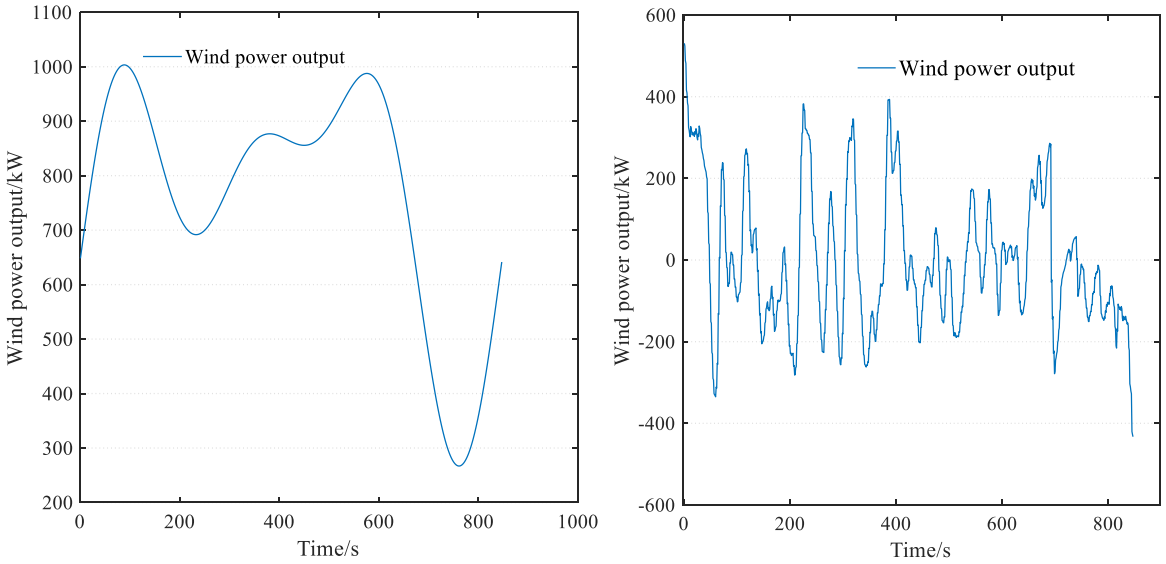

(a) **(b)**

Figure 4.17. The 4th decomposition scheme of the rest power curve: (a) signal feeds to LAES, (b) signal feeds to fast-speed storage

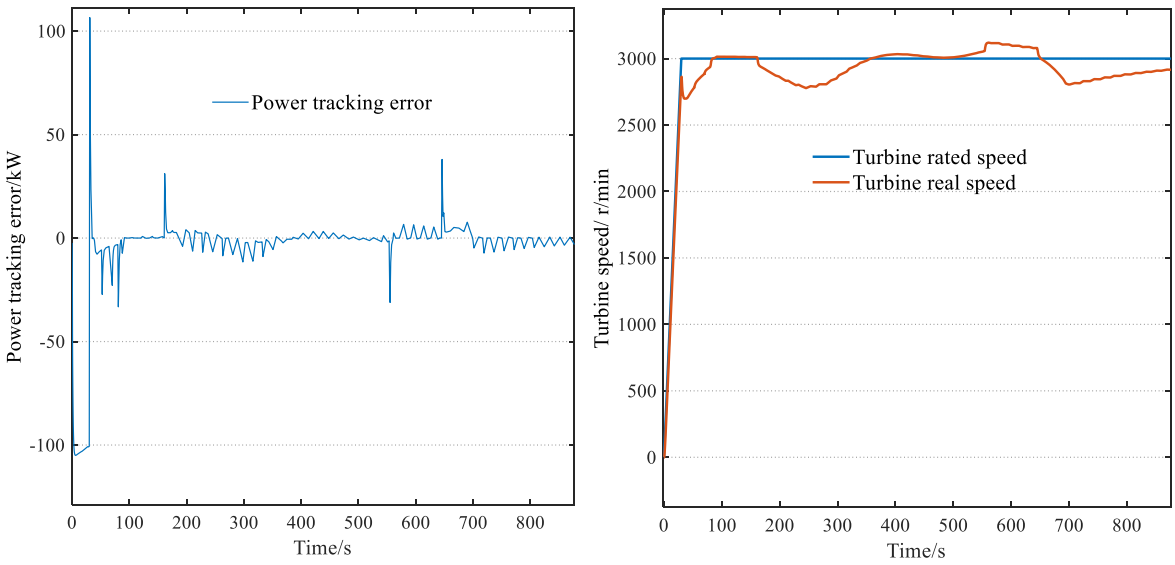

(a) **(b)**

Figure 4.18. LAES time response to the 4th decomposition scheme: (a) LAES power tracking error, (b) LAES rotor speed

Figure 4.17 shows the results when the decomposition time scale of the wind power increases further. The partial energy responded by the LAES (95.06% at 0-0.00375 Hz) is varying at a time scale around 260 s. The part of energy left for a fast storage system (5%) has the peak power at around 450 kW. From Figure 4.18, it can be seen that the tracking errors and instant peaks are almost removed (Figure 4.18 (a)), the existing error peaks are caused by the sudden torque loaded at the start-up process, and the rotor speed can be adjusted more stably and smoothly (Figure 4.18 (b)). Though LAES works more stably and its power following characteristic is more accurate, the peak power and energy capacity of the fast-speed storage increase to 450 kW and 810 kWh, it means higher battery cost as well.

Overall, the first and second decomposition schemes of the wind power curve present high frequencies and small time-scale (< 60s) variations, due to large amount of power tracking errors and instant peaks exist in the LAES response, it is considered that the LAES discharging unit is not suitable for tracking the fast wind power component at time scale less than 60s. The third and fourth decomposition schemes of the wind power curve show smoother variations and lower frequencies. The corresponding power tracking errors and instant peaks of the LAES

response have been reduced remarkably. It is considered that this LAES discharging unit can respond well to the load power at a time scale ~ 120s. Meantime, it also indicated that it needs another fast-speed storage system to respond to the fast wind power component when integrating with wind farms. With the increase of the time-scale of the slow wind power component, the residual power and energy left for the fast-responding storage system are increasing as well. Thus, a combined LAES and fast-speed storage system is needed to achieve a better integration with wind farms, the economic analysis about storage combinations with different response time and power scale was discussed in *section 4.5.2*.

4.5.2 Storage combination scheme and economic comparison

Beside the LAES, battery is adopted to respond to the fast-changing wind power component. Considering different wind power decomposition schemes (as discussed in *section 4.5.1*), different storage combination scenarios (listed in Table 4.3) were proposed to respond to different wind power and energy magnitudes. An economic analysis was conducted to compare different combined storage systems. To facilitate this, it was assumed this piece of wind power curve (800 s) repeats every day in a whole year, a peak power command (1000 kW) is requested at daytime which needs the discharging power from the storage system, an off-peak power command (400 kW) is requested at night which can charge the storage system.

Table 4.3. Different storage system combination and their power and energy capacity

Scenarios	Minimum wind power/kW	Time scale of the fist wind power component	Battery power /kW	LAES power /kW	Charging time per day(h)	Discharging time per day(h)	Running days in a year
Battery	110	\	900	0	12	12	330
LAES1 + Battery1	50	125 s	400	950	12	12	330
LAES2 + Battery2	250	260 s	450	750	12	12	330

From Table 4.3, the first scenario only considered a battery storage to compensate the decrease of wind power, the needed battery power is 900 kW (obtained from Figure 4.9). The second scenario was based on the third wind decomposition scheme (Figure 4.15(b) and Figure 4.16(a)), with the time scale of the first wind power component varying at ~100-120 s, the storage system consists of a 950 kW LAES system and a 400 kW battery system. The third scenario was based on the fourth decomposition scheme (Figure 4.17(b) and Figure 4.18(a)), with the time scale of the first wind power component varying at ~260 s, the storage system consists of a 750 kW LAES system and a 450 kW battery system.

The cost models of LAES subsystems are given in Table 4.4, including the charging unit, discharging unit and storage unit. Various battery technologies commonly used are introduced in Table 4.5 and Table 4.6. The types including lead-acid battery, Li-ion battery and Vanadium redox flow battery were chosen for the economic analysis due to their quick response time, high efficiency and low self-discharge. As the batteries' costs were obtained in 2015, around 50% of cost reduction have been seen by 2021 [247]. The scale learning rate of battery storage technologies was estimated at around 18.5% [248].

Table 4.4. The components cost model of LAES [55,249]

Components	Cost models	Notes
Charging unit	$11406 * (\frac{P_{cha}}{4})^{0.6}$	k$, P_{cha} – charging power, MW
Discharging unit	$5653 * (\frac{P_{dis}}{10})^{0.6}$	k$, P_{dis} – discharging power, MW
Storage unit	$1778 * (\frac{E}{86})^{0.6}$	k$, P_{cha} – stored energy, MWh

The economic analysis and comparison of different storage combinations were conducted considering the annual expenditure, including the amortized capital power and energy cost, as well as the annual operational and maintenance cost and battery replacement cost. The results are shown in Figure 4.19. When the storage system is integrated with a 1 MW

of wind farm (Figure 4.19 (a)), for lead-acid battery, the annual cost of the solely battery case is comparable with another two hybrid storage systems due to the lower power and energy capital cost of this kind of battery. For Li-ion battery and flow battery, the solely battery case presents the highest annual cost, of which the annual costs triple and double those of the ’LAES1+Battery 1’ case (a 950 kW LAES integrated with a 400 kW battery). When the wind farm scale increases to 10 MW (Figure 4.19 (b)), the solely battery scenario is always the highest investment for three kinds of batteries, the cost advantages of another two hybrid storage systemsare more obvious, which are around one third times of that of solely battery case. Compared two hybrid LAES-battery storage systems (’LAES1+Battery 1’ and ‘LAES2+Battery2’) both for 1 MW and 10 MW of wind farms, they present similar cost-effectiveness, but ’LAES1+Battery 1’ case performs better in in terms of its technical advantage, as it presents faster power-following characteristics which match well with the unit start-up time and system inertial.

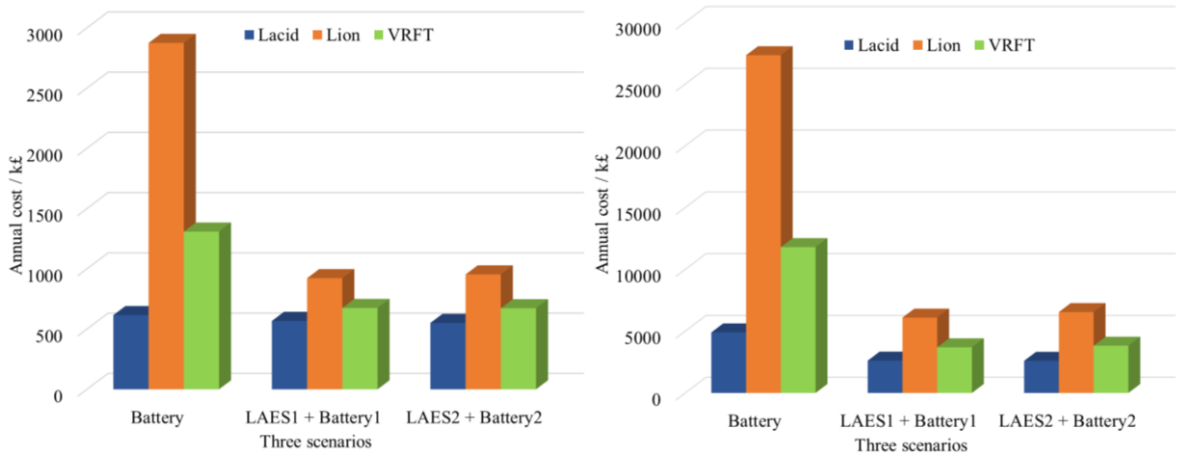

(a) 1 MW wind farm **(b) 10 MW wind farm**

Figure 4.19. The economic comparison of different storage combinations

Table 4.5. The technical details of commonly used batteries [247][250][251]

Battery type	Energy capacity Wh/kg	Power range/MW	Discharge time/ms-h	Overall efficiency	DOD	Self-discharge per day/%	Applications
Lead-acid	30~50	Up to 20	s-h	70% ~ 90%	40% - 50%	0.1~0.3%	Energy time-shift, power quality, UPS, spinning reserve
Na-S	150~230	0.05-8	s-h	75% ~ 85%	30% - 40%	20%	Power time-shift, power quality,
Ni-Cd	~55-75	Up to 40	s-h	60% ~ 73%	10% - 30%	0.2~0.6%	Power quality, emergency reserve
Li-ion	150~350	Up to 10	ms-h	85% ~ 90%	30% - 40%	0.1~0.3%	Frequency regulation, power quality, renewable integration
Vanadium redox flow battery	~10-35	0.03-100	s-10h	65% ~ 85%	0-10%	~0.1%	Peak shaving, renewable integration

Table 4.6. The economic details of commonly used batteries [247][251][252]

Battery type	Power cost $/kW	Energy cost $/kWh	Fixed O&M (€/kW-yr)	Variable O&M (€/kW-yr)	Replacement costs (€/kW)	Life cycles	Expected lifetime
Lead-acid	465	618	3.4	0.37	172	2500	15~20 years
Na-S	366	298	3.6	1.8	180	2500 - 4500	15 years
Ni-Cd	239	780	11	0.6	525	2000-2500	8 years
Li-ion	463	795	6.9	2.1	369	10,000	5~15 years
Vanadium redox flow battery	490	467	8.5	0.9	130	13,000	5~15 years

4.5.3 The dynamic behaviour of LAES with wind farm

From the analysis and comparison in *section 4.5.1* and *section 4.5.2*, the LAES system would be a cost-effectiveness storage option in terms of its response time (~120 s) and investment cost when it serves to compensate the wind power deficiency, the changing trends of key parameters of the LAES discharging unit are presented in Figure 4.20 - Figure 4.22.

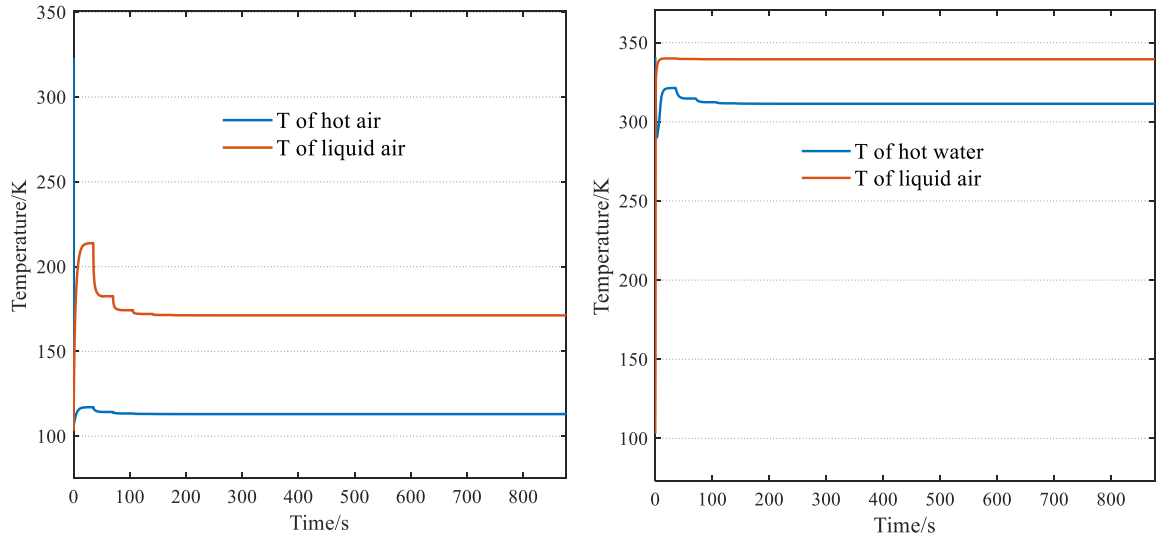

Figure 4.20. Temperature profiles: (a) low-temperature evaporator; (b) re-heaters

Figure 4.20 (a) shows the temperature profile in evaporator. Liquid air is heated by hot air in evaporator, its temperature increases from 103 K to 171.3 K, taking ~120s to reach the steady state due to its large specific heat capacity. But it takes shorter time (~ 70s) for hot air to reach the steady state (113 K) due to its low specific capacity. There is a temperature peak for liquid air, it is due to the large variation in liquid air specific heat capacity (1.8 – 2.9 kJ/kg.K) and density (280 – 870 kg/m^3) at low temperature range (78 K – 188 K), as well as the large initial temperature difference between two fluids, leading to a sudden temperature increase for cold fluid and a decrease for hot fluid. For the temperature profile in re-heater in Figure 4.20 (b), liquid air has turned into gaseous state, its temperature increases quickly to the steady state

(339.5 K). The hot water cools down from 343 K to 311.4 K, its temperature decrease is small due to its large heat capacity (4.2 kJ/kg.K).

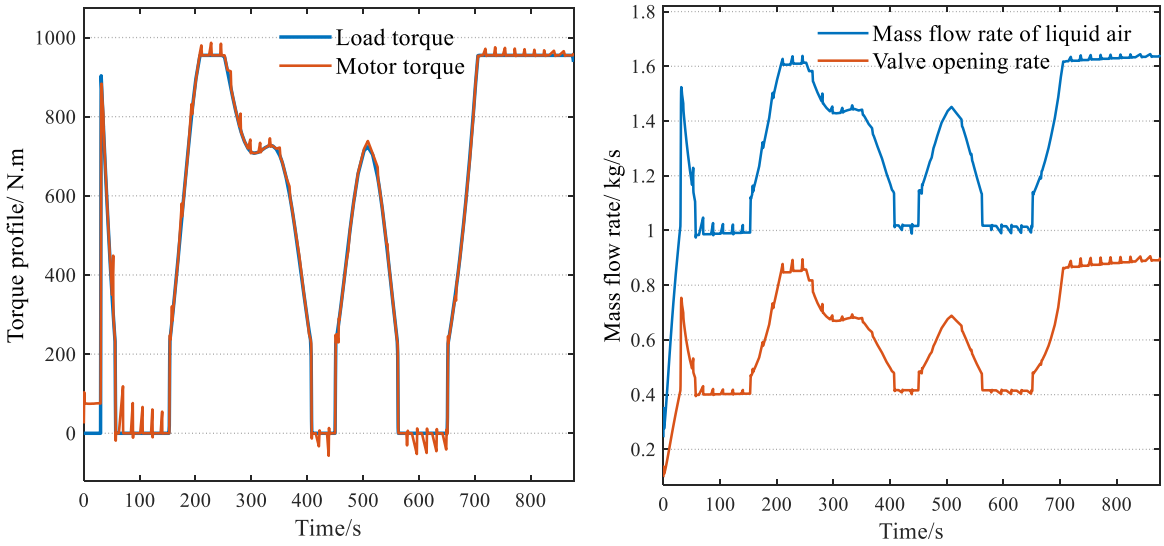

Figure 4.21. The turbine torque and mass flow rate profile: (a) Turbine torque; (b) Air mass flow rate

From Figure 4.21 (a), there is an external load torque signal that is input into the unit controller after the LAES system starts up. In order to keep a constant generator speed, the PID controller delivers the control signal to adjust the opening rate of the inlet valve (0-100%), leading to the variation in air mass flow rate (0-1.6 kg/s) through turbines (Figure 4.21 (b)). Accordingly, the turbine output power and torque are adjusted to follow the input power and torque variation, though there are some tracking errors existing (Figure 4.21 (a)).

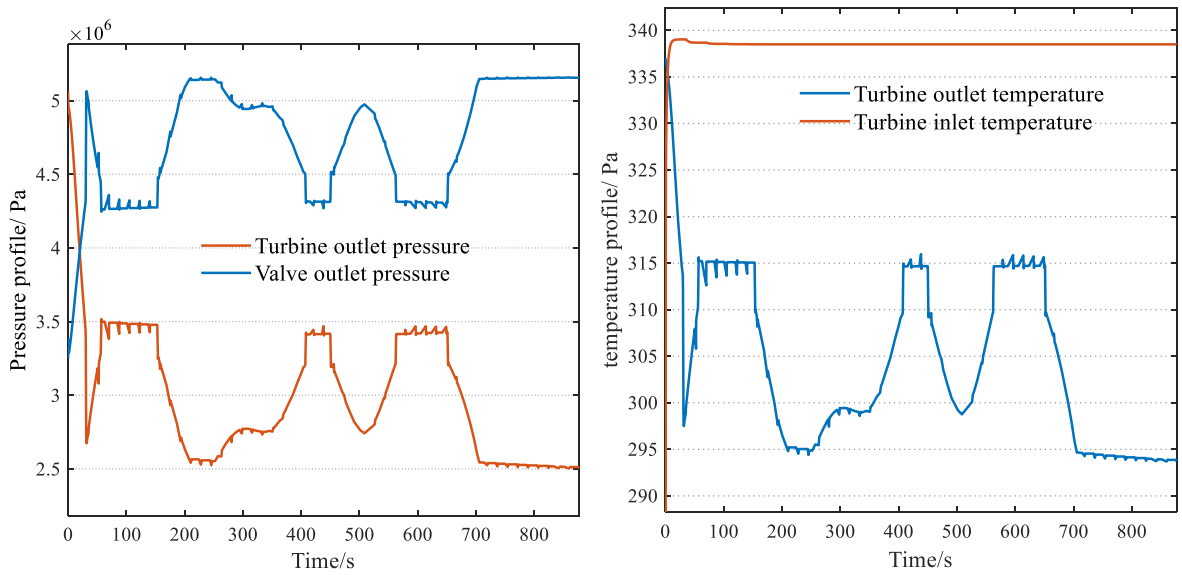

(a)

Figure 4.22. The turbine pressure and temperature profiles: (a) the valve and turbine outlet pressure; (b) the turbine inlet and outlet temperature

Figure 4.22 (a) shows the system pressure variation. For the valve, it is closed at first, the valve outlet pressure increases near to its inlet pressure when it opens, and then decreases to a lower valve when the valve opening rate is reduced. For the turbine, its outlet pressure decreases to ~25 bar when it works under the rated conditions, and then goes up to a higher value (at ~ 35 bar), as the expansion ratio is reduced when it worked under off-design conditions. For turbine temperature profile (Figure 4.22 (a)), its inlet temperature keeps constant when the system reaches steady state after ~120s, while the outlet temperature varies between 295 K and 315 K depending on its working conditions and expansion ratio.

4.6 Summary

This part of work has studied the dynamic behaviour and response time of the LAES discharging unit when integrated with wind power. The dynamic models of LAES components and the system were built and validated based on the experiment results. The empirical wavelet transform technique was adopted to decompose the wind power curve into high-frequency and low-frequency components, which were fed to storage technologies with different response time. For the LAES discharging unit, a PID controller was integrated to control the unit to respond to the power command when wind power is insufficient. Finally, the economic advantages among the different combined storage schemes with LAES and battery technologies were compared. The major results are presented as the followings:

a. The component- and system-level dynamic models of LAES system were established and simulated to understand its practical operational behaviour and control strategy. For a 300 kW LAES discharging unit, its response time was validated as ~130s by experiment results

from a 300 kW pilot LAES plant. Its dynamic characteristics interacting with wind power can be clearly captured.

b. When a LAES discharging unit serves to smooth the varying wind power, different wind power decomposition schemes and power following tests demonstrated that the LAES discharging unit is more suitable for responding to the wind power component varying at a time scale more than its start-up time, which leads to less power tracking errors and smoother speed adjustment, as well as less turbine motor fatigue.

c. The economic comparison among different combined storage schemes indicated: 1) The annual cost of full battery storage is higher than that of the combined LAES and battery storage system for wind farms; 2) For a combined storage system, Lead-acid battery is more suitable for small-scale wind farm, VR flow battery is more suitable for large-scale wind farm, Li-ion battery is more expensive than other two battery technologies; 3) The larger the wind farm, the more obvious the economic advantages of the combined storage system.

5 The optimal design and operation of a hybrid renewable micro-grid with the decoupled liquid air energy storage

5.1 Introduction

5.1.1 Literature review

5.1.1.1 Hybrid renewable energy system design methods

Recent years have seen a growing interest in developing distributed hybrid renewable energy systems (HRESs) [253]. Such systems combine conventional generators with renewables to reduce carbon dioxide emissions. A few studies have investigated HRESs at different scales by using different methods. Based on a concept called 'energy hub', Geidl et al. [121] proposed a general steady-state modelling and optimization framework, involving the conversion, transmission and storage of energy with multiple carriers. Good et al. [254] proposed a modular techno-economic model to study the physical and commercial interactions of different energy vectors within the HRES. Ayele et al. [255] developed a load-flow model based on an extended energy hub approach, and used a nested particle swarm optimization (NPSO) algorithm for the optimisation. Buonomano et al. [256] designed a new HRES and carried out a techno-economic analysis in the TRNSYS (Transient System Simulation) environment. Zakeri et al. [158] adopted the EnergyPLAN to investigate the maximum penetration ratio of different renewables and the optimal combination of different technologies. A new methodology for designing an off-grid hybrid PV-diesel-battery system was developed by Mokhtara et al. [257], which combines demand-supply management (DSM) with particle swarm optimization. The results showed that PV-Li-ion was the optimal configuration, which could achieve 19% and 57% reduction in energy consumption and CO_2 emissions respectively. An overview about the design methodologies, components sizing

and economic indicators of HRES was provided by Lian et al. [258], pointing out that the hybrid methods are the most promising ones for designing HRES.

5.1.1.2 Hybrid renewable energy system with energy storage

As mentioned above, energy storage is essential for supporting the operation of HRESs. A number of studies have discussed the integration of different energy storage technologies with HRESs. This includes the PHES, CAES, LAES, the thermochemical and electrochemical energy storages. Djelailia et al. [184] studied an HRES with PHES, it showed the effectiveness of hydroelectric storage in irrigation, power dispatch, fuel-saving and CO_2 emissions. De Bosio and Verda [259] investigated an HRES with CAES. The thermo-economic analysis indicated that the hybrid system would be cost-effective only when used to solve the grid imbalance. However, PHES and CAES considered in the studies have geographical limitations. Gabrielli et al. [195] proposed a MILP-based model to optimally design a HRES with hydrogen storage, but this technology has a low technical maturity. Martínez Ceseña et al. [260] conducted a techno-economic analysis of a micro-grid with battery storage and thermal energy storage (TES). The storage technologies can provide energy, reserve, and reliability services simultaneously, but the flexibility value of storages was not considered. A comprehensive analysis of a novel system combining LAES and TES was conducted by Nabat et al. [261]. The system can obtain both high energy efficiency (61.1%) and exergy efficiency (52.8%), as well as a promising pay-back period of 3.91 years. Mazzoni S. et al. [262] developed an MILP dispatch model to compare the economic performance of LAES and battery (300-2000 kWh), but the model cannot perform the optimal system design with LAES. Xie et al. [71] assessed the economic value of a decoupled LAES system when participating in the UK electricity service markets. It showed that a large-scale LAES with high-grade waste heat (>150 ℃) would be profitable, but the detailed technical data of LAES was not taken into account. Vecchi et al. [221] conducted a techno-economic analysis of a standalone LAES system within the UK

electricity markets, considering the off-design operation. They also investigated the techno-economic value of LAES to supply electricity, heating and cooling functions simultaneously. The vector-coupling capability of LAES was capable of achieving a 35% of increase in energy efficiency and a 8-12% of decrease in system operational cost [86]. However, the interactions of the gird-scale LAES system with other power generators were not studied.

5.1.2 Research aim

From the above review, one can see little work has been done on the integration of LAES with hybrid renewable micro-grids (HRMGs), nor on the specific value streams of this storage technology in HRMGs. This makes it difficult to understand whether the deployment of LAES in distributed HRMGs would be feasible and valuable. This part of work focused on investigating the key role and optimal selection of LAESs to support future distributed HRMGs. The major novelties of this work lie in the following four aspects:

- The decoupled off-design LAES model was developed, which can adapt to the fluctuating renewables and variable user demands, as well as can achieve the optimal selection of LAES units in a HRMG by using the MILP algorithm.
- The optimal charge and discharge energy to power (E/P) ratios of LAESs were studied for the first time when providing different electricity services. It enables preliminarily determining the LAES capacities when providing the arbitrage, renewable firming and operating reserve functions.
- The multiple functions and revenue streams of LAESs in supporting HRMGs were identified for the first time, which were split into different compositions. The interactions among different value streams were also discussed and compared with those of the battery storage.
- The optimal design and operation of a HRMG with the decoupled LAES by using the hierarchical MILP formulation was achieved. The optimal sizes and operational states

of the decoupled LAES units and other generators in HRMGs can be determined, to incorporate a large portion of renewables with the minimum cost and environmental impact.

This part of work is structured in the following manner. *Section 5.2* describes the components' model and parameters. *Section 5.3* introduces the input profiles and related input parameters. *Section 5.4* presents the MILP methodology and modelling methods. The major results are explained in *Section 5.5*. Finally, conclusions are drawn in *Section 5.6*.

5.2 Case study and input definition

5.2.1 Hybrid renewable micro-grid

A future hybrid renewable micro-grid (HRMG) for the University of Birmingham campus is proposed as the case study, as shown in Figure 5.1. It is to help achieve an independent demand supply with simultaneous economic savings and CO_2 reductions.

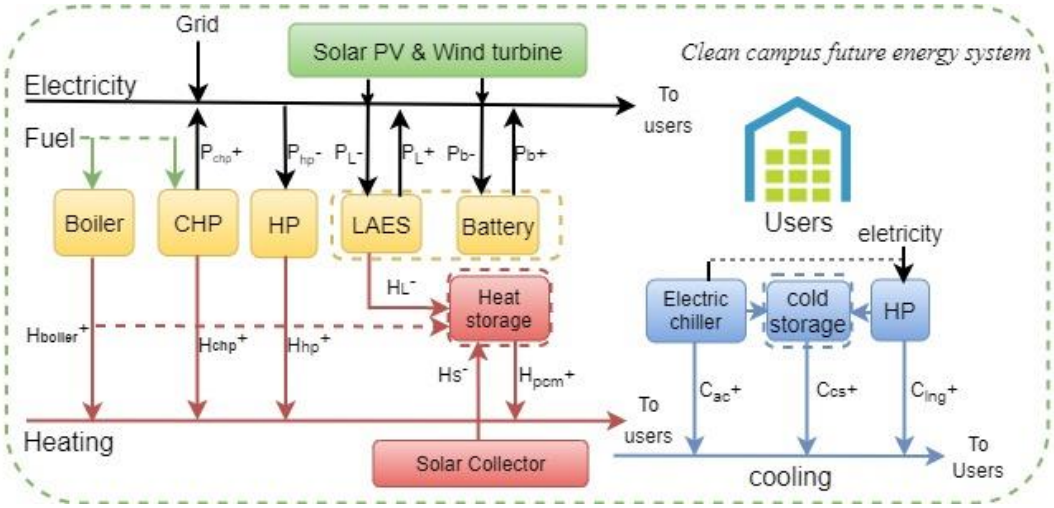

Figure 5.1. Future HRMG scheme for the campus

The future HRMG is an assumed case study, it aims at reducing at least 50% of CO_2 emissions on the 2016 level at the lowest cost as the first-stage transition. The system is connected to the national grid and gas pipelines. It is composed of conventional technologies, like CHPs (combined heat and power technology), boilers and heat pumps (HP); and renewable-based generators, including wind turbines, solar PV and concentrated solar power (CSP); as well as

energy storage systems (ESS), like LAES, battery, heat storage and cold storage. The optimal design and operation framework of the HRMG is formulated as a hierarchical MILP model, in which LAES serves as one of the major electricity energy storages.

5.2.2 Micro-grid components models

The LAES is composed of three major sub-systems, the LFU, the air storage tank and the PRU, shown as in Figure 5.2. The decoupled LAES model was developed, in which the models of the LFU, PRU and storage tank were built separately and explained in detail in *section A1.1* of the supplementary material. The models considered the off-design operation and RTE, the varying power consumption and production, as well as the decoupled costs of subsystems, to achieve cost-effectiveness and practical assessment. The nominal operating parameters of the LAES are presented in Table 5.1, with the optimal parameters chosen on the basis of thermodynamic analysis results reported by She. *et al.* [212].

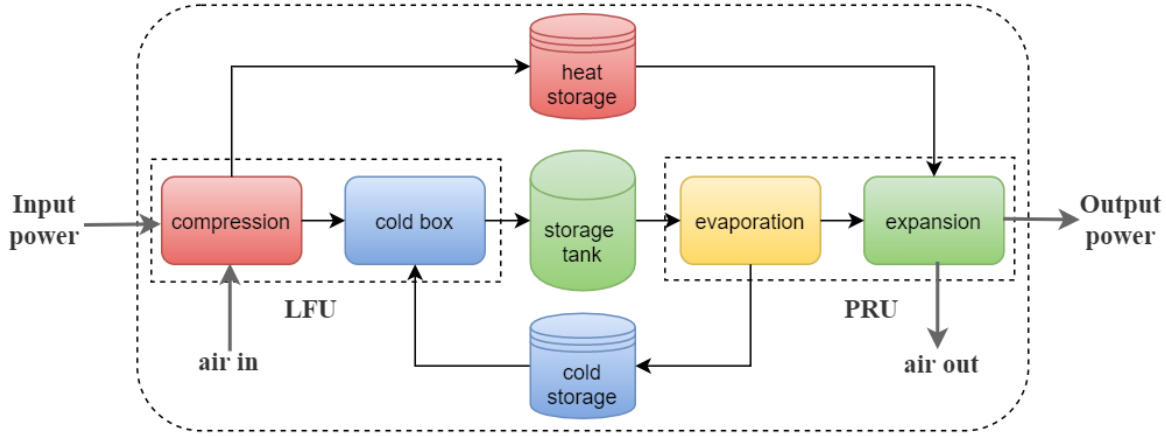

Figure 5.2. The decoupled LAES system

Table 5.1. LAES nominal operating conditions [212][44]

Nominal parameters	value
Charging pressure/MPa	9
Discharging pressure/MPa	12
Turbine inlet temperature / ℃	195
Liquefaction rate	70%
RTE	52.5%

Compressor efficiency	89%
Turbine efficiency	90%
Cryo-turbine efficiency	80%
Intercooler effectiveness	95%
Compression enthalpy kJ/kg	193.00
Expansion enthalpy kJ/kg	145.00

In the HRMG, other components, including the gas engines, heat pumps, electric chillers, gas boilers, battery, solar PV and wind turbines contributed to providing energy for the campus micro-grid as well. Their models and key parameters were explained in *section A1.2- section A1.3* of the supplementary material, summarized as in Table 5.2.

Table 5.2. Technical and economic parameters of other system components

Components	Efficiency	Life time/years	Capital cost/£	O&M cost – % of CAPEX
Gas engine	86% (total)	15	$6962.5 * Pr^{-0.164}$ /kW	5%
Gas boiler	85%	20	80/kW	2%
Electric chiller	2.8	15	$1164.2 \cdot P_r^{-0.284}$ /kW	1.5%
Heat pumps	0.0329*T_{amb}+2.0012	15	$1319.4 \cdot P_r^{-0.268}$ /kW	1.5%
Air compressor	85%	30	$Cost_{c0}(\frac{P_c}{P_{c0}})^{-0.4}$	1%
Air turbine	85%	30	$Cost_{t0}(\frac{P_t}{P_{t0}})^{-0.4}$	1%
Liquid air tank	/	30	44/kWh	1%
Solar PV	16.67%	30	900/kW	3 /year/kW
Wind turbines	/	30	1300/kW	7.5/year/kW
Battery	95% (charge/discharge)	10	420/kWh	2%
Heat storage	95% (charge/discharge)	20	10/kWh	2%

5.2.3 Demand profiles

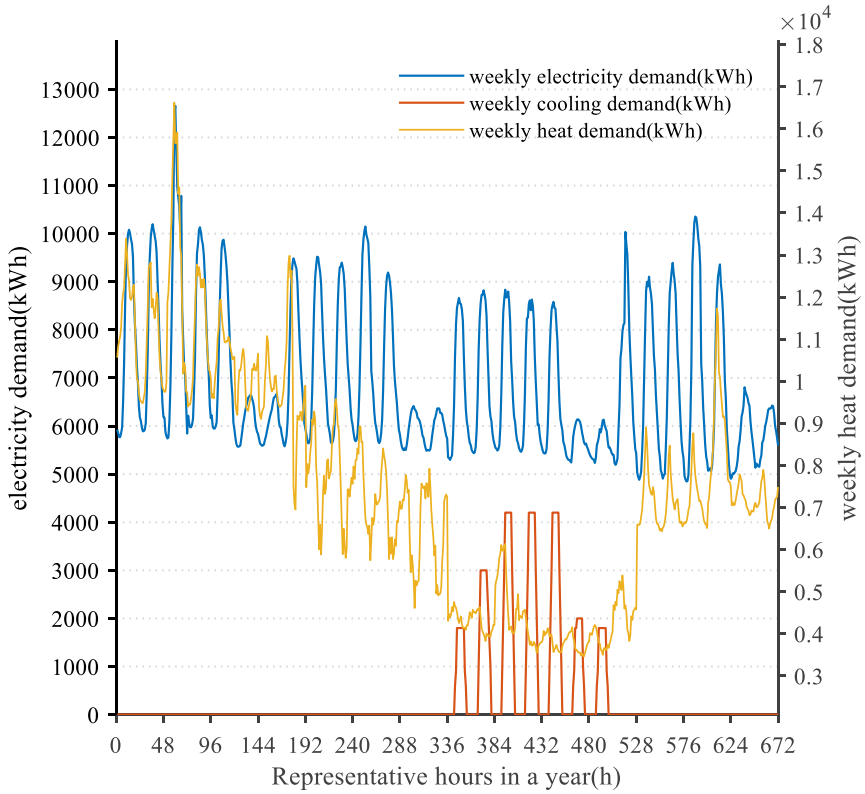

Figure 5.3. The electricity/heat/cooling demands in campus for four representative weeks

The campus of the University of Birmingham was chosen as the case study. Considering the significant complexity and calculation load caused by full-scale optimization, the hourly profiles in four representative weeks in a year are chosen to represent four separate seasons. The profiles include: 1) the electricity, heating and cooling demands (shown in Figure 5.3); 2) the solar and wind capacity factors; 3) the ambient temperature and unit-rate electricity prices. The methods to choose the representative data and profiles are illustrated in *the section A2* of the supplementary material. The annual operational cost and revenue will be calculated by multiplying a weight factor (13) based on the simulation results of the representative weeks [260].

5.2.4 Other input parameters

The campus micro-grid interacts with the national electricity grid, gas network, and other stakeholders. The input parameters of the model were explained in the *section A2.2* of the supplementary material, summarized as in Table 5.3, including the retailing gas prices,

renewable incentives, carbon emission factor and tax, loss of power and curtailment penalty, the search space of variables, and the performance indicators.

Table 5.3. Model other input 'environment' parameters

Components	Parameters	Data	Unit
Energy bill	Gas bill rates	1.04 (summer[1]) / 1.37 (spring[1]) / 2.22 (winter[1])	p[3]/kWh
	Electricity bill rates	-12 ~ 120 (valley[2] ~ peak[2])	p/kWh
Incentives	Renewable heat	2.69	p/kWh
	Solar PV	1.78	p/kWh
	Wind power	0.88	p/kWh
Penalty	Wind curtailment penalty	80	£/MWh
	Loss of power penalty	17000	£/MWh
CO_2 related	NG CO_2 emission factor	185	kg/MWh
	Carbon price	18	£/ton
Reserve related	Loss of load expectation (LOLE)	3	hours/year
	Reserve charge	0.83	£/kW

Notes:

1. 'summer /spring/winter' means the respective electricity price at each season.

2. 'valley/peak' means the electricity prices at valley and peak time.

3. 'p' means pence.

5.3 MILP formulation for micro-grid

5.3.1 MILP algorithm description

The optimal design and operation framework for the micro-grid was formulated as a hierarchical MILP model. It includes two levels, namely the upper design level and the lower operational level. The variables include: the binary variables to represent the selection value, integer variables represent the selected number, and continuous variables to represent design capacities and operational parameters. The model can be described in a general form in eq. (5.1)-(5.3) [195].

$$\mathbf{min}(\boldsymbol{c^T x} + \boldsymbol{d^T y}) \qquad \text{eq. (5.1)}$$

$$\boldsymbol{Ax} + \boldsymbol{By} = \boldsymbol{b} \qquad \text{eq. (5.2)}$$

$$\boldsymbol{x} \geq \mathbf{0} \in \boldsymbol{R}^{\boldsymbol{N_x}}, \boldsymbol{y} \in \{\mathbf{0}, \mathbf{1}\}^{\boldsymbol{N_y}} \quad \text{eq. (5.3)}$$

where, $\boldsymbol{x}$ represents continuous variable vector, $\boldsymbol{y}$ represents binary variable vector, $\boldsymbol{A}$ and $\boldsymbol{B}$ are the corresponding constraints matrices, and $\boldsymbol{b}$ is the constraint known-term vector; N_x and N_y represent the dimensions of $\boldsymbol{x}$ and $\boldsymbol{y}$. $\boldsymbol{c}$ and $\boldsymbol{d}$ represent the cost matrices for continuous and binary variables.

5.3.2 Decision variables

The decision variables are divided into three categories:

i. Design variables, including the selection value ($\boldsymbol{S} \in R^{\boldsymbol{I}}$), selected number ($\boldsymbol{N} \in Z^{\boldsymbol{I_{ep}}}$), and rated sizes of system components ($\boldsymbol{Des}_{ep} \in R^{\boldsymbol{I_{ep}}}$) and storage devices ($\boldsymbol{Des}_{ST} \in R^{I_{ST}}$).

ii. Operational variables, including on/off status ($\boldsymbol{of} \in \{0,1\}^{\boldsymbol{I_{ep}} \times \boldsymbol{T}}$), operating modes ($\boldsymbol{M} \in \{0,1\}^{\boldsymbol{I_{ep}} \times \boldsymbol{T}}$), on/off number ($\boldsymbol{of\_num} \in Z^{\boldsymbol{I_{ep}} \times \boldsymbol{T}}$), input and output power ($\boldsymbol{P_{in}} \in R^{\boldsymbol{I} \times \boldsymbol{T}}, \boldsymbol{P_{out}} \in R^{\boldsymbol{I} \times \boldsymbol{T}}$), as well as the storage level of storage technologies ($\boldsymbol{SOC} \in R^{\boldsymbol{I_{ST}} \times \boldsymbol{T}}$), and the imported electricity and natural gas energy ($\boldsymbol{P}_{ele} \in R^{\boldsymbol{T}}, \boldsymbol{P}_{NG} \in R^{\boldsymbol{T}}$).

iii. Auxiliary variables, which are used to linearize non-linear terms, and to combine design variables and operational variables ($\boldsymbol{Ax} \in R^{\boldsymbol{I_{ep}} \times \boldsymbol{J} \times \boldsymbol{T}}$).

5.3.3 Bounded constraints

In the MILP formulation, the constraints of the problem in this study were distinguished as four categories, technical constraints, operational constraints, economic constraints, and power balance constraints. Here, only the storage system and power balance constraints are given, the rest of constraints can be found in the *section A3.1.2* of the supplementary material.

- Storage system

The energy storage system (ESS) in this study was divided into two categories, namely the coupled and decoupled ESS, which are represented by the battery and LAES and their respective models.

- Coupled battery model

The coupled battery model considers the storage as a whole, and its constraints are expressed as in eq. (5.4) – eq. (5.5).

$$E_{bat}(t) = E_{bat}(t-1) + \eta_{cha} \cdot P^{-}_{cha,bat} \cdot \Delta t - \frac{P^{+}_{dis,bat} \cdot \Delta t}{\eta_{dis}} \quad \text{eq. (5.4)}$$

$$E_{bat,min} \leq E_{bat}(t) \leq E_{bat,max} \quad \text{eq. (5.5)}$$

where, E – the stored energy (kWh), η – efficiency, Δt – the time interval, the subscripts including: bat – battery, cha – the charging process, dis – the discharging process, max – the maximum value, min – the minimum value, the superscripts including: '-' the input power into storage, '+' the output power from storage. Thermal storage is modelled in a similar way.

- Decoupled LAES model

The decoupled LAES model includes the major models of the compressors, turbines and air tanks. The relationships between air mass flow rate, pressure, and power input/output of compressors and turbines are linearized to keep the linearity of MILP formulation. The ramp-up and ramp-down rate, as well as the minimum online and offline time of compressors and turbines are formulated in a similar way to those of gas engines.

Compressors

$$P_{\mathrm{C}}(t) = k_{\mathrm{C}} \cdot \dot{m}_{\mathrm{C}}(t) + C1 \quad \text{eq. (5.6)}$$

$$0 \leq P_{\mathrm{C}}(t) \leq of_{\mathrm{C}}(t) \cdot P_{\mathrm{C},r} \quad \text{eq. (5.7)}$$

Turbines

$$P_{Tr}(t) = k_{Tr} \cdot \dot{m}_{Tr}(t) + C2 \quad \text{eq. (5.8)}$$

$$0 \leq P_{Tr}(t) \leq of_{Tr}(t) \cdot P_{Tr,r} \quad \text{eq. (5.9)}$$

$$0 \leq of_{\mathrm{C}}(t) + of_{Tr}(t) \leq 1 \quad \text{eq. (5.10)}$$

Liquid air tanks

$$m_{la}(t) = m_{la}(t-\Delta t) + \dot{m}_{\mathrm{C}}(t) \cdot \Delta t - \dot{m}_{Tr}(t) \cdot \Delta t \quad \text{eq. (5.11)}$$

$$m_{la,min} \leq m_{la}(t) \leq m_{la,max} \quad \text{eq. (5.12)}$$

where, k_C/ k_{Tr} – the slopes of the regression curves of compressors/turbines, $C1$ / $C2$ – the intercepts of the regression curves of compressors/turbines, P_C / P_{Tr} – the power consumption of compressors/turbines, of_C / of_{Tr}– the on-off status of compressors/ turbines, m – the mass of liquid air in tank, $\dot{m}_C$ / $\dot{m_{Tr}}$ – the air mass flow rates of compressors and turbines, *r*- the rated parameters.

- Power balance constraints

The power and thermal demand and supply should be balanced at each time step, expressed as eq. (5.13) – (5.15).

$$P_{GE}(t) + P_{pv}(t) + P_{wt}(t) - P_{curt,wt}(t) - P_{cha,bat}(t) + P_{dis,bat}(t) - \cdots$$

$$P_{cha,C} + P_{dis,Tr}(t) + P_{los}(t) + P_{grid}(t) - P_{HP}(t) - P_{EC}(t) = P_{L,ele}(t) \quad \text{eq. (5.13)}$$

$$P_{HP}(t) + P_{GB}(t) + P_{ht,GE}(t) - P_{cha,ht}(t) + P_{dis,ht}(t) = P_{L,ht}(t) \quad \text{eq. (5.14)}$$

$$P_{EC}(t) + P_{HP}(t) = P_{L,col}(t) \quad \text{eq. (5.15)}$$

where, symbol P – power, the subscripts represent: *GE* – gas engine, *pv* – solar panels, *wt* – wind turbines, *los* – the loss of power, *grid* – the grid electricity, *HP* – heat pump, *EC* – the electric chiller, *L* – load, *ele* – the electricity, *ht* – the heating, *col* – the cooling, *curt*- the curtailed wind, *t* – the time *t*.

5.3.4 Optimization objectives

The study aims to minimize the total annual system cost and environmental impact, expressed as in eq. (5.16). The objective terms include: the annual equipment capital cost $C_{cpt,tot}$, the operational cost C_{op}, the maintenance cost C_{main}, the CO_2 emission tax C_{CO2}, the renewable curtailment cost C_{cur} and the cost penalty C_{LOP} for loss of power (LOP). At the same time, it manages to increase the renewable penetration by maximizing renewable

incentives C_{inc}. Detailed description of each optimization objective can be found in the *section A3.1.*3 of the supplementary material.

$$min\begin{cases} C_{ann,tot} = C_{cpt,tot} + C_{op} + C_{main} + \cdots \\ C_{CO2} + C_{cur} + C_{LOP} - C_{inc} \end{cases} \quad \text{eq. (5.16)}$$

The commercial software, including MATLAB, YALMIP, and Gurobi, were combined to conduct the simulation in 1-h resolution rolling-horizon. The MILP relative gap (between 0.001-0.02) is used as the convergence criteria. The gap range considers the trade-off between calculation complexity and time consumption. The computer is configured with an Intel (R) CPU i5-6500 3.2 GHz (4) and 8 GB RAM. Besides, the scaling and various parameters tuning methods were used to speed up the simulation process.

5.3.5 The methodology

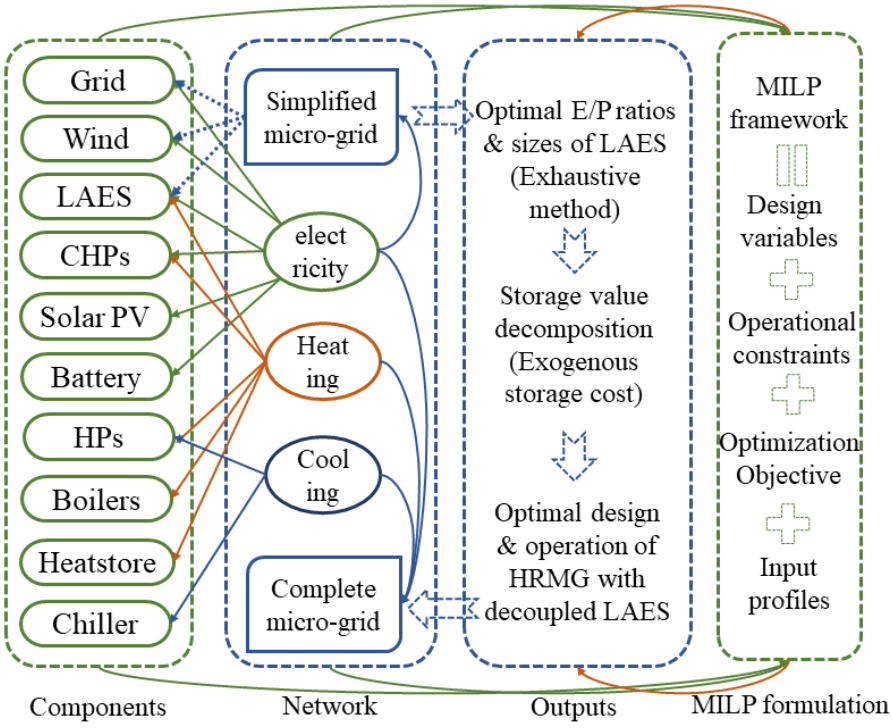

Figure 5.4. The methodology and framework of this work

The methodology of the work is shown as in Figure 5.4. In the MILP design and operation framework, different system components, such as CHPs, wind turbines, solar panels, heat pumps and heat storage (Heat store) etc., have been included to provide the corresponding

energy for different networks (electricity, heating and cooling) within the micro-grid. There are two types of micro-grids developed for the discussion. A simplified micro-grid that only involves electricity network is to study the optimal E/P ratios and sizes of LAES by using exhaustive method. A complete micro-grid involves electricity, heating and cooling networks simultaneously. It is developed to understand the storage value in a comprehensive manner, and eventually to achieve the optimal design and operation of the whole micro-grid.

5.4 Results and discussions

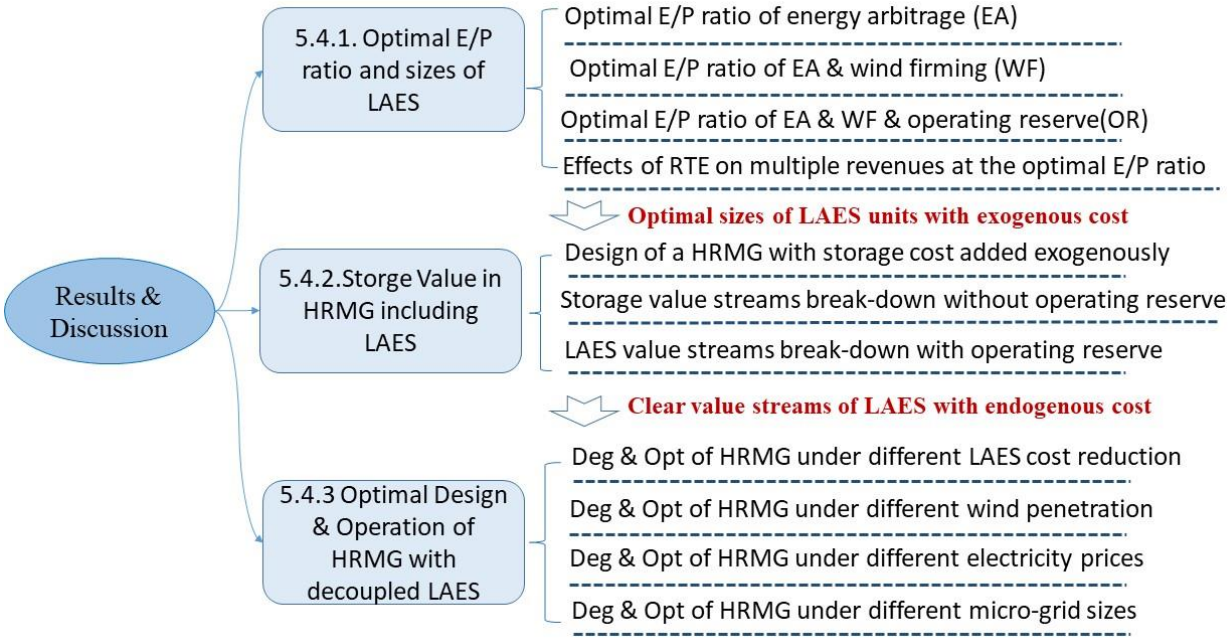

Figure 5.5. The logic and structure of discussion part

In this part, the results' discussion is structured as shown in Figure 5.5. The optimal E/P ratios and sizes of LAES were obtained by using exhaustive method in *section 5.4.1*. Then, the obtained LAES sizes were input into *section 5.4.2*, to analyse the storage value with storage cost being added exogenously. After the storage value streams were identified clearly, the optimal design and operation (Des & Opt) of the HRMG with the decoupled LAES and endogenous storage cost were determined in *section 5.4.3*.

5.4.1 Optimal E/P ratio of LAES

The E/P ratio is the ratio of stored energy (kWh) and the rated charge/discharge power (kW), termed as charge/discharge (Cha/Dis) E/P ratios. For the decoupled LAES, when keeping the rated energy capacity (6 MWh) constant, increasing charge/discharge E/P ratios results in smaller LFUs and PRUs with higher specific costs and longer working durations. ROI is the ratio of net profit and investment cost. It is used to quantify the effects of different E/P ratios of LAES on system economics, higher ROI means better cost-effectiveness.

5.4.1.1 Optimal E/P ratios for energy arbitrage

A simplified micro-grid that only considers the electricity network was assumed as the case study. The LAES is deployed to help conduct the electricity price arbitrage, which is capable of storing electricity at bottom prices and releasing the energy at peak prices to save electricity fee.

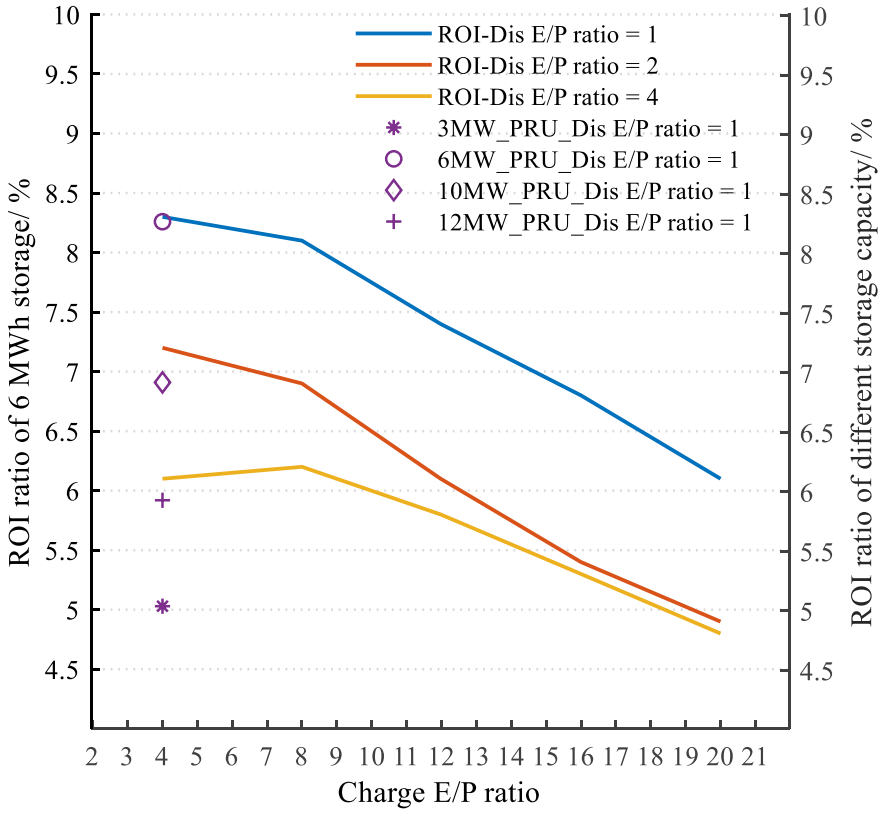

Figure 5.6. Effects of different Cha/Dis E/P ratio on system ROI when achieving energy arbitrage

Under different discharge E/P ratios (curves in Figure 5.6), the arbitrage revenue and ROI decrease when the charge E/P ratios are more than 4h. It is due to that smaller charging units cannot fully capture the low-price electricity to charge the storage tank to full, though they bear lower capital costs. This results in fewer charge and discharge cycles in a year, thus less arbitrage revenue and lower ROI. While larger discharging units are preferred to capture the highest prices to release the stored electricity and to save more electricity fee, but their specific capital costs are far lower than those of charging units. Indicated by four marks in Figure 5.6, keeping the charge/discharge E/P ratios (4/1) constant, the ROI goes up first and then decreases when the sizes of LFU and PRU increase with higher energy capacity of LAES (3 / 6 / 10 / 12 MWh). It can be explained as the value of LAES in the micro-grid has saturated, the capital cost of the larger-scale storage cannot be offset by its revenue. In other words, there exists the optimal sizes of charge/discharge units and storage capacity of LAES for a given-scale micro-grid, which can achieve good cost-effectiveness.

5.4.1.2 Optimal tank sizes for energy arbitrage

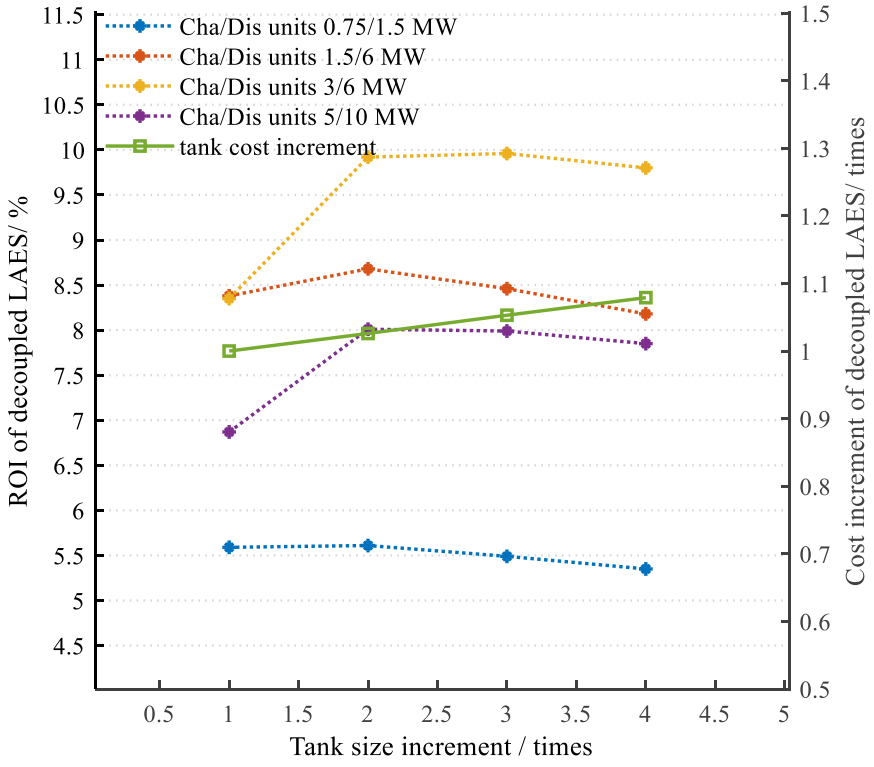

Figure 5.7. The effects of tank sizes on system economics

The effects of tank sizes (tons) on system economics were studied as well when keeping the sizes of liquefiers and turbines constant, shown in Figure 5.7. Take 3MWh, 6MWh, and 10 MWh of LAESs as the cases, the matching tank sizes can only hold the liquid air produced by LFUs during the rated charging hours (the rated charging E/P ratio 4/1). Figure 5.7 shows that there exists an optimal tank volume for LAES with specific sizes of liquefiers and turbines, which is two to three times of the matching tank size. It is due to that much larger reservoir cannot be filled to full in the charging process. Thus, the extra investment on larger storage space cannot be counterbalanced by its extra arbitrage profits, which is consistent with the results of Vecchi et al. [249]. Together with the results in *section 5.4.1.1*, in terms of arbitrage function provided by LAESs, the discharge power at about half of the maximum electricity demand of micro-grids produces better ROI. Accordingly, the storage system presents the optimal charge E/P ratio (8~12 h) and discharge E/P ratio (2~3 h).

5.4.1.3 Optimal E/P ratios for wind firming

When the simplified micro-grid is powered by wind energy (about 50%) and electricity from the grid, the LAES plant is deployed to help achieve wind stabilization. The benefit earned by the LAES is defined as the sum of the avoided curtailment penalty and wind power incentives, the ROI curve is shown in Figure 5.8.

It can be seen that it is not favored to choose a larger PRU when keeping LFU size (3 MW) constant (the left bar group), as it contributes less to absorbing extra wind power, but results in the decrease of arbitrage revenue and ROI. Further, it is due to that the turbines work more often at part-load conditions to avoid wind curtailment, thus cannot fully capture the peak-price electricity to release more stored power and reap more profits. However, if keeping the PRU and matching tank size constant, larger LFUs help absorb more wind power, to avoid wind curtailment and increase arbitrage benefits as well (the middle bar group). It is due to that more free wind energy can be captured quickly by larger LFUs and then stored in the form of

liquid air, but higher capital costs of larger LFUs worsen the system economics (blue curve in Figure 5.8) . Meanwhile, if the matching tank sizes are enlarged by 2-3 times, more extra wind power can be captured and more arbitrage profits can be reaped (the right bar group: ROI 12.4% (matching tank size) to ROI 18.9% (3 times of tank size)). However, an even larger tank (4 times) cannot be charged to full and produce more benefits due to the intermittency of wind energy. Thus, for a LAES with 3 MW LFU and 3MW PRU, the optimal charge and discharge E/P ratios are 12 and 6 h when used for wind firming.

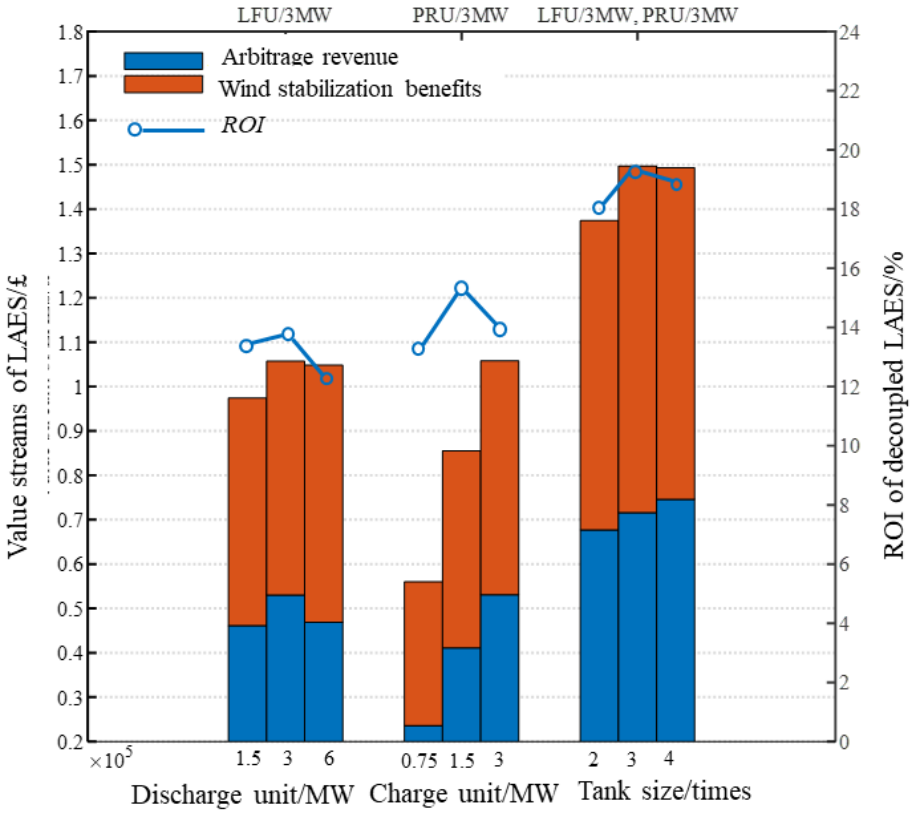

Figure 5.8. Effects of Cha/Dis E/P ratio on LAES revenue and ROI when wind curtailment occurs

5.4.1.4 Optimal E/P ratios for operating reserve

LAES can serve as the secondary upwards reserve (capacity margin for upward regulation) [263].The reserve benefits of LAES was assessed by comparing the avoided penalty of loss of power between systems with and without the operating reserve. The effects of different sizes of LAES plants, namely smaller (0.6/3 MW LFU/PRU), medium (3/3 MW

LFU/PRU), and larger (3/6 MW LFU/PRU) ones, on three revenue streams were studied (shown in Figure 5.9).

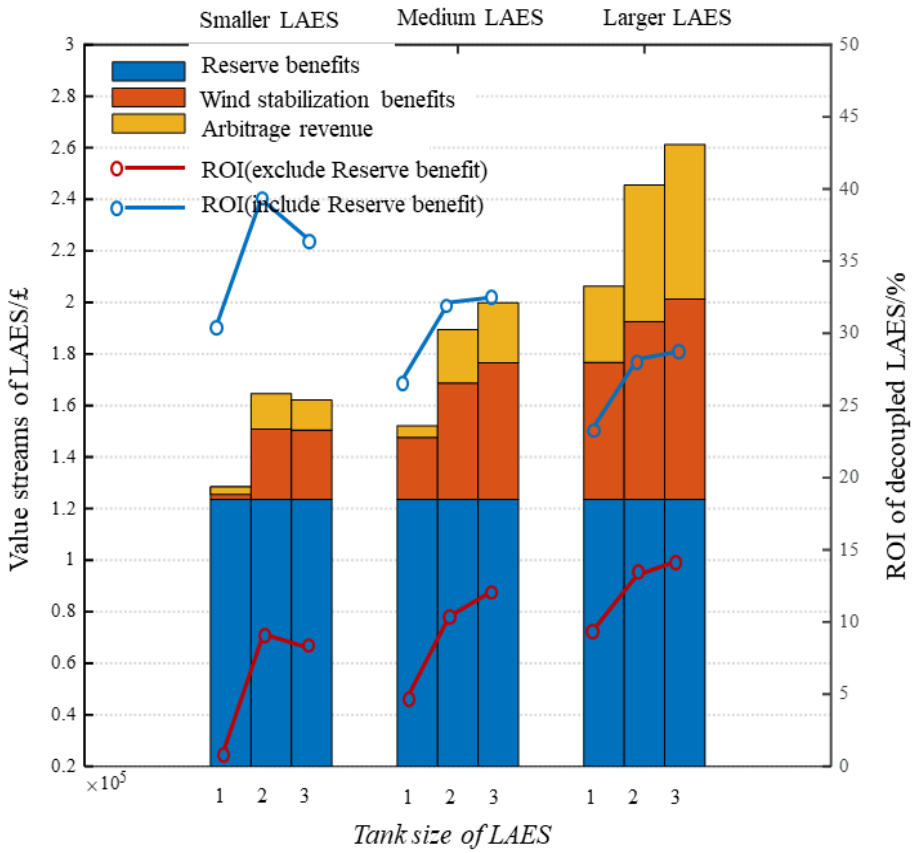

Figure 5.9. Total revenue of LAES with different Cha/Dis E/P ratio

From Figure 5.9, it can be seen that the reserve benefits (a major revenue source) of the LAES are not affected by the increasing capacities of units (blue bars from left to right), as the required reserve level can always be met by adjusting the charge and discharge durations (smaller units is charged for longer charge durations, while larger units for shorter charge hours). But the benefits from wind firming and arbitrage are boosted instantly with units' sizes enlarged (orange and yellow bars from left to right), as larger LAES units are capable of absorbing more low-price electricity and wind energy to keep the reserve level (the LAES capacity is reserved to be no less than 15% of electricidy demand). This leads to more environmental benefits but also higher capital costs and worse system economics (the blue curves). Thus, in the simulated case, the medium LAES (the middle bar group: 3/3 MW

LFU/PRU, Cha/Dis E/P ratio 12/6 h) are chosen to balance the cost-effectiveness and to increase the percentage of wind power as well.

5.4.1.5 Effects of LAES efficiency on the E/P ratio

In the above cases, the nominal RTE of the LAES is 0.52 under the assumed conditions, but there is still much headroom for the efficiency improvement. Thus, the effects of RTE of the LAES (3/3 MW LFU/PRU, Cha/Dis E/P ratio 12/6 h), improving from 0.5 to 0.6 and 0.7 [59], on the value streams were studied in this work (shown in Figure 5.10).

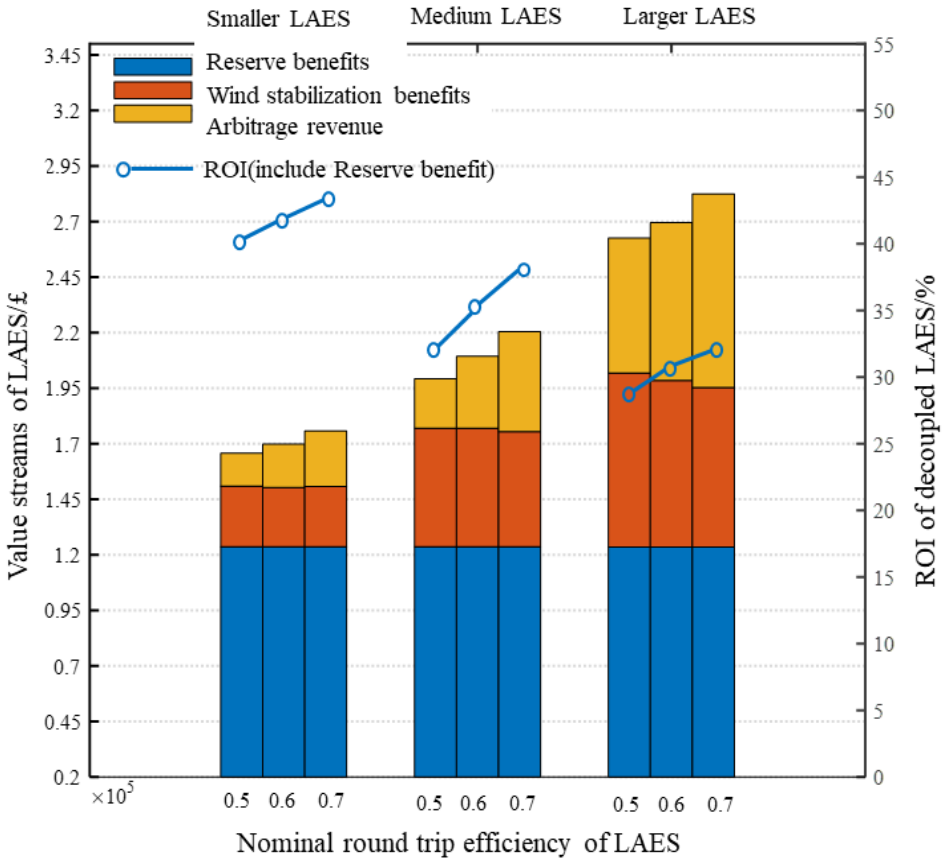

Figure 5.10. Effects of LAES nominal efficiency on economics

From Figure 5.10, it suggests that the reserve revenue (blue bars) is not influenced by the efficiencies, but the arbitrage revenue (yellow bars) instantly benefits from higher efficiencies of the LAES. It is due to that less electricity needs to be bought from the grid, while more power can be released by PRUs to make the most of price differences. But for higher efficiencies, wind firming revenue decreases slightly (orange bars), because the storage level

of liquid air tank increases quickly to full, the spillage of wind energy occurs. Overall, 10%-20% of efficiency improvement results in nearly 2%-3% of enhancement in economics. One of the reasons lies in the lower off-design RTEs of the LAES, which are 41.8% (rated RTE: 52%), 47.9% (rated RTE: 60%) and 56.9% (rated RTE: 70%) respectively. Because the PRUs normally work under off-design conditions to provide enough operating reserve, as well as to avoid wind curtailment.

Based on the exhaustive analysis in *section 5.4.1*, the cost-effective sizes of LAES units for the simplified micro-grid are determined preliminarily to achieve higher ROI. The sizes are 3 MW LFU and 3 MW PRU, as well as the optimal charge and discharge E/P ratios are 12 h and 6 h, and the rated RTE is 0.6.

5.4.2 Optimal design of a micro-grid and energy storage value

In this section, the benefits (value) of LAES, battery storage, and heat storage in a complete micro-grid with various generators were discussed. To be noted, the capacities and costs of LAES and battery were added to the system exogenously before their value streams are fully understood. The model has been validated by comparing the results with Sigarchian et al. [264]. The author adopted the PSO algorithm to determine the optimal sizes of major components in a poly-generation system. The results' comparison was shown in Table 5.4, which confirmed the validity of the MILP design framework in this study. The reason why there is a big difference in the sizes of electric chillers was that the capacities of candidate chillers in the MILP algorithm were in discrete form (200 kW, 500 kW, 800 kW), three chillers with 500 kW each were chosen after the MILP optimization.

Table 5.4. Optimization results comparison

Major system units	Capacity by PSO algorithm	Capacity by this MILP algorithm
CHP unit kW	1000	1000
Boiler kW	2721	3000

Electricity from/to grid kWh	100	113
Electric chiller kW	1100	1500
Heat storage kWh	3000	3000

5.4.2.1 Optimal design of a micro-grid with storage

To achieve the optimal design of a micro-grid, five basic system scenarios were developed and compared, of which candidate equipment is given in Table 5.5 and the design result is shown in Figure 5.11.

Table 5.5. System components candidates

System components	0#	1#	2#	3#	4#	5#
grid	✓	✓	✓	✓	✓	✓
gas boilers	✓	✓	✓	✓	✓	✓
electric chiller	✓	✓	×	×	×	×
gas engines	×	✓	✓	✓	✓	✓
heat pumps	×	×	✓	✓	✓	✓
solar PV	×	×	×	✓	✓	✓
wind power	×	×	×	✓	✓	✓
heat storage(HS)	×	×	×	×	✓	✓
LAES	×	×	×	×	×	✓

0 # system is the conventional campus energy system, 1# system is the existing energy system after 2016, 2# ~ 5# systems are newly-developed hydrid renewable energy system. From Figure 5.11, solar panels cannot be chosen after the optimization due to the scarce solar energy resource in the UK and its high capital cost. Comparing 1 # and 2 # systems, if electric chillers and part of gas boilers are replaced by reversible heat pumps (HPs), the total annual cost decreases by 18.7%, in which the fuel cost and CO_2 tax drop by 17.7% and 8.2% respectively due to the higher efficiency of HPs (averagely 2.83). Comparing 2 # (comparison base), 3 # and 4 # systems, more wind penetration adds more system capital cost by 37.5% (3 # : wind share 17.8%) and 56.2% (4 # : wind share 33.74%). But the respective fuel costs and CO_2 emissions decline by 16% ~ 25% and 15.6% ~ 26.2%, the total system annual costs descend by 2% and 4.6% (taking wind and heat incentives into account). If LAES is added into

the system (5# system), the wind power percentage can be further increased to 47% with less curtailment. Correspondingly, the fuel cost, total annual cost and total CO_2 emissions of 5# system can be cut down by 46.6%, 34.7% and 41.5% when compared with those of 1# system. Overall, it indicates the economic and environmental benefits of distributed renewable energy systems with heat pumps, wind power and energy storage technologies. The specific storage value will be discussed in *section 5.4.2.2*.

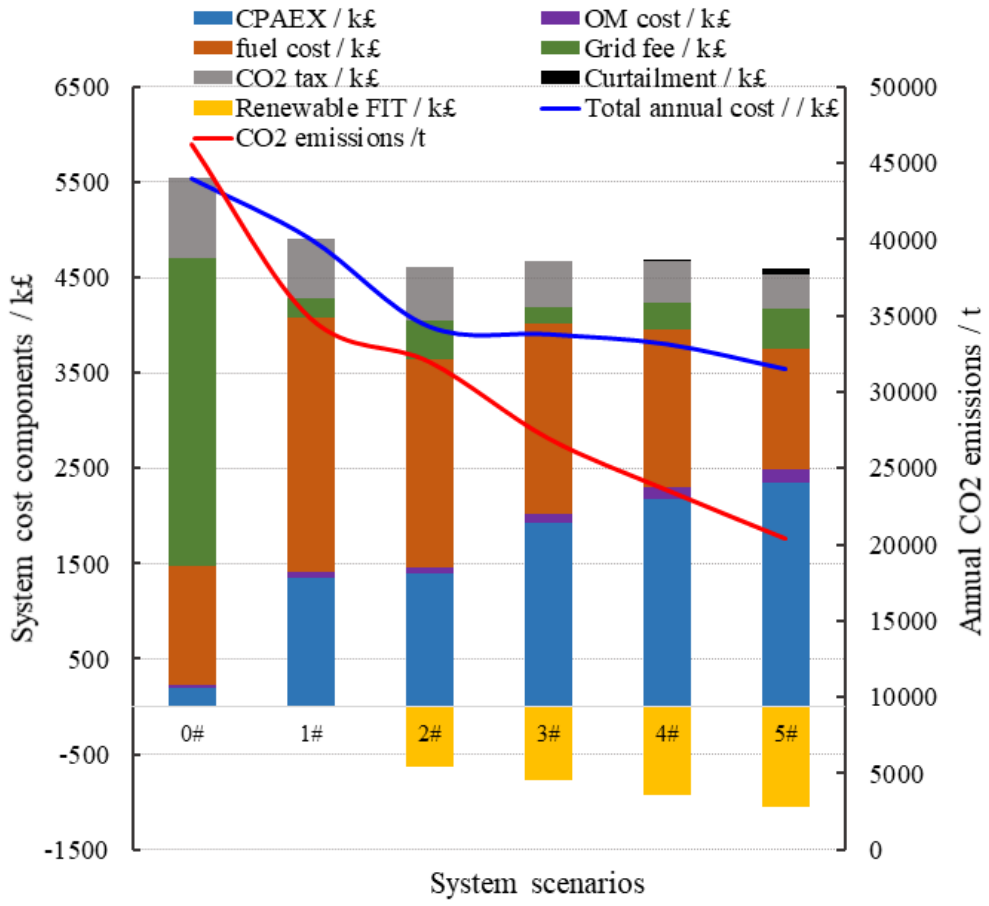

Figure 5.11. Cost comparison of different system scenarios

5.4.2.2 Value of storage in a micro-grid without operating reserve

When wind penetration reaches about 47% (5# system), the effects of heat storage (6MWh), LAES (6 MWh), and battery storage on system annual cost were discussed. A particular focus was put on the benefits analysis of LAES, the value break-downs of each storage are given in Figure 5.12.

From the left pie chart in Figure 5.12, large heat storage helps achieve about 1.65% of annual cost reduction, presenting the high ROI (8.19). Specifically, it saves the fuel cost by 29.2%, reduces the captital cost of peak gas boilers by 11%, as well as boosts the heat pump incentives by 59.8%. When LAES is deployed into the micro-grid, the revenues it creates augment with the increase of wind power percentage (from 17.8% to 33.74% to 46.9%). Take the system with 46.9% of wind penetration as an example, the annual revenue of LAES reaches up to k£ 593, corresponding to 74.7% of its annual amortized cost (not taking the operating reserve into account). The whole benefit can be split into five major revenue streams and their respective percentages, illustrated by the middle pie chart in Figure 5.12. They include: the arbitrage revenue (19.85%), wind stabilization benefits (13.82%), peak units saving (33.74%), flexibility value (25.33%) and waste heat benefits (7.27%).

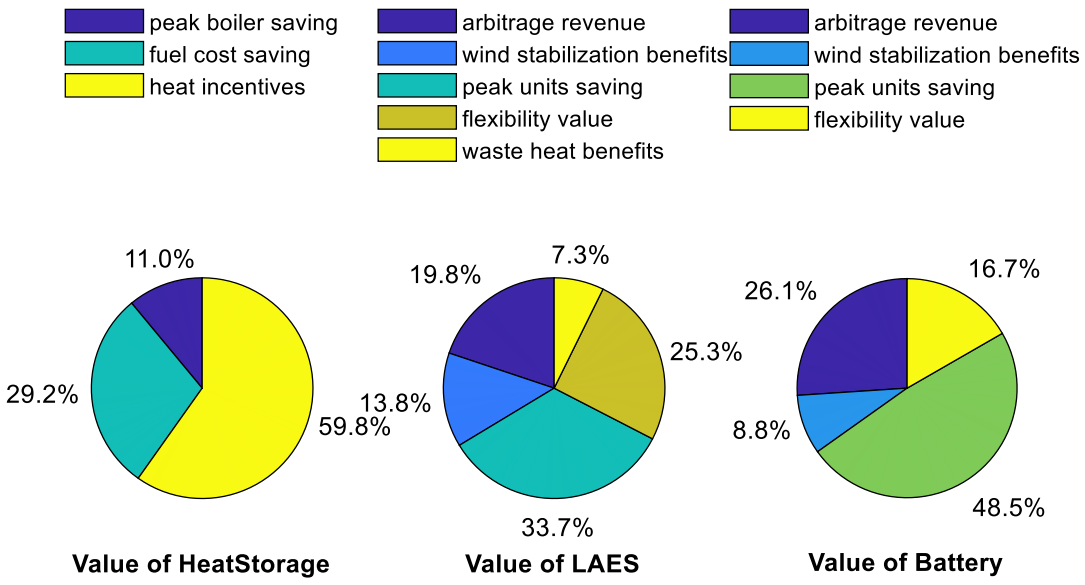

Figure 5.12. Value decomposition of three storage technologies

To be more specific, the arbitrage revenue is to fully utilize the spot electricity price differences to reduce electricity bill. Wind-firming benefit can absorb excess wind energy because of its large storage tank, reducing the wind curtailment by 52.84%. Peak units saving (peak-shaving gain) means the 3MW of LAES discharge unit can replace the 2MW of peak gas engine when the extremely high demand occurs, saving the investment cost of peak gas

engines (the biggest revenue source of LAES). To respond to wind variation quickly and accommodate more renewables, several small gas engines with higher specific costs (system without LAES) are required to meet the flexibility requirement. These engines can be replaced by a large gas engine with lower specific cost when the system is equipped with LAES to provide flexibility, leading to another significant cost saving, termed as the flexibility value of the LAES. Besides, if excess compression heat of LAES is utilized to provide heating energy for the HRMG, it helps save one peak gas boiler (1MW) and the corresponding fuel cost, as well as the carbon emissions from boilers. The effects of the LAES on the HRMG is illustrated in Figure 5.13, in which the wind curtailment reduction, peak-shaving gain and flexibility value were clearly shown.

Battery storage can achieve the similar functions as those of the LAES in micro-grids except for providing waste heat energy. The value contributions of battery were decomposed as arbitrage revenue (26.1%), wind stabilization benefits (8.8%), peak-shaving gain (48.5%) and flexibility value (16.6%), as shown in the right pie chart in Figure 5.12. Its value streams differentiate from those of LAESs, because of the higher efficiency and self-discharge rate of the battery storage, as well as its quick response and no storage tank. Overall, the total value of LAES is higher than that of battery storage by 8.2% when the same investment was made.

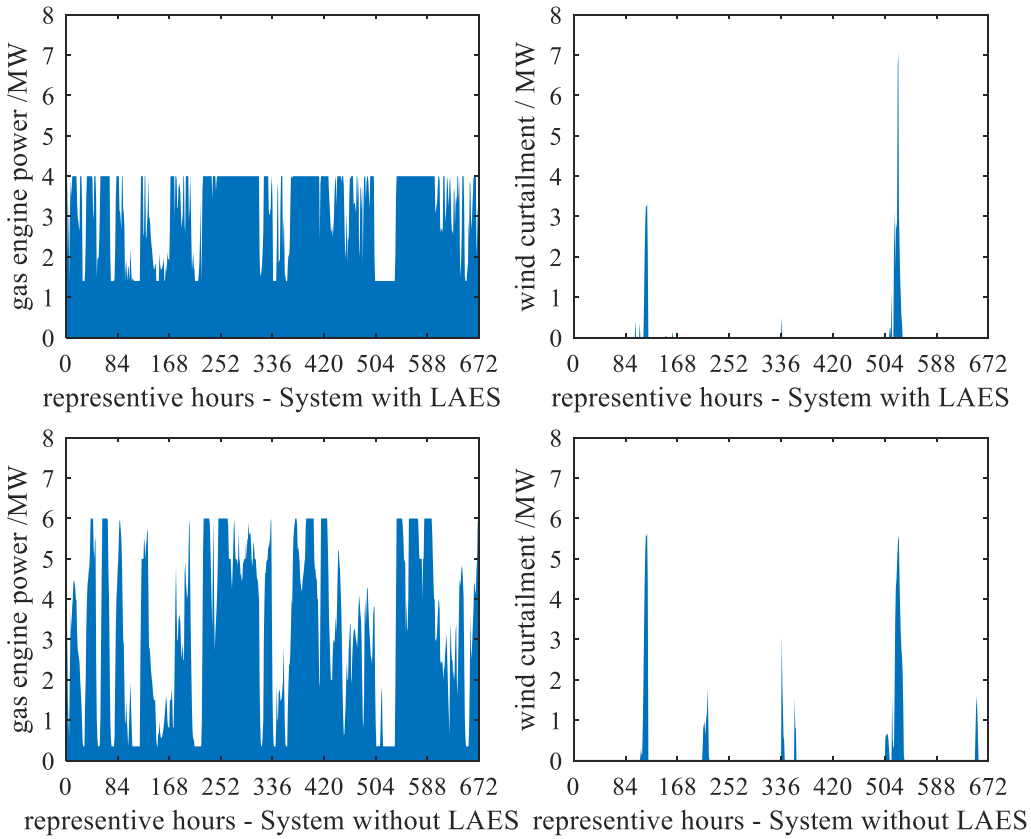

Figure 5.13. LAES effects on gas engine output and wind curtailment

5.4.2.3 Value of LAES in a micro-grid with operating reserve

When LAES is deployed into the micro-grid considering the operating reserve, part of capacities of LAES and gas engines serve as the reserve margins, which is the scheduled output to ensure the robust operation of the system when emergencies occur.

When there is no electric storage, a larger gas engine (5 MW) is equipped to supply electricity and operating reserve simultaneously, resulting in a quite high investment cost of gas engines. However, if the LAES provides part of the reserve capacity, its total value can be augmented by 24.6%, shown as in Figure 5.14. Specifically, the arbitrage revenue of the LAES is reduced by 19.6% to 13.2% when providing part of the operating margin. But in return, the size of the gas engine shrinks to 4 MW, of which capital and fuel cost are cut down by 17% and 45.8% respectively, transferring into the reserve value of the LAES (up to 20.4% of the total value). By now, the stacked revenue of the LAES in the micro-grid reaches up to k£ 715.9

when serving as the operating reserve as well, equivalent to 90.2% of its annual amortized cost. Thus, it is believed that the proper investment of LAESs in micro-grids will be increasingly attractive when more renewables and less CO_2 emissions are required, as Herib Blanco *et al.* [265] argued small storage leads to large benefits.

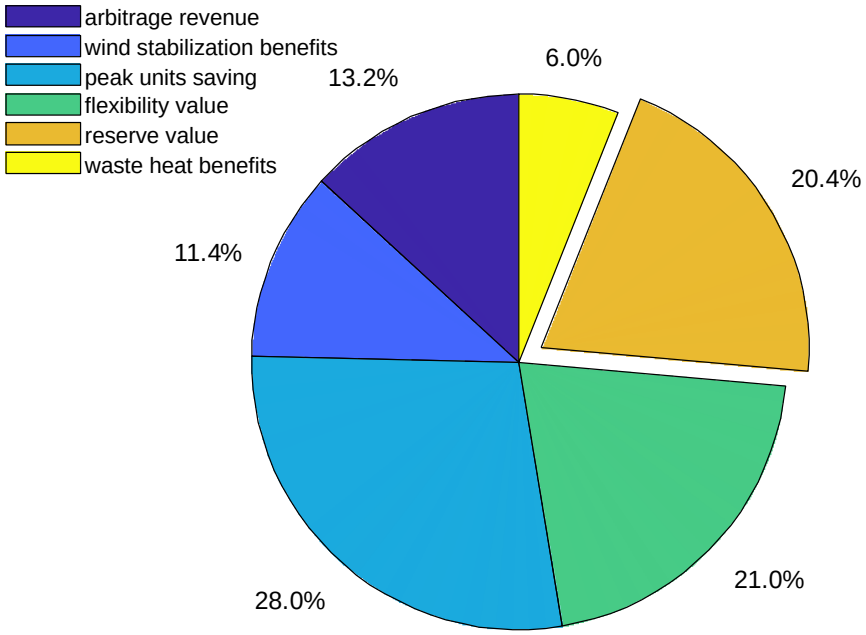

Figure 5.14. Value of LAES serving as an operating reserve in micro-grid

5.4.3 Optimal design and operation of a micro-grid with LAES

In *section 5.4.1* and *section 5.4.2*, the key benefits and specific value streams of LAESs were fully recognized. In this section, the optimal sizes of the LAES in the HRMG are determined endogenously, together with determining other generators' capacities under different scenarios. To be highlighted, only a component is of great value can it be selected in the MILP optimization, which aims at achieving the minimum cost and environmental impact.

To be noted, in this section, the convergence criteria differ from those in *section 5.4.1* and *section 5.4.2* (MIP gap = 1%). Here, three criteria, namely the Time_Limit >= 24h (864000s), Node_Limit >=120000, MIPgap = 2% were set. The optimization terminates when the first convergence criterion is met, which mainly considers the trade-offs between the

solving time and the possible best solution. It is supposed that the objectives achieve the optimum when feasible integer solutions don't update further for enough long time (> 10 h), the converging curves are shown as in Figure 5.15.

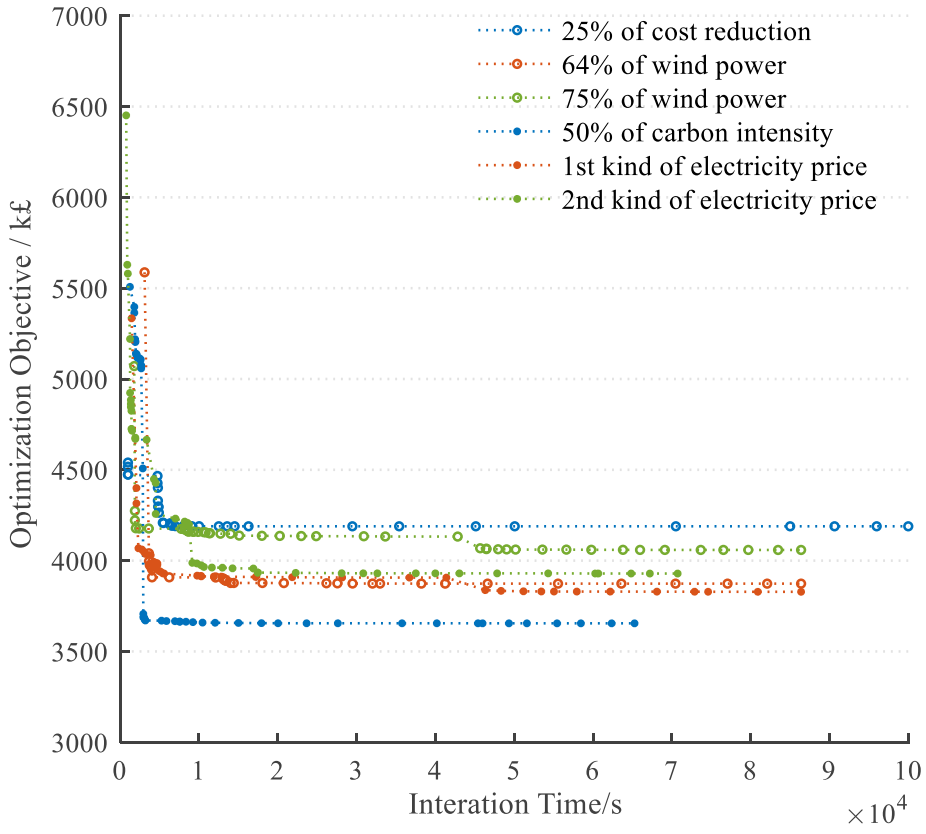

Figure 5.15. MILP optimization iteration curve

5.4.3.1 Effects of the cost reduction of LAES on system design

It is expected that the capital cost of LAESs will be reduced when they are deployed on a large scale and volume. In a micro-grid with 50% of wind penetration, 15% and 25% of cost reduction cases were studied, to reveal the effects of LAES capital cost on system design, shown in Table 5.6. As can be seen, the optimal sizes of the LFU and PRU of the LAES are 3 MW and 3.75 MW respectively. The optimal charge and discharge E/P ratios are 10.4~14h and 5~6.7 h, which is consistent with the exhaustive analysis in *section 5.4.1* and *section 5.4.2*. It indicates the marginal cost reduction of LAESs does not affect the size selection of LFUs and PRUs, as well as the sizes of other system generators. It is due to that the storage value saturates

when its size reaches a specific level in a specified micro-grid. Thus, it does not need larger sizes of LFUs and PRUs when considering economics. But the LAES storage tank size increases from 145 t to 197t, as it can help absorb more wind energy, and reduce wind curtailment and the electricity fee, which is profitable and preferable.

Table 5.6. Optimal design & operation of micro-grid with LAES cost reduction

LAES cost reduction	Engines /MW	WT /MW	Grid /%	HP /MW	Boiler /MW	HS /MWh	LFU /MW	PRU /MW	Tank /tons	System annual cost/k£	LAES annual investment /k£	CO_2 reduction on 2016 level
15%	4	14.63	13.82	5	9	6	3	3.75	145	4277	706.9	41.2%
25%	4	14.60	13.48	5	9	6	3	3.75	197	4190	641.5	41.3%

5.4.3.2 Effects of a higher wind penetration on system design

In this part, two scenarios of wind penetration (64% and 75%) were studied respectively when 25% of LAES cost reduction was assumed, the results are given in Table 5.7 and Figure 5.16. From Table 5.7, it concluded that more wind power percentage is the major driving force to increase the attractiveness of LAES in the micro-grid, the annual investment cost of the LAES increases from k£ 729.2 (64% of wind power) to k£ 958.6 (75% of wind power), as only the value it creates is higher than its investment can the LAES be selected. After the system optimal design, more wind penetration leads to the decrease of gas engines' capacities, as well as the increases in the sizes of LFU, PRU and the tank of the LAES, to absorb and store more wind energy. The rest of power demand is met by purchasing electricity from the grid. As shown in Figure 5.16, the LAES mainly serves as stabilizing wind energy, shaving peak, providing operating reserve and flexibility. The optimal charge/discharge E/P ratios and storage tank size are 27/14 h and 605t when the wind percentage is 75% in the micro-grid. The total CO_2 emissions are reduced by about 55% and 62% in the two scenarios on the 2016 level.

Table 5.7. Optimal design & operation of micro-grid with increasing wind penetration

Wind power %	Engines /MW	WT /MW	Grid /%	HP /MW	Boiler /MW	HS /MWh	LFU /MW	PRU /MW	Tank /tons	System annual cost/k£	LAES annual investment/ k£	CO_2 reduction on 2016 level
64%	2	19.8	20	8	9	10	3	5.2	355	3873.3	729.2	54.6%
75%	1	23.5	20.2	8	11	10	4.8	5.4	605	4058.7	958.6	61.9%

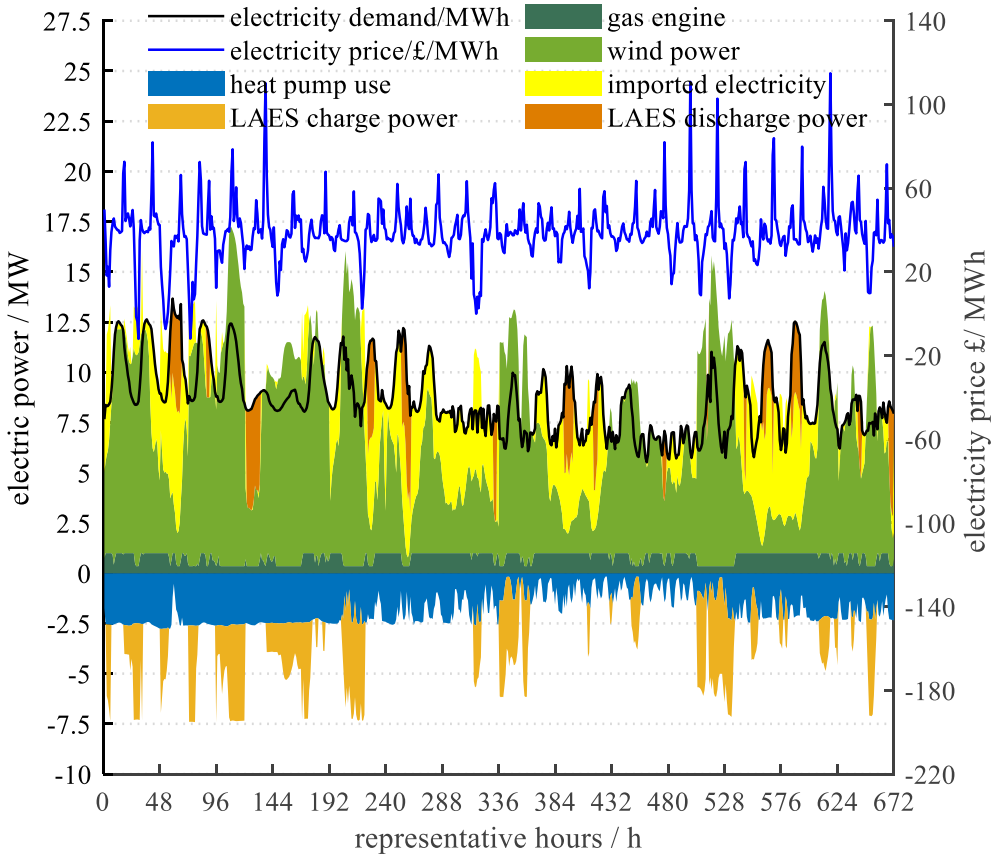

Figure 5.16. Optimal power dispatch of the micro-grid with De-LAES and more wind power

5.4.3.3 Effects of higher electricity prices on system design

In this part, the future grid scenarios were considered, the carbon intensity will drop by 50%, and the electricity prices will go up by 20% and 40% respectively on 2016 level [266]. It is mainly due to higher prices of fuels and more renewables penetration.

Table 5.8. Optimal design & operation of micro-grid with future grid scenarios

Electricity price Increase	Engines /MW	WT /MW	Grid /%	HP /MW	Boiler /MW	HS /MWh	LFU /MW	PRU /MW	Tank /tons	System annual cost / k£	LAES annual investment / k£	CO_2 reduction on 2016 level
20%	3	15.35	20.67	8	10	10	3	4.2	255	3828.4	673.6	57.8%
40%	3	16.38	18.73	8	9	10	3	4.5	279	3928.9	686.9	59.3%

From the results in Table 5.8, when electricity price and the price difference (valley and peak) both go up, the system relies less on the grid but more on wind power, to cut down the operational electricity cost. For LAES selection, the size of LFU keeps unchanged to avoid much increase in its investment cost. But the sizes of PRU and storage tank both increase by respective 7.1% and 9.4%, to capture more electricity price arbitrage opportunities and more excess wind energy. In this scenario, the LAES mainly functions to achieve the electricity arbitrage, peak shaving and operating reserve. In the heating sector, the energy shift from electricity to heat by heat pumps (combined with heat storage) becomes even more active. This is motivated by larger electricity price differences, resulting in the savings on the capital cost of one boiler and the corresponding fuel cost. The system tends to produce more heat and store it when there is low-price electricity and surplus wind energy, and then releases the heating energy to supply heat demand when peak-price electricity occurs. Thus, heat pumps with heat storage is also a good approach to provide system flexibility and absorb excess wind when there is higher renewable penetration, illustrated in Figure 5.17.

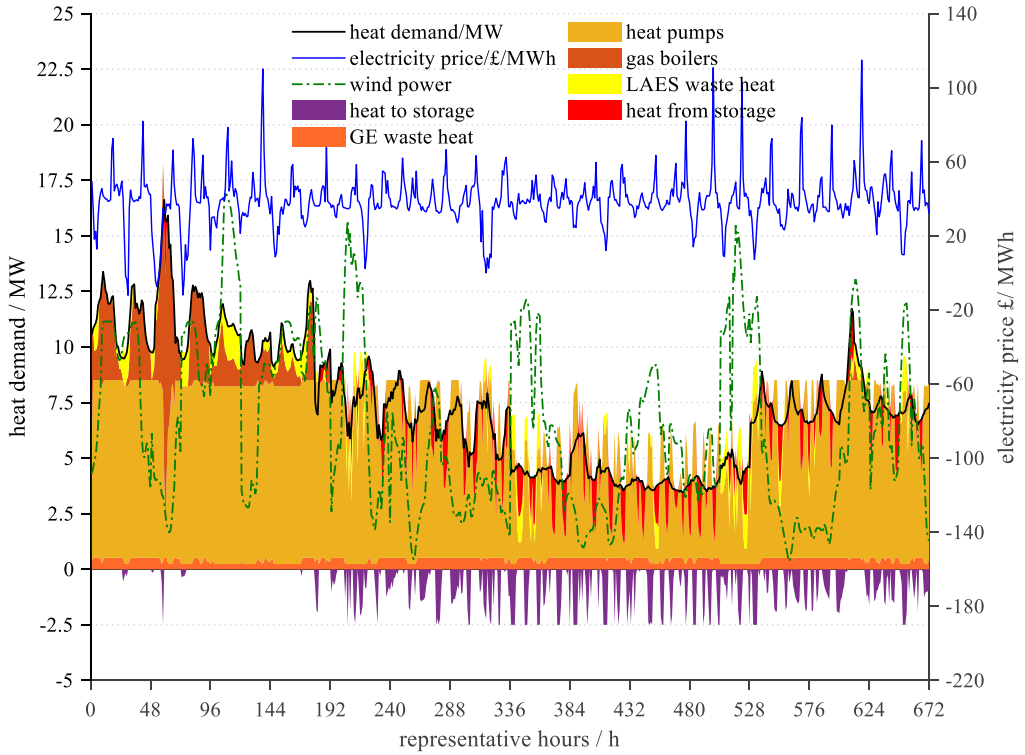

Figure 5.17. Optimal heat dispatch of the micro-grid with De-LAES and larger price differences

5.4.4 Effects of different micro-grid sizes on system design

There is currently no clear threshold for classifying the sizes of micro-grids, but most are in the range of 2 ~ 20 MW [267], few cases can reach up to 50 MW in terms of electric power scale [268]. Thus, to discuss the effects of a high demand on the system design and LAES benefits, the campus power demand is assumed to decrease by 50% (representing a smaller micro-grid) and to increase by 50% (representing a larger micro-grid) on the 2016 level respectively, while keeping at least 50% of renewable power percentage.

Table 5.9. Optimal design & operation considering different sizes of micro-grids

Micro-grid size/times	Wind power ratio/%	Engines/ MW	WT/M W	Grid/ %	HP/M W	Boiler/M W	HS/M Wh	LFU /MW	PRU /MW	Tank/ tons	System annual cost /k£	LAES annual investme nt /k£	CO2 emission s/ tons
0.5	53.15%	0	10.5	43.8	9	2.5	10	3	3	154	1820.1	612.7	5826.7
1.5	50.5%	6	23.9	13.8	12	15	10	3	7.2	450	5478.6	796.1	20537.3

From Table 5.9, in a small micro-grid with lower demands, the LAES can even replace gas engines completely and ideally. The results shows that a single LAES plant is multi-

functional, which is capable of handling peak shaving and excess wind energy, as well as providing the operating reserve, flexibility requirements and waste heat for the micro-grid. However, in a large micro-grid with higher demands, the capacities of the system equipment all increase significantly to meet higher power and heat demands, including the engines, wind turbines, heat pumps and boilers. For the LAES, the LFU size keeps constant at 3 MW because of its low cost-effectiveness. Another reason lies in the capacity of heat pumps increases by 3MW, which can serve as one way to accommodate more wind energy and provide flexibility for the micro-grid. But the sizes of the PRU and storage tank both increase remarkably, to reduce the capacity of the peak gas engine and to provide enough operating reserve. It is due to there are larger differences between the electricity peaks and valleys, as well as a higher requirement for the operating reserve. This case discussion verifies the robustness of the MILP design framework, which is capable of achieving the optimal design and operation of micro-grids with the decoupled LAES under different application scenarios.

5.5 Summary

In this part of work, a decoupled LAES energy storage model under off-design conditions was developed, to adapt to variable renewables and user demands. It was then integrated into a MILP design and operation framework of a hybrid renewable micro-grid (HRMG). The importance of this work lies in it provides the preliminary business model of applying small-scale LAES in hybrid renewable micro-grids, and can promote the optimal deployment of LAES under different scenarios in micro-grids.

Firstly, based upon the framework, the optimal charge/discharge E/P ratios and storage tank sizes of LAES were investigated first by using exhaustive method. It indicates that there exist the optimal sizes of LAES units when it provides different services in a HRMG. The optimal charge/discharge power and storage capacity of LAES vary with the services it

provides. The optimal charge/discharge energy to power ratio are 8/3 h, 12/6 h and 12/6 h corresponding to the arbitrage, wind stabilization and operating reserve.

Secondly, the functions of LAES, TES and battery in the HRMG were analysed, and the total benefits of these storages split into different value streams for the first time. For a micro-grid with 50% of wind power, the LAES in it can help achieve multiple functions, corresponding to six explicit value streams that can be stacked up. They include: the time shifting (13.2%), renewable firming (11.4%), peak shaving (28%), flexibility (21%) and reserve value (20.4%), as well as the waste heat recovery (6%). The total profit of the LAES is 8.2% higher than that of battery storage when the same investments were made

Finally, the optimal design and operation of the HRMG with the decoupled LAES under different scenarios were investigated by the developed MILP framework for the first time. The results indicate the key value of LAESs to support the future HRMGs and its attractiveness in HRMGs, which is mainly motivated by higher requirements on wind power and CO_2 emission reduction. The system design framework can determine the optimal sizes of the micro-grid components and the LAES units. Specifically, the optimal charge/discharge energy to power ratio (27/14 h) and the storage tank size (608 t) of LAES in a micro-grid with 75% wind power are obtained, leading to ~60% of carbon emission reduction on the 2016 level.

6 Achieving a net-zero carbon energy system with liquid air energy storage and the optimal storage combination

6.1 Introduction

6.1.1 Literature review

To build a net-zero carbon energy system, a global effort has been seen in residential, commercial, industry and science areas [3]. A review from Hansen et al. [269] reported that more than 180 of scientific publications about the planning and optimization of 100% renewable energy systems or the net-zero carbon energy systems have been published since 2004. However, it found that most of the articles focused on the power sector, and another problem is that other world areas except for USA, Australia and Europe are not well researched. Diesendorf et al. [270] argued that the transformation of a traditional power system to a 100% renewable system is feasible both technically and economically, but also pointed out this transfer may need more support from government and institutes. It is argued that achieving carbon-free or renewable power systems can be facilitated by the deployment of energy storage technologies at all timescales, including short-, medium- and long-duration storages [271].

6.1.1.1 100% renewable energy system planning

The studies about designing 100% renewable or net-zero carbon energy systems have been conducted across different countries. Budischak et al. [272] developed a renewable grid at the minimum cost in the USA, including onshore wind, offshore wind, solar PV, battery and hydrogen storage. The results indicated that the least-cost system would result in up to three times of excess renewable energy which can be used to replace NG. The electricity cost of a future 99.9% renewable system will be as low as that of today under an optimal mix of

generators and storages (9-72 h). Mathiesen et al. [273] designed a complete renewable energy system including electricity, heating and transport sectors in Denmark, revealing that implementing a 100% renewable energy system will bring economic, climate and social benefits simultaneously. The total emissions of greenhouse gases can be reduced to 10.2% by 2050 compared to 2000 levels. Lenzen et al. [274] studied the possibility of supplying low-carbon electricity for Australia, the LCOE at 20 AU$/kWh can be achieved by the optimal planning. The work also indicated that PHES and biofuel generators are needed to balance the system during periods with low renewables, and showed the significant impacts from transmission networks, biofuel and carbon price. But the system didn't consider multiple energy storage options. Lu et al. [275] also investigated a fully decarbonized and electrified energy system for Australia. The results suggested the cost of such a future energy system for Australia at AU$ 70 - 99/MWh, and confirmed the significance of electricity grids interconnection, demand-side response and mass energy storage.

Brown et al. [276] developed a sector-coupled open energy system model for Europe, which involves electricity, heat and transport sectors, aiming at reducing 95% of CO_2 emissions on 1990 level at a cost-optimal way. The results showed the system investment costs under different scenarios, and revealed the significance of incorporating the battery electric vehicles (BEV), P2G and long-term TES, which can effectively increase the system flexibility, smooth the variability of wind and solar, as well as reduce the total system cost. Child et al. [277] further explored the technical and economic feasibility of a 100% renewable power system for Europe. Two transition pathways, namely regionally-independent and area-interconnected scenarios, were investigated by using LUT (the Lappeenranta University of Technology) energy system transition model. The optimization results indicated that the LCOE of such a system can be reduced from 69 €/MWh to 51 €/MWh when taking the flexible generation and

energy storage into account. Zappa et al. [278] also investigated the feasibility of a 100% renewable power system for Europe. Seven scenarios were developed and studied, the results revealed seven important insights about the future power system development, including the expansions in generation, transmission, wind and solar power capacity, as well as the biomass and biogas capacities etc. It also concluded that the cost of a 100% renewable power system is 30% higher than that of a low-carbon system. Maruf et al. [279] developed an open modelling framework for analysing the feasibility of a 100% renewable and sector-coupled energy system for Germany. The results indicated that such a system is achievable in Germany, the annual investment costs of renewable and heat generators are 17.6~26.6 billion € and 23.7~28.8 billion € respectively. The annual cost of electricity and heat storage is 2.7–3.9 billion €.

Bogdanov et al. [280] developed a 100% renewable energy system with batteries and P2G storage for North-East Asia. The results indicated that the electricity, gas and heat demands can be satisfied by enough renewables at a competitive cost about 69.4 €/MWh (electricity (ele)), and at about 85.6 €/MWh (ele) for a system with higher security. Yue et al. [281] studied the feasibility to achieve a 100% renewable energy system for Ireland, future uncertainties were considered by developing different scenarios. The author suggested that CCS technologies, bioenergy development and imports, as well as the increased annual renewable deployment rate are all crucial for Ireland to achieve the 100% renewable target. Ullah et al. [282] developed a novel energy optimization model to optimize the micro-grid performance, the model considered the uncertainty and non-linearity of renewables by proposing a hybrid demand-response scheme. It combines the multi-objective wind-driven optimization algorithm and the multi-objective genetic algorithm, to reduce the operating cost by 24.5% and the pollution emissions by 19%, as well as to increase the renewable share by ~20%. S. Samsatli and N. J. Samsatli [150] developed a MILP multi-objective optimization

model to achieve the design and operation of multi-vector energy systems. The model was applied into UK to decarbonize the electricity, heat and transport sectors. The results suggested that hydrogen, syngas and electricity are preferable carriers over NG for the future green energy system. The model [140] was also applied to decarbonize domestic transport sector in the UK by developing a wind-hydrogen-electricity network. The results indicated that domestic transport decarbonisation target can be met by combining the onshore wind power and hydrogen, the newly-built hydrogen networks within UK have been planned.

6.1.1.2 Energy storage values in a 100% renewable energy system

There is a growing interest in investigating energy storage value in a 100% renewable energy systems. Haas et al. [283] presented a comprehensive review of energy system expansion planning involving storage technologies. It identified the modelling goal, energy sectors and networks, as well as modelling details, time resolutions and uncertainties of such modelling frameworks. The trends and challenges of storage expansion modelling were proposed as well. Pleßmann et al. [130] developed a model to estimate the energy storage demand for a 100% renewable global power system, the storage technologies include the battery, TES and P2M storage. The results indicated that the average 142 €/MWh of LCOE can be achieved by integrating renewables and optimal energy storage mix (1.5 TWh of batteries, 1,690 TWhth of P2M, and 73.6 TWhth of TES) globally. Weitemeyer et al. [9] investigated the impacts of storage sizes and efficiencies on the integration of 100% renewable power. The results indicated that small and efficient storage technologies help integrate a large portion of renewables, seasonal storage is only needed when the renewable penetration is higher than 80%. Blakers et al. [284] proposed a 100% renewable electricity supply in Australia by using wind and solar energy, as well as hydrogen and biomass energy. It explored the effects of PHES and stronger transmission network on the system performance, concluding that the

estimated LCOE is AU$ 93/ MWh. Child et al. [285] developed a 100% renewable scenario for Finland in 2050, in which the roles of different kinds of storage technologies were discussed. The results indicated the indispensable roles of energy storages in zero-emission energy system, specifically, electricity storage systems provided 21% of electricity demand, and heat storage supplied 4% of heat demands, while gas storage is capable of providing 26% of gas demand in total.

An energy system expansion model REMix was developed by F. Cebulla et al [286], which studied the future generators and storage technologies mix for European countries. The results revealed the capacity requirements, the spatial distribution and dispatch of four different storage technologies, including Li-ion battery, H_2 storage, CAES and PHES. It indicated that 206 GW and 30 TWh of storage systems are needed when the renewable ratio reaches 89%. Haas et al. [287] developed a storage expansion planning model for Chile, which considered the power reserves and energy autonomy, as well as three different storage technologies, including Li-ion battery, PHES and hydrogen storage. Jonathan et al. [288] investigated the effects of three bulk energy storage (BES) technologies, including CO_2-geothermal, CAES and PHES, on the system-wide CO_2 emissions and water requirements. The results showed that the BES can increase the utilization of wind power capacity, as well as the natural gas and coal power capacity. It also suggested that compensation mechanism for BES should be set up to enhance their environmental sustainability. Colbertaldo et al. [89] developed a power system simulation model which incorporates hydrogen as the major storage technology, to manage a high penetration of renewables in California. The results indicated that a combination of wind (94 GW) and solar case (40 GW) requires about 77 GW of electrolysis capacity. The comparison with battery storages indicated that a purely electric battery-based energy system is 55 times more expensive than the system with merely hydrogen storage.

Denholm et al. [289] investigated the impacts of storage duration on reducing renewable curtailment under 55% of renewable penetration in Texas grid. The results indicated that 3% ~ 6% of curtailment reduction can be achieved by deploying 8.5 GW of storage with 4h of duration. Storage with very long duration (like seasonal storage) is not desirable for areas with high renewable penetration. Jafari et al. [290] have investigated the impacts of energy storage systems and their time scales on the renewable integration and system costs in Italy. The results indicated that EES can help reduce the system costs, further, short-term EES (less than 10 h) are more advantageous than long-term EES (~100h) in terms of renewable integration and providing system flexibility. Mao et al. [291] developed an energy system modelling framework considering the dynamic charging/discharging efficiencies and the degradation of Li-ion battery storage. The results indicated that it is acceptable to ignore the dynamic efficiencies to reduce computational volume, but the degradation of battery would lead to different generation expansion scheme. Guerra et al. [271] developed an optimization framework to study the storage portfolio to achieve high (75-90%) or ultrahigh (>90%) renewable integration in the USA power systems. The results suggested that a least-cost carbon-free power system can be achieved with renewable curtailment and a combination of short- and long-duration storage systems. Østergaard et al. [292] discussed the roles and economic effects of electric storage, heat storage and biogas storage in a 100% renewable energy system in Denmark, of which primary resources are wind, solar, geothermal and biomass energy. It concluded that electricity storage is the most influential and costly method for renewable integration. The literature about the planning of 100% renewable energy systems or net zero carbon energy systems were summarized in Table 6.1 for reference and comparison.

Table 6.1. The literature summary of 100% renewable energy systems planning

Authors	Target year	Target area	System Model	Time/space resolution	Type scenario	Major results
Mao et al., 2022	2050	Distributed energy system	Capacity expansion model	Hourly/ One node	Overnight	The degradation of battery storage would affect the generator expansion in 2050 greatly, battery would be an attractive option for deep carbonization by 2050
Islam Maruf et al., 2021	2050	Germany	OSeEM-DE - sector coupled energy system	Hourly/ Two nodes	Overnight	A 100% renewable-based and sector-coupled system for electricity and heat is feasible in Germany with LCOE at ~ 20.26 €/MWh
Lu et al., 2021	2030	Australia	Super grid & smart grid' modelling framework	Half hourly/ Multiple nodes	Transition	A fully decarbonized and electrified energy system for Australia costs at AUS $ 70 - 99/MWh
Omar J. Guerra et al., 2021	2050	America	SDOM (Storage deployment optimization model)	Hourly/ Seven nodes	Overnight	A 85% of renewable energy system for America can be achieved with LCOE at ~ 38.1 - 80.4 $/MWh
Yue et al., 2020	2050	Ireland	Ireland TIMES model	Four season with 5 year interval/ One node	Transition	A maximum 94% of renewables (including onshore and offshore wind, solar and ocean energy, bioenergy import) to power Ireland can be achieved. The transition is more cost-effective with carbon capture technologies
Samsatli et al., 2019	2050	Great Britain	Value Web MILP Model	Hierarchical, non-uniform/ Multi-zone	Transition	Decarbonizing the electricity and heat sectors in UK by deploying renewables and hydrogen storage is feasible.

						Roughly 80% of electric heat and 20% of hydrogen heat is the optimal case
Samsatli et al., 2019	2050	Great Britain	Value Web MILP Model	Hierarchical, non-uniform/ Multi-zone	Transition	The Value Web Model can help determine the investment capacities of generators, resources, and their transport and storage methods for a 100% renewable energy system in UK 2050
Colbertaldo et al., 2019	2030	California	Lumped power system model with storage	Hourly/ one node	Overnight	A 100% renewable power system (94 GW solar and 40 GW wind) for California is feasible with the hydrogen (77 GW electrolysis system) as the primary storage
Child et al., 2019	2050	Europe	LUT Energy System Transition model MOSEK optimiser	Hourly/ 0.45° * 0.45° spatial resolution	Transition	Two transition pathways to a 100% renewable power system for Europe is technically and economically feasibility with LCOE at ~ 51 Euros/MWh
Zappa et al., 2019	2050	Europe	PLEXOS modelling package	Hourly/ 0.75°×0.75° Spatial resolution	Overnight	A 100% renewable power system for Europe is feasible, the cost of such a system is 30% higher than that of a low-carbon system
T. Brown et al., 2018	2030	Europe	PyPSA-Eur-Sec-30	Hourly/ Multiple nodes	Overnight	It revealed the significance of incorporating the battery electric vehicles (BEV), power-to-gas units (P2G) and long-term thermal energy storage into the system

Sadiqa et al., 2018	2050	Pakistan	LUT Energy System Transition model MOSEK optimiser	Hourly/Multiple nodes	Transition	A 100% renewable power and water system for Pakistan primarily relying on solar (96.6%) is feasible with the LCOE at ~ 46.2 €/MWh
J. Haas et al., 2018	2050	Chile	LEELO - linear storage expansion planning model	Hourly/ Four nodes	Overnight	The optimal storage combination and their capacities when providing multiple services were determined. The batteries are the main provider of (short-term) power reserves, assisted by pumped-hydro, hydrogen storage is for providing (long-term) energy autonomy
Blakers et al., 2017	2030	Australia	National electricity power model	Hourly/Multiple cells	Overnight	A 100% renewable energy system, involving wind, solar, hydroelectricity, biomass and strong interconnection, is feasible for Australia at ~ AU$93/MWh of LCOE
Bogdanov et al., 2016	2030	North-East Asian	Linear multi-node energy system optimization model	Hourly / 0.45° * 0.45° Spatial resolution	Overnight	A 100% renewable energy based system is feasible for North-East Asian, the system cost is 69.4 €/MWh
Samsatli et al., 2016	2050	Great Britain	STeMES - Spatial-temporal energy systems model	Half hourly/ Multiple nodes	Overnight	The domestic transport demand in UK can be met by onshore wind turbines and hydrogen-electricity network

6.1.2 Research aim

From the literature review above, there are three gaps that were identified to motivate this part of work, they include: 1) for the UK, few studies have been presented to discuss the net-zero carbon pathways and their comparisons, as well as the role of future CCS technology, which have been ignored. 2) There are few studies that have paid attention to LAES and its roles in helping construct a net-zero carbon energy system, though LAES is a promising storage technology, meanwhile, the comparison and compensation of different storage technologies were not discussed within system planning cases for the UK. 3) Few zonal energy system design models for the UK have been developed to guide the planning of conventional generators with CCS, renewables, heat generators and storage technologies. Thus, the novelties and major work of this study are concluded as the following three ones:

a) A three-zone energy expansion model of the UK has been developed, which couples the power and heat sectors, integrating conventional electric generators, renewables, energy storage technologies, operating reserve and heat generators. The expansion planning and operation of these generators in different zones can be determined by 2050.

b) Different pathways for the UK have been developed to decarbonize the power and heat sectors, including the 100% renewable energy system, the net-zero carbon system and different hydrogenation rates in heat sectors, the comparisons have been made to show the technical feasibility and economic performance of different pathways.

c) The roles of LAES and other storage technologies in different de-carbonization scenarios have been discussed, the required expansion capacities and the optimal storage combination in different zones can be determined.

It is important to highlight that this kind of study involves many assumptions, from technologies, efficiencies and future capital costs to the simplification of grid and heat network topology. Due to that, the significance of investigating future system evolution pathways does

not lay in the exact values obtained as simulation results, but rather in general trends, orders of magnitude, and mutual comparison found for the investigated variables, with the final aim of assessing the potential cost-effective pathways and providing guidance for policy makers to make long-term planning.

The structure of this part of work is constructed as: *Section 6.2* introduces the case study and the demands profiles. *Section 6.3* introduces the techno-economic assumptions of different generators and scenario developments. *Section 6.4* details the energy system expansion model. *Section 6.5* presents the results and discussions. The summary is made in *section 6.6*.

6.2 Case study introduction

6.2.1 Space and time resolution of the case study

Great Britain has pledged to achieve the net-zero carbon emission by 2050 at COP26 [4], which makes it a suitable case study for this work. In the work of Samsatli et al. [140], Great Britain has been divided into 16 zones (shown as in Figure 6.1 (a)) based on the National Grid Seven Year Statement (NGSYS) [140]. Each zone has its own features, including its dynamic electricity, heat and transportation demands, available primary resources, conversion and storage technologies etc. [293]. However, in this study, in order to achieve the proper trade-off between the accuracy and calculationburden, the 16 zones have been aggregated into three major zones, namely Scotland zone (zone 1), Midlands zone (zone 2) and South zone (zone 3), shown as in Figure 6.1(b). Accordingly, the relevant demands, primary resources and capacities of conversion and storage technologies were aggregated as well. It is simplified that there is a transmission line between zone 1 and zone 2, as well as another transmission line between zone 2 and zone 3. For the time resolution, the representative day method was adopted to reduce the computing burden. Specifically, a whole year was distinguished into four seasons, namely the spring, the summer, the autumn, and the winter. Four representative days were selected from each season to represent the low demand (or the lowest renewable capacity factor), the first

medium demand (medium 1, or the first medium renewable capacity factor), the second medium demand (medium 2, or the second medium renewable capacity factor) and the high demand (or the highest renewable capacity factor), which are repeated in each season [34,294].

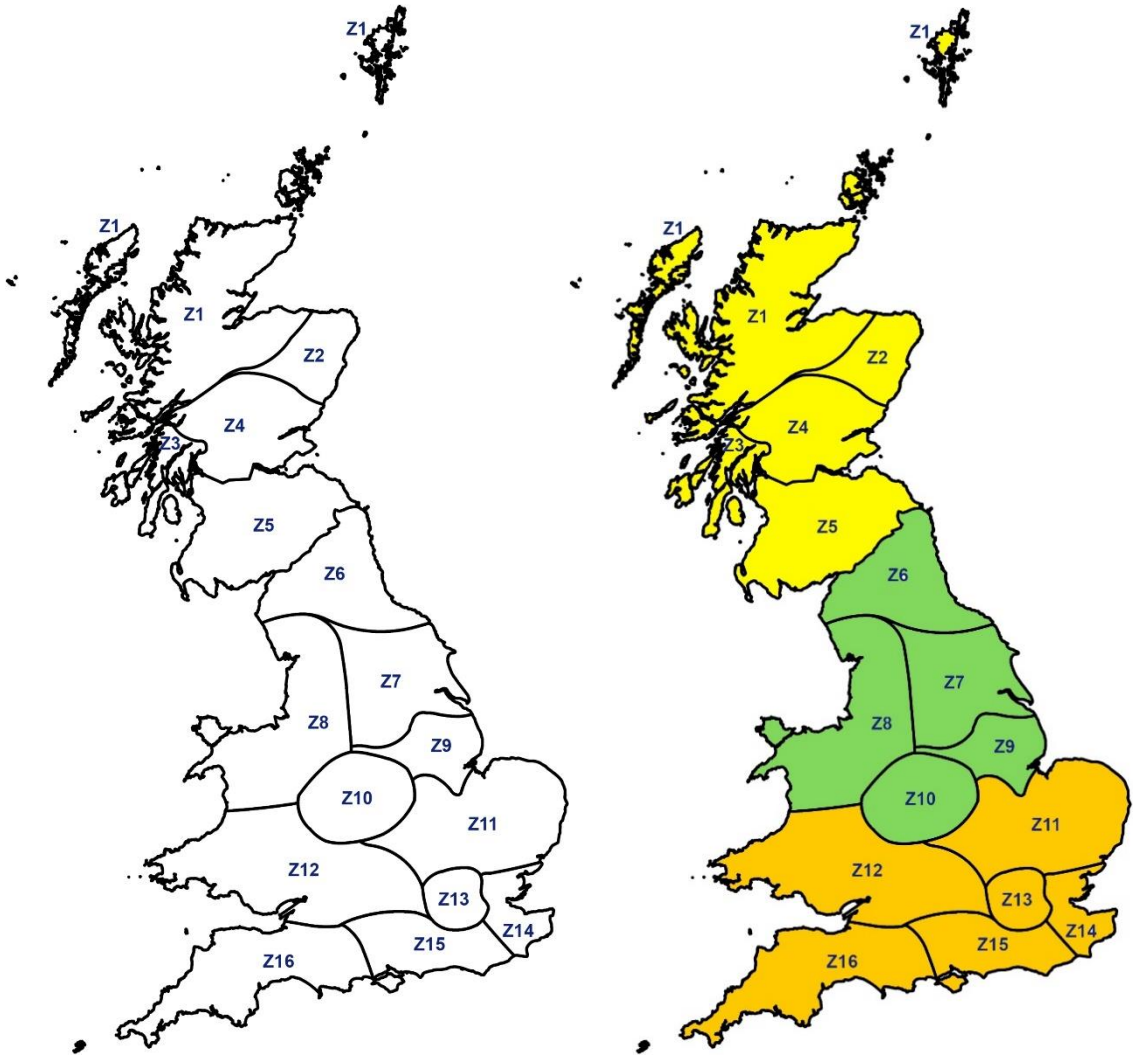

(a) (b)

Figure 6.1. District zones in Great Britain (a) 16 separate zones; (b) three aggregated zones (yellow – zone 1, green – zone 2, orange – zone 3)

6.2.2 Electricity demand

In all three zones, a representative day with hourly electricity load in each season was selected as the electricity demand input. Each representative day was divided into four time periods (t1 - t4) based on the work of Samsatli et al. [150], shown as in Table 6.2. The demand variation in each season was determined by applying a factor (between 90% - 110%) on the

representative data in Table 6.2, which was assumed to characterize the low, medium 1, medium 2 and high demands. A weight factor was applied to consider the repeated cycles of the representative data in each season. Meantime, according to the transport transition plan of the UK [295], high electrification rate is expected by 2050 to meet the net-zero emission pathway, the electricity need from the transport sector will be added into the electricity demand in power sector. The total electricity demand in power sector in Great Britain in 2020 was around 300 TWh, which is expected that there is 42.9% of increase by 2050 [296].

Table 6.2. Electricity demand of different zones in UK in 2020 (unit: GW) [150]

Seasons	Time periods[1]	ZONE 1	ZONE 2	ZONE 3
Spring	t1	1.851	8.455	11.097
	t2	2.312	10.614	13.912
	t3	2.524	11.709	15.298
	t4	2.545	11.612	15.247
Summer	t1	1.605	7.427	9.708
	t2	2.019	9.354	12.225
	t3	2.349	10.949	14.284
	t4	2.314	10.64	13.935
Autumn	t1	1.849	8.504	11.14
	t2	2.331	10.747	14.067
	t3	2.599	12.09	15.78
	t4	2.681	12.227	16.058
Winter	t1	2.223	10.113	13.293
	t2	2.655	12.174	15.959
	t3	2.916	13.484	17.632
	t4	3.055	13.843	18.216

Notes:

1. 'Time periods' representation: 't1' – 12.00 am – 7.00 am, 't2' – 7.00 am – 12.00 am, 't3' – 12.00 am – 6.00 pm, 't4' – 6.00 pm – 12.00 am.

6.2.3 Heat demand

Heat demand in Great Britain was estimated based on the data given by Sansom et al. [297] and Samsatli et al. [298]. It presents large seasonal variability, thus, the average heat demands from 16 successive durations (in consistent with the representative days of electricity demands) were selected, shown as in Figure 6.2 (a) (green short line). The average monthly

demand was further disaggregated into different heat demand periods per day by using the day profiles given by Samsatli et al. [150], shown as in Figure 6.2 (b). The spatial heat demands distribution in three zones were estimated based on the results in the work [298]. The weight factor in heat sector is the same as that in electricity sector. The total annual residential heat demand in 2020 was 480 TWh [297], which was predicted to be reduced by 18.8% when considering the better insulation and more efficient appliances in the future [296].

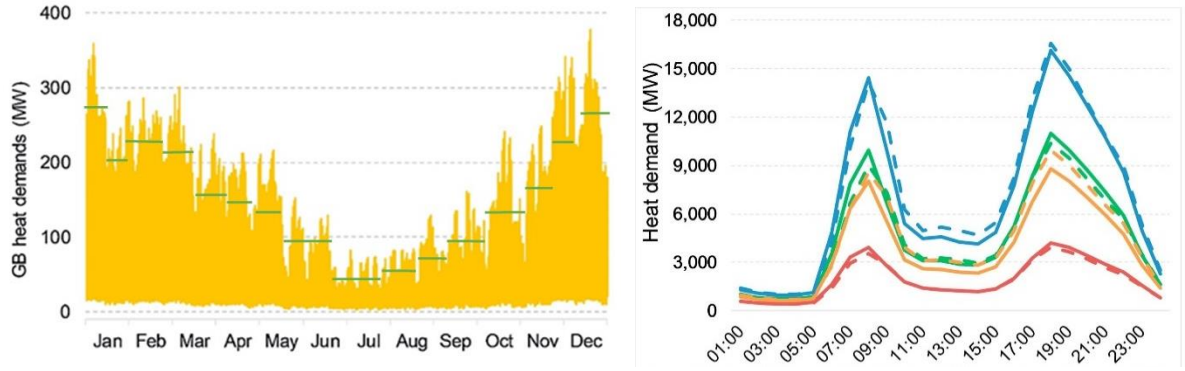

(a) (b)

Figure 6.2. The heat demand profile: (a) Monthly heat demand in a year [298]; (b) Hourly heat demand in a day [150]

6.2.4 Renewable profiles

The widely developed renewables in the UK include onshore wind power, solar PV and offshore wind power. The renewable capacity factor is defined as the availability of wind or solar energy for a specific hour at a certain location [194], which was obtained from the open source website 'Renewables.ninja' [299], the representative capacity factors of onshore wind, offshore wind and solar power are shown in Figure 6.3. As renewables are sporadic and varying sources which do not display the repeating daily, weekly or monthly cycles. Thus, in order to capture the variability of renewables, four representative profiles of each renewable in each season were selected based on the yearly capacity factors of onshore wind power, solar PV and offshore wind power. They represent the lowest, the first medium and the second medium, as well as the highest capacity factors of each season [300]. Finally, a scale factor was used to

scale up or down the representative profiles to make sure the average renewable capacity factor in each season keeps the same value with the original renewable profiles [301]. It was assumed the renewable capacity factors in 2050 in the UK keep the same value as they are nowadays. A weight factor was estimated based on the occurrence rate of each representative renewable profile in a season.

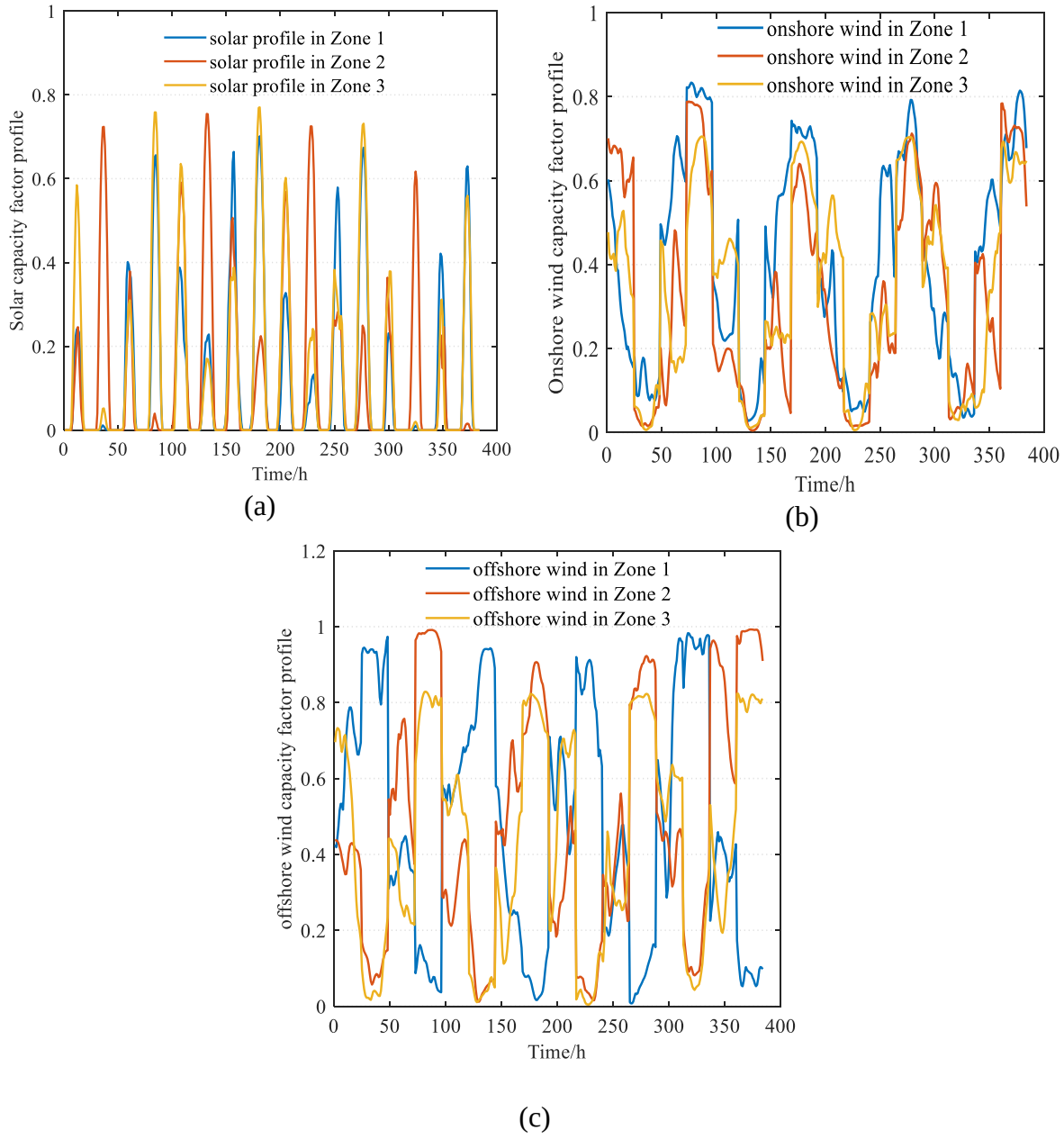

Figure 6.3. The representative renewable capacity factor profiles: (a) Solar energy; (b) Onshore wind energy; (c) Offshore wind energy

6.3 Techno-economic input data

6.3.1 Electricity generators

Currently, the thermal generators for producing electricity in the UK include open cycle gas turbines (OCGT), combined cycle gas turbines (CCGT), biomass plants, hydro run of river power plants, as well as a small number of coal, oil and nuclear plants, of which current capacities were obtained from the work [302]. These thermal generators might be partly or totally retired in the future, depending on the energy transition pathways of the whole country. In this study, the brown-field approach was considered [122], it means the future thermal generators mix and their capacities were to be determined by the energy expansion model based on the current capacities and the decarbonisation scenarios.

In order to reduce the calculation burden, the nuclear and hydro run of river power plants were assumed to provide electricity all year round at the rated capacity considering their small capacities, long lifetime and no carbon emissions. There are no expansions of these two technologies. Besides thermal generators, a large share of electricity generation comes from renewables, including the solar PV, onshore wind power, and offshore wind power. Their current capacities were obtained from the work [296][302], and their available deployment potentials came from the work [150]. The CCS technology and hydrogen CHP were considered to decarbonize the future power system. The capital expenditure (CAPEX), fixed (FOM) and

Table 6.3. The capacities, CAPEX, FOM, VOM and performance metrics of electricity generators [296] [302] [290,303][304,305]

Thermal generators	Current capacity / GW	Minimum load / %	Efficiency / %	CAPEX (£/kW)	FOM (£/kW/year)	VOM (£/kWh)	Lifetime/ years
Coal plant	4.58	50%	33.1	1741.5	37.60	3.73	40
CCGT	20.98	30%	51.7	561.6	13.16	2.03	30
OCGT	11.30	30%	34.1	353.81	13.16	3.08	30
Diesel/oil plant	1.31	50%	34.8	972	16.77	2.24	40
Nuclear plant	7.83	100%	38	3525	78.75	5.85	60
Biomass cogeneration	3.86	30%	34.1	850.5	18.87	2.07	30
Hydro run of river	1.47	\	90	2018.25	7.11	0	40
Pumped hydro storage	2.90	\	90	3071.25	26.33	0.35	40
Onshore wind	12.73	\	\	827.48	10.53	0.195	25
Offshore wind	10.41	\	\	1659.38	24.57	0.27	25
Solar power	11.96	\	\	398.39	8.07	0	25
Import HVDC[1]	5.00	\	95	0.7 (£/kW.km)	0.00075	0	50
CCGT CCS[2]	0	30%	44.7	1290	30.09	2.44	30
OCGT CCS	0	30%	33.1	1082	30.09	3.44	30
Hydrogen CHP[3]	0	35%	40.5	1183.8	31.3	2.03	30

Notes:

1. HVDC - high voltage direct current.
2. CCS – carbon capture and storage.
3. CHP – combined heat and power.

variable (VOM) operation and maintenance costs of these generators were collected from different works, listed in Table 6.3, in which appropriate assumptions have been made based on the technologies' developments.

6.3.2 Heat generators

In order to meet the heat demand (including the domestic and commercial sectors, but excluding industrial sector), the current major heating technologies in the UK are gas boilers (~80%) and district heat networks. The future low-carbon heating technologies include air-source heat pumps (ASHP), ground-source heat pumps (GSHP), biomass boilers and hydrogen boilers, as well as electric heaters [306]. Considering the outdoor temperature variation, the COP of ASHP is varying with temperature and the value was obtained from the work [297], shown as in Figure 6.4. As there are land constraints for GSHP in each zone, it is more suitable for the area with low-density population, while ASHP is appropriate for the area with high-density population [281], the difference is represented in the capacity limitations of these two technologies in different zones.

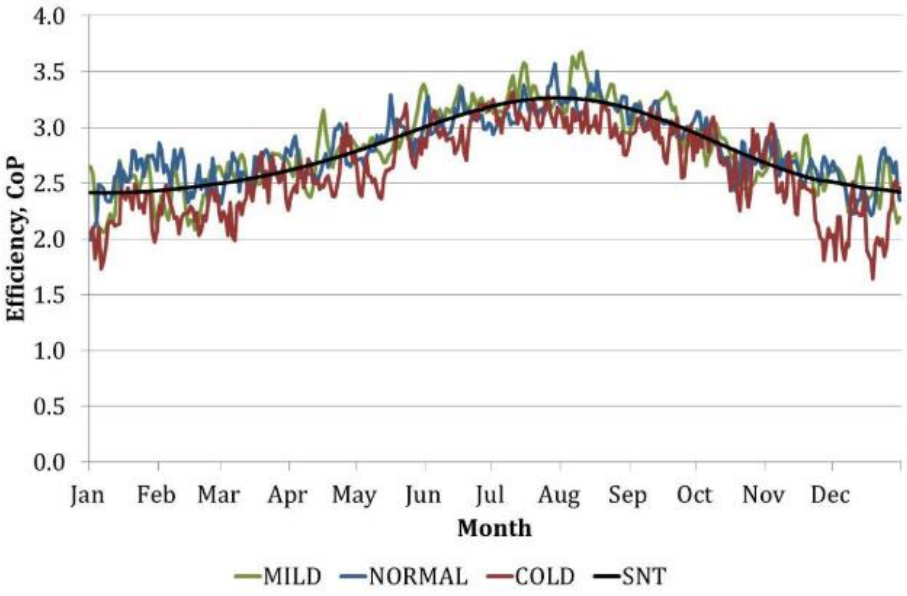

Figure 6.4. The COP of ASHP varying with outdoor temperature [297]

The current capacity of district heat network in the UK is ~22.4 GW [296][307], the major heat sources for district heat network are central gas boilers and gas CHP units, as well as the waste heat from power generators [296]. Oil boilers are to be disused by 2050. It reported that there is a potential of 50% of reduction in the cost of district heat networks [297]. Other renewable heat sources, like geothermal heat and concentrated solar heat, were not included in the model considering their low potential share in the whole system [308]. The installed capacities of different generators were estimated by counting the households and population in each zone [293][309]. The CAPEX and FOM of these generators were collected from several work, listed in Table 6.4. The VOM of heat generators was neglected due to its marginal value. The electricity and heat fuel costs in 2050 (including coal, oil, natural gas, electricity, biomass, H_2) were predicted by the work [303][310][311], collected and listed in the Table 6.5.

Table 6.4. Techno-economic performance parameters for heat generators [306,312,313][276,279,281,298]

Heat generators	Current capacity/GW	Efficiency / %	CAPEX £/kW	FOM (£/kW/year)	lifetime/ years
Gas boiler (Dom[1])	610.4	85	97.9	2.86	15
Oil boiler	51.8	70	109.5	2.86	15
Electric storage heaters[2]	50.4	82	255.88	1.93	15
ASHP (Dom)	2.8	Varying[3]	758.63	1.43	20
GSHP (Dom)	2.8	3.2	1011.5	6.12	20
Electric heaters (Dom)	22.4	90	118.5	1.43	20
H_2 boiler (Dom)	0	90	142.8	3.43	15
Biomass boiler (Dom)	0	80	278.2	2.86	20
District heating network (NG[4])	22.4	82	709	32.4	30
District heating network (H_2[5])	0	82	743	32.4	30

Notes:

1. Dom-domestic application
2. Electric storage heaters refer to the devices consist of an input electric heater (3 kW), a heat storage (23.1 kWh) and an output electric heater (1.5 kW) [297].
3. Varying – refers to the COP of ASHP is varying with outdoor temperature.
4. NG – natural gas, meaning the district heating network is mainly powered by central gas boiler.
5. H_2 – hydrogen, meaning the district heating network is mainly powered by central H_2 boiler.

Table 6.5. Fuel price prediction and CO_2 emissions in 2050 [303][310][311]

Fuel	$ 2013 per barrel of oil equivalent in 2050	£ 2020 per MWh in 2050	CO2 emission intensity kg/MWh
Oil	130	69	238.9
Coal	29	15	341.2
Gas	79	42	180.9
Bio	108	65	0
H_2	\	130	0

6.3.3 Storage technologies

For electric storage technologies, different storages present different efficiencies, durations, energy losses, investment costs and lifetimes etc. There is no one storage system that is perfect to cope with all the relevant problems for a net-zero carbon energy system. A good solution is to consider the storage combination and utilize their compensation characteristics [277].

In the UK, the large-scale deployed storage is PHES, the total discharge power capacity is 2.9 GW, in which 0.74 GW is in zone 1, another 2.16 GW is in zone 3, and there is no PHES existing in zone 2. Considering the geographical constraints, it is assumed that there is no further capacity expansion of PHES in the future [302]. Another promising mid-term energy storage without geographical limitation is LAES, a 5 MW/15 MWh plant has been built near Manchester, and another 50 MW/250 MWh plants will be established in 2022 in the North of England [63]. The major subsystems of LAES are the liquefaction unit, liquid air storage tank and the power recovery unit, of which capital costs were estimated respectively based on the investment of a pilot plant [55].

Besides these two technologies, the Li-ion battery with quick response time and short duration was considered, it is a promising storage technology that can be integrated with intra-day renewables [290]. There is 1.1 GW of battery power capacity within UK at present [314]. In order to achieve net-zero carbon emissions, the long-term storage was considered as well,

H_2 storage is a promising seasonal storage with large amounts of hydrogen stored in reservoirs. This storage technology involves electrolysers to absorb renewables to produce hydrogen, and fuel cells to convert power back to consumers [24]. The stored H_2 can also be injected into gas pipeline and used as heat and transport fuel to support hydrogen economy [297]. The technical and economic performance of these four storage technologies were listed and compared in Table 6.6.

For heat storage, both the short-term and long-term heat storages were considered [276], differentiating in different charging and discharging durations. Short-term heat storage is suitable for domestic applications. At present, there are about 1.8 million homes with electric storage heaters and approximately 11 million homes with hot water tanks (e.g. 400L water tank corresponding to 20-23 kWh per tank) in the UK [315]. Long-term heat storage refers to water tanks with sizes between hundreds to thousands of cubic meters (eg. 300 m^3 tank corresponding to 14 MWh per tank), which are mainly used for districted heating networks and communities [315]. The techno-economic performance parameters of these two heat storage technologies were listed in Table 6.7.

6.3.4 Scenario development

In this work, different decarbonisation scenarios were considered for the UK to compare the techno-economic performance of the future energy systems. As only the power and heat sectors were considered, the base case 1 did not consider the power and heat energy system decarbonisation and coupling, as well as storage systems, other scenarios include different decarbonisation pathways, and different electrification rates and hydrogenation rates in heat sector. The electrification rate and hydrogenation rate are defined as the electricity or hydrogen consumption in the total heat fuel consumption. Case 2 considered sector coupling

Table 6.6. The techno-economic performance parameters of different storage technologies [288][316][317][28][318][280]

Energy storage	Charge power cost £/kW	Discharge power cost £/kW	Energy storage cost £/kWh	Fixed O&M cost £/kW per year	Variable O&M cost £/kWh	Charge efficiency %	Discharge efficiency %	Charge E/P ratio / h	Discharge E/P ratio/h	Self-discharge rate 1/h	Life time/ years
PHES	243	785.2	78	11.92	0.0067	0.95	0.85	100	8	0	40
LAES	714.1	204.2	19.5	13.5	0.0002	0.7	0.85	10	6	0.01%	25
Li-ion	150	156	212.5	6	0.0002	0.95	0.95	5	4	0.25%	15
H2S[1]	450	375	0.85	16.7	0.0004	0.75	0.64	40	20	0	20

Table 6.7. The techno-economic performance parameters of different heat storage

Heat storage	Charge power cost £/kW	Discharge power cost £/kW	Energy storage cost £/kWh	Fixed O&M cost £/kWh per year	Variable O&M cost £/kWh	Charge efficiency %	Discharge efficiency %	Charge E/P ratio / h	Discharge E/P ratio/h	Self-discharge rate 1/h	Life time
Long-term[2]	0	0	16	1.7	Neg	90	90	30	50	Neg	30
Short-term[3]	0	0	40	1.7	Neg	92.5	92.5	8	10	Neg	20

Notes:

1. H2S – it refers to hydrogen to storage.
2. Long-term thermal storage refers to thermal storage that is suitable for distribute heating network.
3. Short-term thermal storage refers to thermal storage that is suitable for domestic applications.
4. All the charge and discharge cost are estimated based on the technology development, the variable O & M cost of heat storage can be neglected.
5. The Fixed O&M costs (£/kW per year) of LAES and H2S storage were estimated based on CAES.
6. The operating costs could be estimated to be around 0.25% of total investment cost and maintenance cost approximately 1%.

and introduced CO_2 tax. Case 3 is a nearly 100% renewable power system (99% of renewable ratio in power sector) and a net-zero carbon (zero carbon emissions) heat system without storage expansion. Case 4 is a 100% renewable power system and a net-zero carbon heat system with storage expansion. Case 5 is a net-zero carbon power system and a net-zero carbon heat system without storage expansion. Case 6 is a net-zero carbon power system and a net-zero carbon heat system with storage expansion. Case 7 is a net-zero carbon power system and a net-zero carbon heat system with storage expansion and 50% of heat hydrogenation rate. These cases were listed in Table 6.8. Except for these scenarios, sensitivity analysis was also conducted to take some future uncertainties into account, including different hydrogenation rates and different storage durations.

Table 6.8. Different future energy system scenarios

Scenarios	Sector coupling & CO_2 tax	A 100% renewable power system	A net-zero carbon power system	A net-zero carbon heat system	Heat hydrogenation rate	Storage expansion
1	×	×	×	×	×	×
2	✓	×	×	×	×	×
3	✓	✓	×	✓	×	×
4	✓	✓	×	✓	×	✓
5	✓	×	✓	✓	×	×
6	✓	×	✓	✓	×	✓
7	✓	×	✓	✓	50%	✓

6.4 Energy system modelling

6.4.1 Modelling framework

In order to achieve the planning and operation optimization of the net-zero carbon energy system in the UK in 2050, the MILP-based energy expansion planning model was developed, which is an extension of the model 'GenX' [319] developed by a research team

from MIT. The model in this work can determine the optimal expansion and retirement capacities of different electricity and heating generators and storage technologies, as well as the optimal dispatches and commitment decisions of these technologies, to meet electricity and heat demand and other constraints at the lowest cost. The design and operational constraints of these technologies are described in details in *section 6.4.2*. The optimization framework is shown as in Figure 6.5.

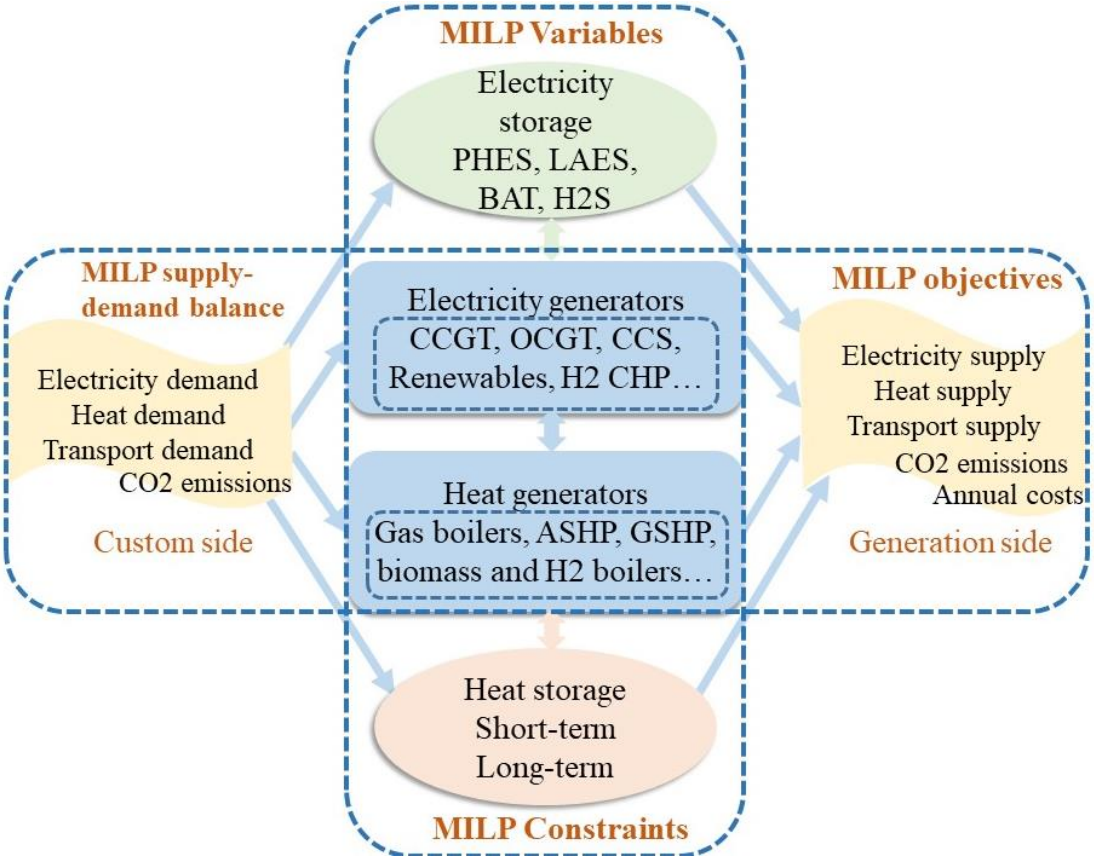

Figure 6.5. Country-level MILP-based energy system expansion model framework

6.4.2 Modelling constraints

6.4.2.1 Electricity generators

As described in *section 6.3.1*, the existing electricity generators and their existing capacities (*P_est_TG*) in the UK are presented in Table 6.3. The brownfield approach was adopted to determine the new (*P_new_TG*) and retired capacities (*P_rtr_TG*), as well as their commitment/start-up/shut-down decisions and numbers (*num_com_TG*, *num_sta_TG*,

num_shut_TG), as well as the dispatched power outputs (*PinG_TG*). It was assumed that the generators clustered in each zone have the identical capacity sizes (P_0*_TG*), the electricity efficiencies (η*_TG_ele*), lifetime (*Lifetime_TG*), minimum power output (*P_min_TG*), ramp up and down rates, and minimum online (*Min_online_TG*) and offline durations (*Min_offline_TG*). In such a way, instead of determining the commitments by using binary numbers , the clustered integer numbers were adopted to reduce the binary variables and improve the computational efficiency. It means the commitment numbers of each generator in each zone vary from zero to the maximum available number. eq. (6.1), eq. (6.2), eq. (6.3), eq. (6.4), and eq. (6.5) express the newly installed, retired, committed, started and shut-down numbers or capacities of generators, which are limited by its maximum, existing and retired numbers or capacities. eq. (6.6) expresses the committed numbers or capacities of generators at the t^{th} time period, which is correlated with those at the t-1^{th} time period. eq. (6.7) - eq. (6.10) state the reserved capacity for providing the primary and secondary reserve (both upward and downward). eq. (6.11) - eq. (6.12) express the power outputs of generators and reserve capacities, which are limited by their allowed minimum and maximum power capacities. eq. (6.13) - eq. (6.14) express the minimum and maximum online and offline durations of generators. eq. (6.15) expresses the fuel consumptions of thermal generators.

$$0 \leq num\_new\_TG_{i,z} \leq num\_max\_TG_{i,z}, \quad \text{eq.(6.1)}$$

$$0 \leq num\_rtr\_TG_{i,z} \leq num\_ext\_TG_{i,z}, \quad \text{eq.(6.2)}$$

$$0 \leq num\_com\_TG_{i,t,z} \leq num\_ext\_TG_{i,z} + \cdots num\_new\_TG_{i,z} - num\_rtr\_TG_{i,z}, \quad \text{eq.(6.3)}$$

$$0 \leq num\_sta\_TG_{i,t,z} \leq num\_ext\_TG_{i,z} + \ldots num\_new\_TG_{i,z} - num\_rtr\_TG_{i,z}, \quad \text{eq.(6.4)}$$

$$0 \leq num\_shut\_TG_{i,t,z} \leq num\_ext\_TG_{i,z} + \ldots num\_new\_TG_{i,z} - num\_rtr\_TG_{i,z}, \quad \text{eq.(6.5)}$$

$$num\_com\_TG_{i,t,z} = num\_com\_TG_{i,t-1,z} + \cdots num\_sta\_TG_{i,t,z} - num\_shut\_TG_{i,t,z}, \quad \text{eq.(6.6)}$$

$$0 \leq rev1\_up\_TG_{i,t,z} \leq P_0\_TG * \ldots$$
$$rev1\_up\_ratio\_TG_{i,z} * num\_com\_TG_{i,t,z}, \quad \text{eq.(6.7)}$$
$$0 \leq rev1\_dn\_TG_{i,t,z} \leq P_0\_TG * \ldots$$
$$rev1\_dn\_ratio\_TG_{i,z} * num\_com\_TG_{i,t,z}, \quad \text{eq.(6.8)}$$
$$0 \leq rev2\_up\_TG_{i,t,z} \leq P_0\_TG * \ldots$$
$$rev2\_up\_ratio\_TG_{i,z} * num\_com\_TG_{i,t,z}, \quad \text{eq.(6.9)}$$
$$0 \leq rev2\_dn\_TG_{i,t,z} \leq P_0\_TG * \ldots$$
$$rev2\_dn\_ratio\_TG_{i,z} * num\_com\_TG_{i,t,z}, \quad \text{eq.(6.10)}$$
$$PinG\_TG_{i,t,z} - rev1\_dn\_TG_{i,t,z} - rev2\_dn\_TG_{i,t,z} \geq \cdots$$
$$P_0\_TG * P\_min\_TG_{i,z} * num\_com\_TG_{i,t,z}, \quad \text{eq.(6.11)}$$
$$PinG\_TG_{i,t,z} + rev1\_up\_TG_{i,t,z} + rev2\_up\_TG_{i,t,z} \leq$$
$$P_0\_TG * P\_max\_TG_{i,z} * num\_com\_TG_{i,t,z}, \quad \text{eq.(6.12)}$$
$$num\_com\_TG_{i,t,z} \geq \sum_{t^*=t-DT\_online\_TG_{i,z}}^{t} num\_sta\_TG_{i,t^*,z}, \quad \text{eq.(6.13)}$$
$$num\_ext\_TG_{i,z} + num\_new\_TG_{i,z} - num\_rtr\_TG_{i,z} - \cdots$$
$$num\_sta\_TG_{i,t,z} > \sum_{t^*=t-DT\_offline\_TG_{i,z}}^{t} num\_shut\_TG_{i,t^*,z} \quad \text{eq.(6.14)}$$
$$fuel\_TG_{i,t,z} = PinG\_TG_{i,t,z}/\eta\_TG_{i}\_ele, \quad \text{eq.(6.15)}$$

where, *TG* – thermal electricity generators, *P* – power capacity or output, *num* – the number of generators. *new* – newly installed, *ext* – the existing number or capacity, *rtr* – the retired number or capacity, *sta* – the start-up number or capacity, *shut* – the shut-down number or capacity. *com* – the committed number or capacity, *rev1* – the primary reserve, *rev2* – the secondary reserve. *ratio* – the capacity percentage, *up* – the upward reserve, *dn* – the downward reserve. *0* – the initial capacity, *min* – the minimum number or capacity, *max* – the maximum number or capacity. *DT* – duration time, *online* – the online number or capacity, *offline* – the offline number or capacity, *fuel* – fuel consumption, *ele* – electricity. CO_2 – carbon dioxide, ems – emissions, *fuel*_CO_2 – the CO_2 content in a kind of fuel, *i* – the i^{th} generator, *t* – the t^{th} time period, *z* – the z^{th} zone.

6.4.2.2 Heat generators

As described in *section 6.3.2*, the existing heat generators and their existing capacities (*P_est_HG*) in the UK are presented in Table 6.4. The number of heat generators were counted in million homes in the work [296]. But in this work, the clustered capacities of different generators were considered to avoid large amount of calculation volume. The committed heat power capacity (*P_com_HG*) is limited by the existing capacity (*P_est_HG*), the newly installed (*P_new_HG*) and retired capacities (*P_rtr_HG*), expressed in eq. (6.16) - eq. (6.18). The heat power capacity injected into the heat network (*PinH_HG*) is limited by the committed heat power capacity, expressed in eq. (6.19). The fuel consumption of heat generators is related to the heat efficiencies (*η_HG_heat*), expressed in eq. (6.20).

$$P\_com\_HG_{\,i,t,z} = P\_est\_HG_{\,i,z} + P\_new\_HG_{\,i,z} - P\_rtr\_HG_{\,i,z} \quad \text{eq.(6.16)}$$

$$0 \le P\_new\_HG_{\,i,z} \le P\_ava\_HG_{\,i,z}, \quad \text{eq.(6.17)}$$

$$0 \le P\_rtr\_HG_{\,i,z} \le P\_est\_HG_{\,i,z}, \quad \text{eq.(6.18)}$$

$$0 \le PinH\_HG_{\,i,t,z} \le P\_com\_HG_{\,i,t,z}, \quad \text{eq.(6.19)}$$

$$Fuel\_HG_{\,i,t,z} = PinH\_HG_{\,i,t,z} / \eta\_HG_i\_heat, \quad \text{eq.(6.20)}$$

where, HG – heat generators, ava – the available numbers or capacities, heat – the heat efficiency.

6.4.2.3 Renewable generators

The existing renewable generators and their existing capacities (*P_est_Rew*) in the UK are presented in Table 6.3. It was assumed there is no retirement of all renewable generators, the numbers of newly built generators (*num_new_Rew*) are limited by the maximum allowed numbers or capacities in eq. (6.21). The committed numbers of renewable generators (*num_com_Rew*) are limited by the existing (*P_est_Rew*) and newly built numbers or capacities, expressed in eq. (6.22). The available renewable power capacity is limited by its capacity factor, expressed in eq. (6.23). The renewable power injected into the grid (*PinG_Rew*) is constrained

by the available power capacity, expressed in eq. (6.24). The curtailed renewable power (*P_curt_Rew*) is expressed in eq. (6.25).

$$0 \leq num\_new\_Rew_{i,z} \leq num\_max\_Rew_{i,z}, \quad \text{eq.(6.21)}$$

$$num\_com\_Rew_{i,z} = (num\_ext\_Rew_{i,z} + \ldots + num\_new\_Rew_{i,z}) * P_0\_Rew_i, \quad \text{eq.(6.22)}$$

$$P\_ava\_Rew_{i,t,z} = capaf\_Rew_{i,t,z} * num\_com\_Rew_{i,t,z} * P_0\_Rew_i \quad \text{eq.(6.23)}$$

$$0 \leq PinG\_Rew_{i,t,z} \leq P\_ava\_Rew_{i,t,z}, \quad \text{eq.(6.24)}$$

$$P\_curt\_Rew_{i,t,z} = P\_ava\_Rew_{i,t,z} - PinG\_Rew_{i,t,z}, \quad \text{eq.(6.25)}$$

where, *capaf* – the renewable capacity factor, *curt* – the curtailed energy.

6.4.2.4 Storage technologies

In this study, four energy storage technologies were considered for the renewable integration. Currently, there are only large-scale PHES systems existing in the UK, battery and LAES have small capacities, hydrogen storage can be considered non-existing. Storage technologies were divided into three subsystems, the charging units, the storage units and discharging units, which have different capital costs and efficiencies. The clustered capacities of storage technologies were considered in the planning process. As these storages are used for integrating renewables, so the charging power (*Pcha_new_sto*) was taken as the newly designed variable, it is constrained by the available storage power capacity (*Pcha_ava_sto*), expressed in eq.(6.26). The storage capacity (*E_new_sto*) and discharging power (*Pdis_new_sto*) are calculated based on the charging (EPR_{cha}) and discharging (EPR_{dis}) energy to power ratio (*EPR*), expressed in eq. (6.27) and eq. (6.28). The power injected into (*PinG_sto*) and withdrawn from (*PfmG_sto*) the power grid are expressed in eq. (6.29) and eq. (6.30). The storage technologies can serve as the primary (*rev1*) and secondary reserve (*rev2*) as well, expressed in eq. (6.31) - eq. (6.34), the discharging power can serve as the upward reserve (*up*), the charging power can serve as downward reserve (*dn*), depending on their response times and reserve capacity ratios. The energy level (*Elevel_sto*) of storage at the t^{th} time period is

correlated with that at the t-1th time period, as well as the charging and discharging power, expressed in eq. (6.37). The charging decision (*Cha_sto*) and discharging decision (*Dis_sto*) are conflicted with each other, expressed in eq. (6.38).

$$0 \le Pcha\_new\_sto_{\,i,z} \le Pcha\_ava\_sto_{\,i,z} \quad \text{eq.(6.26)}$$

$$E\_new\_sto_{\,i,z} = EPR_{cha,i} * Pcha\_new\_sto_{\,i,z} \quad \text{eq.(6.27)}$$

$$Pdis\_new\_sto_{\,i,z} = E\_new\_sto_{\,i,z} / EPR_{dis,i} \quad \text{eq.(6.28)}$$

$$0 \le PinG\_sto_{\,i,t,z} \le Dis\_sto_{\,i,t,z} * Pdis\_eff\_sto_{\,i} * Pdis\_ava\_sto_{\,i,z}, \quad \text{eq.(6.29)}$$

$$0 \le PfmG\_sto_{\,i,t,z} \le Cha\_sto_{\,i,t,z} * Pcha\_ava\_sto_{\,i,z} / Pcha\_eff\_sto_{\,i} \quad \text{eq.(6.30)}$$

$$0 \le rev1\_up\_sto_{\,i,t,z} \le rev1\_up\_ratio\_sto_{i,z} * Pdis\_ava\_sto_{\,i,z} \quad \text{eq.(6.31)}$$

$$0 \le rev1\_dn\_sto_{\,i,t,z} \le rev1\_dn\_ratio\_sto_{i,z} * Pcha\_ava\_sto_{\,i,z} \quad \text{eq.(6.32)}$$

$$0 \le rev2\_up\_sto_{\,i,t,z} \le rev2\_up\_ratio\_sto_{i,z} * Pdis\_ava\_sto_{\,i,z} \quad \text{eq.(6.33)}$$

$$0 \le rev2\_dn\_sto_{\,i,t,z} \le rev2\_dn\_ratio\_sto_{i,z} * Pcha\_ava\_sto_{\,i,z} \quad \text{eq.(6.34)}$$

$$0 \le PinG\_sto_{\,i,t,z} + rev1\_up\_sto_{\,i,t,z} + rev2\_up\_sto_{\,i,t,z} \le \cdots Pdis\_eff\_sto_{\,i} * Pdis\_ava\_sto_{\,i,z} \quad \text{eq.(6.35)}$$

$$0 \le PfmG\_sto_{\,i,t,z} + rev1\_dn\_sto_{\,i,t,z} + rev2\_dn\_sto_{\,i,t,z} \le \cdots Pcha\_ava\_sto_{\,i,z} / Pcha\_eff\_sto_{\,i} \quad \text{eq.(6.36)}$$

$$Elevel\_sto_{\,i,t,z} = Elevel\_sto_{\,i,t-1,z} + PfmG\_TG_{\,i,t,z} * Pcha_{eff_{sto\,i}} - Pdis\_eff\_sto_{\,i} / PinG\_sto_{\,i,t,z} - Eloss\_sto_{\,i,t,z} \quad \text{eq.(6.37)}$$

$$Cha\_sto_{\,i,t,z} + Dis\_sto_{\,i,t,z} \le 1, \quad \text{eq.(6.38)}$$

where, *cha* – the charging process, *dis* - the charging process, *eff* – the efficiency, *EPR* – energy to power ratio, *Eloss* – the energy loss.

6.4.2.5 Balance constraints

The power and thermal demand and supply should be balanced at each time step, eq. (6.39) expresses the power balance, meaning the power generated by thermal generators, renewables and storages minus the power stored by electric storages and the power consumed by heat sectors equals to the electricity demand. eq. (6.40) expresses the heat demand, meaning the heat demand is met by the heat power generated by heat generators and heat storages minus the heat power stored in heat storages.

$$PinG\_TG_{t,z} + PinG\_Rew_{t,z} + PinG\_sto_{t,z} - \cdots$$
$$PfmG\_sto_{t,z} - HG\_ele\_need_{t,z} = Demand\_ele_{t,z}, \quad \text{eq.(6.39)}$$
$$PinG\_HG_{t,z} + PinH\_sto_{t,z} - PfmH\_sto_{t,z} = Demand\_heat_{t,z} \quad \text{eq.(6.40)}$$

6.4.2.6 Optimization objective

The optimization objective is to minimize annual total cost (eq. (6.41)), including the amortized capital cost, fixed and variable operational and maintenance cost of conventional electricity generators, renewables, storage technologies and heat generators, as well as curtailment penalty and CO_2 tax, expressed as in eq. (6.42) – eq. (6.49).

$$Obj = InvC_{tot,TG} + InvC_{tot,Rew} + InvC_{tot,sto} + \cdots$$
$$+ InvC_{tot,HG} + InvC_{tot,Hsto} + Cost_{cur,Rew} + Cost_{tax,CO2} \quad \text{eq.(6.41)}$$

$$InvC_{tot,TG} = \sum_{i=1}^{Num1}(Amf_{TG,i}CAPEX_{TG,i} + FOM_{TG,i} + VOM_{TG,i}) \quad \text{eq.(6.42)}$$

$$InvC_{tot,Rew} = \sum_{i=1}^{Num2}(Amf_{TG,i}CAPEX_{Rew,i} + FOM_{Rew,i} + VOM_{Rew,i}) \quad \text{eq.(6.43)}$$

$$InvC_{tot,sto} = \sum_{i=1}^{Num3}(Amf_{sto,i}CAPEX_{sto,i} + FOM_{sto,i} + VOM_{sto,i}) \quad \text{eq.(6.44)}$$

$$InvC_{tot,HG} = \sum_{i=1}^{Num4}(Amf_{HG,i}CAPEX_{HG,i} + FOM_{HG,i} + VOM_{HG,i}) \quad \text{eq.(6.45)}$$

$$InvC_{tot,Hsto} = \sum_{i=1}^{Num5}(Amf_{Hsto,i}CAPEX_{Hsto,i} + FOM_{Hsto,i} + VOM_{Hsto,i})$$ eq.(6.46)

$$CAPEX_{sto} = \sum CAPEX_{sto,cha} + CAPEX_{sto,dis} + CAPEX_{sto,eng}$$ eq.(6.47)

$$Cost_{curt,Rew} = C_{curt,Rew}P\_curt\_Rew_{tot}, \quad \text{eq.(6.48)}$$

$$Cost_{tax,CO2} = C_{tax,CO2}ems_{tot,CO2}, \quad \text{eq.(6.49)}$$

$$Amf = \frac{IR(1+IR)^{Lf}}{(1+IR)^{Lf}-1}, \quad \text{eq.(6.50)}$$

$$LCOE = \frac{InvC_{tot}+Cost_{curt,Rew}+Cost_{tax,CO2}}{ele_{tot,ann}} \quad \text{eq.(6.51)}$$

$$LCOH = \frac{InvC_{tot}+Cost_{curt,Rew}+Cost_{tax,CO2}}{heat_{tot,ann}} \quad \text{eq.(6.52)}$$

where, *obj* – the optimization objective, *InvC* – investment cost, *Cost* – the incurred cost, *C* – the price cost. *CAPEX* – the capital expenditure, *FOM* – the fixed operational and maintenance cost. *VOM* - the variable operational and maintenance cost, *eng* – the energy capacity of storages. *curt*- the curtailed energy, *ems* – emissions, *CO2* – carbon dioxide, *tot* – total, *Amf* – the amortized factor of a generator. *Num* – the number of generators, *1 - 5* – differentiate different generator set, *IR* – the interest rate. *Lf* – the lifetime of a generator, *LCOE* – levelized cost of electricity, *LCOH* – levelized cost of heat, *ann* – annual production

6.4.3 Model validation

The energy expansion model ‘GenX’ was developed by Jenkins and Sepulveda [319]. A case study in Italy has been investigated based on ‘GenX’ model already by Jafari et al. [303], in which the current thermal power plants and renewables, as well as two types of storage technologies (PHES and battery storage), as well as their technical and economic characteristics were considered. After a whole-year simulation and optimization, the optimal power capacity and annual generation were obtained. Referring to the techno-economic data of generators, as well as the demands and renewable profiles from the work of Jafari et al. [290,303], the extended model developed by this study was applied to the run the simulation for ~500 h (limited by the gained input profiles). The results were obtained and compared with

those of 2030 case of Jafari et al. [303]. The comparison was shown in Figure 6.6. It can be seen that the installed capacities and hourly generation of different generators were roughly in consistent with the results in [303]. But the major differences lie inthe major the onshore wind power capacity (32.8 GW (this study) vs. 23 GW [303]) and its generation profile, as well as the installed capacities of CCGT, OCGT and Biomass generators This can be explained by the differentsimulation durations, as only 500 h of simulation was conducted in this study due to the limited input data accessed

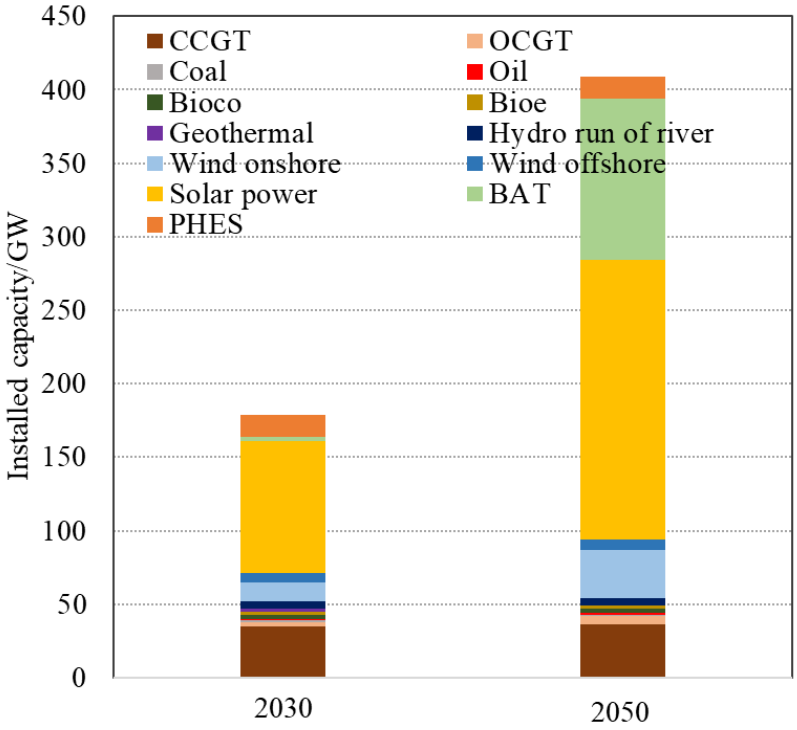

Figure 6.6. The validation results of the case study in Italy

6.5 Results and discussions

6.5.1 Different pathways for a net-zero carbon energy system

6.5.1.1 The effects of different pathways on power sector

As has been stated in *section 6.3.4*, there are seven de-carbonization pathways (scenarios or cases), the optimization results in power sector were shown in Figure 6.7 and Figure 6.8. As can be seen in Figure 6.7, in base case 1 (non-decarbonization, non-coupling

and no CO_2 tax), the installed capacity of CCGT (37.4 GW) is less than that of renewables (70.8 GW), the total CO_2 emissions were ~140 million tons. Case 2 showed less installed capacity of CCGT but more capacities of CCGT-CCS (9 GW), onshore wind power (46.4 GW) and solar power (25 GW), which is mainly due to the minor effect of the imposed CO_2 tax. From an electricity generation view in Figure 6.8, in case 1 and case 2, half electricity generation is from conventional generators (CCGT, OCGT and CCGT-CCS), and another half is from renewables. The renewable share only increased from 51.7% (case 1) to 55.8% (case 2).

In order to achieve a nearly 100% renewable power system and a net-zero carbon heat system without storage technologies in case 3, renewable generators' capacities were increased by 2.94 times (Figure 6.7), amounting to 245.4 GW. 31.9 GW of biomass plants provide 42.1% of electricity generation, and 213.4 GW of wind and solar power provides 51% of electricity, the rest installed capacity is 58.4 GW of CCGT to provide flexibility together with biomass plants. But when storage technologies were added on the base of case 3, the total installed capacities of thermal generators decrease by 16.3% in case 4. It is mainly due to that storage technologies can replace CCGT and biomass plants to provide system flexibility, and can also absorb large amounts of wasted renewable energy, the renewable curtailment ratio is reduced from 37.1% (case 3) to 9.2% (case 4). To be noted, as the renewable ratio is not exactly 100% (>99%), thus, there are still ~15-48 million tons of CO2 emissions in case 3 and case 4 (Figure 6.8).

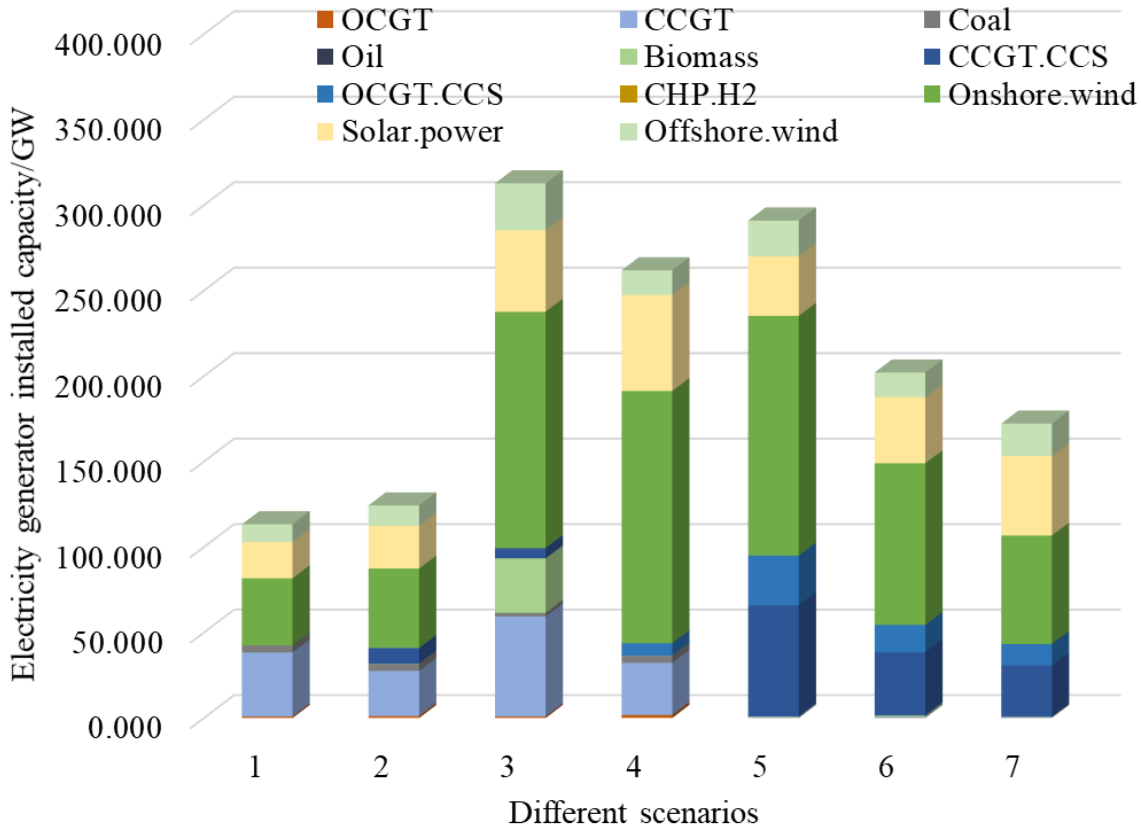

Figure 6.7. The installed capacity of electricity generators of different scenarios

Case 5 represents a net-zero carbon power system and a net-zero carbon heat system without storage expansion. It can be seen from Figure 6.7 that the total renewable capacities are 196.4 GW. The CCGT-CCS (65 GW) and OCGT-CCS (29 GW) plants are installed to achieve net-zero carbon emissions in power sector, both provide about half of electricity generation shown in Figure 6.8. Biomass plants does not run frequently, as the fuel cost of biomass is much higher than that of NG . When there are storage technologies added on base of case 5, the total installed capacities of generators are reduced by 30.5% in case 6. The installed capacities of CCGT-CCS, OCGT-CCS, onshore wind power, solar power and offshore wind power were 37 GW, 16 GW, 94.5 GW, 38.7 GW and 14.4 GW respectively. The renewable curtailment ratio is reduced from 41.7% to 7.3%, it means energy stores can help firm more renewable energy (renewable generation 74.2% in Figure 6.8), to meet peak power and provide flexibility.

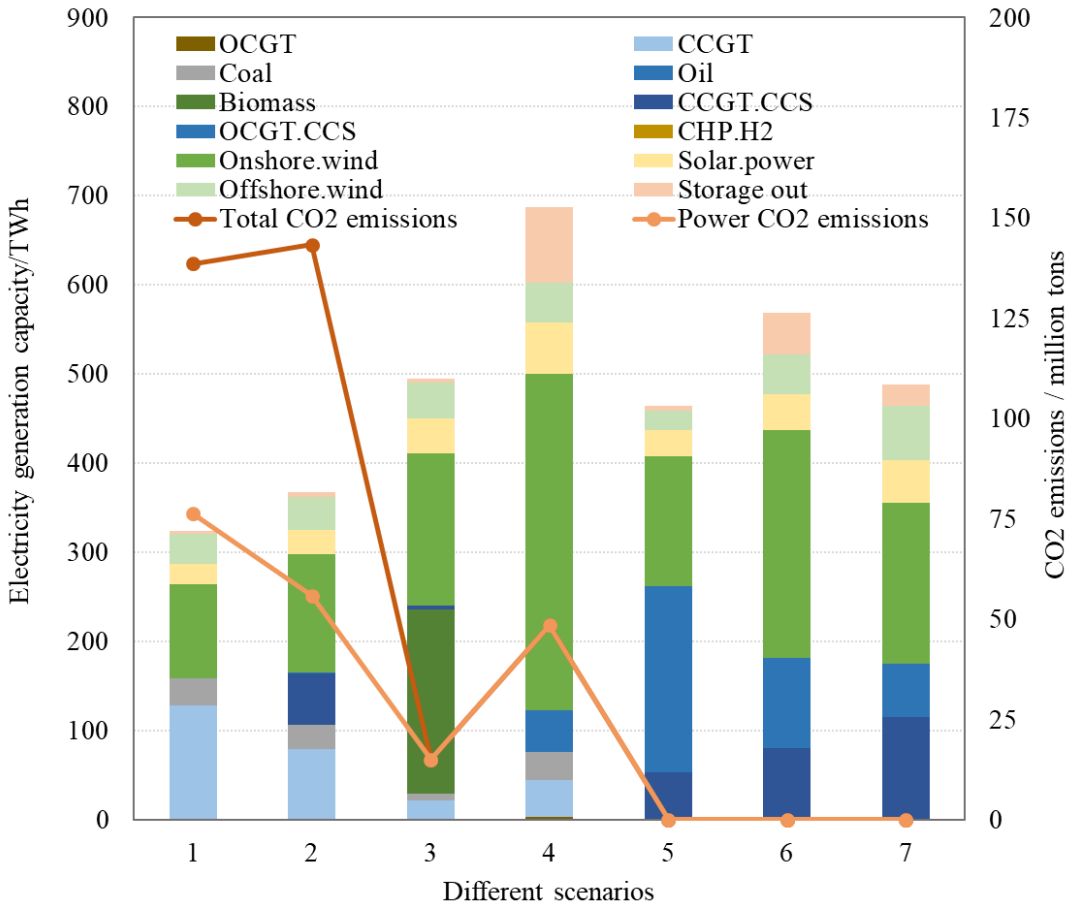

Figure 6.8. The annual generation capacity of electricity generators of different scenarios

Case 7 was developed on the base of case 6, the heat hydrogenation rate increases from 0 to 50%. From Figure 6.8, the total installed capacity of thermal generators is reduced further by 14.8%, as more H_2 boilers are used in heat sectors. The operation of heat pumps and their electricity consumption are reduced significantly, which requires less electric generators and electricity. Overall, the major power expansions lie in onshore wind power, solar power, CCGT-CCS and OCGT-CCS, to build a future net-zero carbon power system. It also clearly shows the crucial roles of storage technologies in absorbing large share of renewables and reducing curtailment, as well as providing system flexibility and operating reserve, to reduce the total generator installed capacities.

6.5.1.2 The effects of different pathways on heat sector

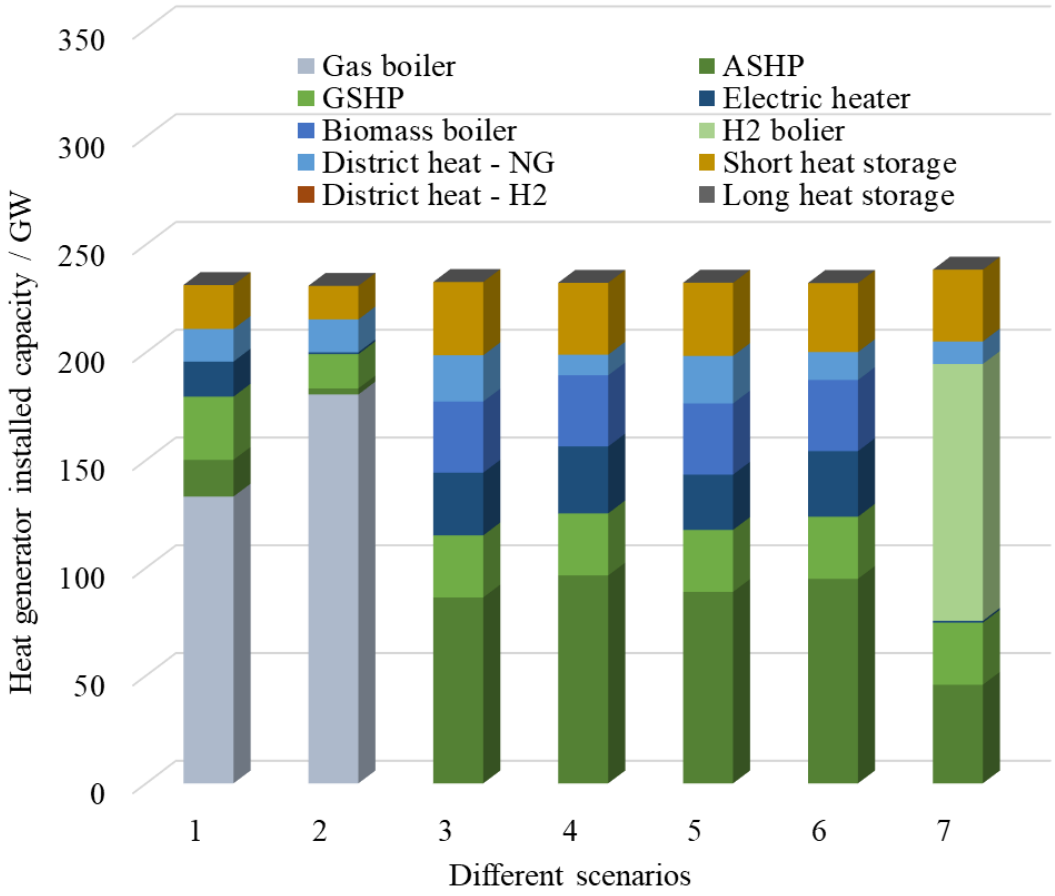

Figure 6.9. The installed capacity of heat generators of different scenarios

The heat sector results under different scenarios are shown in Figure 6.9, Figure 6.10 and Figure 6.11. Figure 6.9 shows the installed capacities of heat generators under different scenarios. It can be seen that gas boilers are the major heat generators when there is no heat decarbonisation requirements (case 1 and case 2), of which installed capacities amount to over 130 GW in total. However, for a net-zero carbon heat energy system (case 3 – case 6), gas boilers are disused to reduce carbon emissions, the largest share (~80 – 90 GW) of heat generator is ASHP. Other generators, including GSHP, electric heaters and biomass boilers account for the similar share (~ 30 GW). To be noted, the expansion capacity of GSHP was constrained due to its large land occupation. The installed capacities of district heat network depend on the waste heat from electricity generators (CHPs), varying between 10 GW and 20

GW. But when there is 50% of heat hydrogenation rate in case 7, the installed capacities of H_2 boilers increase to ~120 GW, while those of ASHP and GSHP are reduced significantly to supply the base heat demand. The short-term heat storage (domestic application) also would play a crucial role due to its low cost and capability to provide heat system flexibility, its installed capacities are about 20 GW.

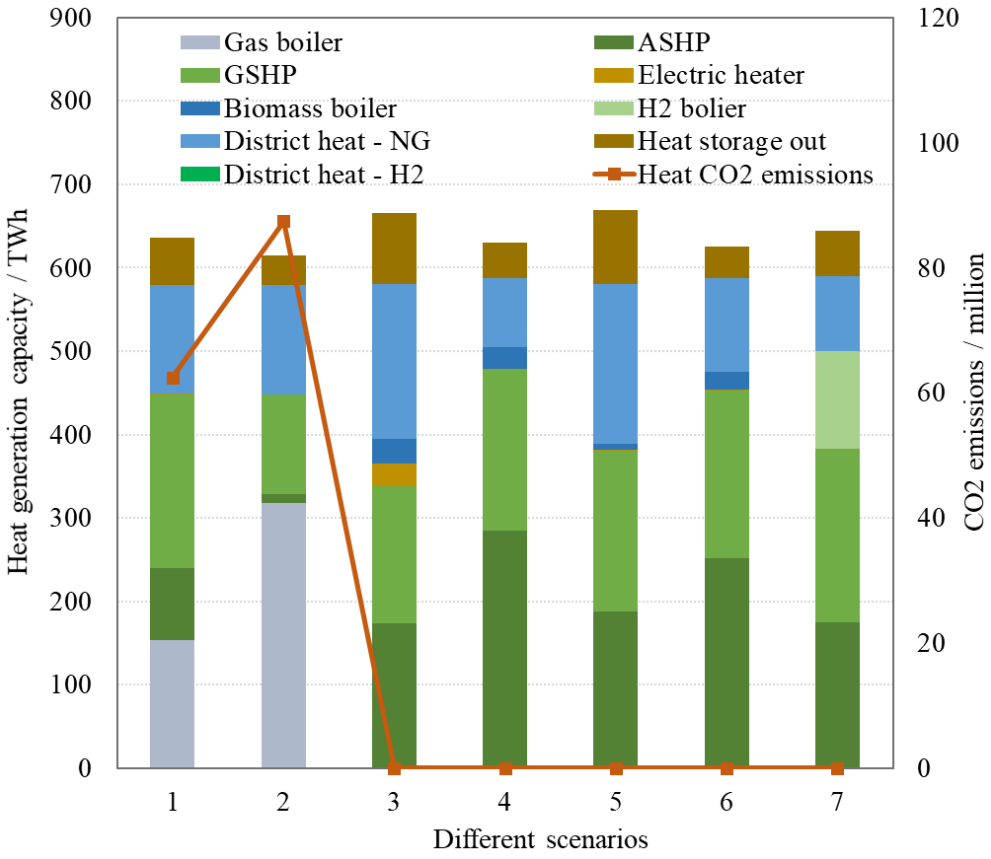

Figure 6.10. The annual generation capacity of heat generators of different scenarios

Accordingly, from a heat generation view in Figure 6.10, gas boilers produce 150 TWh and 310 TWh of heat in case 1 and case 2 as the major generators, there is almost no generation from ASHP in case 2 due to its lower efficiency and higher electricity consumption than those of GSHP. From case 3 to case 7, the heat generations from ASHP and GSHP present the similar share, as GSHP is used as the base heat generators and ASHP serves as the peak heat generators. There is only a small portion of heat generation from electric heaters and biomass boilers due to their high fuel consumptions (electricity and biomass) and high fuel costs, which just serve

as back-up generators. Another big part of heat generation comes from the district heat network, to recover wasted heat energy from CHP units and to reduce system operational cost (fuel cost). In case 7, H_2 boilers provide about 117 TWh of heat energy, they only serve as the peak electric generators due to the lower efficiency and higher price of H_2 in 2050.

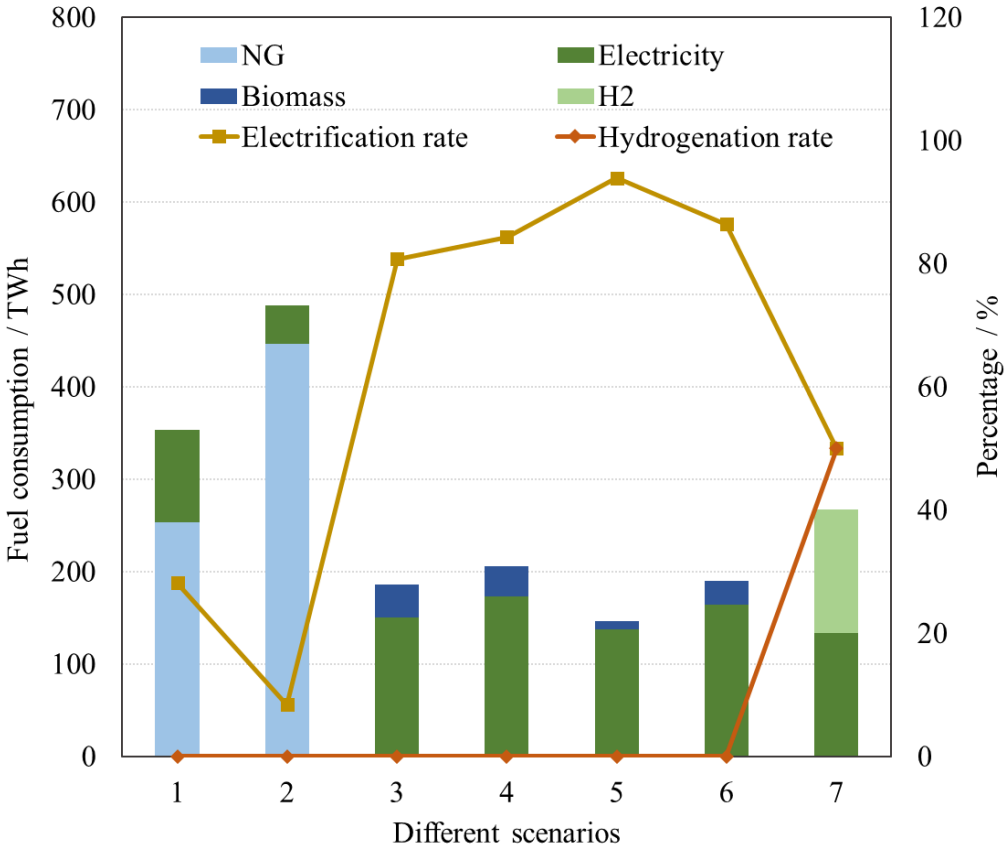

Figure 6.11. The fuel consumption of heat generators of different scenarios

From the heat fuel consumption view in Figure 6.11, it can be seen that the total fuel consumptions in case 1 (~350 TWh) and case 2 (490 TWh) are close to the heat generation capacities, in which the majority of fuel is NG (70% - 90%). But the total fuel consumption is reduced remarkably from case 3 to case 6. It is mainly due to that the COP of ASHP (2.3~3) and GSHP (~3.2) can help reduce the electricity consumption significantly, accordingly, the electrification rates of these cases are all over 83% (highest at 94% in case 5). The electrification and hydrogenation rates in case 7 are 50% respectively, the total hydrogen consumption in heat sector is ~135 TWh.

6.5.1.3 The economic performance of different pathways

Compared the annual investment costs, LCOE and LCOH of seven scenarios, the results are shown in Figure 6.12. When there is no decarbonisation in case 1 and case 2, the major annual investment costs are from electricity and heat fuel costs, as thermal generators and gas boilers consume large amounts of NG, the rest comes from the operational costs of conventional generators. The LCOEs of these two cases are also the lowest at 52.3 £/MWh and 58.5 £/MWh respectively. From case 3 to case 7, half of the annual expenditure is mainly spent on increasing the capacities of renewables (rising by 1.5 - 2.5 times than the base case) and zero-emission generators. These include the biomass plants in case 3, CCGT-CCS and OCGT-CCS in case 5 and case 6, as well as ASHP and GSHP from case 3 to case 6, and H_2 boilers in case 7. The annual investments and LCOEs present the highest value in case 3 and case 5, as there are no energy storage expansions, which reduce the cost-effectiveness of the newly installed renewables. But in case 4 and case 6, when only ~10-12% of investments are made on storage technologies, the annual total costs are reduced by ~28% and 15.1% respectively, accordingly, the LCOEs decrease from 133.1 £/MWh (case 3) to 63 £/MWh (case 4), and from 126.7 £/MW (case 5) to 82 £/MWh (case 6) respectively. The LCOHs from case 1 to case 6 vary slightly between 40.1 £/MWh to 47.2 £/MWh, but increases to 63 £/MWh in case 7, which is mainly due to the high hydrogen consumption and cost (H_2 price at ~130 £/MWh). To be noted, the LCOE of a net-zero carbon power system (case 6) is higher than that of a 100% renewable power system (case 4), it is mainly due to that the renewable power ratio in case 4 is not exactly 100% but 99%, resulting in a small amount of generation and CO_2 emissions from CCGT. But overall, a future 100% renewable (net-zero carbon) power system and a net-zero carbon heat system are affordable with LCOE at 65~80 £/MWh and LCOH at 45~63 £/MWh.

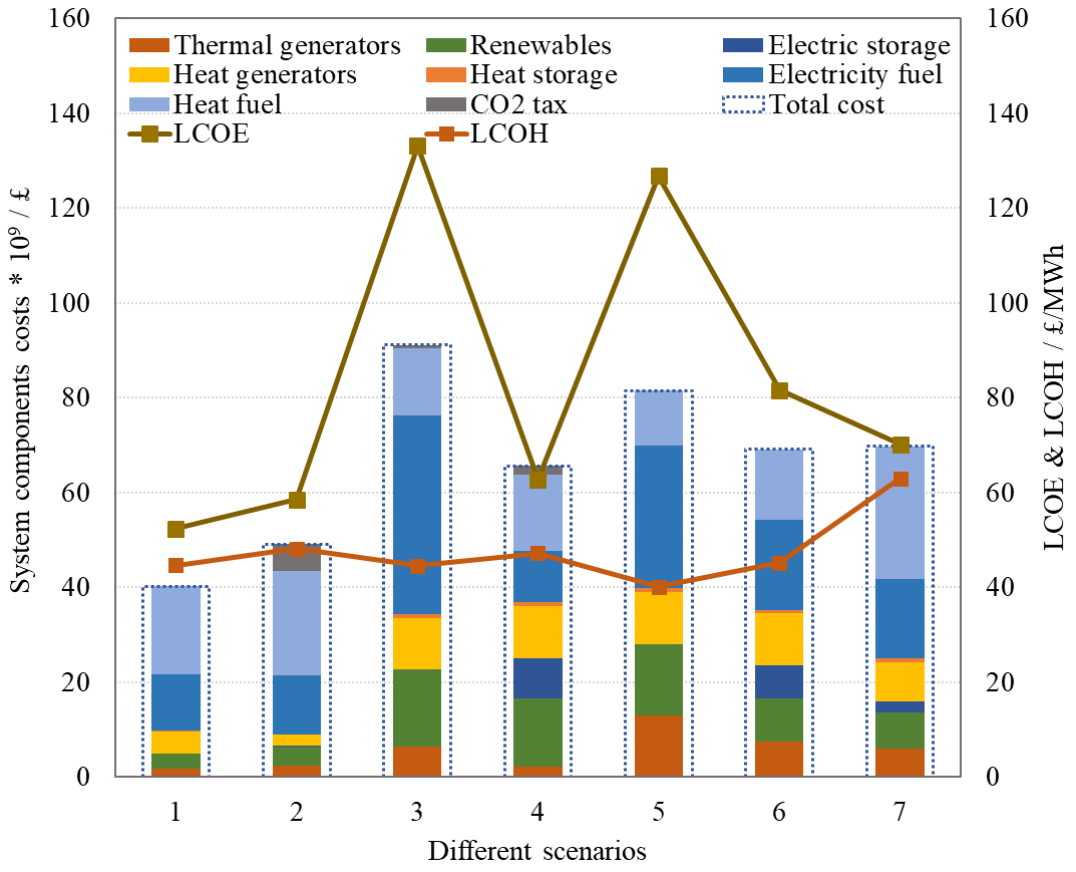

Figure 6.12. The annual investment cost, LCOE and LCOH of different scenarios

6.5.1.4 Renewable deployment in different zones

The Figure 6.13 clearly shows the renewable development in different zones and curtailment capacities in the future, as there are different distributions of renewable resources in three zones, the average renewable capacity factors in three zones are shown in

Table 6.9. It can be seen that onshore wind (~8-10 GW) and offshore wind power (~ 5 GW) are mainly installed to provide renewable electricity to decarbonize zone 1 (Figure 6.13(a)), there is almost no solar power expansion due to its low capacity factor in this zone. But in zone 2 (Figure 6.13(b)), overall, the installed capacities of solar power are comparable (case1, case 2, case 4 and case 6) with (case 3, case 5 and case 7) those of onshore wind power due to its relatively lower onshore wind capacity factor. Obviously, the storage technologies in case 4 and case 6 help enhance the installed capacities of onshore wind power significantly,

but the offshore wind power capacities are only ~5-10 GW due to its high capital and operational costs.

Table 6.9. The average capacity factor of renewables in different zones

Renewable capacity factor	Value	Renewable capacity factor	Value	Renewable capacity factor	Value
onwd_avg_z1	0.41	solar_avg_z1	0.11	ofwd_avg_z1	0.484
onwd_avg_z2	0.329	solar_avg_z2	0.12	ofwd_avg_z2	0.491
onwd_avg_z3	0.343	solar_avg_z3	0.13	ofwd_avg_z3	0.433

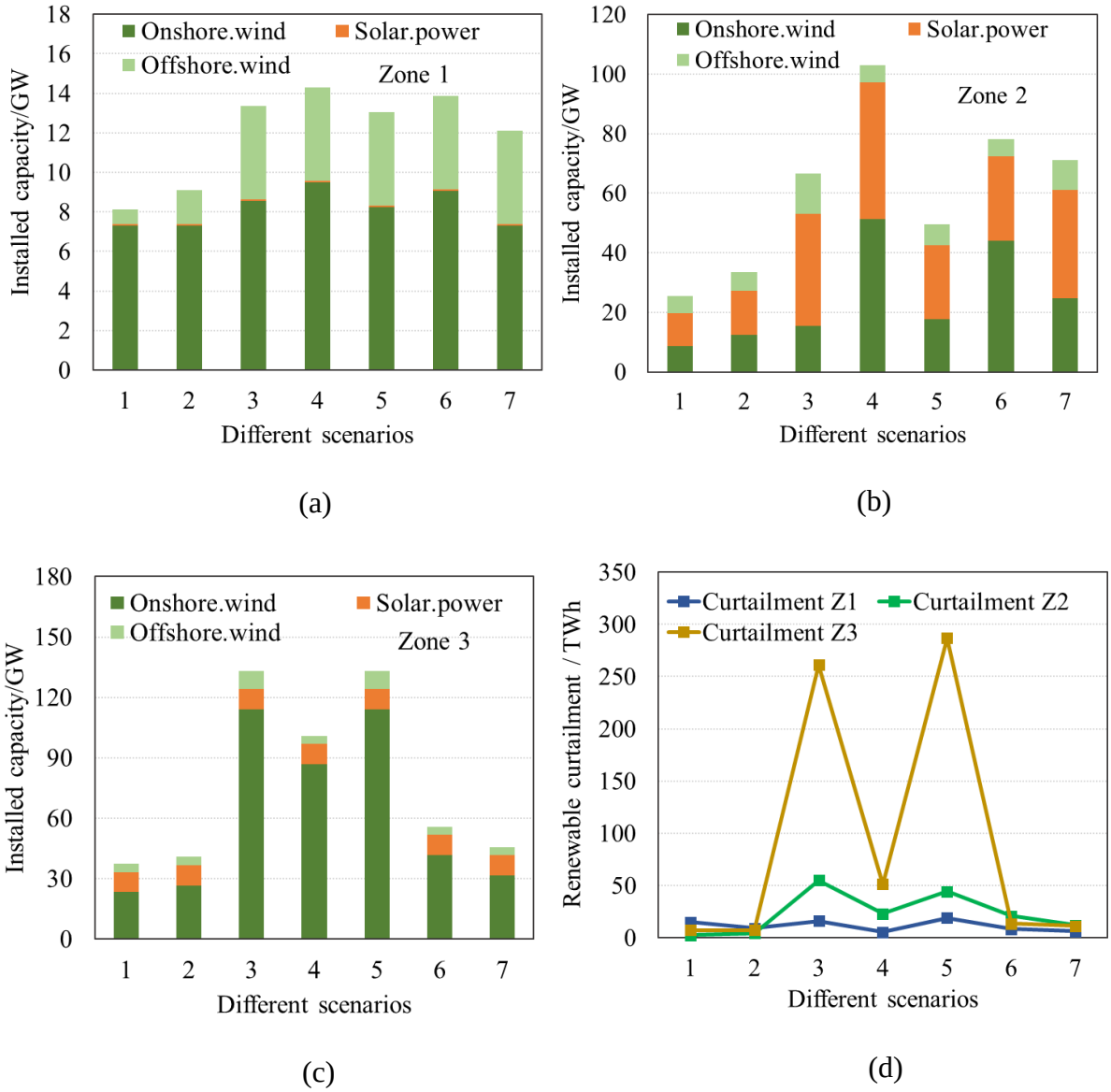

Figure 6.13. The renewable development in different zones

In zone 3 (Figure 6.13(c)), the installed capacity of onshore wind power is remarkably higher than those of solar and offshore wind power, which amounts to ~ 90 – 115 GW (case 3

to case 5). It is due to the relatively higher onshore wind capacity factor in this zone and its low capital and operational costs, leading to almost no solar and offshore wind power expansion on the existing capacity. To be noted, when storage technologies are added in zone 3, the total renewable capacities are reduced significantly from around 133 GW (case 3 and case 5) to 100 GW (case 4) and 55.6 GW (case 6) respectively. It can be explained by the renewable curtailment in Figure 6.13(d), large amounts of renewable curtailments occur in case 3 and case 5 in zone 3, which also means much more wasted renewable energy. But the curtailments can be reduced by 80-95% when storage technologies were added in case 4 and case 6 in this zone. But in zone 1, the annual renewable curtailments are below 15 TWh due to its low renewable expansion capacities. In zone 2, the annual curtailments are high at around 55 TWh when there are no electricity storages, but can be reduced to below 20 TWh when storages are added into the system.

6.5.2 The analysis of different storage technologies

In this study, in case 1, only PHES was included in the power system, it was seen as the base case and assumed there will be no PHES expansion due to geographical constraints. In case 4, case 6 and case 7, other three types of electricity storage technologies were included to help manage large share of renewables, they are battery (BAT), LAES and hydrogen storage (H2S), which have different charge/discharge durations, costs and RTEs (seen from Table 6.6). Two kind of heat storage technologies were considered, they are short-term and long-term heat storages, which feature different charge/discharge durations, costs and RTEs (seen from Table 6.7).

6.5.2.1 The total capacity expansion of LAES and other storages

From Figure 6.14, it can be seen that the major storage expansion lies in LAES in power sector and the short-term heat storage in heat sector. For a 100% renewable power system (case 4), the invested total electric storage energy capacity and discharge power capacity are 541.85

GWh and 49.2 GW, in which LAES is 492.4 GWh (discharge power capacity is 41 GW if discharge E/P ratio is 12 h), PHES is 29 GWh (discharge power is 2.9 GW if the discharge E/P ratio is 10 h), and battery is 20.4 GWh (discharge power is 4 GW if the discharge E/P ratio is 5 h).

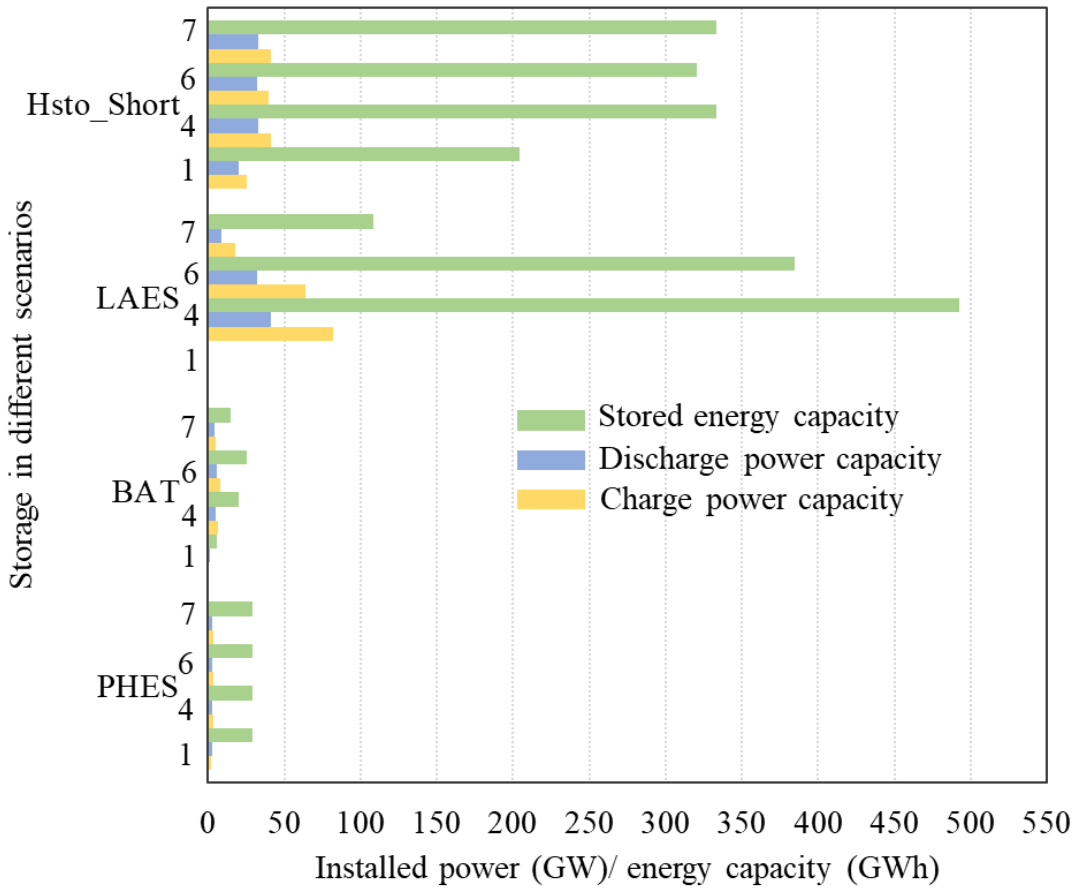

Figure 6.14. The capacity expansions of LAES and other storages (Hsto short stands for heat store for short time period)

For a net-zero carbon power system, the invested total storage energy capacity is 439 GWh, in which LAES is 384 GWh (discharge power capacity is 32.1 GW), PHES is 29 GWh and battery is 25.6 GWh (discharge power was 6.2 GW). When the heat electrification rate is 50%, the invested total storage energy capacity is 152.3 GWh, in which LAES is 108.3 GWh (discharge power is 9.1 GW), PHES is 29 GWh, and battery is 15 GWh (discharge power is 4.1 GW). There is no investment in H_2 storage for storing electricity due to its characteristics with too long charge and discharge durations, as well as the selected representative demand

profiles. In heat sector, it is advantageous to build short-term heat storage (~30 GW power capacity and 330 GWh energy capacity in total) as much as possible to help save more heat fuel cost, as its charge and discharge duration fit in well with the daily heat demand variation characteristics (to be charged at low heat demand at night, and to discharge at high heat demand at daytime).

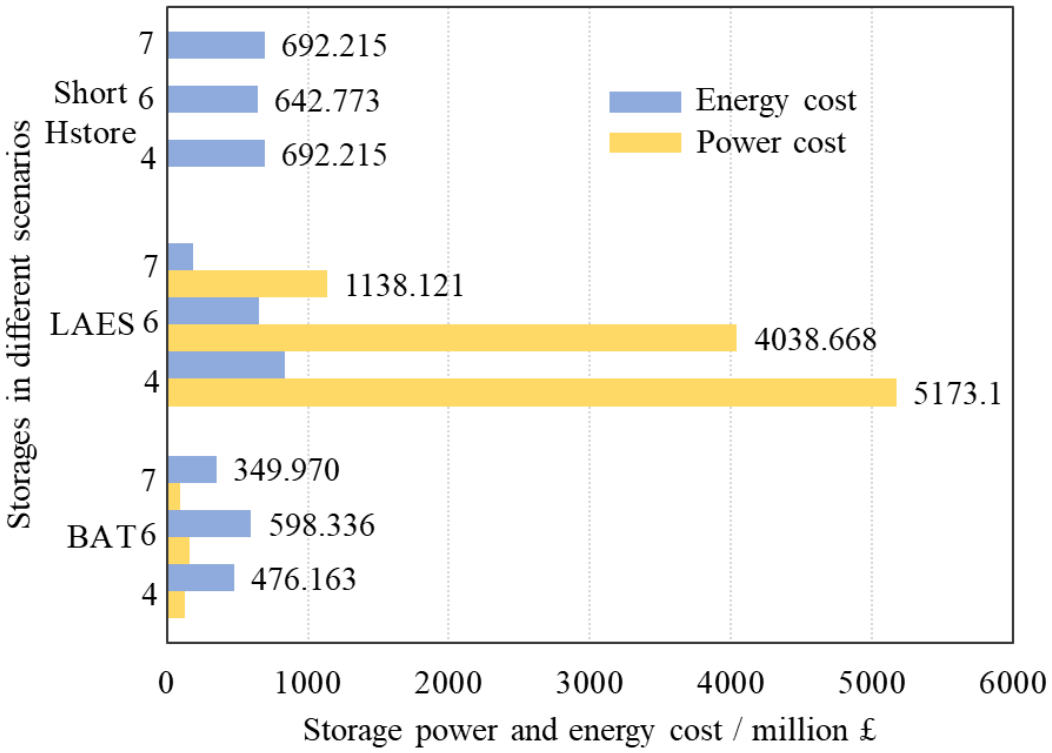

Figure 6.15. The power and energy investment costs of LAES and other storages

There are two reasons explaining why there are large amounts of investment in LAES: 1) its charge and discharge E/P ratios match well with the wind power curtailment pattern and daily variation in electricity demand. When the electricity demand is low but wind power prevails at night, wind curtailment normally sustains for about tens of hours, the excess wind energy can be accommodated by large storage tanks of LAES. The stored energy can be injected back into the grid when low wind power occurs for tens of hours; 2) the specific storagetank cost of LAES (19.5 £/kWh) is much lower than that of battery (212.5 £/kWh), which facilitates the investment in LAES especially for the applications where large energy capacity is needed. This can be clearly seen from Figure 6.15. For battery, its energy capacity

costs (~ million £ 400 – 700) are much higher than its power capital costs (~ million £ 96 – 160) in all cases. But for LAES, its power investment costs are about million £ 5173, million £ 4038 and million £ 1138 for case 4, case 6 and case 7 respectively, which are all more than 6 times of its energy capital costs (million £ 184 – 836). For short-term heat storage, the capital expenditure is mainly spent on its energy capital cost, which is about million £ 700, the power capital cost is neglected.

6.5.2.2 The zonal capacity expansion of LAES and other storages

Figure 6.16, Table 6.10, and Figure 6.17 show the expansion capacity and generation of various storage technologies in different zones. Case 1 is the base case without storage expansion, there are only the existing capacities (Figure 6.16 and Table 6.10) and generations (Figure 6.17) of PHES, battery and short-term heat storage. But in case 4 and case 6 in all three zones in Figure 6.16, it shows that the newly installed storages are mainly LAES and short-term heat storage, it is due to large renewable deployment in these two cases, the new capacities of LAES are proportional to the renewables' capacities to capture the excess onshore wind power.

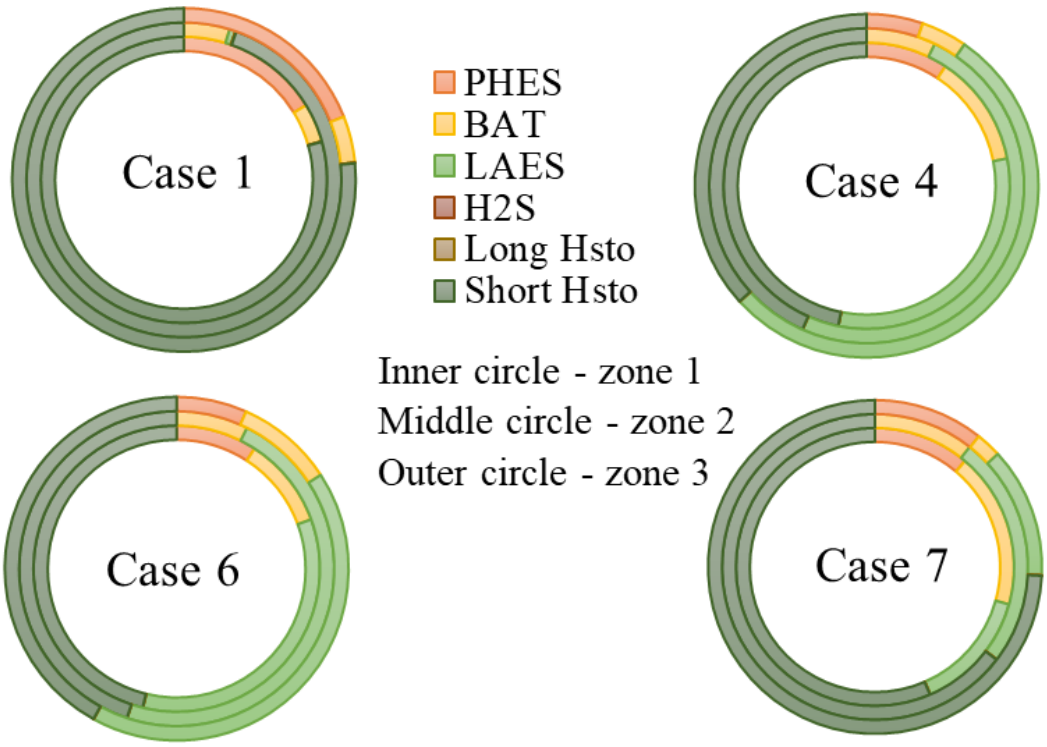

Figure 6.16. The installed discharge power capacities of LAES and other storages in different zones

Quantitatively in Table 6.10, the capacity ratio of LAES and renewables in case 4 is about 16.2% (16.7 GW, zone 2) - 21.7% (21.9 GW, zone 3), and in case 6 is around 19.9% (15.5 GW, zone 2) – 24.8% (13.8 GW, zone 3), case 6 has lower installed renewable capacities than case 4. However, the capacity ratio of LAES to renewables in case 7 is ~ 5.6% (2.6 GW, zone 3) – 7.8% (5.6 GW, zone 2) due to significantly lower renewable deployment capacities. For battery, the capacity expansions in case 4 and case 6 in three zones are remarkably less than those of LAES due to its high cost and short charge durations. The new capacities of battery in zone 1 are all higher than those in other two zones in all cases. It is due to that the installed battery in zone 1 is enough to deal with renewable curtailment and add system flexibility considering the low renewable deployment and demands in zone 1.

Table 6.10. The discharge power capacity expansion in different zones and cases (unit: GW)

\	Storages	zone 1	zone 2	zone 3	\	zone 1	zone 2	zone 3
case 1	PHES	0.74	0.00	2.16	case 4	0.74	0.00	2.16
	BAT	0.20	0.40	0.50		1.01	2.40	1.77

	LAES	0.00	0.06	0.00		2.49	16.71	21.88
	Short heat store	3.61	8.09	8.71		3.73	14.60	15.00
	Renewable capacity	8.12	25.38	37.35		14.32	102.9	100.9
	LAES/renewable capacity ratio	0	0	0		17.4%	16.2%	21.7%
case 6	PHES	0.74	0.00	2.16	case 7	0.74	0.00	2.16
	BAT	0.83	2.40	3.00		1.20	2.40	0.50
	LAES	2.78	15.53	13.78		0.94	5.59	2.56
	Short heat store	3.73	14.60	13.69		3.73	14.60	15.00
	Renewable capacity	13.87	78.10	55.65		12.12	71.22	45.60
	LAES/renewable capacity ratio	20.1%	19.9%	24.8%		7.7%	7.8%	5.6%

From the storage generation view in Figure 6.17, in case 4, the annual energy generation ratio of LAES to total generation from storage in zone 1, zone 2 and zone 3 are 55%, 85% and 80%. There are large amounts of onshore wind power installed in zone 2 and zone 3 to meet 99% of renewable ratio, leading to more wind energy capture and generation from LAES in these two zones. Similarly, in case 6, the annual energy generation ratio of LAES in zone 1, zone 2 and zone 3 are 42.7%, 78% and 59.3%, but more generation from PHES and battery can be seen. In case 7, LAES generation ratio in zone 1, zone 2 and zone 3 are 27.2%, 76.2% and 36.9%, as the installed power capacities of renewable and LAES are reduced significantly, PHES and battery are more often used to help absorb and discharge excess renewable power and provide system flexibility.

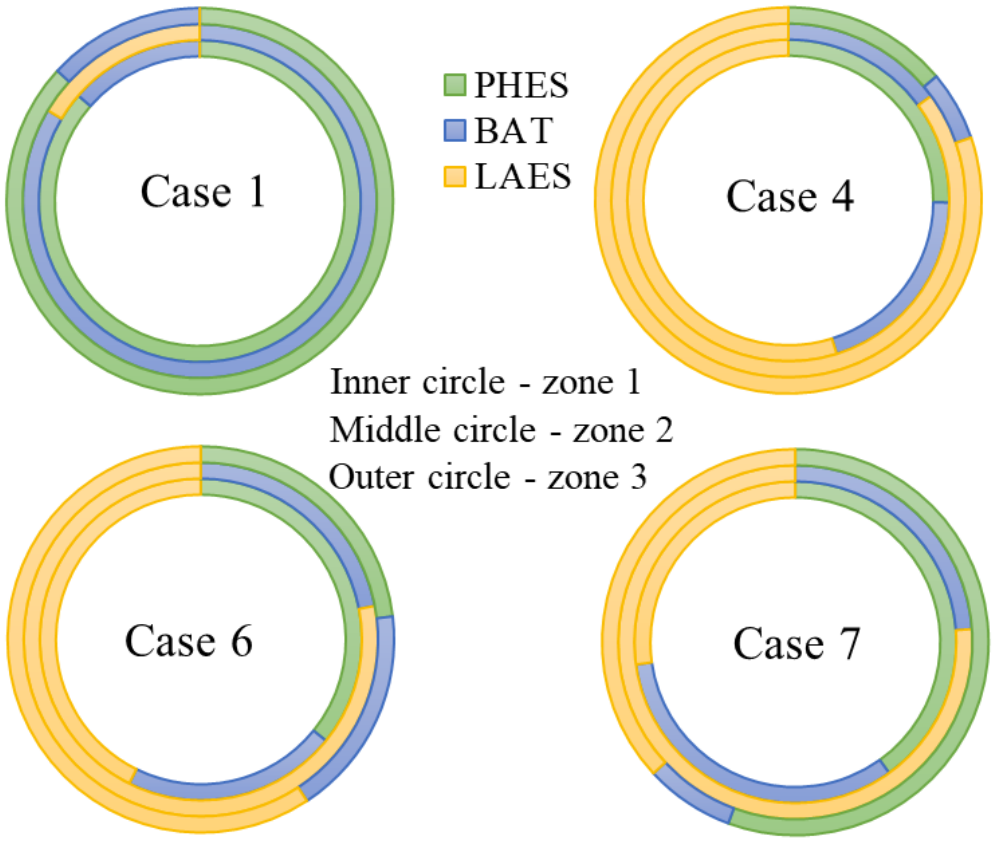

Figure 6.17. The annual storage generation in different zones

6.5.3 Sensitivity analysis

6.5.3.1 Different heat hydrogenation rate

Figure 6.18 showed the effects of different heat hydrogenation rates on system costs. With the hydrogenation rates increasing from 20% (sensitivity case 1) to 50% (sensitivity case 2) to 90% (sensitivity case 3), the installed capacities of H_2 boilers increased from 86 GW to 163 GW, it brings about more hydrogen fuel cost (heat fuel cost) and higher LCOH (varying from 55.8 to 63 to 89.7 £/MWh) in Figure 6.18.

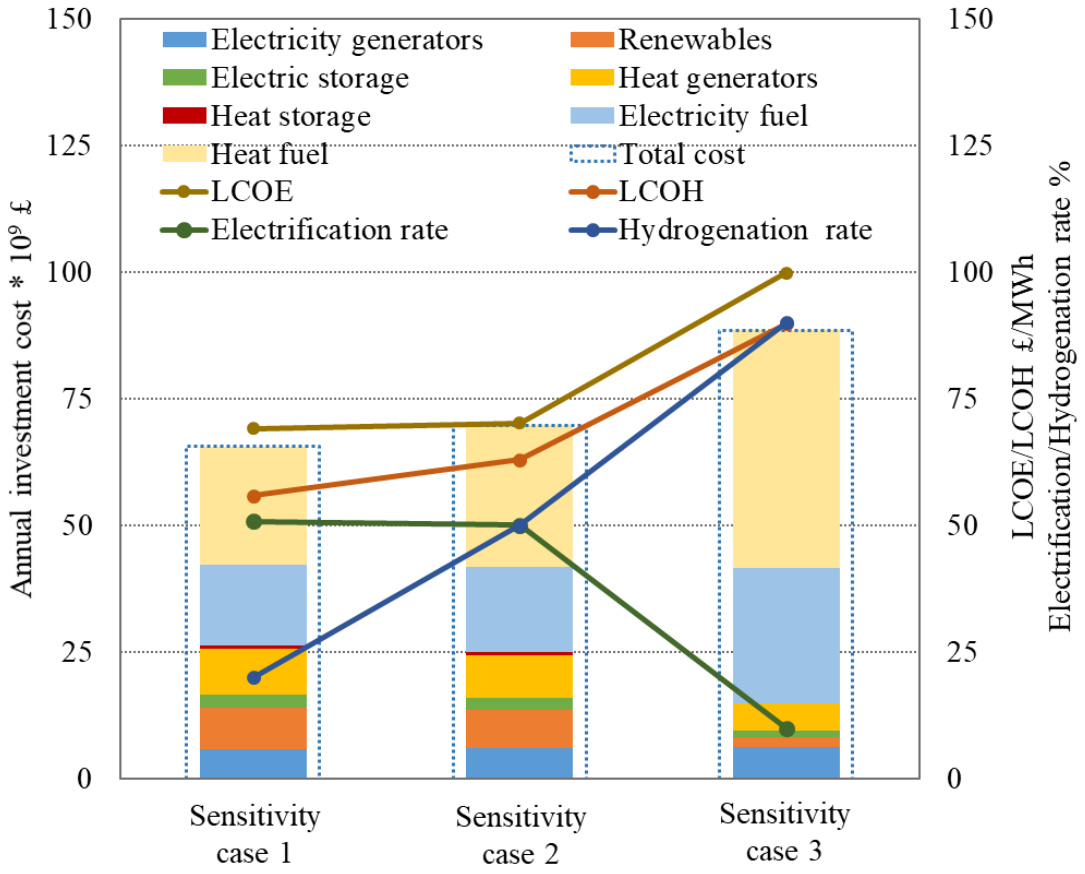

Figure 6.18. The effects of different hydrogenation rates on system costs

While the capacity of ASHP decreases from 48.6 GW to 2.8 GW, it leads to less electricity consumption, and less renewable electricity shift from electricity sector to heat sector. Thus, it results in less the annual investment costs on renewables and electricity storages. More electricity produced by CCGT-CCS and OCGT-CCS result in higher electricity fuel cost and higher LCOE, rising from 69 to 70 to 99.8 £/MWh. It is concluded that higher heat hydrogenation rates would lead to higher system costs, LCOE and LCOH, unless the hydrogen price can be reduced to a lower value, like as cheap as NG. Meanwhile, higher heat hydrogenation rates would weaken the coupling of electricity and heat networks, and reduce the reply upon electric and heat storage systems.

6.5.3.2 Different storage duration

Figure 6.19 shows the effect of different storage durations on storage capacities and renewable generation. In sensitivity cases 4, 5, 6, the charge/discharge durations of battery and

LAES are shown in Figure 6.19, ‘LAES 6/12 h’ means the charge/discharge durations of LAES are 6h and 12h. It can be seen that the battery capacities decrease with the charging durations increasing in zone 1 and zone 2 in all sensitivity cases, and does not change obviously in zone 3, it indicates that battery performs better at short durations. For LAES in zone 2, its energy capacity expands from 102.6 GWh (sensitivity case 4) to 160 GWh (sensitivity case 5), and then shrink to 121.7 GWh (sensitivity case 6), but in zone 3, the energy capacity of LAES constantly rises from 80.8 GWh to 132.6 GWh to 162.4 GWh. It indicates the optimal charge/discharge E/P ratio of LAES is 8/14 h in zone 2, but is 10/15 h in zone 3, which depends on the renewable profiles and wind curtailment patterns in these two zones. However, different storage durations do not affect too much on system annual investment costs and LCOEs (72.8 £/MWh (case 4), 68.6 £/MWh (case 5) and 68.9 £/MWh (case 6)). This sensitivity case study suggested that battery is more suitable for short-duration application (~4/5h), while the durations of LAES can be tailored depending on the renewable profiles. For the wind-dominated case in the UK, the more suitable charge and discharge durations of LAES are 8~10 h and 14~15 h respectively..

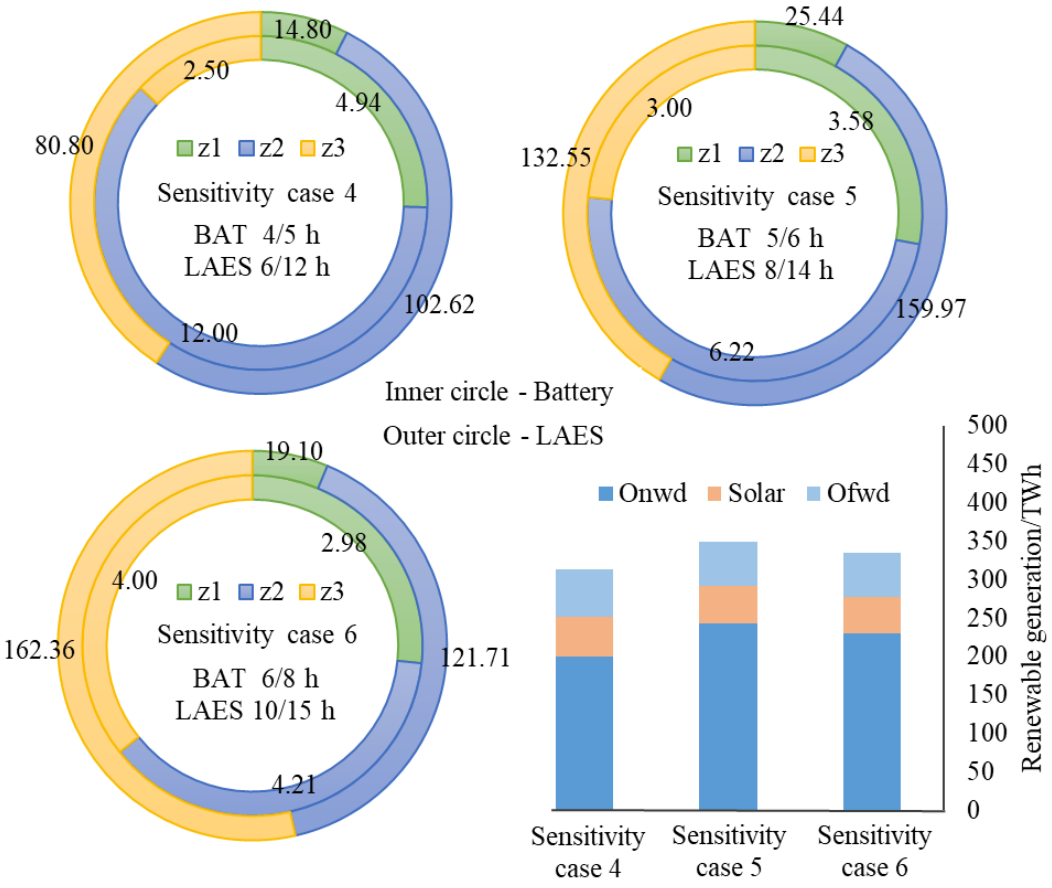

Figure 6.19. The effect of different storage durations on storage capacities and renewable generation

6.6 Summary

This part of work aimed to assess different decarbonisation pathways and theirtechno-economic performances for the UK by 2050. In order to achieve this, a MILP-based energy expansion model was developed based on 'GenX' model.The model is capable of determining the expansion capacities, commitment and operational capacities of different electricity and heat generators and energy storage technologies in different zones. Upon this country-level energy system design and operation framework, seven decarbonisation scenarios were proposed, optimized and discussed to assess both the technical and economic feasibility. A particular focus was put on the expansion planning and investment of renewables and storages in different zones. The sensitivity analyses of different hydrogenation rates in heat sectors and

energy storage durations were also discussed to reveal their effects. Overall, the major conclusions are drawn as the following ones:

a) To build a future net-zero carbon power system, the optimal expansion capacities lie in onshore wind power (94.5 GW), solar power (38.7 GW), offshore wind power (14.4 GW), CCGT-CCS (37 GW) and OCGT-CCS (16 GW), there is a need to cut down the investment cost of offshore wind power to increase its attractiveness.

b) To build a future net-zero carbon heat system, gas boilers will be disused, the major expansion capacity is in ASHP (~80 - 90 GW), other heat generators, including GSHP, electric heaters and biomass boilers account for the similar share (~ 30 GW). The district heat network capacity varies between 10 GW and 20 GW depending the coupling of heat and electricity sectors. However, higher heat hydrogenation rates would lead to higher system costs, LCOE and LCOH, unless the hydrogen price can be reduced to a lower value, like as cheap as NG. Higher hydrogenation rate would also weaken the coupling of electricity and heat networks, and reduce the reply upon electric and heat storage systems.

c) The crucial roles of storage technologies elaborate in its capability of absorbing large share of renewables, reducing curtailment, as well as providing system flexibility and operating reserve, to reduce the total installed generator capacities and system costs. When only ~10-12% of investments were made on storage technologies, the annual total costs were reduced by ~15.1%-28%. For a net-zero carbon power and heat system, the major storage expansions are LAES (384 GWh) and short-term heat storage (330 GWh).

d) The newly deployed renewable capacities in different zones depend on the relative renewable capacity factors, their investment costs and storage capacities. The installed capacities, optimal E/P ratios and generation of storage technologies in different zones depend on the daily electricity and heat demand profiles, as well as the renewable capacities and

curtailment patterns. Specifically, the LAES and renewable capacity ratio for a net-zero carbon power system is around 20%.

e) A future 100% renewable (net-zero carbon) power system and a net-zero carbon heat system are techno-economically feasible, which can be affordable with LCOE at 65~80 £/MWh and LCOH at 45~63 £/MWh. The durations of LAES can be tailored depending on the renewable profiles, the more suitable charge and discharge durations are 8~10 h and 14~15 h for the wind-dominated case in the UK.

7 Conclusion and recommendations

7.1 Major conclusions

The thermo-economic multi-objective optimization of the stand-alone LAES system by using GA can determine the optimal design and operational parameters of LAES systems. The optimal charging and discharging pressure, as well as the optimal inlet and outlet temperature of air-propane cold box can be obtained. These parameters can further indicate the optimal heat transfer areas of coolers, heaters, cold boxes and evaporators, as well as the optimum mass flow rates of propane, methanol and thermal oil. The optimization can directly provide guidance in selecting system design and operational parameters under different system configurations and scenarios. The Pareto Front of RTE and capital cost obtained from the multi-objective optimization of LAES can provide the proper investment advice for system operators.

The dynamic simulation based on the dynamic models of LAES system is crucial to understand its practical operational behaviour and control strategy. After investigating the dynamic characteristics of a LAES discharging unit when integrated with a wind farm, it concluded that the LAES system is more suitable for responding to the wind power component varying at a time scale more than 100s, which leads to less power tracking errors,smoother speed adjustment, and less turbine motor fatigue. The economic comparison of different combined storage schemes also indicated the suitable storage system for different scales of wind farms. Overall, the annual cost of full battery storage is always higher than that of the combined LAES and battery storage system for wind farms. LAES with Lead-acid battery is more suitable for small-scale wind farms, while LAES with VR flow battery is more suitable for large-scale wind farms.

The developed MILP-based design and optimization framework of a hybrid renewable micro-grid (HRMG) can help determine the optimal components (including LAES units) and

their sizes for the micro-grid, to minimize the investment costs and CO_2 emissions. In HRMG, LAES can help provide multiple functions, including the time shifting, renewable firming, peak shaving, flexibility and reserve value, as well as the waste heat recovery, the percentages of these value streams and their interactions within the HRMG have been clearly identified. The total profit of the LAES is 8.2% higher than that of battery storage with the same investment cost. It clearly demonstrated the key role of LAESs and its attractiveness in supporting the future HRMGs with high renewable share.

The MILP-based energy expansion model of a country-level energy system was developed to assess the techno-economic performance of different decarbonisation pathways for the UK by 2050. The model can determine the expansion capacities, commitment and operational capacities of different electricity and heat generators and energy storage technologies in different zones. To build a net-zero carbon power and heat system, the optimal expansion capacities lie in onshore wind power (94.5 GW) in power sector and ASHP (~80 - 90 GW) in heat sectors. The LCOE and LCOH of such a system are at 65~80 £/MWh and 45~63 £/MWh respectively.

The crucial roles of storage technologies especially LAES lie in its capability of absorbing large share of renewables, reducing curtailment, as well as providing system flexibility and operating reserve, to reduce the total installed capacities of generators and system costs. When only ~10-12% of investments were made on storage technologies, the total annual costs were reduced by ~15.1%-28%. For a net-zero carbon power and heat system, the major storage expansions are LAES (384 GWh) and short-term heat storage (330 GWh). A LAES system with the charge durations at 8~10 h and discharge durations at 14~15 h is more suitable for the wind-dominated case in the UK than short-duration batteries (~4/5h). The capacity ratio of LAES to renewables for a net-zero carbon power system is around 20%.

7.2 Future research recommendations

The future recommendations for studies in the LAES area include:

a) The thermo-economic multi-objective optimization of different hybrid LAES systems and more complex systems are needed, to provide guideline on system design and operational parameters to minimize system costs and environment impacts.

b) The energy capacity and time response optimization of different LAES systems for different wind farms, as well as the studies about detailed dynamic characteristics and development of alternative control strategies for the LAES system, like the combined pump and inlet valve control method, are needed to promote the deployment of LAES in practical case.

c) Other potential benefits of LAESs in hybrid renewable micro-grid, like the investment deferral of the network, increasing system stability and avoiding equipment fatigue, as well as stabilizing renewables and other profounding environment benefits should be investigated and quantified in the future.

d) The uncertainties in the assumptions in technology costs, energy costs, future renewable and demand profiles of the MILP design framework should be considered and studied. The expansion of transmission system, the transport sectors and coupling, the demand response including the electric vehicles and domestic applications should be included in the net-zero carbon energy system design in the future.

Supplementary materials A

A1 Components models in hybrid renewable micro-grid

A1.1 Decoupled liquid air storage model

A1.1.1 The model of air turbines

The stored liquid air is drawn from tanks to expand through multi-stage turbines to produce power. As users' loads varying, turbines would work at part-load conditions. Thus, the off-design turbine model with simplified assumptions are explained as follows:

a. Three stages of air turbines were adopted to achieve full isentropic expansion. The rotational speed was controlled to be constant at the nominal speed by PID controller [239].

b. The inlet temperatures of turbines are kept constant at around 195 ℃ via controlling the volume of heat transfer fluid [199], which comes from the waste compression heat of LAES.

c. The head control strategy of variable-speed pump to maintain the inlet pressure of turbines nearly constant, the mass flow rate varies with the rotating speed of the cryogenic pump [233].

The operation of each turbine is described by the reduced characterized performance parameters and Flugel formula [236], shown as in eq. (A.1) - eq. (A.7).

$$RP_{Tr}(t) = \frac{W_{Tr}}{W_{Tr,0}} = f\left(\frac{\eta_{Tr}}{\eta_{Tr,0}} \cdot \frac{\dot{m}_{Tr}}{\dot{m}_{Tr,0}} \cdot \frac{T_{in}}{T_{in,0}} \cdot \frac{\beta_{Tr}}{\beta_{Tr,0}}\right) \quad \text{eq.(A.1)}$$

$$\frac{\eta_{Tr}}{\eta_{Tr,0}} = \left(1 - t(1-n')^2\right)\frac{n'}{\dot{m}'}\left(2 - \frac{n'}{\dot{m}'}\right) \quad \text{eq.(A.2)}$$

$$n' = \frac{\bar{n}}{\bar{n}_0} \quad \text{eq.(A.3)}$$

$$\bar{n} = \frac{n}{\sqrt{T_{in}}} \quad \text{eq.(A.4)}$$

$$\dot{m}' = \frac{\bar{\dot{m}}}{\bar{\dot{m}}_0} \quad \text{eq.(A.5)}$$

$$\bar{\dot{m}} = \frac{\dot{m}\sqrt{T_{in}}}{P_{in}} \quad \text{eq.(A.6)}$$

$$RM_{Tr}(t) = \frac{\dot{m}_{Tr}}{\dot{m}_{Tr,0}} = \alpha\sqrt{\frac{T_{in,0}}{T_{in}}}\sqrt{\frac{{\beta_{Tr}}^2-1}{{\beta_{Tr,0}}^2-1}} \quad \text{eq.(A.7)}$$

where, the subscripts 0 – the design state, in – inlet state, Tr – expansion turbine, the superscripts '′' means the normalized parameters, '-' means the reduced parameters, W- the power output, $\dot{m}$ – the mass flow rate, T- the temperature, η- the isentropic efficiency, P – pressure, RP – the pressure ratio, RM – the mass flow rate ratio, β- the expansion ratio, n – the turbine speed.

Based on the assumptions and eq.(A.1) - eq.(A.7), a linear relationship relating $RP_{Tr}(t)$ to $RM_{Tr}(t)$ was obtained, shown in eq. (A.8), the linearization was conducted via a linear regression on the curve obtained, the coefficients a, b vary with the specified nominal conditions.

$$RP_{Tr}(t) = a \cdot RM_{Tr}(t) + b \quad \text{eq.(A.8)}$$

A1.1.2 The model of air compressors

In LAES system, air compressors serve as the major component to draw power from the grid or renewables, which work off the design conditions when absorbing intermittent renewable energy. Thus, variable-speed motor of compressors were adopted to adapt to the varying loads. Some assumptions were made before building the part-load performance of compressors, explained as follows:

a. The power drawn by compressors was mainly affected by air flow rate, as the variable speed control strategy was adopted to keep the discharge pressure at a specified small range [320], accordingly the liquid yield ratio (the ratio of liquid air produced and total air mass flow) was assumed nearly constant at 0.7 at charging pressure 10 MPa [204,212].

b. For the three-stage adiabatic compression process, the compression ratio is the same for each stage [204]. The air compression heat was assumed to be partly used in the power recovery process, and the excess part (20%-45%) was recovered for heat loads in campus [43].

c. The co-axial counter intercoolers and after-coolers were adopted, the heat transfer process is isobaric [44], the varying volume of cooling media kept nearly the same inlet temperature for each stage compressors.

Similar to air turbines, two ratios were defined to describe the part-load conditions of industrial air compressors, namely the air mass flow rate ratio RM_{C} and power ratio RP_{C}, of which regression linear correlation is expressed as in eq. (A.9) - (A.12), the coefficients p, q were derived for typical compressors, but can vary with the specific compressor, the difference is within 3% [320].

$$RM_{\mathrm{C}}(t) = f\big(RP_{\mathrm{C}}(t)\big) = p \cdot RP_{\mathrm{C}}(t) + q \qquad \text{eq.(A.9)}$$

$$RM_{\mathrm{C}}(t) = \frac{\dot{m}_{C}(t)}{\dot{m}_{C0}} \qquad \text{eq.(A.10)}$$

$$RP_{\mathrm{C}}(t) = \frac{P_{\mathrm{C}}(t)}{P_{\mathrm{C0}}} \qquad \text{eq.(A.11)}$$

$$Q_{rh}(t) = \eta_{hex}\dot{m}_{\mathrm{C}}(t)\big(h_{\mathrm{C},o} - h_{\mathrm{C},in}\big) = \eta_{hex}\, P_{\mathrm{C}}(t) \qquad \text{eq.(A.12)}$$

where, subscripts C – the compressor, *0* – the design state, *rh* – the recoverable heat, *o* – the outlet state, in- the inlet state, h – the enthalpy, Q - the compression heat energy, hex- the heat exchanger, η- the heat recovery efficiency of the heat exchanger, assumed as 0.9.

For air compressors and turbines, the manufacture data and the thermodynamic analysis of LAES were referred to determine the nominal operating conditions, which were presented in the work [42,44,45].

A1.1.3 The model of liquid air tanks

For the air storage tank, it receives liquid air from the liquefaction unit and supplies liquid air for expansion, at any time t, the storage volume V_{LAES} (m3) is expressed in eq. (A.13) - (A.14), which is bounded by the allowed minimum and maximum volume in eq. (A.14) [241].

$$V_{LA}(t) = V_{LA}(t-1) + \int_{t}^{t+\Delta t} \frac{\dot{m}_{LA,in}(t)}{\rho_{LA}}\, dt - \int_{t}^{t+\Delta t} \frac{\dot{m}_{LA,o}(t)}{\rho_{LA}}\, dt \qquad \text{eq.(A.13)}$$

$$V_{min} \leq V_{LAES}(t) \leq V_{max} \quad \text{eq.(A.14)}$$

where, V- the volume of liquid air tank (m^3), $\dot{m}_{LA,in}$- the liquid air inflow (kg/s), $\dot{m}_{LA,o}$- the liquid air outflow (kg/s), ρ_{LA}- the density of liquid air (kg/m^3). Subscripts min – the minimum level, max – the maximum level, t – the time.

A1.2 The model of gas engines

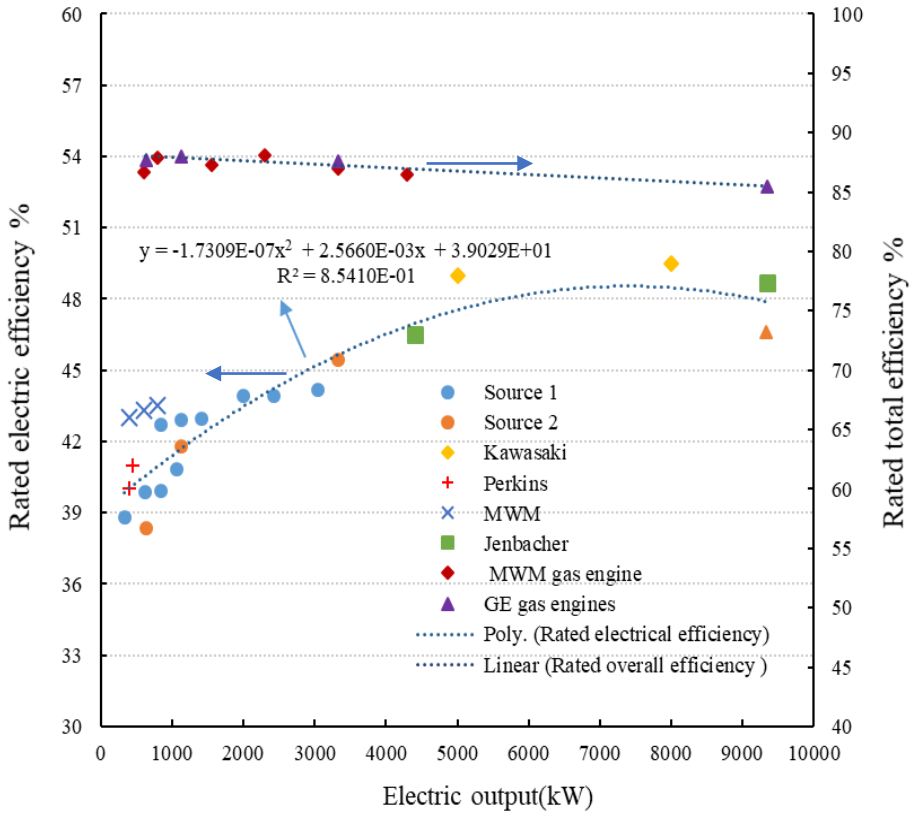

Figure A.1. Relationship between the rated efficiency and electric output power

Multiple engines with power output less than 5 MW are preferable in this work, based on the manufacture data [321–324] and the data sources from literature [325–328], the performance of gas engines at part-load conditions, including the rated and part-load efficiencies, the relationships among the normalized power output, fuel consumption and recoverable heat were obtained through curve regressions [174], shown in Figure A.1 and Figure A.2, which are expressed as eq. (A.15) - (A.17).

$$\eta_{r,GE} = -1.731 \cdot 10^{-7} \cdot P_{r,GE}{}^{2} + \cdots$$
$$2.566 \cdot 10^{-3} \cdot P_{r,GE} + 39.03 \qquad \text{eq.(A.15)}$$

$$P_{GE}(t) = 1.13 \cdot \eta_{r,GE} \cdot Q_{f,GE}(t) - 0.131 \cdot P_{r,GE} \qquad \text{eq.(A.16)}$$

$$Q_{rh,GE}(t) = (\eta_{tot,GE} - \eta_{r,GE}) \cdot \cdots$$
$$(0.94 \cdot Q_{f,GE}(t) + 0.057 \cdot \frac{P_{r,GE}}{\eta_{r,GE}}) \qquad \text{eq.(A.17)}$$

where, subscripts *r*- rated parameters, *GE*- gas engine, *P*- electric power (MW), Q_h - heat power (MW), Q_f - fuel power (MW), η – the efficiency.

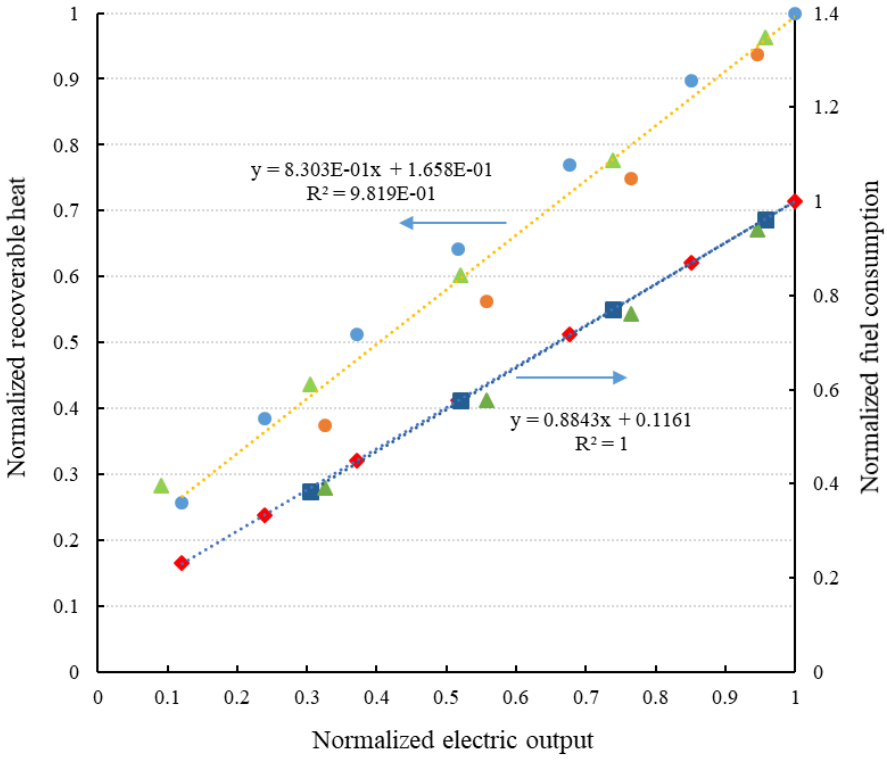

Figure A.2. Relationships between normalized electric output, fuel consumption and recoverable heat

A1.3 The model of heat pumps

Heat pump is now considered as one of key heating technologies for the 4th generation district heating network, it features the low running cost, high efficiency, and zero emissions (electricity consumption from renewable energy) [329,330]. Besides, heat pumps also can be reversed to supply cooling demand for houses in summer [331]. Thus, governments offers attractive renewable heat incentives to encourage this heating technology [332].

$$P_{HP}(i,t) = \mathrm{COP}_{HP}(T_{amb}) \cdot P_{ele}(i,t) \qquad \text{eq.(A.18)}$$

$$\mathbf{COP}_{HP}(T_{amb}) = \begin{cases} \mathbf{2.8}, & T_{amb} \in \textit{cooling season} \\ \mathbf{0.0329} * T_{amb} + \mathbf{2.0012}, & T_{amb} \in \textit{heating season} \end{cases} \quad \text{eq.(A.19)}$$

where, subscripts *HP* – heat pumps, *amb* – ambience, *ele* – electricity, COP - coefficient of performance.

Except for these two key technologies in hybrid renewable micro-grid (HRMG), other components, including gas boilers, electric chillers, solar PV and wind turbines, as well as heat storage and battery, the key performance parameters, capital and O&M costs (operational and maintenance cost) are shown in Table A.1.

Table A.1. Performance parameters of system components

Components	Efficiency	Life time/years	Capital cost/£	O&M cost /%[4]	Reference
Gas engine	86%(overall)[1]	15	$6962.5 * Pr^{-0.164}$ /kW[2]	0.05	[326]
Gas boiler	85%	20	80/kW	0.02	[264]
Electric chiller	2.8	15	$1164.2 \cdot P_r^{-0.284}$ /kW	0.015	[264]
Heat pumps	0.0329*T_{amb}+2.0012[3]	15	$1319.4 \cdot P_r^{-0.268}$ /kW	0.015	[264]
Air compressor	85%	30	$11406 * (\frac{P_{cha}}{4})^{0.6}$	0.01	[221]
Air turbine	85%	30	$5653 * (\frac{P_{dis}}{10})^{0.6}$	0.01	[221]
liquid air tank	/	30	$1778 * (\frac{E}{86})^{0.6}$	0.01	[221]
Solar PV	16.67%	30	900/kW	3 /year/kW	[333]
Wind turbines	/[5]	30	1300/kW	7.5 /year/kW	[334]
Battery	95% (charge/discharge)	10	420/kWh	0.02	[262]
Heat storage	95% (charge/discharge)	20	10/kWh	0.02	[264]

[1]. Overall efficiency of gas engine means the summation of electric and heat efficiency;

[2]. P_r refers to the rated power output of equipment.

[3]. Heat pumps efficiency is related to the outside temperature, the correlation was obtained from the curve regression of manufacture data .

[4]. The operational and maintenance costs of equipment are considered as a fraction of its annual capital cost .

[5]. Wind turbine overall efficiency includes aerodynamic efficiency, mechanical efficiency, and electricity conversion efficiency.

A2 Input profiles and parameters

A2.1 Demand profiles

Considering the seasonal climate conditions, the electricity, heat and cooling demands, and ambient temperature present high similarities and repeatability, thus the average demand profiles in four seasons (including the maximum demand and extreme conditions, like a windless day with high electricity and heat demand) were selected from the whole-year campus data in 2016. The cooling demand was estimated by considering the average cooling load in the UK, the total office area and ambient temperature to demonstrate the reversible heat pump's cooling function [172][335][336].

For the solar and wind energy available in the micro-grid, the capacity factor is used, which means the availability of wind or solar energy for a specific hour at a certain location and ambient temperature based on historical data. The solar and wind energy capacity factor, as well as the ambient temperature were obtained from the authorized website (renewables.ninja) [299]. As renewables do not display the repeating daily or weekly cycles, in order to capture the variability and representative, a scale factor was used to scale up or down the data to represent the average renewable capacity factor in each season [337], and the weeks with the largest aggregated variations will be chosen as the representative ones, in order to verify the flexibility of energy storage in the system [338]. A similar method was adopted to select electricity price, which is greatly affected by renewables. The demand input profiles and renewable capacity factors are shown as in Figure A.3-Figure A.6.

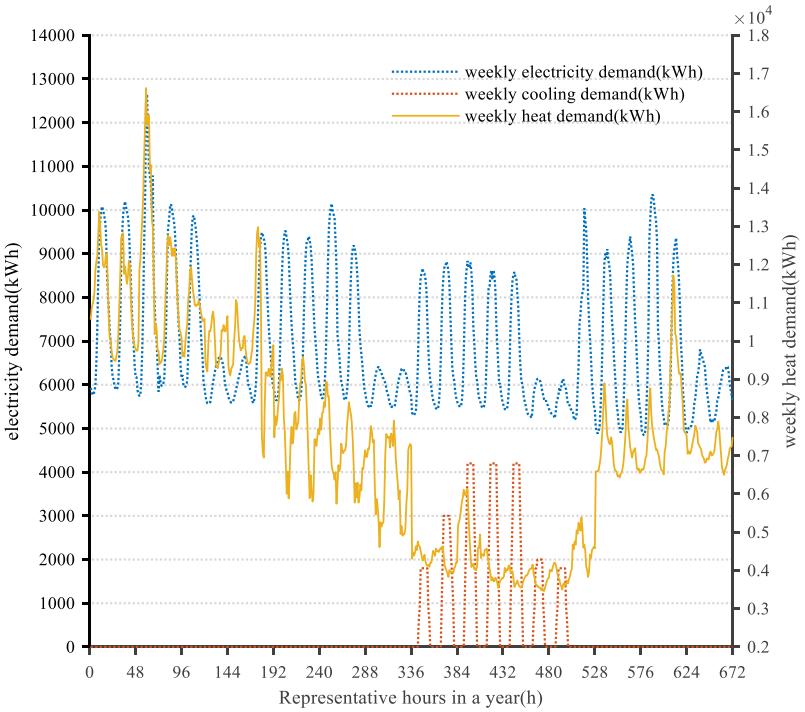

Figure A.3. Representative electricity/heat/cooling demands in campus

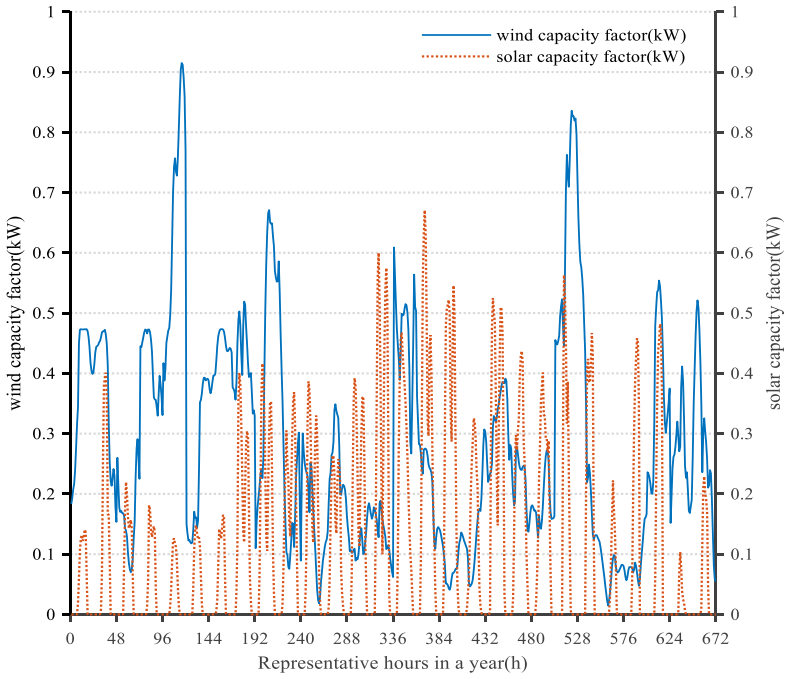

Figure A.4. Representative renewable capacity factors in campus

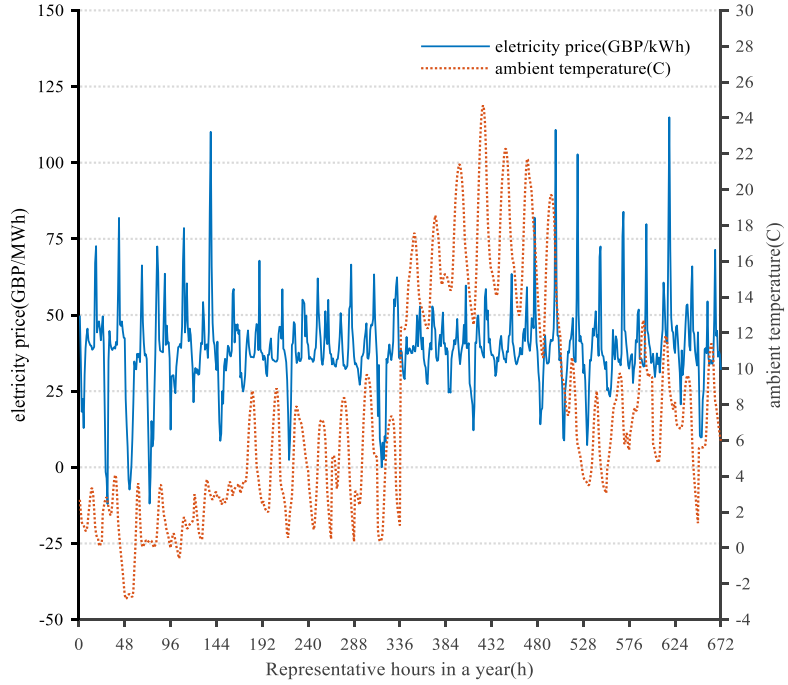

Figure A.5. Representative unit-rate electricity price and ambient temperature in campus

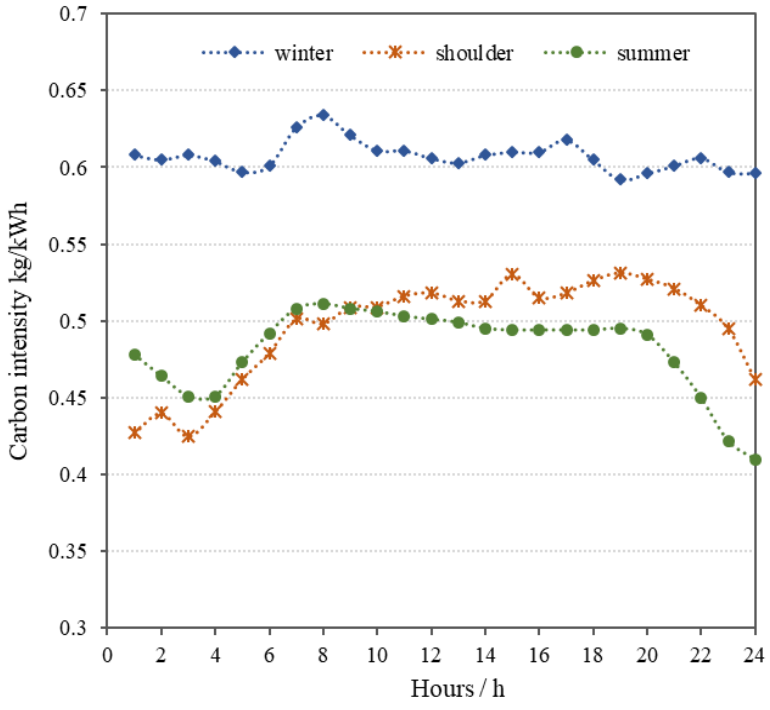

Figure A.6. Daily grid carbon intensity in different seasons in the UK

A2.2 Other input parameters

As the campus micro-grid is connected to the national gas and electricity network, so total bills of gas and electricity was considered. The retail gas prices were considered as

constant separately during summer, intermediate and winter seasons, which were 1.04, 1.37, and 2.22 p/kWh respectively [339,340].The emission factor of natural gas is 0.185 kg CO_2/kWh, and the average carbon intensity of the electricity grid in the UK is varying with time due to different generators mix, which is shown in Figure A.6 [260]. The recommended carbon price for the power sector in the UK is £ 0.018/kg CO2 since 2013 [341].

With regard to the electricity bills, for a university campus as a business case, the bill is composed of five major parts by analysing the campus bill and referring to the data from Ofgem [340], they include the wholesale cost (~60%), environmental obligation cost (~18%), transmission cost (~10%), operating cost (~9%) and others (levies, ~3%). The wholesale cost was charged based on the retail electricity prices shown in Figure A.5, and the demand charge (1.1£/kVA/month) and transmission charge (218.6 £/day) also constitute the large parts in the bill, the environmental obligation cost was charged by applying CO_2 tax in this study. The yearly average electricity demand was 6.6 MW and the peak demand was 12.6 MW.

To achieve CO_2 emission reduction targets, renewable energy and clean technologies were encouraged by governments by implementing renewable heat incentives (RHI) and Feed-In Tariffs (FITs) policies, which were considered in this study. The commercial incentives were 2.69 p/kWh, 0.05 p/kWh, and 0.88 p/kWh for ASHP (7 years), solar PVs, and wind turbines [342].

When a higher ratio of renewables penetrates the micro-grid, curtailments would occur to keep demand and supply balanced, which is not expected, as it reduces the renewable incentives, the cost-effectiveness of the wind farm and the environmental benefits. Thus, a curtailment penalty was imposed, which was assumed as £ 80/MWh in the UK market [343].

In a highly-independent micro-grid with high renewable penetration, it is required to keep enough operating reserve (surplus operating capacity) to respond to sudden load and renewable variations. Generally, the operating reserve can be categorized into three types based

on European guidelines [344], namely the primary reserve, the secondary reserve and the tertiary reserve, depending on their response time and dynamics. In this study, the secondary reserve value was set as 10% of hourly load and 15% of hourly wind power output [345]. The charge for the reserve capacity was taken as 0.83 £/kW [260].

Considering the loss of power would occur accidentally, which would impose a heavy economic loss on business and commercial parties, the loss of power penalty was imposed at a rate of 17000 £/MWh [260]. In the system without reserve margin, the loss of power probability (LOPP) should be less than the predefined loss of load expectation (LOLE, 3 hours/year), which is aligned with the requirement of the UK grid security code [260]. While in the system with operating reserve, the LOPP was expressed as the piece-wise linear function of capacity margin at each time step, the aggregated LOPP should be less than LOLE [260] [346].

After all the input the parameters were introduced above, they were collected and listed in Table A.2.

Table A.2. Model input 'environment' parameters

Components	Parameters	Data	Unit
Energy bill	Gas bill rates	1.04 / 1.37 / 2.22	p/kWh
	Electricity bill rates	Fig.5.	p/kWh
Incentives	Renewable heat	2.69 (7 years)	p/kWh
	Solar PV	1.78	p/kWh
	Wind power	0.88	p/kWh
Penalty	Wind curtailment penalty	80	£/MWh
	Loss of power penalty	17000	£/MWh
CO2 related	NG CO2 emission factor	185	kg/MWh
	Carbon price	18	£/t
Reserve related	LCOE	3	hours/year
	Reserve charge	0.83	£/kW

A2.3 Search space of variables

For the MILP optimal design and operation, the capacity ranges of system components were set for the MILP simulation, which are listed in Table A.3.

Table A.3. Capacity ranges of system components

Components	Capacity range	Limits statement
Gas engines	1000-5000 kW	Industry recommends
Electric chiller	500-2000 kW	Cooling demand
Heat pump	500-2000 kW	Industrial heat pump scale
Gas boiler	1000-5000 kW	Industrial boiler scale
LAES	0-12000 kWh	Maximum electricity demand
Battery	0-13000 kWh	Maximum electricity demand
Hot water storage	0-10000 kWh	heat demand and tank volume
Solar PV	0-3000 m^2	Limited installation area
Wind turbine	0-400(number)	Limited installation area

A2.4 Other performance indicators

The E/P ratio is defined as the ratio of stored energy (kWh) and the rated charge/discharge power (kW), called charge/discharge (Cha/Dis) E/P ratio. It describes the temporal characteristics of energy storage technologies. The recommended E/P ratio of the battery is 4h and considered as short-term storage, while for PHES and CAES, the E/P ratio are set as 7h and 16h [338]. But for the decoupled LAES, the ratio was not yet studied and defined before, moreover, LAES is capable of providing different services in the electricity market, like energy arbitrage, wind stabilization, short-term operating reserve, and fast reserve [221], which require different E/P ratios.

ROI is defined as the ratio of net profit and investment cost, it is used to quantify the effects of different E/P ratios of LAES on system economics, higher ROI means better cost-effectiveness. To be noted, The capital costs of LFUs, PRUs, and storage tanks were estimated based on the investment cost of a 10 MW of commercial LAES plant, the size scale factor is 0.6 [347]. The storage capacity and cost were added into the system exogenously before the value streams of LAES were fully recognized. For the decoupled LAES system, when keeping the rated energy capacity (6MWh) the same and increasing Cha/Dis E/P ratios, smaller LFUs and PRUs with higher specific costs and longer working durations were applied.

A3 MILP formulation methodology

A3.1 MILP algorithm description

The optimal design and operation framework for the micro-grid was formulated as a hierarchical MILP model. It has two levels, namely the upper design level and the lower operation level, introducing the binary variables, integer variables, and continuous variables to represent the selection value, the selected number, other design and operational parameters. It can be described in a general form in eq. (A.20)-(A.21) [348].

$$\mathbf{min}(\boldsymbol{c^T x} + \boldsymbol{d^T y}) \qquad \textbf{eq.(A.20)}$$

$$\boldsymbol{Ax} + \boldsymbol{By} = b \qquad \textbf{eq.(A.21)}$$

$$\boldsymbol{x} \geq \mathbf{0} \in \boldsymbol{R^{N_x}}, \boldsymbol{y} \in \{\mathbf{0}, 1\}^{N_y} \qquad \textbf{eq.(A.22)}$$

where, $\boldsymbol{x}$ represents continuous variable vector, $\boldsymbol{y}$ represents binary variable vector, $\boldsymbol{A}$ and $\boldsymbol{B}$ are the corresponding constraints matrices, and $\boldsymbol{b}$ is the constraint known-term; N_x and N_y represent the dimensions of $\boldsymbol{x}$ and $\boldsymbol{y}$. $\boldsymbol{c}$ and $\boldsymbol{d}$ represent the cost matrices for continuous and binary variables.

A3.1.1 Decision variables

The decision variables were divided into three categories:

i. Design variables, including the selection value ($\boldsymbol{S} \in R^{\boldsymbol{I}}$), selected number ($\boldsymbol{N} \in Z^{\boldsymbol{I_{ep}}}$), and rated size of system components ($\boldsymbol{Des_{ep}} \in R^{\boldsymbol{I_{ep}}}$) and storage devices ($\boldsymbol{Des_{ST}} \in R^{I_{ST}}$).

ii. Operation variables, including on/off status ($\boldsymbol{of} \in \{0,1\}^{\boldsymbol{I_{ep} \times T}}$), operating modes ($\boldsymbol{M} \in \{0,1\}^{\boldsymbol{I_{ep} \times T}}$), on/off number ($\boldsymbol{of\_num} \in Z^{\boldsymbol{I_{ep} \times T}}$), input and output power ($\boldsymbol{P_{in}} \in R^{\boldsymbol{I \times T}}, \boldsymbol{P_o} \in R^{\boldsymbol{I \times T}}$), as well as the storage level of storage technologies ($\boldsymbol{SOC} \in R^{\boldsymbol{I_{ST} \times T}}$), as well as the imported electricity and gas energy ($\boldsymbol{P_{ele}} \in R^{\boldsymbol{T}}, \boldsymbol{P_{gs}} \in R^{\boldsymbol{T}}$).

iii. Auxiliary variables, which are used to linearize non-linear terms, and to combine design variables and operation variables ($\boldsymbol{Ax} \in R^{\boldsymbol{I_{ep} \times J \times T}}$).

A3.1.2 Bounded constraints

In the MILP formulation, the constraints of the problem are described as four categories:

i. Technical constraints, determining the conversion relationship of input and output power, as well as other technical limits, like the efficiency, lifetime, minimum and maximum load and the available installation space, which are based on performance curve and manufactured data of equipment, as well as the first principle of energy.

ii. Operation constraints, representing the operation limits when equipment is running, like ramp-up/down rates, minimum online/ offline time durations, optimal charge/discharge rates, renewable curtailments and operating reserve margins.

iii. Economic constraints, including the capital cost and the O&M cost of system components, amortized cost, CO_2 tax, renewable incentives, curtailment penalty, the unserved load penalty and the revenue of energy storage devices.

iv. Power balance constraints, describing the balance between the power flow, heat flow, and cooling flow at each time step based on the components output and the first principle of energy.

These constraints are illustrated by different components separately as followings.

- Gas engine

Gas engines are used to produce electricity and heat simultaneously by consuming natural gas. The constraints are described as in eq. (A.23) - eq.(A.24).

Electric power output:

$$P_{GE}(i,t) = 1.13 \cdot \eta_{r,GE}(i) \cdot Q_{f,GE}(i,t) - 0.131 P_{r,GE}(i) \quad \text{eq.(A.23)}$$

Recoverable heat:

$$Q_{rh,GE}(i,t) = (\eta_{tot,GE}(i) - \eta_{r,GE}(i)) \cdot \left(0.94 \cdot Q_{f,GE}(i,t) + \frac{0.57 \cdot P_{r,GE}(i)}{\eta_{r,GE}(i)}\right) \quad \text{eq.(A.24)}$$

Operational range:

$$P_{min,GE}(i) * of_{GE}(i,t) * P_{r,GE}(i) \leq P_{GE}(i,t) \leq of_{GE}(i,t) * P_{r,GE}(i) \quad \text{eq.(A.25)}$$

Ramp_up/down rate limits:

$$P_{dn,GE}(i,t) \leq P_{GE}(i,t) \leq P_{up,GE}(\boldsymbol{i},\boldsymbol{t}) \quad \text{eq.(A.26)}$$

Minimum online/offline duration:

$$online_{GE}(i,j,t{:}\,t_{on}) \geq online_{GE}(i,j,t) - online_{GE}(i,j,t-1) \quad \text{eq.(A.27)}$$

CO_2 emission constraint:

$$ems_{GE} = \sum Q_{f,GE}(i,t) * emf_{NG} \quad \text{eq.(A.28)}$$

where, *P* – electricity power capacity, Q – heat power, *online* – the state of gas engines that are in operation, *ems* – emission of CO_2, *emf* – emission factor, *i* – the i^{th} equipment candidate, *t* – the t^{th} time step, η - efficiency. Subscripts *GE* – gas engine, *NG* – natural gas, *f* – fuel consumption, *rh* - recoverable heat power (MW), *tot* – total efficiency, *r* – rated power, *up*- ramp up, *dn* – ramp down, *on* – online, *min* – minimum.

- Heat pump

Reversible heat pumps consumes electricity to produce heat or cooling power. They can also be considered as a method to shift off-peak electricity to heat. The performance is described in eq. (A.29) – (A.30), of which the correlation of coefficient of performance (COP) with ambient temperature (T_{amb}) was obtained from the regression.

$$Q_{HP}(\boldsymbol{i},t) = \mathrm{COP}_{HP}(T_{amb}) \cdot P_{ele}(\boldsymbol{i},t) \quad \text{eq.(A.29)}$$

$$\mathrm{COP}_{HP}(T_{amb}) = \begin{cases} 2.8, & T_{amb} \in cooling\ season \\ 0.0329 * T_{amb} + 2.0012, & T_{amb} \in heating\ season \end{cases} \quad \text{eq.(A.30)}$$

where, *T* – temperature. Subscripts *HP* – heat pump, *ele* – electricity.

Considering the nearly constant ambient temperature when it is used to provide cooling power from June to August, it is reasonable to assume a constant COP. But in heating seasons, the COP of heat pumps was considered varying with ambient temperature, the regression

relationship was obtained from manufacture test data. Heat pumps start to work in heat mode when the external temperature is below a threshold temperature (14 °C) [260].

For reversible heat pumps, a binary variable $\boldsymbol{M}_{HP} \in \{0,1\}^T$ was introduced to control the operational modes (heating or cooling mode) of heat pumps. Its operational range, ramp up/down rate limits and online /offline duration were expressed in a similar way to those of gas engines.

- Gas boiler

Gas boilers produce heat power by consuming natural gas, of which heat power provided is expressed as in eq. (A.31) - (A.33).

$$P_{GB}(\boldsymbol{i},\boldsymbol{t}) = \eta_{GB} \cdot Q_{f,GB}(\boldsymbol{i},\boldsymbol{t}) \quad \text{eq.(A.31)}$$

$$0 \leq Q_{f,GB}(\boldsymbol{i},\boldsymbol{t}) \leq Q_{f,max}(\boldsymbol{i}) \quad \text{eq.(A.32)}$$

$$ems_{GB} = \sum Q_{f,GB}(i,t) * emf_{NG} \quad \text{eq.(A.33)}$$

where, *GB*- gas boilers, η_{GB}- efficiency of the gas boiler, it is assumed as constant when ignoring the size dependency. *max* – maximum.

- Solar PV & wind turbines

The generated power by solar PV panels and wind turbines are expressed as in eq. (A.34) - (A.35). The capacity factor was used, which means the availability of wind or solar energy for a specific hour at a certain location. Considering the scarce solar resource in the UK, only the wind power curtailment was considered.

$$P_{pv}(t) = CF_{pv} \cdot P_{r,pv} \quad \text{eq.(A.34)}$$

$$P_{wt}(t) <= CF_{wt} \cdot P_{r,wt} \quad \text{eq.(A.35)}$$

But due to the limited top roof area and land available for installing wind turbines, two constraints were imposed for these two renewables.

$$0 \leq A_{pv} \leq A_{pv,max} \quad \text{eq.(A.36)}$$

$$0 \leq N_{wt} \leq N_{wt,max} \quad \text{eq.(A.37)}$$

where, pv – solar PV panels, wt – wind turbines, CF- capacity factor, A – deployment area, N- the number of wind turbines.

- Operating reserve constraints

In the model, gas engines and LAES were considered to provide operating reserve when wind penetration is high. The reserve constraints are expressed in eq. (A.38) – eq.(A.43) [260,349].

$$R_{GE}(i,t) + R_{ST}(t) \leq \boldsymbol{R}(t) \quad \text{eq.(A.38)}$$

$$R_{GE}(i,t) = R_{GE\_capa}(i,t) - P_{GE}(\boldsymbol{i},t) \quad \text{eq.(A.39)}$$

$$0 \leq R_{ST}(t) \leq R1_{ST,capa}(t) \quad \text{eq.(A.40)}$$

$$0 \leq R_{ST}(t) \leq R2_{ST,capa}(t) \quad \text{eq.(A.41)}$$

$$R1_{ST\_capa}(i,t) \leq P_{ST\_ava}(t) \quad \text{eq.(A.42)}$$

$$R2_{ST\_capa}(t) \leq P_{r,\mathrm{Tr}} - P_{\mathrm{Tr}}(t) + P_{\mathrm{C}}(t) * \mathbf{RTE} \quad \text{eq.(A.43)}$$

where, R – the needed reserve power (MW), $R1$ – the primary reserve power, $R2$ – the secondary reserve power**,** P_{Tr} – the power output of turbines of LAES, P_{C} – the power input of compressors of LAES, RTE – the round trip efficiency of LAES. Subscripts ST – storage, $ST, capa$ – storage reserve capacity, GE_capa – gas engine reserve capacity, ST_ava - the available storage capacity.

- Linearization of non-linear terms

In order to keep the linearity of the MILP formulation, the non-linear terms should be transformed by certain methods with additional auxiliary variables and constraints. The common used methods are the 'big-M' method to transform if-then constraints, and the piece-wise linear approximation which is capable of linearizing non-linear performance curves.

1) 'Big-M' method [350]

It is assumed there is an appropriate 'big' number '*M*', which is determined based on the application, leaving it large enough to activate or deactivate the linear constraints. *x*(*t*) is the continuous variable, a binary variable $\Lambda(t)$ is introduced to construct the expression in eq.(A.44) - eq.(A.46).

$$M_2 \cdot \Lambda(t) \le x(t) \le M_1 \cdot \Lambda(t) \quad \text{eq.(A.44)}$$

$$z(t) - \big(1 - \Lambda(t)\big) \cdot M_1 \le x(t) \le z(t) \quad \text{eq.(A.45)}$$

$$0 \le z(t) \le Z_1 \quad \text{eq.(A.46)}$$

M_2, M_1 are two big '*M*' numbers, when $\Lambda(t)$ is switched on to 1, $x(t)$ is activated and limited by the appropriate upper and lower limits, and $x(t) = z(t)$ is satisfied. When $\Lambda(t)$ is switched off to 0, $x(t) = 0$, the variable is deactivated.

2) Piece-wise linear approximation [351]

It is assumed there is a non-linear function *z* of continuous variable *x*, the piece-wise linear approximation is used to linearize the non-linear curve, the procedures are described as follows.

$$z = f(x), x_1 \le x \le x_n \quad \text{eq.(A.47)}$$

a. The space of variable *x* is discretized into *n* elements, expressed as [$x_1, x_{2,\dots,} x_n$], $x_1 = x_{min}, x_n = x_{max}$;

b. The corresponding discrete function values [$z_1, z_{2,\dots,} z_n$] are calculated.

c. Introduce a set of auxiliary continuous variables α_i, which relate x_i to z_i.

$$\sum_{i=1}^{n} \alpha_i x_i = x \quad \text{eq.(A.48)}$$

$$\sum_{i=1}^{n} \alpha_i z_i = z \quad \text{eq.(A.49)}$$

$$\sum_{i=1}^{n} \alpha_i = 1, 0 \le \alpha_i \le 1, i = 1, 2, \dots, n \quad \text{eq.(A.50)}$$

d. Introduce another *n*-1 of binary variables β_i, satisfying the following constraints:

$$\sum_{i=1}^{n-1} \beta_i = 1 \quad \text{eq.(A.51)}$$

$$\alpha_1 - \beta_1 \le 0 \quad \text{eq.(A.52)}$$

$$\alpha_i - \beta_{i-1} - \beta_i \leq 0, i = 2,3,n-1 \quad \text{eq.(A.53)}$$

$$\alpha_n - \beta_{n-1} \leq 0 \quad \text{eq.(A.54)}$$

The variables α_i and β_i are optimally solved by MILP algorithm, then, the optimal value of x and y can be determined.

A3.1.3 Optimization objectives

The study aimed to minimize the total annual cost and the environmental impact of the system, including the equipment annual capital cost $C_{cpt,tot}$, the operational cost C_{op} and maintenance cost C_M, and CO_2 emission tax C_{CO2}, as well as renewable curtailment penalty C_{cur} and loss of power penalty C_{LOP}, at the same time, it aimed to increase the renewable penetration by maximizing renewable incentives C_{inc}, expressed as in eq. (A.55).

$$min\begin{cases} C_{ann,tot} = C_{cpt,tot} + C_{op} + C_M + \cdots \\ C_{CO2} + C_{cur} + C_{LOP} - C_{inc} \end{cases} \quad \text{eq.(A.55)}$$

To conduct a one-year economic analysis and to consider the time value of monetary, the amortized capital cost of equipment was adopted [170]. It means amortizing the initial investments over the entire lifetime of system components, the interest rate *IR* was assumed as 7%, given by eq. (A.56) – eq. (A.58).

$$C_{cpt,tot} = \sum_{i=1}^{I} Amf_i \cdot C_{cpt}(i) \quad \text{eq.(A.56)}$$

$$Amf_i = \frac{IR(1+IR)^{Lf_i}}{(1+IR)^{Lf_i}-1}, \forall\, i \in I \quad \text{eq.(A.57)}$$

$$C_M = \sum_{i=1}^{I} f_i \cdot C_{cpt}(i) + \sum_{k=1}^{rew} f_k \cdot P_{rew}(k) \quad \text{eq.(A.58)}$$

where, Amf_i is the amortized factor of the i^{th} equipment, Lf is the lifetime of equipment, f is the maintenance cost factor, *IR* – the interest rate, C_{cpt} – the capital cost of each equipment, P_{rew} - the power produced by renewables, *rew* – renewables, *k* – the k^{th} type of renewable.

The CO_2 tax was imposed to reduce the environmental impacts of traditional technologies and to encourage to adopt new green technologies. A carbon price Tax_{co2} was

introduced to implement the CO_2 tax based on the CO2 emissions from equipment $ems(i,t)$ and the grid electricity $ems_{grid}(t)$.

$$C_{CO2} = \sum_{t=1}^{T} \sum_{i=1}^{I} Tax_{co2} \cdot ems(i,t) + \sum_{t=1}^{T} Tax_{co2} \cdot ems_{grid}(t) \quad \text{eq.(A.59)}$$

The operational cost C_{op} of the system mainly comes from consuming natural gas (gas cost C_f) and electricity (electricity cost C_{ele}) from the grid (P_{grid}), the price of electricity Pr_{ele} and gas Pr_{gs} were assumed based on the retail prices. C_{op} is expressed in eq. (A.60).

$$C_{op} = C_{ele} + C_f = \sum_{t=1}^{T} Pr_{ele}(t) \cdot P_{grid}(t) + \cdots$$

$$\sum_{t=1}^{T} \sum_{i=1}^{I} Pr_{gs}(t) \cdot Q_f(i,t) \quad \text{eq.(A.60)}$$

In the wind prevailing seasons, wind curtailment cost C_{cur} would occur, the curtailment penalty Pr_{cur} was imposed on the curtailed wind power $P_{wt,cur}$, to increase the renewable penetration, and maintain the stable frequency and power quality of the network, which is expressed as in eq. (A.61).

$$C_{cur} = \sum_{t=1}^{T} Pr_{cur} P_{wt,cur}(t) \quad \text{eq.(A.61)}$$

For a micro-grid with high independence and renewables penetration, it is necessary to maintain the operating reserve to manage the variability and uncertainties of resources and demands. The loss of power penalty C_{LOP} was introduced to avoid loss of power P_{los} as much as possible. The cost penalty Pr_{LOP} was defined as 17000 £ / MWh in this study.

$$C_{LOP} = \sum_{t=1}^{T} Pr_{LOP} P_{los}(t) \quad \text{eq.(A.62)}$$

The renewable heat, solar, and wind energy incentives were also taken into account in the study, which are expressed as in eq. (A.63).

$$C_{inc,tot} = \sum_{t=1}^{T} \sum_{k=1}^{rew} FIT_k \cdot P_{rew}(t) + \sum_{t=1}^{T} FIT_{HP} \cdot Q_{HP}(t) \quad \text{eq.(A.63)}$$

where, $C_{inc,tot}$ – the incentives of renewable technologies, FIT – the feed in tariff rate, P – the produced electricity from renewables, *HP* – heat pumps, *rew* – the renewable energy.

Bibliography

[1] Roeder M, Hill F, Mander S, Conor W, Kuriakose J, Glynn S, et al. The impacts of climate change on UK energy demand. Infrastruct Asset Manag 2015;2:107–19. https://doi.org/10.1680/iasma.14.00039.

[2] IEA. Net Zero by 2050: A Roadmap for the Global Energy Sector. Int Energy Agency 2021:224.

[3] The Paris Agreement. United Nations 2016. https://www.un.org/en/climatechange/paris-agreement.

[4] COP26: Together for our planet. United Nations 2021.

[5] EUA. The Upfront Cost of Decarbonising Your Home 2021:0–36.

[6] United States Department of State. The Long-Term Strategy of the United States: Pathways to Net-Zero Greenhouse Gas Emissions by 2050. United States Dep State United States Exec Off Pres 2021:1–63.

[7] Gielen D, Boshell F, Saygin D, Bazilian MD, Wagner N, Gorini R. The role of renewable energy in the global energy transformation. Energy Strateg Rev 2019;24:38–50. https://doi.org/10.1016/j.esr.2019.01.006.

[8] De Vita A, Kielichowska I, Mandatowa P, Capros P, Dimopoulou E, Evangelopoulou S, et al. a s s e t July, 2 0 1 8 Technology pathways in decarbonisation scenarios 2018.

[9] Weitemeyer S, Kleinhans D, Vogt T, Agert C. Integration of Renewable Energy Sources in future power systems: The role of storage. Renew Energy 2015;75:14–20. https://doi.org/10.1016/j.renene.2014.09.028.

[10] Strbac G, Aunedi M, Pudjianto D. Strategic Assessment of the Role and Value of Energy Storage Systems in the UK Low Carbon Energy Future Improving Offline Security Rules for Dynamic Security Assessment View project Smarter Network Storage View project 2012. https://doi.org/10.13140/RG.2.1.1418.5684.

[11] Das T, Krishnan V, McCalley JD. Assessing the benefits and economics of bulk energy storage technologies in the power grid. Appl Energy 2015;139:104–18. https://doi.org/10.1016/j.apenergy.2014.11.017.

[12] Gür TM. Review of electrical energy storage technologies, materials and systems: Challenges and prospects for large-scale grid storage. Energy Environ Sci 2018;11:2696–767. https://doi.org/10.1039/c8ee01419a.

[13] Gallo AB, Simões-Moreira JR, Costa HKM, Santos MM, Moutinho dos Santos E. Energy storage in the energy transition context: A technology review. Renew Sustain Energy Rev 2016;65:800–22. https://doi.org/10.1016/j.rser.2016.07.028.

[14] He W, King M, Luo X, Dooner M, Li D, Wang J. Technologies and economics of electric energy storages in power systems: Review and perspective. Adv Appl Energy 2021;4:100060. https://doi.org/10.1016/j.adapen.2021.100060.

[15] AL Shaqsi AZ, Sopian K, Al-Hinai A. Review of energy storage services, applications, limitations, and benefits. Energy Reports 2020;6:288–306. https://doi.org/10.1016/j.egyr.2020.07.028.

[16] Luo X, Wang J, Dooner M, Clarke J. Overview of current development in electrical energy storage technologies and the application potential in power system operation. Appl Energy 2016;137:511–36.

[17] Liang T, Zhang T, Li Y, Tong L, Wang L, Ding Y, et al. Thermodynamic Analysis of Liquid Air Energy Storage (LAES) System. Encycl. Energy Storage, vol. 2020, 2023.

[18] Ting Liang, Tongtong Zhang, Xipeng Lin TA. Liquid air energy storage technology: a comprehensive review of research, development and deployment. Prog Energy 2023.
[19] Olympios A, McTigue J, Farres Antunez P, Tafone A, Romagnoli A, Li Y, et al. Progress and prospects of thermo-mechanical energy storage – A critical review. Prog Energy 2021. https://doi.org/10.1088/2516-1083/abdbba.
[20] Liang T, Vecchi A, Knobloch K, Sciacovelli A, Engelbrecht K, Li Y, et al. Key components for Carnot Battery : Technology review , technical barriers and selection criteria. Renew Sustain Energy Rev 2022;163:112478. https://doi.org/10.1016/j.rser.2022.112478.
[21] Andrea Vecchi, Kai Knobloch, Ting Liang, Adriano Sciacovelli, Kurt Engelbrecht, Yongliang Li YD. Carnot Battery (CB): a State-of-art Review on CB System Performance and Applications. J Energy Storage 2022.
[22] Steinmann WD. The CHEST (Compressed Heat Energy STorage) concept for facility scale thermo mechanical energy storage. Energy n.d.;69:543–52. https://doi.org/10.1016/j.energy.2014.03.049.
[23] Moradi R, Groth KM. Hydrogen storage and delivery: Review of the state of the art technologies and risk and reliability analysis. Int J Hydrogen Energy 2019;44:12254–69. https://doi.org/10.1016/j.ijhydene.2019.03.041.
[24] Andersson J, Grönkvist S. Large-scale storage of hydrogen. Int J Hydrogen Energy 2019;44:11901–19. https://doi.org/10.1016/j.ijhydene.2019.03.063.
[25] Chen H, Cong TN, Yang W, Tan C, Li Y, Ding Y. Progress in electrical energy storage system: A critical review. Prog Nat Sci n.d.;19:291–312. https://doi.org/10.1016/j.pnsc.2008.07.014.
[26] Subburaj AS, Kondur P, Bayne SB, Giesselmann MG, Harral MA. Analysis and review of grid connected battery in wind applications. IEEE Green Technol Conf 2014:1–6. https://doi.org/10.1109/GREENTECH.2014.14.
[27] Is W, Storage E. Energy Storage in California 2018:1–8.
[28] Mongird K, Viswanathan V, Balducci P, Alam J, Fotedar V, Koritarov V, et al. Energy Storage Technology and Cost Characterization Report | Department of Energy. US Dep Energy 2019:1–120.
[29] Olympios A V, McTigue JD, Farres-Antunez P, Tafone A, Romagnoli A, Li Y, et al. Progress and prospects of thermo-mechanical energy storage—a critical review. Prog Energy 2021;3:022001. https://doi.org/10.1088/2516-1083/abdbba.
[30] International Energy Agency. Global Energy Review: CO2 Emissions in 2021 Global emissions rebound sharply to highest ever level. Iea 2022:1–14.
[31] Groscurth H, Bruckner TH, Kummel R. Pergamon M O D E L I N G OF E N E R G Y - S E R V I C E S S U P P L Y S Y S T E M S 1995;20:941–58.
[32] Grosspietsch D, Saenger M, Girod B. Matching decentralized energy production and local consumption: A review of renewable energy systems with conversion and storage technologies. Wiley Interdiscip Rev Energy Environ 2019;8:1–18. https://doi.org/10.1002/wene.336.
[33] Grosspietsch D. Fostering Technological Change for a Sustainable Built Environment: The Role of Policy, System Design and Performance 2018:233.
[34] Gabrielli P. Optimal design of multi-energy systems: From technology modeling to system optimization 2019:334.
[35] Oecd/Iea. World Energy Model Documentation 2012.
[36] Pfenninger S. Dealing with multiple decades of hourly wind and PV time series in energy models: A comparison of methods to reduce time resolution and the planning implications of inter-annual variability. Appl Energy 2017;197:1–13.

https://doi.org/10.1016/j.apenergy.2017.03.051.
[37] Mancarella P, Andersson G, Peças-Lopes JA, Bell KRW. Modelling of integrated multi-energy systems: drivers, requirements, and opportunities Index Terms— multi-energy systems, integrated energy systems, whole-energy systems, energy systems modelling, energy systems integration, energy systems modelling tools 2016.
[38] Hawkes AD, Leach MA. Modelling high level system design and unit commitment for a microgrid. Appl Energy 2009;86:1253–65. https://doi.org/10.1016/j.apenergy.2008.09.006.
[39] Cardoso G, Brouhard T, DeForest N, Wang D, Heleno M, Kotzur L. Battery aging in multi-energy microgrid design using mixed integer linear programming. Appl Energy 2018;231:1059–69. https://doi.org/10.1016/j.apenergy.2018.09.185.
[40] Fazlollahi S, Mandel P, Becker G, Maréchal F. Methods for multi-objective investment and operating optimization of complex energy systems. Energy 2012;45:12–22. https://doi.org/10.1016/j.energy.2012.02.046.
[41] Peng X. LIQUID AIR ENERGY STORAGE: PROCESS OPTIMIZATION AND PERFORMANCE ENHANCEMENT. The University of Birmingham, 2018.
[42] Guizzi GL, Manno M, Tolomei LM, Vitali RM, Leo Guizzi G, Manno M, et al. Thermodynamic analysis of a liquid air energy storage system. Energy 2015;93:1639–47. https://doi.org/10.1016/j.energy.2015.10.030.
[43] Peng X, She X, Li Y, Ding Y. Thermodynamic analysis of Liquid Air Energy Storage integrated with a serial system of Organic Rankine and Absorption Refrigeration Cycles driven by compression heat. Energy Procedia 2017;142:3440–6. https://doi.org/10.1016/j.egypro.2017.12.227.
[44] Sciacovelli A, Vecchi A, Ding Y. Liquid air energy storage (LAES) with packed bed cold thermal storage – From component to system level performance through dynamic modelling. Appl Energy 2017;190:84–98. https://doi.org/10.1016/j.apenergy.2016.12.118.
[45] She X, Peng X, Nie B, Leng G, Zhang X, Weng L, et al. Enhancement of round trip efficiency of liquid air energy storage through effective utilization of heat of compression. Appl Energy n.d.;206:1632–42. https://doi.org/10.1016/j.apenergy.2017.09.102.
[46] Ting Liang, Xiaohui She, Yongliang Li, Tongtong Zhang YD. Thermo-economic multi-objective optimization of the liquid air energy storage system 2022.
[47] Chino K, Araki H. Evaluation of energy storage method using liquid air. Heat Transf - Asian Res 2000;29:347–57. https://doi.org/10.1002/1523-1496(200007)29:5<347::AID-HTJ1>3.0.CO;2-A.
[48] Abdo RF, Pedro HTC, Koury RNN, Machado L, Coimbra CFM, Porto MP. Performance evaluation of various cryogenic energy storage systems. Energy 2015;90:1024–32. https://doi.org/10.1016/j.energy.2015.08.008.
[49] Borri E, Tafone A, Comodi G, Romagnoli A. Improving liquefaction process of microgrid scale Liquid Air Energy Storage (LAES) through waste heat recovery (WHR) and absorption chiller. Energy Procedia 2017;143:699–704. https://doi.org/10.1016/j.egypro.2017.12.749.
[50] Zhang T, Zhang X, Xue X, Wang G, Mei S. Thermodynamic analysis of a hybrid power system combining Kalina cycle with liquid air energy storage. Entropy 2019;21:220. https://doi.org/10.3390/e21030220.
[51] Hamdy S, Moser F, Morosuk T, Tsatsaronis G. Exergy-based and economic evaluation of liquefaction processes for cryogenics energy storage. Energies 2019;12. https://doi.org/10.3390/en12030493.

[52] Liang T, Zhang T, Lin X, Alessio T, Legrand M, He X, et al. Liquid air energy storage technology: a comprehensive review of research, development and deployment. Prog Energy 2023;5. https://doi.org/10.1088/2516-1083/aca26a.
[53] Peng X, She X, Cong L, Zhang T, Li C, Li Y, et al. Thermodynamic study on the effect of cold and heat recovery on performance of liquid air energy storage. Appl Energy n.d.;221:86–99. https://doi.org/10.1016/j.apenergy.2018.03.151.
[54] Peng H, Shan X, Yang Y, Ling X. A study on performance of a liquid air energy storage system with packed bed units. Appl Energy 2018;211:126–35. https://doi.org/10.1016/j.apenergy.2017.11.045.
[55] Liang T, Webley PA, Chen YC, She X, Li Y, Ding Y. The optimal design and operation of a hybrid renewable micro-grid with the decoupled liquid air energy storage. J Clean Prod 2022;334:130189. https://doi.org/10.1016/j.jclepro.2021.130189.
[56] Tafone A, Borri E, Comodi G, Romagnoli A. Parametric performance maps for design and selection of Liquid Air Energy Storage system for mini to micro-grid scale applications. Energy Procedia, vol. 158, 2019, p. 5053–60. https://doi.org/10.1016/j.egypro.2019.01.649.
[57] Li Y, Chen H, Ding Y. Fundamentals and applications of cryogen as a thermal energy carrier: A critical assessment. Int J Therm Sci 2010;49:941–9. https://doi.org/10.1016/j.ijthermalsci.2009.12.012.
[58] Hamdy S, Morosuk T, Tsatsaronis G. Cryogenics-based energy storage: Evaluation of cold exergy recovery cycles. Energy 2017;138:1069–80. https://doi.org/10.1016/j.energy.2017.07.118.
[59] Tafone A, Borri E, Comodi G, van den Broek M, Romagnoli A. Liquid Air Energy Storage performance enhancement by means of Organic Rankine Cycle and Absorption Chiller. Appl Energy n.d.;228:1810–21. https://doi.org/10.1016/j.apenergy.2018.06.133.
[60] SMITH EM. STORAGE OF ELECTRICAL ENERGY USING SUPERCRITICAL LIQUID AIR. Proc Inst Mech Eng 1977;191:289–98.
[61] K.Aoyama, K.Kishimoto, Y.Yoshida, K.Toda, M.Atsumi HK. Gas turbine inlet air cooling system with liquid air. Am Soc Mech Eng 1983;6:1–6.
[62] Energy storage-revolution in the air. Mod Power Syst 2013:32–3.
[63] Highview Power to Develop Multiple Cryogenic Energy Storage Facilities in the UK and to Build Europe's Largest Storage System. n.d.
[64] Power H. Highview Power to Develop Multiple Cryogenic Energy Storage Facilities in the UK and to Build Europe's Largest Storage System 2020.
[65] Xue XD, Wang SX, Zhang XL, Cui C, Chen LB, Zhou Y, et al. Thermodynamic Analysis of a Novel Liquid Air Energy Storage System. Phys Procedia n.d.;67:733–8. https://doi.org/10.1016/j.phpro.2015.06.124.
[66] Liu Z, Yu H, Gundersen T. Optimization of Liquid Air Energy Storage (LAES) using a Genetic Algorithm (GA). vol. 48. Elsevier Masson SAS; 2020. https://doi.org/10.1016/B978-0-12-823377-1.50162-2.
[67] Ameel B, T'Joen C, De Kerpel K, De Jaeger P, Huisseune H, Van Belleghem M, et al. Thermodynamic analysis of energy storage with a liquid air Rankine cycle. Appl Therm Eng 2013;52:130–40. https://doi.org/10.1016/j.applthermaleng.2012.11.037.
[68] Vecchi A, Li Y, Mancarella P, Sciacovelli A. Integrated techno-economic assessment of Liquid Air Energy Storage (LAES) under off-design conditions: Links between provision of market services and thermodynamic performance. Appl Energy n.d.;262. https://doi.org/10.1016/j.apenergy.2020.114589.
[69] Hamdy S, Morosuk T, Tsatsaronis G. Exergoeconomic optimization of an adiabatic cryogenics-based energy storage system. Energy n.d.;183:812–24.

https://doi.org/10.1016/j.energy.2019.06.176.
[70] Incer-Valverde J, Hamdy S, Morosuk T, Tsatsaronis G. Improvement perspectives of cryogenics-based energy storage. Renew Energy 2021;169:629–40. https://doi.org/10.1016/j.renene.2021.01.032.
[71] Xie C, Hong Y, Ding Y, Li Y, Radcliffe J. An economic feasibility assessment of decoupled energy storage in the UK: With liquid air energy storage as a case study. Appl Energy 2018;225:244–57. https://doi.org/10.1016/j.apenergy.2018.04.074.
[72] Lin B, Wu W, Bai M, Xie C. Liquid air energy storage: Price arbitrage operations and sizing optimization in the GB real-time electricity market. Energy Econ 2019;78:647–55. https://doi.org/10.1016/j.eneco.2018.11.035.
[73] Wang C, Akkurt N, Zhang X, Luo Y, She X. Techno-economic analyses of multi-functional liquid air energy storage for power generation, oxygen production and heating. Appl Energy n.d.;275. https://doi.org/10.1016/j.apenergy.2020.115392.
[74] Tafone A, Romagnoli A, Li Y, Borri E, Comodi G. Techno-economic Analysis of a Liquid Air Energy Storage (LAES) for Cooling Application in Hot Climates. Energy Procedia n.d.;105:4450–7. https://doi.org/10.1016/j.egypro.2017.03.944.
[75] Guizzi GL, Manno M, Tolomei LM, Vitali RM. Thermodynamic analysis of a liquid air energy storage system. Energy n.d.;93:1639–47. https://doi.org/10.1016/j.energy.2015.10.030.
[76] Tafone A, Ding Y, Li Y, Xie C, Romagnoli A. Levelised Cost of Storage (LCOS) analysis of liquid air energy storage system integrated with Organic Rankine Cycle 2020. https://doi.org/10.1016/j.energy.2020.117275.
[77] Ebrahimi A, Ghorbani B, Skandarzadeh F, Ziabasharhagh M. Introducing a novel liquid air cryogenic energy storage system using phase change material, solar parabolic trough collectors, and Kalina power cycle (process integration, pinch, and exergy analyses). Energy Convers Manag 2021;228. https://doi.org/10.1016/j.enconman.2020.113653.
[78] Zhang T, Zhang XL, He YL, Xue XD, Mei SW. Thermodynamic analysis of hybrid liquid air energy storage systems based on cascaded storage and effective utilization of compression heat. Appl Therm Eng 2020;164:114526. https://doi.org/10.1016/j.applthermaleng.2019.114526.
[79] Nabat MH, Sharifi S, Razmi AR. Thermodynamic and economic analyses of a novel liquid air energy storage (LAES) coupled with thermoelectric generator and Kalina cycle. J Energy Storage 2022;45:103711. https://doi.org/10.1016/j.est.2021.103711.
[80] Nabat MH, Zeynalian M, Razmi AR, Arabkoohsar A, Soltani M. Energy, exergy, and economic analyses of an innovative energy storage system; liquid air energy storage (LAES) combined with high-temperature thermal energy storage (HTES). Energy Convers Manag 2020;226:113486. https://doi.org/10.1016/j.enconman.2020.113486.
[81] Liu Q, He Z, Liu Y, He Y. Thermodynamic and parametric analyses of a thermoelectric generator in a liquid air energy storage system. Energy Convers Manag 2021;237:114117. https://doi.org/10.1016/j.enconman.2021.114117.
[82] Tafone A, Borri E, Comodi G, van den Broek M, Romagnoli A. Liquid Air Energy Storage performance enhancement by means of Organic Rankine Cycle and Absorption Chiller. Appl Energy 2018;228. https://doi.org/10.1016/j.apenergy.2018.06.133.
[83] She X, Zhang T, Peng X, Wang L, Tong L, Luo Y, et al. Liquid Air Energy Storage for Decentralized Micro Energy Networks with Combined Cooling, Heating, Hot Water and Power Supply. J Therm Sci 2020;29:1–17. https://doi.org/10.1007/s11630-020-1396-x.
[84] Cui S, Song J, Wang T, Liu Y, He Q, Liu W. Thermodynamic analysis and efficiency assessment of a novel multi-generation liquid air energy storage system. Energy 2021;235:121322. https://doi.org/10.1016/J.ENERGY.2021.121322.

[85] Al-Zareer M, Dincer I, Rosen MA. Analysis and assessment of novel liquid air energy storage system with district heating and cooling capabilities. Energy 2017;141:792–802. https://doi.org/10.1016/j.energy.2017.09.094.

[86] Vecchi A, Li Y, Mancarella P, Sciacovelli A. Multi-energy liquid air energy storage: A novel solution for flexible operation of districts with thermal networks. Energy Convers Manag 2021;238:114161.

[87] Briola S, Gabbrielli R, Delgado A. Energy and economic performance assessment of the novel integration of an advanced configuration of liquid air energy storage plant with an existing large-scale natural gas combined cycle. Energy Convers Manag 2020;205:112434. https://doi.org/10.1016/j.enconman.2019.112434.

[88] Hanak DP, Powell D, Manovic V. Techno-economic analysis of oxy-combustion coal-fired power plant with cryogenic oxygen storage. Appl Energy 2017;191:193–203. https://doi.org/10.1016/j.apenergy.2017.01.049.

[89] Colbertaldo P, Agustin SB, Campanari S, Brouwer J. Impact of hydrogen energy storage on California electric power system: Towards 100% renewable electricity. Int J Hydrogen Energy 2019;44:9558–76. https://doi.org/10.1016/j.ijhydene.2018.11.062.

[90] Krawczyk P, Szabłowski Ł, Karellas S, Kakaras E, Badyda K. Comparative thermodynamic analysis of compressed air and liquid air energy storage systems. Energy 2018;142:46–54. https://doi.org/10.1016/j.energy.2017.07.078.

[91] Barsali S, Ciambellotti A, Giglioli R, Paganucci F, Pasini G. Hybrid power plant for energy storage and peak shaving by liquefied oxygen and natural gas. Appl Energy 2018;228:33–41. https://doi.org/10.1016/j.apenergy.2018.06.042.

[92] Kim J, Noh Y, Chang D. Storage system for distributed-energy generation using liquid air combined with liquefied natural gas. Appl Energy n.d.;212:1417–32. https://doi.org/10.1016/j.apenergy.2017.12.092.

[93] Li Y, Cao H, Wang S, Jin Y, Li D, Wang X, et al. Load shifting of nuclear power plants using cryogenic energy storage technology. Appl Energy n.d.;113:1710–6. https://doi.org/10.1016/j.apenergy.2013.08.077.

[94] Cetin TH, Kanoglu M, Yanikomer N. Cryogenic energy storage powered by geothermal energy. Geothermics 2019;77:34–40. https://doi.org/10.1016/j.geothermics.2018.08.005.

[95] Park J, Lee I, Moon I. A Novel Design of Liquefied Natural Gas (LNG) Regasification Power Plant Integrated with Cryogenic Energy Storage System. Ind Eng Chem Res 2017;56:1288–96. https://doi.org/10.1021/acs.iecr.6b04157.

[96] Park J, Lee I, Yoon H, Kim J, Moon I. Application of Cryogenic Energy Storage to Liquefied Natural Gas Regasification Power Plant. Comput. Aided Chem. Eng., vol. 40, Elsevier B.V.; 2017, p. 2557–62. https://doi.org/10.1016/B978-0-444-63965-3.50428-1.

[97] Lee I, Park J, Moon I. Conceptual design and exergy analysis of combined cryogenic energy storage and LNG regasification processes: Cold and power integration. Energy 2017;140:106–15. https://doi.org/10.1016/j.energy.2017.08.054.

[98] Lee I, You F. Systems design and analysis of liquid air energy storage from liquefied natural gas cold energy. Appl Energy 2019;242:168–80. https://doi.org/10.1016/j.apenergy.2019.03.087.

[99] Lee I, Park J, You F, Moon I. A novel cryogenic energy storage system with LNG direct expansion regasification: Design, energy optimization, and exergy analysis. Energy 2019;173:691–705. https://doi.org/10.1016/j.energy.2019.02.047.

[100] Zhang T, Chen L, Zhang X, Mei S, Xue X, Zhou Y. Thermodynamic analysis of a novel hybrid liquid air energy storage system based on the utilization of LNG cold energy. Energy 2018;155:641–50. https://doi.org/10.1016/j.energy.2018.05.041.

[101] He T, Lv H, Shao Z, Zhang J, Xing X, Ma H. Cascade utilization of LNG cold energy by integrating cryogenic energy storage, organic Rankine cycle and direct cooling. Appl Energy 2020;277. https://doi.org/10.1016/j.apenergy.2020.115570.
[102] Qi M, Park J, Kim J, Lee I, Moon I. Advanced integration of LNG regasification power plant with liquid air energy storage: Enhancements in flexibility, safety, and power generation. Appl Energy 2020;269. https://doi.org/10.1016/j.apenergy.2020.115049.
[103] Peng X, She X, Li C, Luo Y, Zhang T, Li Y, et al. Liquid air energy storage flexibly coupled with LNG regasification for improving air liquefaction. Appl Energy 2019;250:1190–201. https://doi.org/10.1016/j.apenergy.2019.05.040.
[104] Park J, You F, Cho H, Lee I, Moon I. Novel massive thermal energy storage system for liquefied natural gas cold energy recovery. Energy 2020;195. https://doi.org/10.1016/j.energy.2020.117022.
[105] Zhang T, She X, Ding Y. A power plant for integrated waste energy recovery from liquid air energy storage and liquefied natural gas. Chinese J Chem Eng 2021. https://doi.org/10.1016/j.cjche.2021.02.008.
[106] She X, Zhang T, Cong L, Peng X, Li C, Luo Y, et al. Flexible integration of liquid air energy storage with liquefied natural gas regasification for power generation enhancement. Appl Energy n.d.;251. https://doi.org/10.1016/j.apenergy.2019.113355.
[107] Park J, Cho S, Qi M, Noh W, Lee I, Moon I. Liquid Air Energy Storage Coupled with Liquefied Natural Gas Cold Energy: Focus on Efficiency, Energy Capacity, and Flexibility. Energy 2020:119308. https://doi.org/10.1016/j.energy.2020.119308.
[108] Li Y, Wang X, Jin Y, Ding Y. An integrated solar-cryogen hybrid power system. Renew Energy 2012;37:76–81. https://doi.org/10.1016/j.renene.2011.05.038.
[109] Xu M, Zhao P, Huo Y, Han J, Wang J, Dai Y. Thermodynamic analysis of a novel liquid carbon dioxide energy storage system and comparison to a liquid air energy storage system. J Clean Prod 2020;242:118437. https://doi.org/10.1016/j.jclepro.2019.118437.
[110] Nabat MH, Soltani M, Razmi AR, Nathwani J, Dusseault MB. Investigation of a green energy storage system based on liquid air energy storage (LAES) and high-temperature concentrated solar power (CSP): Energy, exergy, economic, and environmental (4E) assessments, along with a case study for San Diego, US. Sustain Cities Soc 2021;75:103305. https://doi.org/10.1016/j.scs.2021.103305.
[111] Legrand M, Rodríguez-Antón LM, Martinez-Arevalo C, Gutiérrez-Martín F. Integration of liquid air energy storage into the spanish power grid. Energy 2019;187. https://doi.org/10.1016/j.energy.2019.115965.
[112] Legrand M, Labajo-Hurtado R, Rodríguez-Antón LM, Doce Y. Price arbitrage optimization of a photovoltaic power plant with liquid air energy storage. Implementation to the Spanish case. Energy 2022;239. https://doi.org/10.1016/j.energy.2021.121957.
[113] Ji W, Zhou Y, Sun Y, Zhang W, Pan CZ, Wang JJ. Thermodynamic characteristics of a novel wind-solar-liquid air energy storage system. IOP Conf. Ser. Mater. Sci. Eng., vol. 278, Institute of Physics Publishing; 2017, p. 012070. https://doi.org/10.1088/1757-899X/278/1/012070.
[114] Cetin TH, Kanoglu M, Bedir F. Integration of cryogenic energy storage and cryogenic organic cycle to geothermal power plants. Geothermics 2020;87:101830. https://doi.org/10.1016/j.geothermics.2020.101830.
[115] Damak C, Leducq D, Hoang HM, Negro D, Delahaye A. Liquid Air Energy Storage (LAES) as a large-scale storage technology for renewable energy integration – A review of investigation studies and near perspectives of LAES. Int J Refrig 2020;110:208–18. https://doi.org/10.1016/j.ijrefrig.2019.11.009.

[116] Wu S, Zhou C, Doroodchi E, Moghtaderi B. Techno-economic analysis of an integrated liquid air and thermochemical energy storage system 2020. https://doi.org/10.1016/j.enconman.2019.112341.
[117] Farres-Antunez P, Xue H, White AJ. Thermodynamic analysis and optimisation of a combined liquid air and pumped thermal energy storage cycle. J Energy Storage 2018;18:90–102. https://doi.org/10.1016/j.est.2018.04.016.
[118] Georgiou S, Shah N, Markides CN. A thermo-economic analysis and comparison of pumped-thermal and liquid-air electricity storage systems. Appl Energy 2018;226:1119–33. https://doi.org/10.1016/j.apenergy.2018.04.128.
[119] Kantharaj B, Garvey S, Pimm A. Compressed air energy storage with liquid air capacity extension. Appl Energy 2015;157:152–64. https://doi.org/10.1016/j.apenergy.2015.07.076.
[120] Pimm AJ, Garvey SD, Kantharaj B. Economic analysis of a hybrid energy storage system based on liquid air and compressed air. J Energy Storage 2015;4:24–35. https://doi.org/10.1016/j.est.2015.09.002.
[121] Geidl M, Andersson G. Integrated Modeling and Optimization of Multi-Carrier Energy Systems. Power Syst Lab 2007;Doctor of:143.
[122] Mancarella P. MES (multi-energy systems): An overview of concepts and evaluation models. Energy 2014;65:1–17. https://doi.org/10.1016/j.energy.2013.10.041.
[123] Cai YP, Huang GH, Tan Q, Yang ZF. Planning of community-scale renewable energy management systems in a mixed stochastic and fuzzy environment. Renew Energy 2009;34:1833–47. https://doi.org/10.1016/j.renene.2008.11.024.
[124] Schütz T, Hu X, Fuchs M, Müller D. Optimal design of decentralized energy conversion systems for smart microgrids using decomposition methods. Energy 2018;156:250–63. https://doi.org/10.1016/j.energy.2018.05.050.
[125] Rieder A, Christidis A, Tsatsaronis G. Multi criteria dynamic design optimization of a small scale distributed energy system. Energy 2014;74:230–9. https://doi.org/10.1016/j.energy.2014.06.007.
[126] Wouters C, Fraga ES, James AM. An energy integrated, multi-microgrid, MILP (mixed-integer linear programming) approach for residential distributed energy system planning - A South Australian case-study. Energy 2015;85:30–44. https://doi.org/10.1016/j.energy.2015.03.051.
[127] Thellufsen JZ, Lund H, Sorknæs P, Østergaard PA, Chang M, Drysdale D, et al. Smart energy cities in a 100% renewable energy context. Renew Sustain Energy Rev 2020;129. https://doi.org/10.1016/j.rser.2020.109922.
[128] Elliston B, MacGill I, Diesendorf M. Comparing least cost scenarios for 100% renewable electricity with low emission fossil fuel scenarios in the Australian National Electricity Market. Renew Energy 2014;66:196–204. https://doi.org/10.1016/j.renene.2013.12.010.
[129] Rodriguez RA, Becker S, Greiner M. Cost-optimal design of a simplified, highly renewable pan-European electricity system. Energy 2015;83:658–68. https://doi.org/10.1016/j.energy.2015.02.066.
[130] Pleßmann G, Erdmann M, Hlusiak M, Breyer C. Global energy storage demand for a 100% renewable electricity supply. Energy Procedia 2014;46:22–31. https://doi.org/10.1016/j.egypro.2014.01.154.
[131] McPherson M, Johnson N, Strubegger M. The role of electricity storage and hydrogen technologies in enabling global low-carbon energy transitions. Appl Energy 2018;216:649–61. https://doi.org/10.1016/j.apenergy.2018.02.110.
[132] Barton PI, Li X. Optimal design and operation of energy systems under uncertainty.

IFAC Proc Vol 2013;10:105–10. https://doi.org/10.3182/20131218-3-IN-2045.00038.
[133] Gan LK, Shek JKH, Mueller MA. Hybrid wind-photovoltaic-diesel-battery system sizing tool development using empirical approach, life-cycle cost and performance analysis: A case study in Scotland. Energy Convers Manag 2015;106:479–94. https://doi.org/10.1016/j.enconman.2015.09.029.
[134] Ogunjuyigbe ASO, Ayodele TR, Akinola OA. Optimal allocation and sizing of PV/Wind/Split-diesel/Battery hybrid energy system for minimizing life cycle cost, carbon emission and dump energy of remote residential building. Appl Energy 2016;171:153–71. https://doi.org/10.1016/j.apenergy.2016.03.051.
[135] Wang J, Lu Y, Yang Y, Mao T. Thermodynamic performance analysis and optimization of a solar-assisted combined cooling, heating and power system. Energy 2016;115:49–59. https://doi.org/10.1016/j.energy.2016.08.102.
[136] Khan MJ, Yadav AK, Mathew L. Techno economic feasibility analysis of different combinations of PV-Wind-Diesel-Battery hybrid system for telecommunication applications in different cities of Punjab, India. Renew Sustain Energy Rev 2017;76:577–607. https://doi.org/10.1016/j.rser.2017.03.076.
[137] Rubio-Maya C, Uche-Marcuello J, Martínez-Gracia A, Bayod-Rújula AA. Design optimization of a polygeneration plant fuelled by natural gas and renewable energy sources. Appl Energy 2011;88:449–57. https://doi.org/10.1016/j.apenergy.2010.07.009.
[138] Giannakoudis G, Papadopoulos AI, Seferlis P, Voutetakis S. Optimum design and operation under uncertainty of power systems using renewable energy sources and hydrogen storage. Int J Hydrogen Energy 2010;35:872–91. https://doi.org/10.1016/j.ijhydene.2009.11.044.
[139] Abedi S, Alimardani A, Gharehpetian GB, Riahy GH, Hosseinian SH. A comprehensive method for optimal power management and design of hybrid RES-based autonomous energy systems. Renew Sustain Energy Rev 2012;16:1577–87. https://doi.org/10.1016/j.rser.2011.11.030.
[140] Samsatli S, Staffell I, Samsatli NJ. Optimal design and operation of integrated wind-hydrogen-electricity networks for decarbonising the domestic transport sector in Great Britain. Int J Hydrogen Energy 2016;41:447–75. https://doi.org/10.1016/j.ijhydene.2015.10.032.
[141] Casisi M, Pinamonti P, Reini M. Optimal lay-out and operation of combined heat & power (CHP) distributed generation systems. Energy 2009;34:2175–83. https://doi.org/10.1016/j.energy.2008.10.019.
[142] Lund R, Mathiesen BV. Large combined heat and power plants in sustainable energy systems. Appl Energy 2015;142:389–95. https://doi.org/10.1016/j.apenergy.2015.01.013.
[143] Kavvadias KC, Tosios AP, Maroulis ZB. Design of a combined heating, cooling and power system: Sizing, operation strategy selection and parametric analysis. Energy Convers Manag 2010;51:833–45. https://doi.org/10.1016/j.enconman.2009.11.019.
[144] Li H, Nalim R, Haldi PA. Thermal-economic optimization of a distributed multi-generation energy system - A case study of Beijing. Appl Therm Eng 2006;26:709–19. https://doi.org/10.1016/j.applthermaleng.2005.09.005.
[145] Calise F, de Notaristefani di Vastogirardi G, Dentice d'Accadia M, Vicidomini M. Simulation of polygeneration systems. Energy 2018;163:290–337. https://doi.org/10.1016/j.energy.2018.08.052.
[146] Liu P, Gerogiorgis DI, Pistikopoulos EN. Modeling and optimization of polygeneration energy systems. Catal Today 2007;127:347–59. https://doi.org/10.1016/j.cattod.2007.05.024.

[147] Ahmadi P, Rosen MA, Dincer I. Multi-objective exergy-based optimization of a polygeneration energy system using an evolutionary algorithm. Energy 2012;46:21–31. https://doi.org/10.1016/j.energy.2012.02.005.
[148] Ghaem Sigarchian S, Malmquist A, Martin V. The choice of operating strategy for a complex polygeneration system: A case study for a residential building in Italy. Energy Convers Manag 2018;163:278–91. https://doi.org/10.1016/j.enconman.2018.02.066.
[149] Liu X, Mancarella P. Modelling, assessment and Sankey diagrams of integrated electricity-heat-gas networks in multi-vector district energy systems. Appl Energy 2016;167:336–52. https://doi.org/10.1016/j.apenergy.2015.08.089.
[150] Samsatli S, Samsatli NJ. A multi-objective MILP model for the design and operation of future integrated multi-vector energy networks capturing detailed spatio-temporal dependencies. Appl Energy 2018;220:893–920. https://doi.org/10.1016/j.apenergy.2017.09.055.
[151] Orehounig K, Evins R, Dorer V. Integration of decentralized energy systems in neighbourhoods using the energy hub approach. Appl Energy 2015;154:277–89. https://doi.org/10.1016/j.apenergy.2015.04.114.
[152] Maroufmashat A, Elkamel A, Fowler M, Sattari S, Roshandel R, Hajimiragha A, et al. Modeling and optimization of a network of energy hubs to improve economic and emission considerations. Energy 2015;93:2546–58. https://doi.org/10.1016/j.energy.2015.10.079.
[153] Stadler M, Marnay C, Kloess M, Cardoso G, Mendes G, Siddiqui A, et al. Optimal Planning and Operation of Smart Grids with Electric Vehicle Interconnection. J Energy Eng 2012;138:95–108. https://doi.org/10.1061/(asce)ey.1943-7897.0000070.
[154] Xie S, Wang X, Qu C, Wang X, Guo J. Impacts of different wind speed simulation methods on conditional reliability indices. Int Trans Electr Energy Syst 2013;20:1–6. https://doi.org/10.1002/etep.
[155] Mancarella P. Cogeneration systems with electric heat pumps: Energy-shifting properties and equivalent plant modelling. Energy Convers Manag 2009;50:1991–9. https://doi.org/10.1016/j.enconman.2009.04.010.
[156] Mancarella P, Chicco G. Real-time demand response from energy shifting in distributed multi-generation. IEEE Trans Smart Grid 2013;4:1928–38. https://doi.org/10.1109/TSG.2013.2258413.
[157] Samsatli S, Samsatli NJ. The role of renewable hydrogen and inter-seasonal storage in decarbonising heat – Comprehensive optimisation of future renewable energy value chains. Appl Energy 2019;233–234:854–93. https://doi.org/10.1016/j.apenergy.2018.09.159.
[158] Zakeri B, Syri S, Rinne S. Higher renewable energy integration into the existing energy system of Finland e Is there any maximum limit? Energy 2014;92:244–59. https://doi.org/10.1016/j.energy.2015.01.007.
[159] Ghenai C, Merabet A, Salameh T, Pigem EC. Grid-tied and stand-alone hybrid solar power system for desalination plant. Desalination 2018;435:172–80. https://doi.org/10.1016/j.desal.2017.10.044.
[160] Askarzadeh A, dos Santos Coelho L. A novel framework for optimization of a grid independent hybrid renewable energy system: A case study of Iran. Sol Energy 2015;112:383–96. https://doi.org/10.1016/j.solener.2014.12.013.
[161] Lagorse J, Simões MG, Miraoui A, Costerg P. Energy cost analysis of a solar-hydrogen hybrid energy system for stand-alone applications. Int J Hydrogen Energy 2008;33:2871–9. https://doi.org/10.1016/j.ijhydene.2008.03.054.
[162] Rosen J, Tietze-Stöckinger I, Rentz O. Model-based analysis of effects from large-scale

wind power production. Energy 2007;32:575–83. https://doi.org/10.1016/j.energy.2006.06.022.
[163] Sveinbjörnsson D, Ben Amer-Allam S, Hansen AB, Algren L, Pedersen AS. Energy supply modelling of a low-CO2 emitting energy system: Case study of a Danish municipality. Appl Energy 2017;195:922–41. https://doi.org/10.1016/j.apenergy.2017.03.086.
[164] Maleki A, Pourfayaz F. Optimal sizing of autonomous hybrid photovoltaic/wind/battery power system with LPSP technology by using evolutionary algorithms. Sol Energy 2015;115:471–83. https://doi.org/10.1016/j.solener.2015.03.004.
[165] Dong W, Li Y, Xiang J. Optimal sizing of a stand-alone hybrid power system based on battery/hydrogen with an improved ant colony optimization. Energies 2016;9. https://doi.org/10.3390/en9100785.
[166] Maleki A, Ameri M, Keynia F. Scrutiny of multifarious particle swarm optimization for finding the optimal size of a PV/wind/battery hybrid system. Renew Energy 2015;80:552–63. https://doi.org/10.1016/j.renene.2015.02.045.
[167] Sharafi M, ElMekkawy TY. A dynamic MOPSO algorithm for multiobjective optimal design of hybrid renewable energy systems. Int J Energy Res 2014;38:1949–63. https://doi.org/https://doi.org/10.1002/er.3202.
[168] Urbanucci L. Limits and potentials of Mixed Integer Linear Programming methods for optimization of polygeneration energy systems. Energy Procedia 2018;148:1199–205. https://doi.org/10.1016/j.egypro.2018.08.021.
[169] Yokoyama R, Shinano Y, Taniguchi S, Ohkura M, Wakui T. Optimization of energy supply systems by MILP branch and bound method in consideration of hierarchical relationship between design and operation. Energy Convers Manag 2015;92:92–104. https://doi.org/10.1016/j.enconman.2014.12.020.
[170] Yang Y, Zhang S, Xiao Y. An MILP (mixed integer linear programming) model for optimal design of district-scale distributed energy resource systems. Energy 2015;90:1901–15. https://doi.org/10.1016/j.energy.2015.07.013.
[171] Weber C, Shah N. Optimisation based design of a district energy system for an eco-town in the United Kingdom. Energy 2011;36:1292–308. https://doi.org/10.1016/j.energy.2010.11.014.
[172] Arcuri P, Florio G, Fragiacomo P. A mixed integer programming model for optimal design of trigeneration in a hospital complex. Energy 2007;32:1430–47. https://doi.org/10.1016/j.energy.2006.10.023.
[173] Bischi A, Taccari L, Martelli E, Amaldi E, Manzolini G, Silva P, et al. A detailed MILP optimization model for combined cooling, heat and power system operation planning. Energy 2014;74:12–26. https://doi.org/10.1016/j.energy.2014.02.042.
[174] Deetjen TA, Vitter JS, Reimers AS, Webber ME. Optimal dispatch and equipment sizing of a residential central utility plant for improving rooftop solar integration. Energy 2018;147:1044–59. https://doi.org/10.1016/j.energy.2018.01.110.
[175] Tu T, Rajarathnam GP, Vassallo AM. Optimization of a stand-alone photovoltaic–wind–diesel–battery system with multi-layered demand scheduling. Renew Energy 2019;131:333–47. https://doi.org/10.1016/j.renene.2018.07.029.
[176] Zhou Z, Liu P, Li Z, Pistikopoulos EN, Georgiadis MC. Impacts of equipment off-design characteristics on the optimal design and operation of combined cooling, heating and power systems. Comput Chem Eng 2013;48:40–7. https://doi.org/10.1016/j.compchemeng.2012.08.007.
[177] Liu X, Yan Z, Wu J. Optimal coordinated operation of a multi-energy community considering interactions between energy storage and conversion devices. Appl Energy

2019;248:256–73. https://doi.org/10.1016/j.apenergy.2019.04.106.
[178] Pina EA, Lozano MA, Serra LM. Optimal design of polygeneration systems supported with renewable energy sources and energy storage for a Brazilian hospital. ECOS 2018 - Proc 31st Int Conf Effic Cost, Optim Simul Environ Impact Energy Syst 2018.
[179] Carvalho M, Lozano MA, Serra LM. Multicriteria synthesis of trigeneration systems considering economic and environmental aspects. Appl Energy 2012;91:245–54. https://doi.org/10.1016/j.apenergy.2011.09.029.
[180] Wang J, Zhai ZJ, Jing Y, Zhang C. Optimization design of BCHP system to maximize to save energy and reduce environmental impact. Energy 2010;35:3388–98. https://doi.org/10.1016/j.energy.2010.04.029.
[181] Sawle Y, Gupta SC, Bohre AK. Socio-techno-economic design of hybrid renewable energy system using optimization techniques. Renew Energy 2018;119:459–72. https://doi.org/10.1016/j.renene.2017.11.058.
[182] Dufo-López R, Cristóbal-Monreal IR, Yusta JM. Optimisation of PV-wind-diesel-battery stand-alone systems to minimise cost and maximise human development index and job creation. Renew Energy 2016;94:280–93. https://doi.org/10.1016/j.renene.2016.03.065.
[183] Macedo LH, Franco JF, Romero R, Rider MJ. An MILP model for the analysis of operation of energy storage devices in distribution systems. 2016 IEEE PES Transm Distrib Conf Expo Am PES T D-LA 2016 2017:1–6. https://doi.org/10.1109/TDC-LA.2016.7805610.
[184] Djelailia O, Kelaiaia MS, Labar H, Necaibia S, Merad F. Energy hybridization photovoltaic/diesel generator/pump storage hydroelectric management based on online optimal fuel consumption per kWh. Sustain Cities Soc 2019;44:1–15. https://doi.org/10.1016/j.scs.2018.09.037.
[185] Li B, Roche R, Miraoui A. Microgrid sizing with combined evolutionary algorithm and MILP unit commitment. Appl Energy 2017;188:547–62. https://doi.org/10.1016/j.apenergy.2016.12.038.
[186] Li B, Roche R, Paire D, Miraoui A. Sizing of a stand-alone microgrid considering electric power, cooling/heating, hydrogen loads and hydrogen storage degradation. Appl Energy 2017;205:1244–59. https://doi.org/10.1016/j.apenergy.2017.08.142.
[187] Martínez Ceseña EA, Good N, Syrri ALA, Mancarella P. Techno-economic and business case assessment of multi-energy microgrids with co-optimization of energy, reserve and reliability services. Appl Energy 2018;210:896–913. https://doi.org/10.1016/j.apenergy.2017.08.131.
[188] Quashie M, Marnay C, Bouffard F, Joós G. Optimal planning of microgrid power and operating reserve capacity. Appl Energy 2018;210:1229–36. https://doi.org/10.1016/j.apenergy.2017.08.015.
[189] Khan ASM, Verzijlbergh RA, Sakinci OC, De Vries LJ. How do demand response and electrical energy storage affect (the need for) a capacity market? Appl Energy 2018;214:39–62. https://doi.org/10.1016/j.apenergy.2018.01.057.
[190] Akhavan-Hejazi H, Mohsenian-Rad H. Optimal operation of independent storage systems in energy and reserve markets with high wind penetration. IEEE Trans Smart Grid 2014;5:1088–97. https://doi.org/10.1109/TSG.2013.2273800.
[191] Byrne RH, Silva-Monroy CA. Estimating the Maximum Potential Revenue for Grid Connected Electricity Storage: Arbitrage and Regulation. Sand2012-3863 2012:64.
[192] Pudjianto D, Aunedi M, Djapic P, Strbac G. Whole-systems assessment of the value of energy storage in low-carbon electricity systems. IEEE Trans Smart Grid 2014;5:1098–109. https://doi.org/10.1109/TSG.2013.2282039.

[193] Moreno R, Moreira R, Strbac G. A MILP model for optimising multi-service portfolios of distributed energy storage. Appl Energy 2015;137:554–66. https://doi.org/10.1016/j.apenergy.2014.08.080.
[194] de Sisternes FJ, Jenkins JD, Botterud A. The value of energy storage in decarbonizing the electricity sector. Appl Energy 2016;175:368–79. https://doi.org/10.1016/j.apenergy.2016.05.014.
[195] Gabrielli P, Gazzani M, Martelli E, Mazzotti M. Optimal design of multi-energy systems with seasonal storage. Appl Energy 2018;219:408–24. https://doi.org/10.1016/j.apenergy.2017.07.142.
[196] Lee I, Park J, Moon I. Conceptual design and exergy analysis of combined cryogenic energy storage and LNG regasification processes: Cold and power integration. Energy 2017;140:106–15. https://doi.org/10.1016/j.energy.2017.08.054.
[197] Tafone A, Romagnoli A, Borri E, Comodi G. New parametric performance maps for a novel sizing and selection methodology of a Liquid Air Energy Storage system. Appl Energy 2019;250:1641–56. https://doi.org/10.1016/j.apenergy.2019.04.171.
[198] Cui S, Song J, Wang T, Liu Y, He Q, Liu W. Thermodynamic analysis and efficiency assessment of a novel multi-generation liquid air energy storage system. Energy 2021;235:121322. https://doi.org/10.1016/j.energy.2021.121322.
[199] Li Y, Wang X, Jin Y, Ding Y. An integrated solar-cryogen hybrid power system. Renew Energy 2012;37:76–81. https://doi.org/10.1016/j.renene.2011.05.038.
[200] Khani H, Dadash Zadeh MR. Real-time optimal dispatch and economic viability of cryogenic energy storage exploiting arbitrage opportunities in an electricity market. IEEE Trans Smart Grid 2015;6:391–401. https://doi.org/10.1109/TSG.2014.2357253.
[201] Pimm AJ, Garvey SD, Kantharaj B. Economic analysis of a hybrid energy storage system based on liquid air and compressed air. J Energy Storage 2015;4:24–35. https://doi.org/10.1016/j.est.2015.09.002.
[202] Morgan R, Nelmes S, Gibson E, Brett G. Liquid air energy storage - Analysis and first results from a pilot scale demonstration plant. Appl Energy 2015;137:845–53. https://doi.org/10.1016/j.apenergy.2014.07.109.
[203] Morgan R, Nelmes S, Gibson E, Brett G. An analysis of a large-scale liquid air energy storage system. Proc Inst Civ Eng Energy 2015;168:135–44. https://doi.org/10.1680/ener.14.00038.
[204] Peng X, She X, Cong L, Zhang T, Li C, Li Y, et al. Thermodynamic study on the effect of cold and heat recovery on performance of liquid air energy storage. Appl Energy 2018;221:86–99. https://doi.org/10.1016/j.apenergy.2018.03.151.
[205] Hamdy S, Morosuk T, Tsatsaronis G. Exergetic and economic assessment of integrated cryogenic energy storage systems. Cryogenics (Guildf) 2019;99:39–50. https://doi.org/10.1016/j.cryogenics.2019.02.009.
[206] Wang C, Zhang X, You Z, Zhang M, Huang S, She X. The effect of air purification on liquid air energy storage – An analysis from molecular to systematic modelling. Appl Energy 2021;300:117349. https://doi.org/10.1016/j.apenergy.2021.117349.
[207] Ghasemkhani A, Farahat S, Naserian MM. Multi-objective optimization and decision making of endoreversible combined cycles with consideration of different heat exchangers by finite time thermodynamics. Energy Convers Manag 2018;171:1052–62. https://doi.org/10.1016/j.enconman.2018.06.046.
[208] Punnathanam V, Kotecha P. Multi-objective optimization of Stirling engine systems using Front-based Yin-Yang-Pair Optimization. Energy Convers Manag 2017;133:332–48. https://doi.org/10.1016/j.enconman.2016.10.035.
[209] Al Jubori AM, Al-Dadah R, Mahmoud S. Performance enhancement of a small-scale

organic Rankine cycle radial-inflow turbine through multi-objective optimization algorithm. Energy 2017;131:297–311. https://doi.org/10.1016/j.energy.2017.05.022.
[210] Morandin M, Mercangöz M, Hemrle J, Maréchal F, Favrat D. Thermoeconomic design optimization of a thermo-electric energy storage system based on transcritical CO2 cycles. Energy 2013;58:571–87. https://doi.org/10.1016/j.energy.2013.05.038.
[211] Berhane HG, Gonzalo GG, Laureano J, Dieter B. Design of environmentally conscious absorption cooling systems via multi-objective optimization and life cycle assessment. Appl Energy 2009;86:1712–22. https://doi.org/10.1016/j.apenergy.2008.11.019.
[212] She X, Peng X, Nie B, Leng G, Zhang X, Weng L, et al. Enhancement of round trip efficiency of liquid air energy storage through effective utilization of heat of compression. Appl Energy 2017;206:1632–42. https://doi.org/10.1016/j.apenergy.2017.09.102.
[213] Hatcher P, Khalilpour R, Abbas A. Optimisation of LNG mixed-refrigerant processes considering operation and design objectives. Comput Chem Eng 2012;41:123–33. https://doi.org/10.1016/j.compchemeng.2012.03.005.
[214] Antúnez PF. Modelling and development of thermo-mechanical energy storage. University of Cambridge, 2018.
[215] Le VL, Kheiri A, Feidt M, Pelloux-Prayer S. Thermodynamic and economic optimizations of a waste heat to power plant driven by a subcritical ORC (Organic Rankine Cycle) using pure or zeotropic working fluid. Energy 2014;78:622–38. https://doi.org/10.1016/j.energy.2014.10.051.
[216] Loh HP, Lyons J, White CW. Process equipment cost estimation. Natl Energy Technol Cent 2002:74.
[217] Vecchi A, Li Y, Ding Y, Mancarella P, Sciacovelli A. Liquid air energy storage (LAES): A review on technology state-of-the-art, integration pathways and future perspectives. Adv Appl Energy 2021;3:100047. https://doi.org/10.1016/j.adapen.2021.100047.
[218] Al-Dujaili A, Suresh S. A MATLAB toolbox for surrogate-assisted multi-objective optimization: A preliminary study. GECCO 2016 Companion - Proc 2016 Genet Evol Comput Conf 2016:1209–16. https://doi.org/10.1145/2908961.2931703.
[219] Bradford E, Schweidtmann AM, Lapkin A. Efficient multiobjective optimization employing Gaussian processes, spectral sampling and a genetic algorithm. J Glob Optim 2018;71:407–38. https://doi.org/10.1007/s10898-018-0609-2.
[220] Garg A, Liu C, Jishnu AK, Gao L, Le Phung ML, Tran VM. A Thompson Sampling Efficient Multi-Objective Optimization Algorithm (TSEMO) for Lithium-Ion Battery Liquid-Cooled Thermal Management System: Study of Hydrodynamic, Thermodynamic, and Structural Performance. J Electrochem Energy Convers Storage 2021;18:1–13. https://doi.org/10.1115/1.4048537.
[221] Vecchi A, Li Y, Mancarella P, Sciacovelli A. Integrated techno-economic assessment of Liquid Air Energy Storage (LAES) under off-design conditions: Links between provision of market services and thermodynamic performance. Appl Energy 2020;262. https://doi.org/10.1016/j.apenergy.2020.114589.
[222] Wang C, Akkurt N, Zhang X, Luo Y, She X. Techno-economic analyses of multi-functional liquid air energy storage for power generation, oxygen production and heating. Appl Energy 2020;275. https://doi.org/10.1016/j.apenergy.2020.115392.
[223] Guo L, Ji W, Gao Z, Fan X, Wang J. Dynamic characteristics analysis of the cold energy transfer in the liquid air energy storage system based on different modes of packed bed. J Energy Storage 2021;40:102712. https://doi.org/10.1016/j.est.2021.102712.
[224] Wang C, Bian Y, You Z, Luo Y, Zhang X, Peng H, et al. Dynamic analysis of a novel standalone liquid air energy storage system for industrial applications. Energy Convers

Manag 2021;245:114537. https://doi.org/10.1016/j.enconman.2021.114537.
[225] Guo H, Xu Y, Zhang X, Liang Q, Wang S, Chen H. Dynamic characteristics and control of supercritical compressed air energy storage systems. Appl Energy 2021;283:116294. https://doi.org/10.1016/j.apenergy.2020.116294.
[226] Cui S, He Q, Shi X, Liu Y, Du D. Dynamic characteristics analysis for energy release process of liquid air energy storage system. Renew Energy 2021;180:744–55. https://doi.org/10.1016/j.renene.2021.08.115.
[227] Cui S, Lu C, Shi X, Du D, He Q, Liu W. Numerical investigation of dynamic characteristics for expansion power generation system of liquefied air energy storage. Energy 2021;226:120372. https://doi.org/10.1016/j.energy.2021.120372.
[228] Lu C, He Q, Cui S, Shi X, Du D, Liu W. Evaluation of operation safety of energy release process of liquefied air energy storage system. Energy 2021;235:121403. https://doi.org/10.1016/j.energy.2021.121403.
[229] Tackett HH, Cripe JA, Dyson G. Positive displacement reciprocating pump fundamentals- power and direct acting types. Proc Twenty-Fourth Int Pump User Symp 2008:45–58.
[230] Johnston DN. Numerical Modelling of Reciprocating Pumps with Self-Acting Valves. Proc Inst Mech Eng Part I J Syst Control Eng 1991;205:87–96. https://doi.org/10.1243/pime_proc_1991_205_318_02.
[231] Sharma V. Reynolds Transport Theorem. Multiph Flow Fluid 1994:423–7. https://doi.org/10.1016/b978-0-08-051226-6.50022-4.
[232] Lee JK, Kim TY, Kim HS, Chai JB, Lee JW. Estimation of Probability Density Functions of Damage Parameter for Valve Leakage Detection in Reciprocating Pump Used in Nuclear Power Plants. Nucl Eng Technol 2016;48:1280–90. https://doi.org/10.1016/j.net.2016.04.007.
[233] Li M, Foss R, Stelson KA, Van De Ven JD, Barth EJ. Design, Dynamic Modeling, and Experimental Validation of A Novel Alternating Flow Variable Displacement Hydraulic Pump. IEEE/ASME Trans Mechatronics 2019;24:1294–305. https://doi.org/10.1109/TMECH.2019.2906859.
[234] Huang ZF. Transient Modelling of a Positive Displacement Pump for Advanced Power Cycle Applications 2017.
[235] BPMA, Gambica. Variable Speed Driven Pumps - Best Practical Guide. 2009.
[236] Zhang N, Cai R. Analytical solutions and typical characteristics of part-load performances of single shaft gas turbine and its cogeneration. Energy Convers Manag 2002;43:1323–37. https://doi.org/10.1016/S0196-8904(02)00018-3.
[237] Na Zhang RC. Analytical solutions and typical characteristics of part-load performances of single shaft gas turbine and its cogeneration. Energy Convers Manag 2002;43:1323–1337.
[238] Luo X, Dooner M, He W, Wang J, Li Y, Li D, et al. Feasibility study of a simulation software tool development for dynamic modelling and transient control of adiabatic compressed air energy storage with its electrical power system applications. Appl Energy 2018;228:1198–219. https://doi.org/10.1016/j.apenergy.2018.06.068.
[239] He W, Wang J, Ding Y. New radial turbine dynamic modelling in a low-temperature adiabatic compressed air energy storage system discharging process. Energy Convers Manag 2017;153:144–56. https://doi.org/10.1016/j.enconman.2017.09.059.
[240] Zhu B, Xu J, Yan C, Xie J. The general supercritical heat transfer correlation for vertical up-flow tubes: K number correlation. Int J Heat Mass Transf 2020;148. https://doi.org/10.1016/j.ijheatmasstransfer.2019.119080.
[241] Li Y, Miao S, Luo X, Yin B, Han J, Wang J. Dynamic modelling and techno-economic

analysis of adiabatic compressed air energy storage for emergency back-up power in supporting microgrid. Appl Energy 2020;261:114448. https://doi.org/10.1016/j.apenergy.2019.114448.
[242] He W, Wang J, Wang Y, Ding Y, Chen H, Wu Y, et al. Study of cycle-to-cycle dynamic characteristics of adiabatic Compressed Air Energy Storage using packed bed Thermal Energy Storage. Energy 2017;141:2120–34. https://doi.org/10.1016/j.energy.2017.11.016.
[243] Kim CK, Lee SM, Jang CM. Performance analysis of a ball valve used for gas pipelines by introducing nondimensional parameters. Adv Mech Eng 2019;11:1–10. https://doi.org/10.1177/1687814018823350.
[244] Sciacovelli A, Smith D, Navarro H, Li Y, Ding Y. Liquid air energy storage – Operation and performance of the first pilot plant in the world. ECOS 2016 - Proc 29th Int Conf Effic Cost, Optimisation, Simul Environ Impact Energy Syst 2016.
[245] Zeiler A, Faltermeier R, Keck IR, Tomé AM, Puntonet CG, Lang EW. Empirical mode decomposition - An introduction. Proc Int Jt Conf Neural Networks 2010;1. https://doi.org/10.1109/IJCNN.2010.5596829.
[246] Doenges K, Egido I, Sigrist L, Lobato Miguelez E, Rouco L. Improving AGC Performance in Power Systems with Regulation Response Accuracy Margins Using Battery Energy Storage System (BESS). IEEE Trans Power Syst 2020;35:2816–25. https://doi.org/10.1109/TPWRS.2019.2960450.
[247] Zakeri B, Syri S. Electrical energy storage systems: A comparative life cycle cost analysis. Renew Sustain Energy Rev 2015;42:569–96. https://doi.org/10.1016/j.rser.2014.10.011.
[248] Mauler L, Duffner F, Zeier WG, Leker J. Battery cost forecasting: A review of methods and results with an outlook to 2050. Energy Environ Sci 2021;14:4712–39. https://doi.org/10.1039/d1ee01530c.
[249] Vecchi A, Naughton J, Li Y, Mancarella P, Sciacovelli A. Multi-mode operation of a Liquid Air Energy Storage (LAES) plant providing energy arbitrage and reserve services – Analysis of optimal scheduling and sizing through MILP modelling with integrated thermodynamic performance. Energy 2020;200:117500. https://doi.org/10.1016/j.energy.2020.117500.
[250] Rodrigues EMG, Fernandes CAS, Godina R, Bizuayehu AW, Catalao JPS. NaS battery storage system modeling and sizing for extending wind farms performance in Crete. 2014 Australas Univ Power Eng Conf AUPEC 2014 - Proc 2014:1–6. https://doi.org/10.1109/AUPEC.2014.6966547.
[251] Cole W, Frazier AW, Augistine C. Cost Projections for Utility-Scale Battery Storage: 2021 Update. Natl Renew Energy Lab 2021:21.
[252] AL Shaqsi AZ, Sopian K, Al-Hinai A. Review of energy storage services, applications, limitations, and benefits. Energy Reports 2020;6:288–306. https://doi.org/10.1016/j.egyr.2020.07.028.
[253] Met Office. UK Climate Projections: Headline Findings 2021:1–12.
[254] Good N, Martínez Ceseña EA, Zhang L, Mancarella P. Techno-economic and business case assessment of low carbon technologies in distributed multi-energy systems. Appl Energy 2016;167:158–72. https://doi.org/10.1016/j.apenergy.2015.09.089.
[255] Ayele GT, Mabrouk MT, Haurant P, Laumert B, Lacarrière B. Optimal placement and sizing of heat pumps and heat only boilers in a coupled electricity and heating networks. Energy 2019;182:122–34. https://doi.org/10.1016/j.energy.2019.06.018.
[256] Buonomano A, Calise F, Ferruzzi G, Vanoli L. A novel renewable polygeneration system for hospital buildings: Design, simulation and thermo-economic optimization.

Appl Therm Eng 2014;67:43–60. https://doi.org/10.1016/j.applthermaleng.2014.03.008.
[257] Mokhtara C, Negrou B, Bouferrouk A, Yao Y, Settou N, Ramadan M. Integrated supply–demand energy management for optimal design of off-grid hybrid renewable energy systems for residential electrification in arid climates. Energy Convers Manag 2020;221:113192. https://doi.org/10.1016/j.enconman.2020.113192.
[258] Lian J, Zhang Y, Ma C, Yang Y, Chaima E. A review on recent sizing methodologies of hybrid renewable energy systems. Energy Convers Manag 2019;199:112027. https://doi.org/10.1016/j.enconman.2019.112027.
[259] de Bosio F, Verda V. Thermoeconomic analysis of a Compressed Air Energy Storage (CAES) system integrated with a wind power plant in the framework of the IPEX Market. Appl Energy 2015;152:173–82. https://doi.org/10.1016/j.apenergy.2015.01.052.
[260] Martínez Ceseña EA, Good N, Syrri ALA, Mancarella P. Techno-economic and business case assessment of multi-energy microgrids with co-optimization of energy, reserve and reliability services. Appl Energy 2018;210:896–913. https://doi.org/10.1016/j.apenergy.2017.08.131.
[261] Nabat MH, Zeynalian M, Razmi AR, Arabkoohsar A, Soltani M. Energy, exergy, and economic analyses of an innovative energy storage system; liquid air energy storage (LAES) combined with high-temperature thermal energy storage (HTES). Energy Convers Manag 2020;226:113486. https://doi.org/10.1016/j.enconman.2020.113486.
[262] Mazzoni S, Ooi S, Tafone A, Borri E, Comodi G, Romagnoli A. Liquid Air Energy Storage as a polygeneration system to solve the unit commitment and economic dispatch problems in micro-grids applications. Energy Procedia 2019;158:5026–33. https://doi.org/10.1016/j.egypro.2019.01.660.
[263] Luo X, Wang J, Wojcik JD, Wang J, Li D, Draganescu M, et al. Review of voltage and frequency grid code specifications for electrical energy storage applications. Energies 2018;11. https://doi.org/10.3390/en11051070.
[264] Ghaem Sigarchian S, Malmquist A, Martin V. Design Optimization of a Small-Scale Polygeneration Energy System in Different Climate Zones in Iran. Energies 2018;11. https://doi.org/10.3390/en11051115.
[265] Blanco H, Faaij A. A review at the role of storage in energy systems with a focus on Power to Gas and long-term storage. Renew Sustain Energy Rev 2018;81:1049–86. https://doi.org/10.1016/j.rser.2017.07.062.
[266] Annex M. BEIS 2018 Updated Energy & Emissions Projections: Growth assumptions and prices 2018. https://assets.publishing.service.gov.uk/government/uploads/system/uploads/attachment_data/file/802478/Annex-m-price-growth-assumption_16-May-2019.ods.
[267] Aram A. Microgrid Market in the USA. Hitachi Rev 2017;66:454–5.
[268] Giraldez J, Flores-espino F, Macalpine S, Asmus P. Phase I microgrid cost study: data collection and analysis of microgrid costs in the United States. Golden, CO Natl Renew Energy Lab 2018:1–63.
[269] Hansen K, Breyer C, Lund H. Status and perspectives on 100% renewable energy systems. Energy 2019;175:471–80. https://doi.org/10.1016/j.energy.2019.03.092.
[270] Diesendorf M, Elliston B. The feasibility of 100% renewable electricity systems: A response to critics. Renew Sustain Energy Rev 2018;93:318–30. https://doi.org/10.1016/j.rser.2018.05.042.
[271] Guerra OJ, Eichman J, Denholm P. Optimal energy storage portfolio for high and ultrahigh carbon-free and renewable power systems. Energy Environ Sci 2021;14:5132–46. https://doi.org/10.1039/d1ee01835c.
[272] Budischak C, Sewell D, Thomson H, MacH L, Veron DE, Kempton W. Cost-minimized

combinations of wind power, solar power and electrochemical storage, powering the grid up to 99.9% of the time. J Power Sources 2013;225:60–74. https://doi.org/10.1016/j.jpowsour.2012.09.054.
[273] Mathiesen BV, Lund H, Karlsson K. 100% Renewable energy systems, climate mitigation and economic growth. Appl Energy 2011;88:488–501. https://doi.org/10.1016/j.apenergy.2010.03.001.
[274] Lenzen M, McBain B, Trainer T, Jütte S, Rey-Lescure O, Huang J. Simulating low-carbon electricity supply for Australia. Appl Energy 2016;179:553–64. https://doi.org/10.1016/j.apenergy.2016.06.151.
[275] Lu B, Blakers A, Stocks M. 90–100% renewable electricity for the South West Interconnected System of Western Australia. Energy 2017;122:663–74. https://doi.org/10.1016/j.energy.2017.01.077.
[276] Brown T, Schlachtberger D, Kies A, Schramm S, Greiner M. Synergies of sector coupling and transmission reinforcement in a cost-optimised, highly renewable European energy system. Energy 2018;160:720–39. https://doi.org/10.1016/j.energy.2018.06.222.
[277] Child M, Kemfert C, Bogdanov D, Breyer C. Flexible electricity generation, grid exchange and storage for the transition to a 100% renewable energy system in Europe. Renew Energy 2019;139:80–101. https://doi.org/10.1016/j.renene.2019.02.077.
[278] Zappa W, Junginger M, van den Broek M. Is a 100% renewable European power system feasible by 2050? Appl Energy 2019;233–234:1027–50. https://doi.org/10.1016/j.apenergy.2018.08.109.
[279] Maruf MNI. Open model-based analysis of a 100% renewable and sector-coupled energy system–The case of Germany in 2050. Appl Energy 2021;288:116618. https://doi.org/10.1016/j.apenergy.2021.116618.
[280] Bogdanov D, Breyer C. North-East Asian Super Grid for 100% renewable energy supply: Optimal mix of energy technologies for electricity, gas and heat supply options. Energy Convers Manag 2016;112:176–90. https://doi.org/10.1016/j.enconman.2016.01.019.
[281] Yue X, Patankar N, Decarolis J, Chiodi A, Rogan F, Deane JP, et al. Least cost energy system pathways towards 100% renewable energy in Ireland by 2050. Energy 2020;207:118264. https://doi.org/10.1016/j.energy.2020.118264.
[282] Ullah K, Hafeez G, Khan I, Jan S, Javaid N. A multi-objective energy optimization in smart grid with high penetration of renewable energy sources. Appl Energy 2021;299:117104. https://doi.org/10.1016/j.apenergy.2021.117104.
[283] Haas J, Cebulla F, Cao K, Nowak W, Palma-Behnke R, Rahmann C, et al. Challenges and trends of energy storage expansion planning for flexibility provision in low-carbon power systems – a review. Renew Sustain Energy Rev 2017;80:603–19. https://doi.org/10.1016/j.rser.2017.05.201.
[284] Blakers A, Lu B, Stocks M. 100% renewable electricity in Australia. Energy 2017;133:471–82. https://doi.org/10.1016/j.energy.2017.05.168.
[285] Child M, Breyer C. The Role of Energy Storage Solutions in a 100% Renewable Finnish Energy System. Energy Procedia 2016;99:25–34. https://doi.org/10.1016/j.egypro.2016.10.094.
[286] Cebulla F, Naegler T, Pohl M. Electrical energy storage in highly renewable European energy systems: Capacity requirements, spatial distribution, and storage dispatch. J Energy Storage 2017;14:211–23. https://doi.org/10.1016/j.est.2017.10.004.
[287] Haas J, Cebulla F, Nowak W, Rahmann C, Palma-Behnke R. A multi-service approach for planning the optimal mix of energy storage technologies in a fully-renewable power supply. Energy Convers Manag 2018;178:355–68.

https://doi.org/10.1016/j.enconman.2018.09.087.
[288] Ogland-Hand JD, Bielicki JM, Wang Y, Adams BM, Buscheck TA, Saar MO. The value of bulk energy storage for reducing CO2 emissions and water requirements from regional electricity systems. Energy Convers Manag 2019;181:674–85. https://doi.org/10.1016/j.enconman.2018.12.019.
[289] Denholm P, Mai T. Timescales of energy storage needed for reducing renewable energy curtailment. Renew Energy 2019;130:388–99. https://doi.org/10.1016/j.renene.2018.06.079.
[290] Jafari M, Korpås M, Botterud A. Power system decarbonization: Impacts of energy storage duration and interannual renewables variability. Renew Energy 2020;156:1171–85. https://doi.org/10.1016/j.renene.2020.04.144.
[291] Mao J, Jafari M, Botterud A. Planning Low-carbon Distributed Power Systems: Evaluating the Role of Energy Storage. Energy 2020;238:121668. https://doi.org/10.1016/j.energy.2021.121668.
[292] Østergaard PA. Comparing electricity, heat and biogas storages' impacts on renewable energy integration. Energy 2012;37:255–62. https://doi.org/10.1016/j.energy.2011.11.039.
[293] Quarton CJ, Samsatli S. Resource and technology data for spatio-temporal value chain modelling of the Great Britain energy system. Data Br 2020;31:105886. https://doi.org/10.1016/j.dib.2020.105886.
[294] Papavasiliou A, Oren SS, O'Neill RP. Reserve Requirements for Wind Power Integration: A Scenario-Based Stochastic Programming Framework. IEEE Trans Power Syst 2011;26:2197–206. https://doi.org/10.1109/tpwrs.2011.2121095.
[295] Innovate UK. UK Transport Vision 2050 2021.
[296] National Grid. Future Energy Scenarios Navigation 2020:1–124.
[297] Sansom R, Robert. Decarbonising low grade heat for low carbon future. PhD Thesis 2015.
[298] Samsatli S, Samsatli NJ. The role of renewable hydrogen and inter-seasonal storage in decarbonising heat – Comprehensive optimisation of future renewable energy value chains. Appl Energy 2019;233–234:854–93. https://doi.org/10.1016/j.apenergy.2018.09.159.
[299] Stefan Pfenninger; Iain Staffell. renewables.ninja n.d.
[300] Poncelet K, Hoschle H, Delarue E, Virag A, Drhaeseleer W. Selecting representative days for capturing the implications of integrating intermittent renewables in generation expansion planning problems. IEEE Trans Power Syst 2017;32:1936–48. https://doi.org/10.1109/TPWRS.2016.2596803.
[301] Thomas L. Baldwin and SAL. Power Systems Power Systems 2013;40:1183–90.
[302] GOV.UK. Power Stations in the United Kingdom 2020.
[303] Jafari M, Delmastro C, Grosso D, Bompard E, Botterud A. Electrify Italy : The Role of Renewable Energy. Appl Energy Symp MIT A+B 2019.
[304] HM Government. Energy White Paper: Powering our Net Zero Future. vol. 44. 2020.
[305] Care W, Future B. CHP-Technology for green produced hydrogen as fuel 2021.
[306] National Grid ESO. Heat decarbonisation modelling - Impact of our new Regional Heat model for FES 2021 2021:1–3.
[307] Department for Business Energy & Industical Strategy. Experimental statistics on heat networks 2018:80–5.
[308] Rawlins J, Ashcroft M. Small-scale Concentrated Solar Power - A review of current activity and potential to accelerate deployment. Carbon Trust 2013:50.

[309] Park N. Population estimates for the UK. Off Natl Stat 2019.
[310] Capros P. Energy, transport and GHG emissions Trends to 2050. 2016. https://doi.org/10.2833/9127.
[311] International Energy Agency. The Future of Hydrogen: Seizing today's opportunities. IEA Publ 2019:203.
[312] Gahan L, East J, Baker M, Provins A. Heating our homes in a Net Zero Future: Understanding what matters to consumers Study team The Future of Heat 2020;44.
[313] Ofgem. The Decarbonisation of Heat. Ofgem's Futur Insights Ser 2016:3–4.
[314] Norris R. UK Battery Storage Project Database Report. 2022.
[315] Ltd DE& E. Evidence Gathering: Thermal Energy Storage (TES) Technologies. Dep Business, Energy Ind Strateg 2016.
[316] Mongird K, Viswanathan V, Alam J, Vartanian C, Sprenkle V, Baxter R. 2020 Grid Energy Storage Technology Cost and Performance Assessment. US Dep Energy 2020:1–20.
[317] ARPA-E. Duration Addition to electricitY Storage (DAYS) Overview. Dep Energy 2018:1–12.
[318] Department for Business, Energy & Industrial Strategy U. Hydrogen production costs by production source 2021.
[319] Jenkins J, Sepulveda N. Enhanced Decision Support for a Changing Electricity Landscape: the GenX Configurable Electricity Resource Capacity Expansion Model. MIT Energy Initiat Work Pap 2017:1–67.
[320] Schimidt C, Kissock K. Power Characteristics of Industrial Air Compressors. J Chem Inf Model 2003;53:1689–99.
[321] Waukesha. Waukesha gas engine products list 2019.
[322] MWM. MWM Gas Engines and Gensets – Output. Reliability. Economy. MWM Off Website 2019.
[323] Kawasaki. Green Gas Engine 2019.
[324] Jenbacher GE. Jenbacher Gas Engines. Website 2019.
[325] Li H, Nalim R, Haldi PA. Thermal-economic optimization of a distributed multi-generation energy system—A case study of Beijing. Appl Therm Eng n.d.;26:709–19. https://doi.org/10.1016/j.applthermaleng.2005.09.005.
[326] Ken Darrow James Wang RT. Technology Characterization – Reciprocating Internal Combustion Engines. Rep from US Environ Prot Agency Comb Heat Power Partnersh 2015.
[327] Manzela AA, Hanriot SM, Cabezas-Gómez L, Sodré JR. Using engine exhaust gas as energy source for an absorption refrigeration system. Appl Energy n.d.;87:1141–8. https://doi.org/10.1016/j.apenergy.2009.07.018.
[328] Sun Z-G. A combined heat and cold system driven by a gas industrial engine. Energy Convers Manag n.d.;48:366–9. https://doi.org/10.1016/j.enconman.2006.07.008.
[329] Ayele GT, Mabrouk MT, Haurant P, Laumert B, Lacarrière B. Optimal placement and sizing of heat pumps and heat only boilers in a coupled electricity and heating networks. Energy n.d.;182:122–34. https://doi.org/10.1016/j.energy.2019.06.018.
[330] Blarke M, Lund H. Large-scale heat pumps in sustainable energy systems: System and project perspectives. Therm Sci n.d.;11:143–52. https://doi.org/10.2298/tsci0703143b.
[331] Renedo CJ, Ortiz A, Mañana M, Delgado F. A more efficient design for reversible air–air heat pumps. Energy Build n.d.;39:1244–9. https://doi.org/10.1016/j.enbuild.2007.01.008.
[332] Nowak T. Large scale heat pumps in Europe. Rep from EHPA n.d.

[333] Ghenai C, Bettayeb M. Modelling and performance analysis of a stand-alone hybrid solar PV/Fuel Cell/Diesel Generator power system for university building. Energy n.d.;171:180–9. https://doi.org/10.1016/j.energy.2019.01.019.
[334] Ramli MAM, Bouchekara HREH, Alghamdi AS. Optimal sizing of PV/wind/diesel hybrid microgrid system using multi-objective self-adaptive differential evolution algorithm. Renew Energy n.d.;121:400–11. https://doi.org/10.1016/j.renene.2018.01.058.
[335] Kemna R. Average EU building heat load for HVAC equipment. Rep from Eur Comm 2014.
[336] Paolo Zangheri Marco Pietrobon RA. Heating and cooling energy demand and loads for building types in different countries of the EU 2014.
[337] Ma J, Silva V, Belhomme R, Kirschen DS, Ochoa LF. Evaluating and Planning Flexibility in Sustainable Power Systems. IEEE Trans Sustain Energy 2013;4:200–9. https://doi.org/10.1109/tste.2012.2212471.
[338] de Sisternes FJ, Jenkins JD, Botterud A. The value of energy storage in decarbonizing the electricity sector. Appl Energy 2016;175:368–79. https://doi.org/10.1016/j.apenergy.2016.05.014.
[339] Ofgem. Gas prices: Day-ahead contracts – monthly average (GB). Website Page n.d.
[340] ofgem. Understand your gas and electricity bills 2020;July 2020. https://www.ofgem.gov.uk/consumers/household-gas-and-electricity-guide/understand-your-gas-and-electricity-bills.
[341] Renaldi R, Kiprakis A, Friedrich D. An optimisation framework for thermal energy storage integration in a residential heat pump heating system. Appl Energy 2017;186:520–9. https://doi.org/10.1016/j.apenergy.2016.02.067.
[342] Ofgem. Feed-In Tariff (FIT) rates n.d.
[343] Joos M, Staffell I. Short-term integration costs of variable renewable energy: Wind curtailment and balancing in Britain and Germany. Renew Sustain Energy Rev 2018;86:45–65. https://doi.org/10.1016/j.rser.2018.01.009.
[344] Michael Milligan Debra Lew PD. Operating Reserves and Wind Power Integration: An International Comparison. Rep by Natl Renew Energy Lab Rep 2010.
[345] Movahediyan Z, Askarzadeh A. Multi-objective optimization framework of a photovoltaic-diesel generator hybrid energy system considering operating reserve. Sustain Cities Soc 2018;41:1–12. https://doi.org/10.1016/j.scs.2018.05.002.
[346] Pudjianto D, Aunedi M, Djapic P, Strbac G. Whole-Systems Assessment of the Value of Energy Storage in Low-Carbon Electricity Systems. IEEE Trans Smart Grid 2014;5:1098–109. https://doi.org/10.1109/tsg.2013.2282039.
[347] Sarkadi L, Brett G, Barnett M, Kroó N, Armaroli N, Ongena J, et al. The application of liquid air energy storage for large scale long duration solutions to grid balancing. EPJ Web Conf n.d.;79. https://doi.org/10.1051/epjconf/20147903002.
[348] Gabrielli P, Fürer F, Mavromatidis G, Mazzotti M. Robust and optimal design of multi-energy systems with seasonal storage through uncertainty analysis. Appl Energy 2019;238:1192–210. https://doi.org/10.1016/j.apenergy.2019.01.064.
[349] Akhavan-Hejazi H, Mohsenian-Rad H. Optimal Operation of Independent Storage Systems in Energy and Reserve Markets With High Wind Penetration. IEEE Trans Smart Grid 2014;5:1088–97. https://doi.org/10.1109/tsg.2013.2273800.
[350] Morales E, Latorre JM, Ramos A. Tight and Compact MILP Formulation for the Thermal Unit Commitment Problem. IEEE Trans Power Syst 2013;28:4897–908. https://doi.org/10.1109/tpwrs.2013.2251373.
[351] Yokoyama R, Shinano Y, Taniguchi S, Ohkura M, Wakui T. Optimization of energy

supply systems by MILP branch and bound method in consideration of hierarchical relationship between design and operation. Energy Convers Manag 2015;92:92–104. https://doi.org/10.1016/j.enconman.2014.12.020.